Integrated lab-scale continuous manufacturing of pharmaceutical products

A thesis presented for the degree of
Doctor of Philosophy
in the Faculty of Science
of the University of Strathclyde

by

Vishal Raval

Strathclyde Institute of Pharmacy and Biomedical Sciences
Nov, 2022

Declaration of Author's Rights

This thesis is the result of the author's original research. It has been composed by the author and has not been previously submitted for the examination, which has led to the award of a degree.

Signed:

Date:

Acknowledgements

Firstly I would like to thank my supervisor Professor Alastair Florence for the opportunity to work with him and his esteemed team here at the Centre for Continuous Manufacturing and Advanced Crystallisation (CMAC) at Strathclyde University. His guidance and support have been invaluable to my research and development as a researcher over the last few years. I would also like to thank Dr Humera Siddique, Dr Cameron Brown, Dr Thomas McGlone, Dr Naomi Briggs, Dr Kenny Smith, Mark McGowan and Jack Creswick for their contributions to this thesis and continued support. I would like to thank CMAC for providing a collaborative research environment, a well-equipped National Facility and helpful expert colleagues. I would also like to express my gratitude to the University of Strathclyde for supporting me in doing a part-time PhD along with my day job.

I would also like to dedicate this thesis to the late Dr Lihua Zhao for inspiring me to start this PhD and to my late father Atul Raval, you will always remain in my heart.

Finally, I would like to thank all my friends and family, particularly my school and society friends and also to my wife Tanushree, daughter Darshani, mother Jayshree and sister Nirali for their endless sacrifices and support, love and encouragement throughout my study.

Abstract

Art relates to something to be done or produced by skill, whilst science must be known, discovered, or invented. Crystallisation is a purification and separation process with a long history, and it can be said often falls somewhere in the middle of the two. Research on crystallisation continues to move our understanding closer to that of science. However, crystallisation on the industrial scale is still partly an art, with experience and intuition commonly important in its successful daily operation. However, this leads to processes that are not repeatable, robust or predictable.

Innovation in the pharmaceutical industry has focussed for a long time to the research and development of new active compounds; meanwhile, production, dominated by batch-wise technologies, has only recently started to change. As has already been demonstrated in several other industrial sectors, continuous manufacturing (CM) has many advantages over batch processes. The faster, cheaper, and more flexible processes can be developed with a significantly higher level of quality assurance. The stirred tank reactor (STR) is still favoured as a straightforward manufacturing approach for mixing and reaction. The benefits of moving to continuous include; more efficient use of raw materials, minimisation of waste, improved yield, and improved process reliability, which may have otherwise been limited in a batch-type setup. Improved heat/mass transfer, reductions in energy consumption for running processes in addition to reactor downtime for maintenance and cleaning, more efficient use of physical plant space, a significant reduction in process development required for scale-up and better handling of hazardous materials, including dangerous and unstable intermediates

Chapters 1, 2 and 3 of this thesis detail an Introduction, literature review, aims and objectives of the research and the materials and methods used throughout this work, respectively. Chapter 4 focuses on the design, development and characterisation of the novel lab-scale continuous platform for better control over particle attributes. This research has developed a Cascade of Moving

Baffle Oscillatory Crystalliser (CMBOC), which has a combination of moving baffles in vessels and continuous operation achieved through connecting sections in series, providing an alternative technology to the cascade of CSTR. Due to uniform oscillation provided over the whole vessel section, with no damping of oscillation caused by entrained bubbles, the CMBOC has the added benefits of uniform mixing, enhanced heat and mass transfer and is exceptionally flexible and so it is well suited for multistage processes. The platform was also characterised for mixing and flow with liquids and slurries, confirming excellent mixing performance for residence times in the range of 20–120 min. Heat transfer characteristics were determined and shown to be well suited to the demands of cooling crystallisation processes. Under this research, the platform was also tested for its suitability to perform continuous cooling crystallisation of alpha lactose monohydrate (ALM) and Paracetamol (PCM) running for more than ten residence times with both substances.

Chapter 5 deals with optimising the continuous lactose crystallisation process in the CMBOC by developing a cooling crystallisation population balance equation model using a sequential parameter estimation approach using gPROMS Formulated Products modelling software. A set of experiments were performed in a batch crystalliser to estimate primary and secondary nucleation and crystal growth kinetics. These estimated parameters were utilised in designing a continuous crystallisation process (seeded and unseeded) aiming to dial a particle size. Predictions from the models were validated against the product collected from the continuous trial. Reasonably good agreements were obtained between the experimental measurements and model predictions within the defined model boundaries and uncertainties.

Chapter 6 deals with implementing particle engineering methods via spherical agglomeration to control the final product attributes. Spherical agglomeration can simplify downstream processing dramatically and improve the handling of difficult, needle-shaped crystals. As this research progressed, it was identified that there was a gap in the method to produce smaller spherical agglomerates

(<500 μm) with tuneable final product properties (dissolution rate, compressibility, flow property, porosity) suitable for direct compression.

Contents

List of Figures

List of Tables

Chapter 1. General Introduction

1.1 Pharmaceutical manufacturing

The pharmaceutical industry has faced many challenges in recent years, including increased competition from the generic market associated with the 'patent cliff' [1, 2]. The increased cost of new drug research and development (R&D) whilst patient populations are increasing. Product volumes have reduced due to the increased number of products and increasing potency means there is a greater need for personalised product supply (**Figure 1-1**) [3, 4]; moreover, the regulatory demand for product safety and to achieve greener processes all act as drivers for the industry to adopt more efficient manufacturing processes [5]. Systematic implementation of process intensification (PI) can help overcome these challenges. PI is a hot topic in the pharmaceutical sector to reduce costs and develop processes quickly and safely. One aspect that has received significant attention over the last 10-15 years has been moving from batch processing to continuous manufacture (CM) [6, 7].

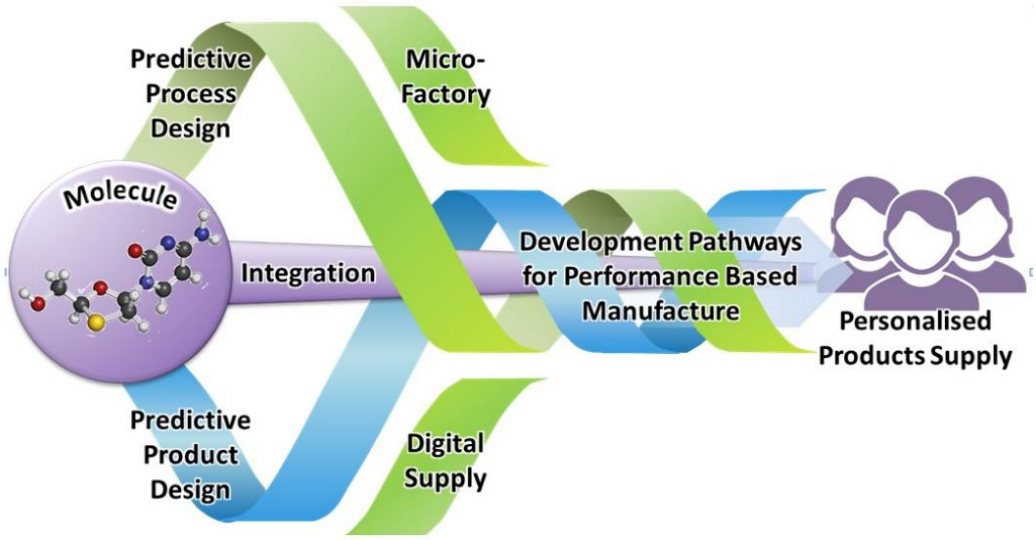

Figure 1-1 Personalised product supply, adapted from the CMAC website [3].

The need for pharmaceutical manufacturing innovation is widely recognised [8, 9], along with the potential benefits this can bring [10, 11]. In recent years,

one particular area that has received attention has been moving from batch to continuous crystallisation [12]. Although batch is the most common method and the methodologies for developing these crystallisation processes are reasonably well understood and widely implemented, there are still significant issues with batch-to-batch variability, which can lead to substantial issues in the downstream processing of isolated material [13] or use of non-value additional steps such as milling to impart property control or complex formulation and/or secondary manufacturing methods to overcome sub-optimal physical attributes. Advanced processing and particle engineering can be useful assets in this context, delivering consistent processes with a material whose properties are designed to achieve the manufacturability, stability and performance demanded by pharmaceutical products and applications. However, the benefits of these approaches are often best viewed from an end-to-end system perspective. This has not been the norm in pharmaceutical manufacturing but is now recognised as a long term goal (e.g. Aliskiren Hemifumarate [14] and an exemplary small-molecule drug [15] are examples of this).

Continuous crystallisation can be viewed within the PI approaches framework that generally applies (**Figure 1-2**)[16]. While crystallisation has perhaps seen less focussed effort around PI approaches in general than synthesis, for example, the need for efficient, robust, scalable processes that can achieve control over crystal size distribution, shape, and solid-state form is clear. Poor control or variability over these material attributes can significantly impact downstream processing, *i.e*. filtration, drying, milling and tabletting [15].

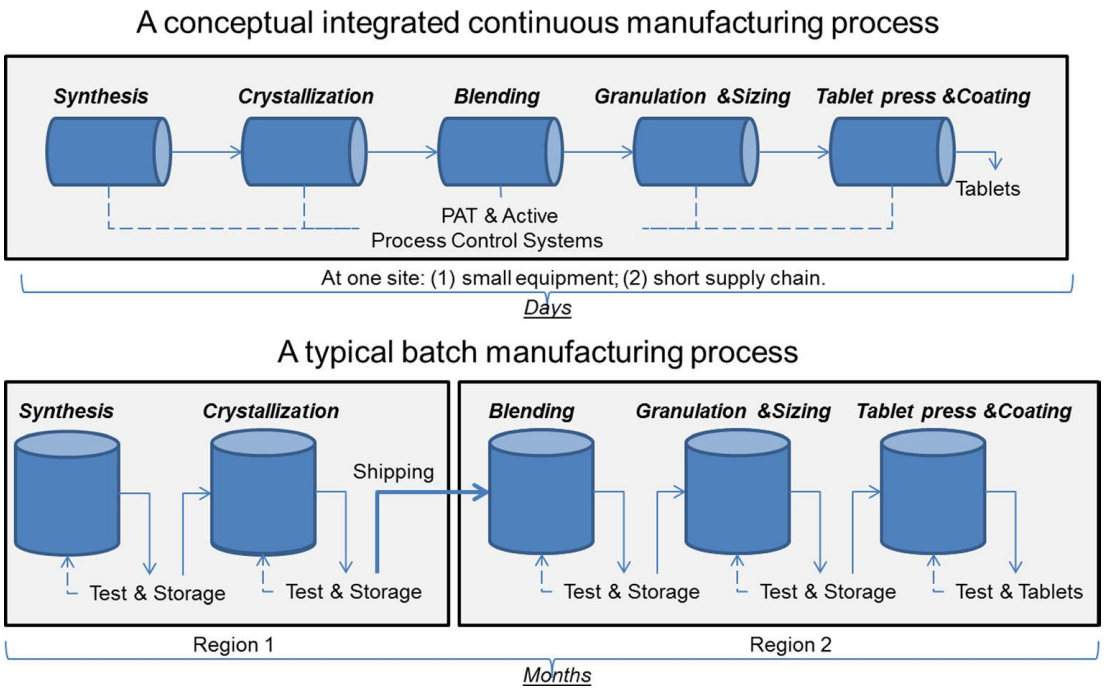

*Figure 1-2 A conceptual fully integrated continuous manufacturing process and a typical batch manufacturing process for tablets are also presented for comparison. Adapted from lee 2015 [*17*].*

1.2 Crystallisation

Crystallisation is one of the most important unit operations in manufacturing pharmaceutical and fine chemicals. Crystallisation processes are widely used for particle formation, purification and separation. Many fine chemical products and active pharmaceutical ingredients (API) are synthesised in solution and then crystallised downstream as solid materials. The ability to separate the desired compound from the bulk solution is essential because it often contains by-products from chemical reactions and impurities from the input materials. Solution crystallisation using either cooling or anti-solvent is widely used to drive and control particle formation. The crystallisation process requires considerable time and energy resources. Several economic factors must also be considered in selecting process technology, including the efficiency of solvent recycling, separation of impurities, consumption of raw material, and increasing yield [18]. Despite the importance of crystallisation on the final

product properties, it has often been approached as a ‘low-tech’ area of chemical production, resulting in low purity and often poor control over the physical form and crystal attributes. These views are changing for pharmaceutical manufacturing with the increasing importance of control for quality and safety, the high costs and the reputational impacts of crystallisation failure (e.g. reverting back to clinical trials formulations and reformulating Ritonavir [19]), coupled with the increased scientific and technological capabilities to design and control robust, scalable and efficient crystallisation processes that are becoming available.

The dominant method for performing crystallisation in the pharmaceutical industry is to use stirred tank reactors (STRs) in batch mode. In pharmaceutical R&D, process development and scale-up have historically taken place over long timelines and face challenges with uncertain project outcomes in converting promising candidate drugs to viable, safe and effective commercial-scale medicines whilst meeting regulatory requirements [20, 21]. Increasingly the development and key chemical, manufacturing and control steps involved in process development are placed under pressure to accelerate process development to ensure products are available for clinical testing and, if successful, commercial-scale production as quickly as possible, especially in the current challenging times like covid 19 pandemic. These objectives are compounded by the challenges of poor scalability [22], poor control [23] and poor yield [24], often seen in batch processes in pharmaceutical industries.

1.3 Crystallisation theory and practice

Therapeutic treatments are most commonly distributed to patients as solid dosage forms containing an active pharmaceutical ingredient (API). APIs are categorised as crystalline or amorphous based on their chemical structure arrangement. A crystalline solid consists of many molecules in an ordered structural arrangement. It has long-range order results in crystalline particles with a regular arrangement of molecules repeatedly repeating over the entire crystal. Crystalline materials are grouped into polymorphs, co-crystals,

solvates and salts, depending on how the components arrange themselves in the crystal lattice (**Figure 1-3**).

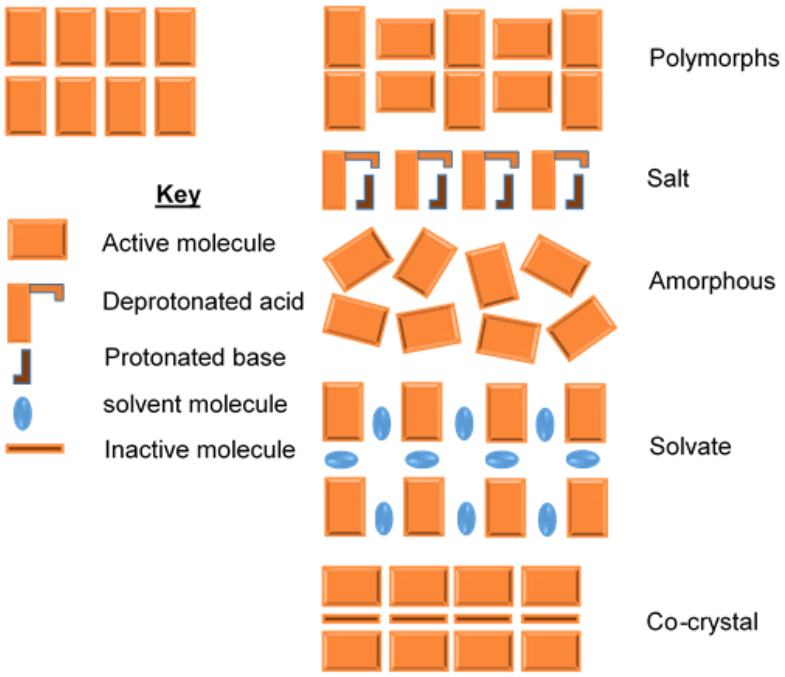

Figure 1-3: Solid API classification. (Adapted from Mullin, 2001)

Amorphous solids consist of particles with an irregular shape, and their internal arrangement is such that any order is only observed over short structural distances. Due to the constituent structural arrangement differences, the two types of solids differ in their properties. For example, crystalline solids have definitive melting points. On the other hand, amorphous solids soften over a temperature range and can be moulded into various shapes, which might be important for formulation purposes. On heating, they can become crystalline at a certain temperature. These differences between crystalline and amorphous solids are summarised in **Table 1.1** [21]. Stable crystalline materials tend to be present in most pharmaceutical products administered to patients [18] due to increased stability.

Table 1-1 Difference between crystalline and amorphous solids [21]

Property	**Crystalline solids**	**Amorphous solids**
Shape	Definitive shape	Irregular shape
Melting point	Definitive temperature	Gradually softens over a temperature range
Heat of fusion	Definitive heat of fusion	No definitive heat of fusion
Anisotropy	Anisotropic in nature	Isotropic in nature
Nature	True solids	Pseudo solids or super cooled liquids
Order in the arrangement of constituent particles	Long-range order	Short-range order

There are several different methods by which crystallisation can be carried out; evaporation, cooling, melt, and anti-solvent. Sometimes more than one of these methods is combined to improve crystallisation process control and product crystal properties [25-27]. The most common pharmaceutical industry approach is cooling crystallisation.

1.3.1 Solubility and Meta stable zone width

Before any crystallisation process development, phase diagrams are essential. They provide vital data on the possible phases of crystallising, likely process yields, and the number of variables utilised to control a process [28]. During crystallisation development, including multi-component solids, the solubility curve (usually displayed as solubility vs temperature) describes the liquid and solid-liquid regions' boundaries in the phase diagrams.

Solubility is a thermodynamic quantity that defines the maximum amount of solute which can be dissolved in a particular solvent at a given temperature and pressure. When a solid is added to a solvent, the solute dissolves, and concentration increases in the solution. This process is known as dissolution.

Some of the dissolved molecules in solution encounter suspended crystals and attach to the crystal surface by a process called crystallisation. A state of dynamic equilibrium is reached when the two processes occur at the same rate. At this stage, the solution's solute concentration will remain constant under the given temperature and pressure. A saturated solution is described as a solution in which no more solute can be dissolved. An unsaturated solution is one in which more solute can be dissolved at the same temperature. The solution in dynamic equilibrium is saturated and contains the maximum amount of solute dissolved in a given amount of solvent. Thus, the concentration of solute in such a solution is its solubility [29].

The metastable zone width (MSZW) is the area between the solubility curve and the metastable limit curve, which is important to control any crystallisation process. The concept of the MSZW is illustrated in **Figure 1-4**. At point A, the solution is undersaturated, and as the solution is cooled from point A to B along the red line, the solution gets more and more saturated until point B. At this point, the solution is at equilibrium with any excess crystalline material suspended in it. The curve on which point B lies (black curve) is known as the solubility curve. Further cooling along the green line results in a phase where the solution's concentration is greater than the equilibrium concentration at the given temperature. The solution is supersaturated, which is known as the unstable region. However, a solid will not spontaneously precipitate or crystallise until it has reached point C. Point C is known as the solution's metastable boundary. The curve at which point C lies (blue curve) is the MSZW curve, where the solution conditions are met. Along this line, the solution will spontaneously nucleate, and it is called the MSZW curve.

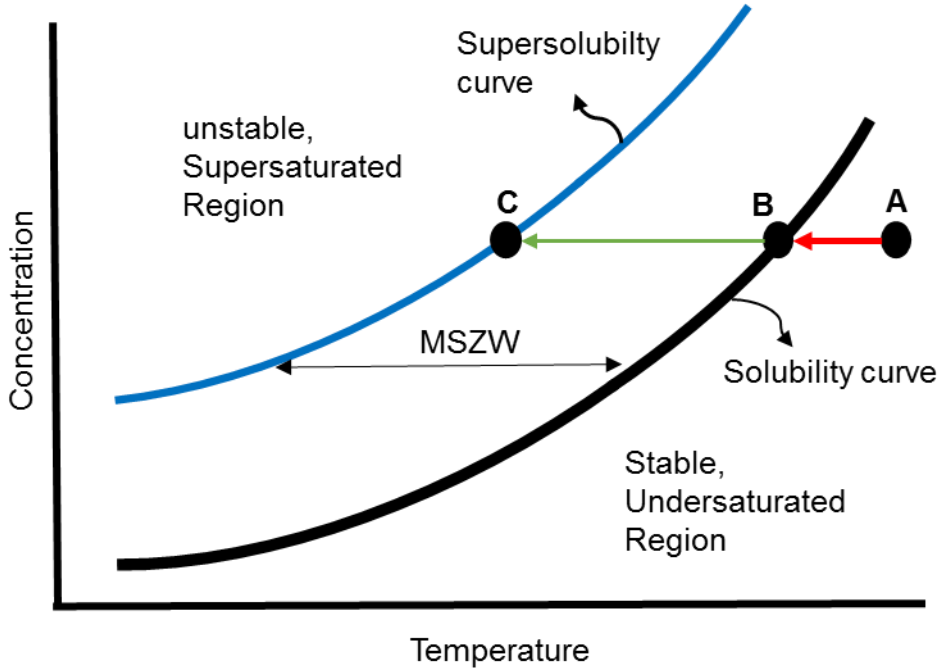

Figure 1-4: Graphical presentation of MSZW and solubility curves illustrating saturation within a solution.

The MSZW can be measured by monitoring turbidity, refractive index, or focused beam reflectance measurement (FBRM) [30]. The MSZW is dependent on the nucleation kinetics and can be influenced by cooling rate, mixing, solution history, fluid dynamics and impurities [31, 32].

1.3.2 Nucleation mechanism

Nucleation occurs in a supersaturated solution where dissolved molecules associate, forming stable, critical nuclei that act as crystal growth sites. There are two mechanisms by which stable nuclei are produced, primary and secondary nucleation. Primary nucleation takes place when no crystalline matter is present. Secondary nucleation refers to the nucleation that is induced as a result of crystals present in the solution.

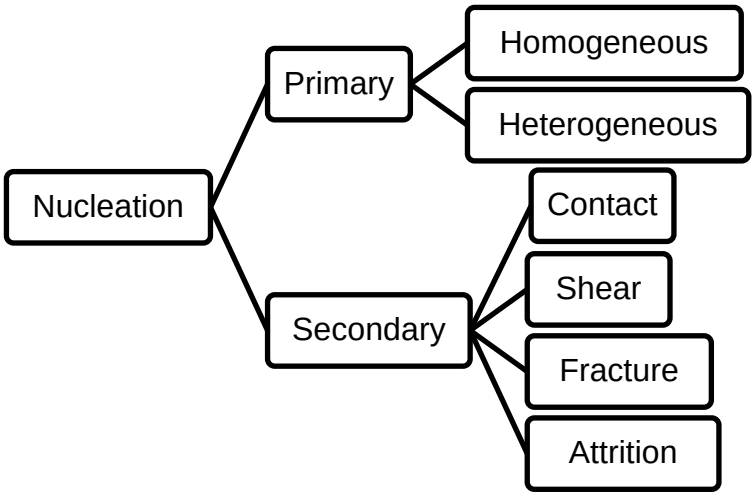

*Figure 1-5 Classification nucleation mechanisms for primary and secondary adapted from Mullin,2001 [*21*].*

1.3.2.1 Primary nucleation

Primary nucleation takes place in two ways; homogeneous nucleation and heterogeneous nucleation. During homogeneous nucleation, the association of molecules in a solution occurs randomly and spontaneously, whereas, in heterogeneous nucleation, foreign particles act as sites for nucleation. Heterogeneous nucleation is most common as many systems will likely contain some suspended or insoluble impurities. These foreign entities reduce the free energy required for nucleation, making nuclei appear more readily and at lower supersaturations than homogeneous nucleation. The rate of nucleation, J, can be expressed in the form of the Arrhenius equation:

$$\boldsymbol{J = A\, exp\left(-\frac{\Delta G}{KT}\right)} \qquad \textbf{Equation 1-1}$$

Where the number of nuclei formed per unit time per unit volume (J) = # $s^{-1}.m^{3}$, rate constant (A) = #. $s^{-1}.m^{-3}$, free surface energy (ΔG)= N/m, Boltzmann constant (K) = 1.3805 x 10^{-23} $J.K^{-1}$ and temperature (T) = K are expressed.

Classical Nucleation Theory (CNT) is the most widely used theory to describe the nucleation process [33]. Whilst CNT has offered a starting point for explaining nucleation; it makes several assumptions [34]. The assumptions

are: the nuclei are considered as spherical droplets, the formation of nuclei is by single addition of solute monomers, the nuclei formed have the same structure as the final crystal, and the size of the nuclei is the only factor used to determine whether formed nuclei are stable or unstable.

Due to CNT's several assumptions and not considering the influence of process conditions or impurities, this nucleation theory has been reconsidered in a two-step nucleation theory [34, 35]. In two-step nucleation, dense pre-nucleation clusters of solute molecules are produced. These take the form of oil-like droplets; once an intermediate size is reached, the clusters restructure themselves to an organised crystalline nucleus within this droplet [36].

1.3.2.2 Secondary nucleation

Secondary nucleation occurs when there are parent crystals present in the solution. These parent crystals induce the formation of new nuclei through several methods, typically contact nucleation. Crystals can impact the vessel walls, the impeller, or each other and break, releasing smaller crystals and nuclei into the bulk solution. Fluid shear forces may also be sufficient to produce secondary nuclei from a crystal surface [37]. Secondary nucleation occurs at lower supersaturations than primary nucleation, having its own characteristic metastable zone width. It is generally an unfavourable process during crystallisation as it can lead to broad distributions in crystal sizes. However, in some cases, secondary nucleation can be desired where the production of new nuclei in the solution having the same characteristic as the parent crystals is targeted, for example, in seeding processes. Secondary nucleation also influences crystallisation yield via the surface area of crystals available for growth. A high secondary nucleation rate dependence on supersaturation indicates that it will be difficult to grow large crystals regardless of the equipment. The overall rate process of secondary nucleation can be described by [37],

$$B = K_b M^j N^k \Delta C^b \qquad \textbf{Equation 1-2}$$

Where the secondary nucleation rate (B), a specified function of the vessel geometry (K_b), the concentration of crystals in solution (M), stirrer speed (N) supersaturation and exponents (J, k and b) are parameters determined by the assumptions of the model [37].

In continuous processes, insufficient secondary nucleation can have negative effects because supersaturation may rise due to the lack of crystal growth surface. The system will then reach a metastable zone of activated nucleation that largely affects the crystal growth state [38].

1.3.3 Crystal growth

Crystal growth is the latter stage of crystallisation following nucleation, where the nuclei grow into larger, stable, crystalline particles. As long as the system remains supersaturated, the crystals present will continue to grow. This rate depends on several factors, i.e. impurities, supersaturation, temperature, agglomeration and agitation/mixing.

The growth process can be considered a two-step event involving mass transport, diffusion from the bulk to the crystal surface, followed by surface interaction. The solute molecules are integrated into the crystal lattice and defined by **Equation 1-3** [21].

$$\boldsymbol{G = A\,exp\left(\frac{-E_G}{RT}\right)\Delta C^g} \qquad \textbf{Equation 1-3}$$

Where, G = linear growth rate, A = rate constant, E_G = activation energy (KJ.mol^{-1}), g = order of overall crystal growth, and ΔC is change in concentration

1.3.4 Supersaturation and control

Crystallisation processes are driven by supersaturation, and it is important to control the supersaturation profile, which defines the product's size, shape, and solid-state [39]. High supersaturation levels lead to excessive nucleation of fine particles, whereas low supersaturation leads to larger crystal growth. The balance between nucleation and growth determines the physical and

mechanical properties of the product crystals and how well the growing crystal rejects chemical impurities.

Supersaturation is typically expressed in two common ways, namely the supersaturation ratio (S) and relative supersaturation (σ):

$$S = \frac{c}{c^*} \qquad \textbf{Equation 1-4}$$

where C = solution concentration and C^* = equilibrium solution concentration (at a constant temperature and pressure) and the relative supersaturation (σ) is given by:

$$\sigma = \frac{c - c^*}{c^*} \qquad \textbf{Equation 1-5}$$

At low supersaturation, crystals can grow faster than they nucleate, resulting in a larger crystal size that includes impurities. However, at higher supersaturation, the crystal nucleation rate dominates the crystal growth rate resulting in smaller crystals which sometimes cause filtration problems downstream. This is a problem of relatively low total thermodynamic driving force (high positive input of surface free energy being in opposition to the negative volume free energy) at low supersaturation, which can be enhanced by nucleation on earlier formed crystals. If supersaturation is high, further effective nucleation and growth will be limited. Supersaturation is usually maintained low in well-designed industrial crystallisation processes to achieve the desired particle size distribution (PSD) [21]. There are numerous methods to control supersaturation within a solution, i.e. cooling, anti-solvent and evaporative crystallisation (**Figure 1-6**) [39]. Specific systems will nucleate at varying supersaturation levels, and this physical process is sensitive to a wide range of process conditions, including cooling rate, agitation, temperature and impurities [21].

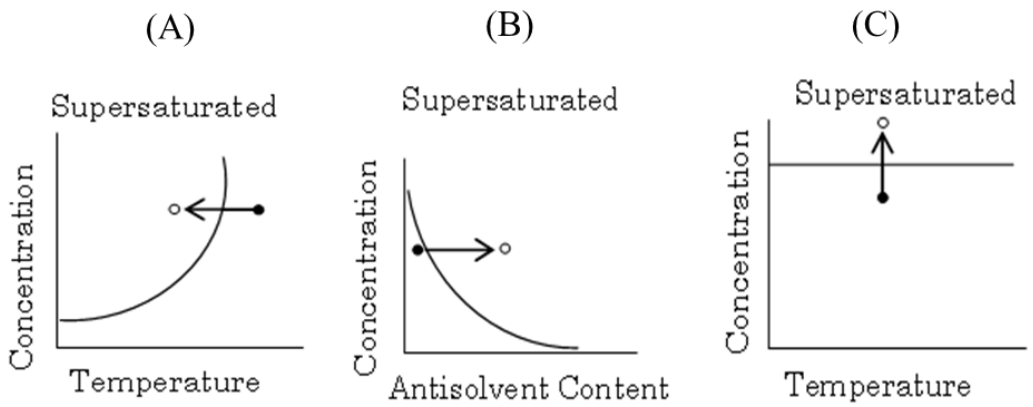

Figure 1-6 Mechanism of supersaturation formation on phase diagrams during (A) Cooling Crystallisation, (B) Antisolvent crystallisation (C) Evaporative crystallisation.

Cooling crystallisation is implemented where the solid's solubility has strong temperature dependence, and supersaturation can be created by reducing the process temperature. A typical batch cooling crystallisation begins with hot unsaturated feed charged to a jacketed stirred reactor. Supersaturation is created by applying cooling, after which nucleation occurs, crystals grow, and the supersaturation is depleted. The final product PSD is dependent on the supersaturation profile created over the batch time and the applied cooling rate. If natural cooling is employed, the vessel's temperature will fall exponentially. On the other hand, the supersaturation increases very quickly in the early stages and peaks when nucleation occurs after exceeding the metastable limit. This sequence of events leads to an uncontrolled performance and results in small crystals with a wide PSD. However, a distinct performance improvement can be obtained if the supersaturation peak is eliminated. This may be done by choosing a working level of supersaturation at which the primary nucleation rate is likely negligible by seeding the solution and maintaining the supersaturation within the metastable zone throughout the batch time. This operation mode, called 'controlled cooling', requires the cooling curve to fall slowly in the early stages and move quickly towards the

end where more crystal surface area is available to deplete the supersaturation [21].

Another method to create supersaturation is antisolvent crystallisation, in which more than one solvent is used. Antisolvent crystallisation can be achieved by adding the antisolvent to a dissolved solid solution (normal mode) or by a dissolved solid solution added to antisolvent (reverse mode). Antisolvent addition reduces the API's solubility in a solvent with reasonable solubility and generates supersaturation at that solvent composition which induces the crystallisation. The addition of antisolvent typically generates local supersaturation at the addition points; therefore, nucleation typically occurs at the point of addition, after which crystal growth happens in the bulk solution. Due to this local supersaturation effect can be difficult to operate and control the antisolvent crystallisation process.

The evaporative crystallisation method is applied when the solubility of a solid does not show a strong temperature dependence and is mainly applied on a large scale for bulk chemical production (common salt) and in pharmaceutical industries has been confined to for small scale discovery of new chemicals and their associated forms [29].

1.3.5 Desirable crystal attributes

The general aims of industrial crystallisation are high manufacturing efficiency and high yield, processable end products. Desirable crystal attributes commonly referred to in the literature are summarised in **Figure 1-7**, which shows the attributes produced from the crystallisation process and their impact on subsequent process steps[40].

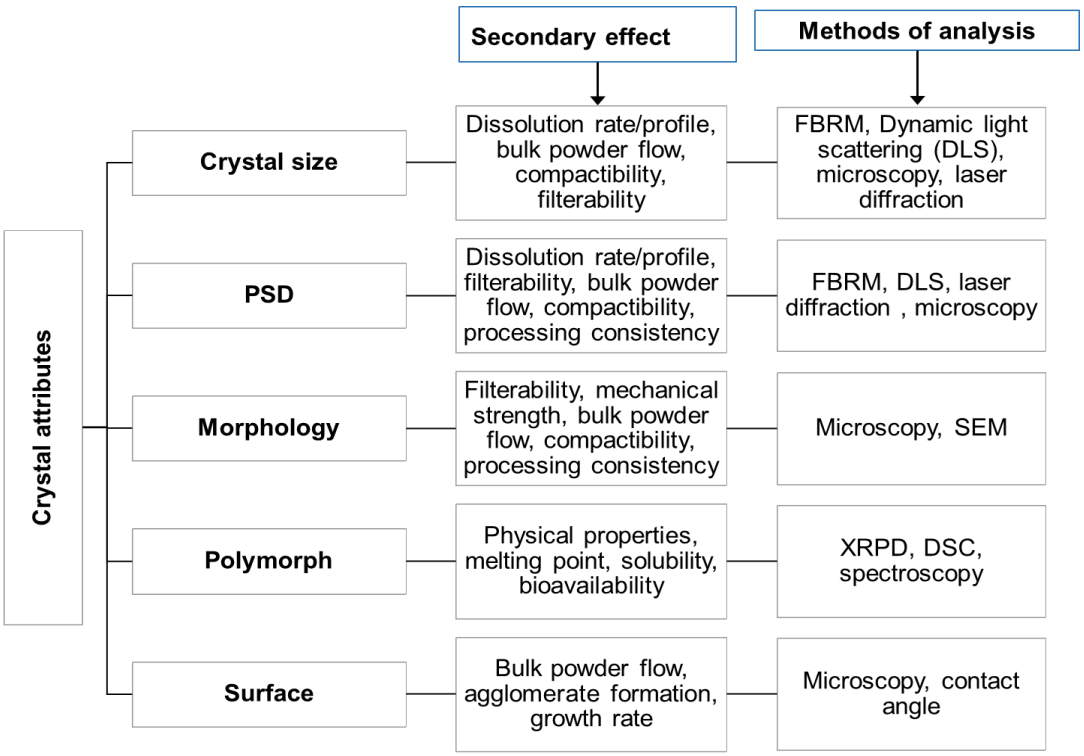

Figure 1-7 Desirable crystal attributes resulting from crystallisation and how these affect product performance. Typical techniques for measurement are also shown.

Polymorphism is the existence of more than one crystalline form of a compound [41]. Different polymorphs show different physiochemical properties, including solubility and stability, particle properties, such as particle size distribution (PSD) and morphology, and potentially influence bioavailability and downstream processability. Thus, controlling polymorph nucleation, subsequent growth, and possible transformations is a fundamental requirement for developing robust pharmaceutical crystallisation processes [39, 40]. Ostwald's rule of stages explains that the metastable form (if one exists) appears first during crystallisation and transforms to a more stable form with lower free energy [42]. Thermodynamically stable polymorphs are generally the most desirable form in pharmaceutical manufacturing. Control over the polymorphic form can be achieved by nucleation temperature, seeding with a desired polymorph [43], controlling the supersaturation [44], choice of solvent [45], using additives [46], and surfactants [47].

Crystal size and PSD are also important attributes that affect bioavailability. If variations in physical form or PSD significantly affect the drug substance's performance, these must be controlled as a priority, once the product attributes that dictate therapeutic requirements are met from a process, optimisation of other parameters, including product yield and cycle time, becomes a focus to maximise efficiency and productivity. These desired targets generally have no direct impact on the end-user but rather on the drivers for economically viable processes in highly cost-effective and safer manufacturing processes [40].

There are many routes by which crystalline material can be tailored to result in more favourable characteristics; for example, needle and flake-like crystal habits are the most difficult to handle from a manufacturing point of view as they are challenging to filter, dry and formulate. APIs with poor solubility in water affect the dissolution rate, resulting in the drug bioavailability [48]. The Biopharmaceutical Classification system (BCS) differentiates drugs based on their solubility, permeability and dissolution properties. An API's particle size and PSD play an important role in the drug's dissolution process [49]. Smaller particles are generally preferred from a bioavailability perspective. However, smaller particles are difficult to handle from a secondary processing perspective.

Generally, APIs are more readily absorbed by the body with a reduced particle size as the surface area available for dissolution increases, thus improving the dissolution behaviour. Depending on the targeted administration route, different particle sizes of API can be desired. Poor control of the PSD during the crystallisation process can significantly hinder downstream secondary manufacturing processes. For example, uncontrolled secondary nucleation during crystallisation can produce fines, a population of smaller particles co-existing with the bulk population of larger particles. These fines can lead to broad and bimodal PSDs, significantly increasing the filtration time and leading to blockages during filtration. Fines tend to arise from either secondary nucleation or attrition. Secondary nucleation can occur when crystals already present in a saturated solution have a catalysing effect on the nucleation

process; here, nucleation is induced again but at supersaturation levels lower than spontaneous primary nucleation. Controlled crystal growth will reduce the likelihood of spontaneous secondary nucleation [50, 51]. Fines can also appear due to the breakage of crystals during crystallisation, known as attrition. This occurs due to collisional or fluid mechanical breakup, resulting from crystal-crystal, crystal-agitator and crystal-wall collisions. The possibility of breakage depends on the mechanical strength of the crystal and the applied braking forces; for this reason, attrition can be somewhat more difficult to control [51-53]. Troublesome regions for attrition within crystallisers are located in the highest shear areas, typically around the impeller. Aggregation and agglomeration are further processes that can occur during crystallisation and affect crystal growth and the resulting crystal size distributions. Aggregates are clusters of loosely bound crystals, easily disintegrated, whereas agglomerates are clusters where the crystals have become tightly interlocked and only disintegrate under considerable force. These are generally undesired processes during crystallisation due to their impact on growth rates and complications with processing and sizing.

In some cases, it can be advantageous to manipulate this process to produce particles with improved attributes. One such example of favourable agglomeration during crystallisation is that of spherical crystallisation. Here control over the agglomeration process results in spherical crystalline agglomerates with improved physical and mechanical properties such as flowability, compatibility and bioavailability [54].

1.4 Process Intensification in Continuous Crystallisation

Van Gerven and Stankiewicz have presented a systematic overview of PI methods for pharmaceutical crystallisation [16]. They have classified different approaches that can be explored when seeking to intensify a process under four general areas or domains: space, time, function and energy (**Figure 1-8**) [55]. Continuous crystallisation provides opportunities for intensification within the time domain over batch processing. However, many researchers have

demonstrated the opportunity to combine multiple domains to achieve and optimise a PI process. These include continuous microfluidic approaches [56], the use of external fields such as coupling continuous with ultrasound [57] and continuous particle engineering approaches such as spherical agglomeration (SA) [58, 59].

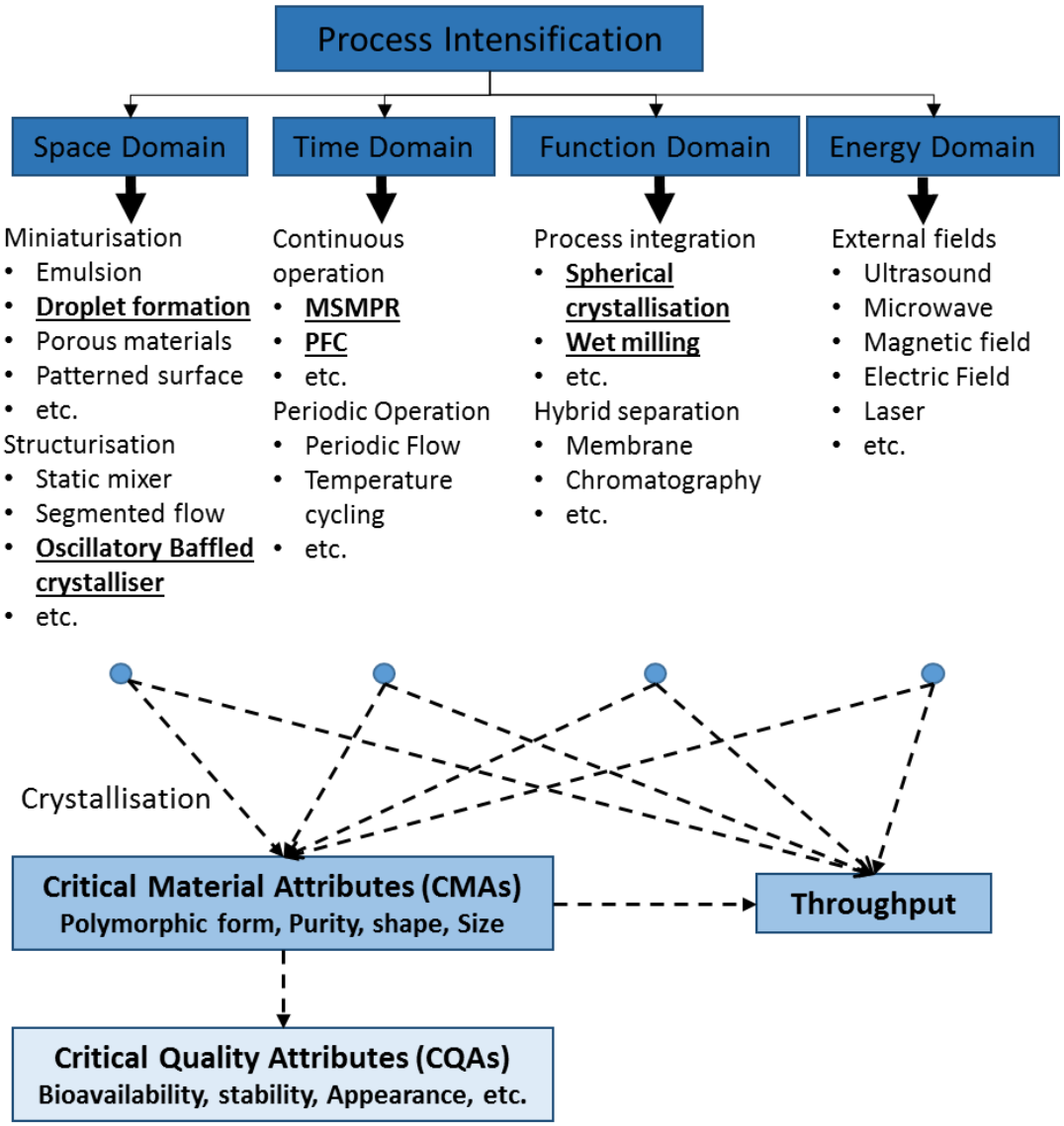

*Figure 1-8 An overview of PI in pharmaceutical crystallisation. The underlined area is the focus of this thesis. Adapted from Wang et al. [*55*].*

Continuous crystallisation and particle engineering are the two important PI domains (time and function, respectively) for pharmaceutical crystallisation. The claimed benefits of continuous crystallisation include improved product

quality and improved manufacturing processes [8]. Studies have shown that 40-60 % of current batch processes can be operated continuously [5, 32, 60]. Continuous crystallisation also offers the advantages of reduced waste and energy consumption due to increased yields, smaller footprint and associated capital costs, and achieving greater process control by steady-state operation combined with closed-loop control and PAT and reduced costs [61].

1.5 Types of crystalliser

In drug substance production, crystallisation is essential to deliver purity and achieve consistent particles with desirable quality attributes, including size, shape, and form, impacting manufacturability, stability, and performance. With increasing interest in the industrial adoption of continuous manufacturing, there is a need for robust, well-characterised continuous crystallisation process equipment.[4, 62] Several continuous crystallisers are currently used in the bulk chemical industry. However, these have been less applied in the pharmaceutical and fine chemical sectors due to the scale of operations and crystals' often challenging physical properties. In recent years, increased research efforts have been made to develop and assess new crystallisers to achieve efficient process operation and enhanced particle control. These include Continuous Stirred Tank Reactor (CSTR) with single or multiple stages (cascade) [24, 63], Plug Flow Crystallisers (PFC) [43, 64] segmented flow crystallisers [65] and Taylor-Couette crystallisers [66-68]. Also, well-characterised experimental and digital design methodologies for process design, scale-up, and optimisation of processes using these technologies have received considerable attention [39].

Another important consideration in the design of a crystalliser is its suitability for operating different crystallisation processes, including antisolvent, cooling, combined antisolvent-cooling, and reactive or pH-controlled crystallisations [13, 69]. Each crystallisation type requires a means of control over particular process parameters. For example, a smooth temperature profile and efficient heat transfer are required in cooling crystallisation (dealing with narrow MSZW

processes). Controlled mixing of components is often required for antisolvent and pH-controlled crystallisation. Thus, for maximum utility, a crystalliser will ideally support different supersaturation control methods via flexible addition points for antisolvent or buffers, control different temperature profiles,, use, and cleaning [70].

1.5.1 Stirred tank crystallisers

Stirred tank crystallisers (STCs) largely remain the standard technology for crystallisation from early-stage discovery to commercial manufacturing for pharmaceutical product mass production. However, they can suffer from batch-to-batch variability and the need for costly and time-consuming scale up to meet increased production demands [4]. The drawback of the STC at a larger scale includes poor heat and mass transfer, concentration gradients within the solution, larger shear rate distributions, i.e. particles around the impeller and the experience of different conditions in the vessel's other areas. Temperature gradients across the vessel diameter are also large due to the low wall temperature needed to meet desired cooling, significantly affecting the nucleation phenomena as the entire solution is not under the same conditions. The STC is quite possibly the simplest of its kind having just three main components, a vessel, a mixer and a jacket. Crystallisation in stirred tanks can be achieved in either batch or continuous mode (**Figure 1-9**).

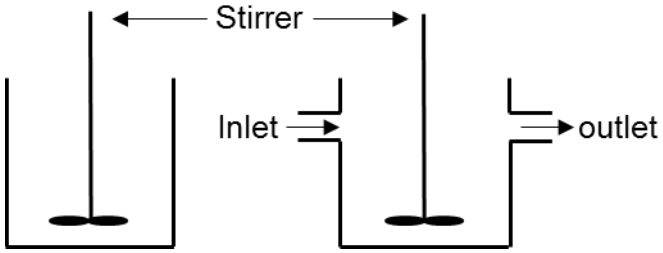

Figure 1-9 Schematic of a Stirred tank Crystalliser, batch (left), continuous (right).

The scaling-up process of the STC can also be challenging. Mixing gradients are often found in large-scale mixing within the STC, which cannot be linearly

scaled up. As a result, the final crystal attributes can be affected, and in some cases, it is not easy to obtain a consistent product [22].

1.5.2 Continuous stirred tank reactor (CSTR)

Crystallisation in an MSMPR is carried out in a single vessel or by connecting one or more well-stirred crystallisers in series for multiple-stage operations. CSTRs remain the most widely utilised platform for continuous crystallisation due to familiarity with operation and control compared to existing batch equipment (As each crystalliser operates at a constant temperature). These have been successfully operated at a range of 1–10 L scale [14]. However, some disadvantages documented by CSTRs include localised high shear near the impeller/agitator, non-uniform and slow heat transfer due to low surface-to-volume ratio and non-linear process scalability [13, 71]. This non-uniform heat transfer, wider residence time distribution and localised high shear affect the final crystal product attributes (wider crystal size distribution) [72, 73].

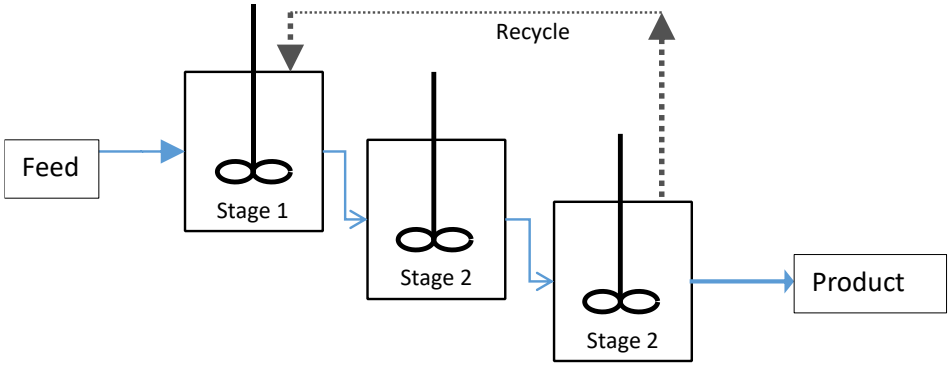

Figure 1-10 Schematic of CSTRs in series.

1.5.3 Oscillatory Baffled Crystallisers

The first conception of the oscillatory baffled crystalliser (OBC) was proposed by Mackley in 1989 [74]. There are mainly two modes of oscillatory mixing: moving baffle (MB), where baffles are moved within the column oscillated [75-78] and moving fluid, where baffles are fixed, and the fluid is oscillated [77, 79]. The OBC consists of a tubular vessel surrounded by a jacket used for heating/chilling the contained liquid. The vessel contains periodically spaced

baffles; these baffles must be placed the same distance apart, ensuring the solution is experiencing the same mixing conditions along the baffle length. The production of eddies generates the mixing in these crystallisers (**Figure 1-11**). Eddies are created on either side as the baffles move through the solution, depending on the baffles, moving up or down. The constant production of eddies allows efficient and constant mixing throughout the system.

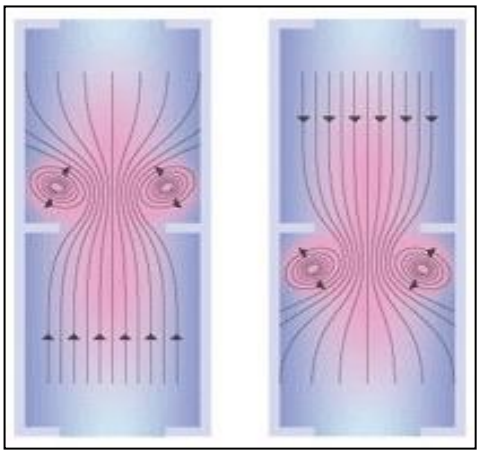

Figure 1-11 Production of eddies while oscillating the fluid, Upstroke (left), Downstroke (right).

The OBC allows uniform process conditions of the solution and, in doing so, produces higher quality crystals and significantly more reproducible results when compared to an STC [80].

When considering a continuous operation, the system should be operated such that the maximum oscillatory velocity is at least double the velocity of the fluid flowing through the tube. This means the flow is always fully reversing with the fluid interaction at the baffles. The mixing generated in the zones between baffles is then uniform, and the tube itself can behave as a series of well-mixed stirred tanks. Importantly, mixing is independent of the throughput velocity, meaning it is possible to have a low net flow velocity but maintain good mixing and plug-flow performance through control of the oscillatory conditions.

1.5.3.1 Continuous Oscillatory Baffled Crystallisers (COBC)

COBCs typically comprise a tubular vessel containing periodically spaced annular baffles. The detailed design and operations of a COBC are described in a number of literature examples [43, 64, 70, 81]. Processes are operated by passing a fluid through the vessel whilst superimposing an oscillatory motion of the fluid. COBCs allow longer residence times to be achieved in a shorter reactor whilst maintaining near plug flow conditions as turbulent mixing is controlled by the oscillatory conditions and decoupled from the net flow rate [43, 81-86]. Scale-up and conversion from a batch to a continuous process with the COBC are easier than conventional stirred tank reactors by increasing the reactor's length rather than the diameter [87]. Several PhD theses are also dedicated to the COBCs [88-92]. **Figure 1-12** shows a typical set-up of a COBC for a crystallisation process, consisting of 8-10 cooling sections, each with half an hour of residence time. The setup can have a number of access ports for PAT probes and/or sampling points across the length. Oscillation can be generated at the inlet and/or outlet of the crystalliser using bellows, pistons or diaphragms.

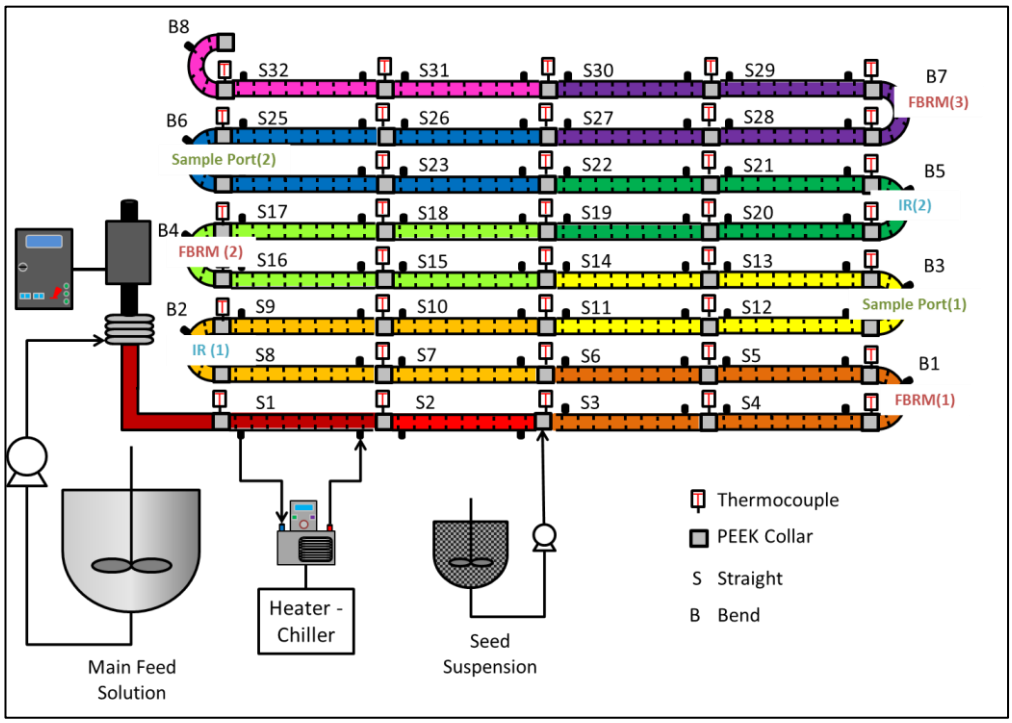

Figure 1-12 Typical COBC setup (adapted from Briggs et al., 2015)

COBCs offer a range of favourable characteristics for controlling continuous crystallisation, such as enhanced heat and mass transfer capabilities, linear scalability, minimal concentration gradients and simple implementation of process analytical technology (PAT). However, they also present some operating restraints, i.e., poor handling of high solid loadings (typically > 20 wt %) and the need to degas the crystalliser to avoid damping of the oscillation. [81, 93].

1.5.3.2 Moving-Baffled Oscillatory Crystalliser (MBOC)

A moving baffle is an alternative technology that allows mixing by moving the baffles within the crystalliser(**Figure 1-13**). Moving baffles has several potential benefits, including handling high solid loadings via the control of oscillatory conditions. More uniform mixing is achieved than in a stirred tank by distributing the moving baffles uniformly throughout each vessel [73, 94]. Importantly, this crystalliser setup's scale-up, as with other oscillatory baffled crystallisers, follows well-defined rules maintaining a consistent baffle to orifice ratio and baffle spacing as the size of the reactor changes [81, 95, 96].

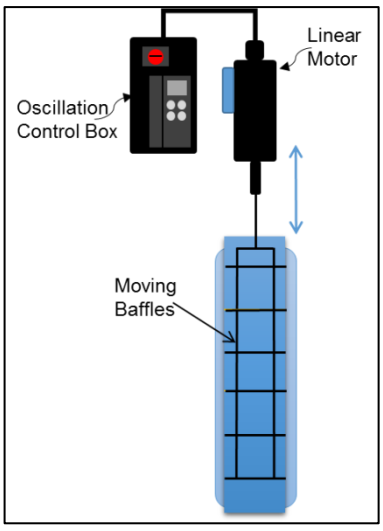

Figure 1-13 Batch Moving-Baffled Oscillatory Crystalliser (MBOC) setup.

Yiging C. Liu *et al.* showed that the Moving-Baffled crystalliser has considerable potential to produce narrow product particle size distributions and offers stable and reliable cooling crystallisation operation in a single-stage

MSMPR in continuous mode compared to a traditional STC [97, 98]. Heat transfer enhancement in terms of the Nusselt number (Nu) due to oscillatory flow by a factor of 10-30 has also been reported previously [99-104]. Callahan *et al.* have studied the influence of the hydrodynamic environment in a moving baffle on the nucleation mechanism of chiral crystallisation [87].

Moving-Baffle crystalliser also benefits less/no fouling due to close moving baffles around the vessel wall. They also tend to provide consistent nucleation performance, which is important for crystallisation processes. They can also control PSD and yield due to uniform mixing. They can further be used in gas/liquid reactions, enhancing yield and giving higher conversion as they can promote higher gas retention/hold up within the reactor. The Design and characterisation of MBOC will be covered in much more detail in Chapter 4.

1.5.4 Segmented flow crystallisers

Reactive precipitation, cooling crystallisation and antisolvent crystallisation have been demonstrated over the years with segmented flow [65, 105-107]. Segmented flow tubular crystallisation can achieve a near plug flow condition with narrow residence time distribution. Robertson *et al.* demonstrated small scale crystallisation using segmented flow to achieve consistent nucleation events and prevent fouling. The segmented flow helps avoid any back mixing in the system, enabling the product to experience the same crystallisation process conditions over the length of the crystalliser (**Figure** 1-14) [65].

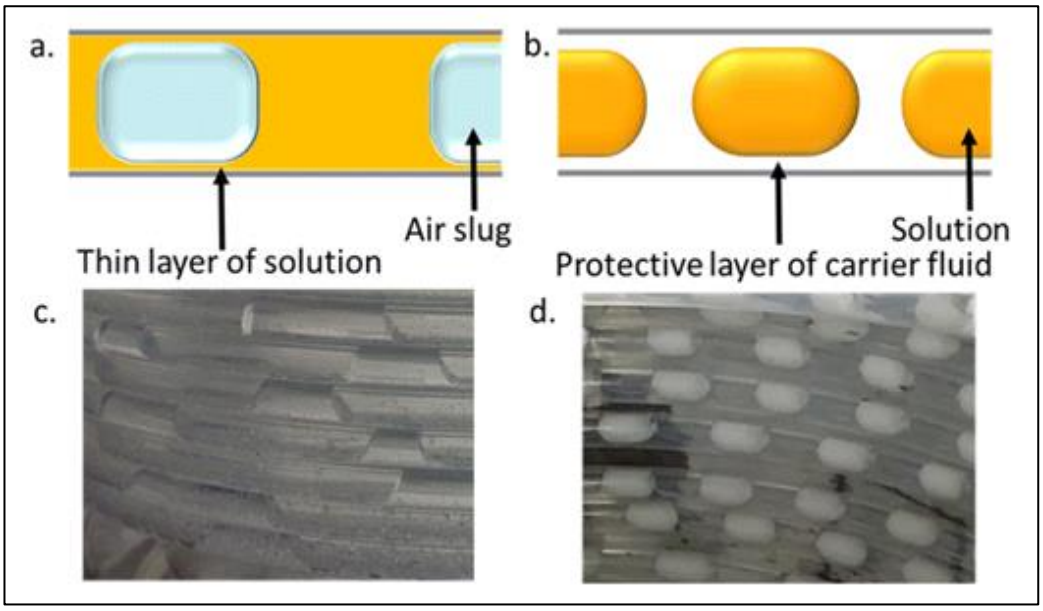

Figure 1-14 Schematic showing a) air-segmented flow. (b) Liquid-segmented flow (c) Air segmented tubing coil (d) Liquid segmented tubing coil. (Adapted from Robertson, 2015)

1.5.5 Fluidised bed crystallisers

A typical fluidised bed crystalliser (also known as Oslo) is the oldest type of crystalliser known for producing large, coarse crystals, as shown in **Figure 1-15**. Where feed solution enters the crystalliser vessel at inlet of the circulating pipe. Saturated solution from the upper section of the vessel along with the feed solution circulated by the pump through the heat exchanger which is cooled rapidly by forced circulation of water. On cooling, the solution becomes supersaturated. This supersaturated solution flows down the pipe and come out in the crystalliser from the bottom of the tube directly into the mass of crystals growing in the vessel. The rate of circulation is such that the crystal is maintained in a fluidised state in the vessel, and classification occurs by a hindered setting process. Crystals that have grown to the required size fall to the bottom of the vessel and are discharged. [12, 21]. Due to geometric limitations, it is challenging to build this unit on a smaller scale. As a result, theoretical work on this crystalliser is limited, which raises problems in scale-

up or troubleshooting operations. Therefore, understanding an OSLO is case-specific and based on empirical evidence.

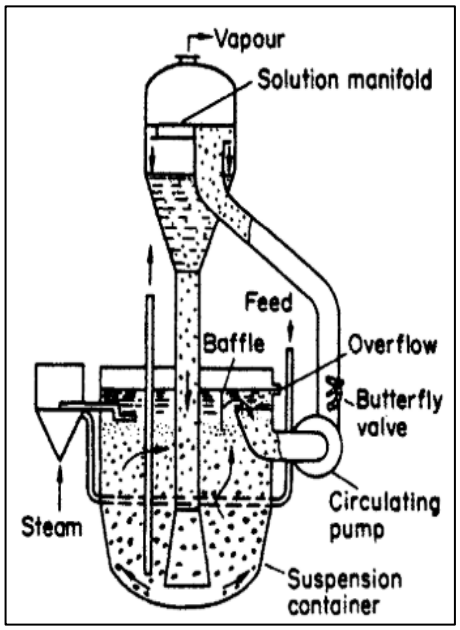

Figure 1-15 Schematic of an Oslo fluidised bed Crystalliser (adapted from Mullin 2001).

1.5.6 Draft tube and baffle crystallisers

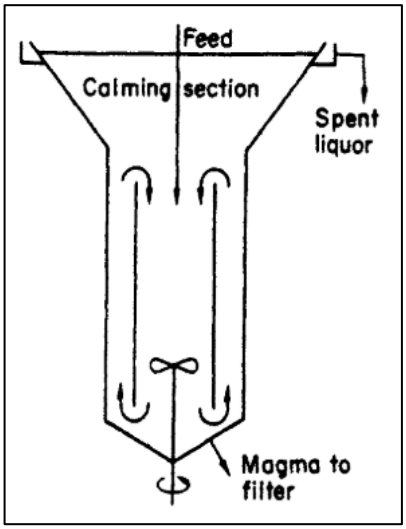

Figure 1-16 Schematic diagram of the Draft tube and baffle crystalliser (adapted from Mullin 2001).

In the last fifty years, draft tube and baffle (DTB) crystallisers have been commonly used for industrial crystallisation as an alternative to the Oslo crystalliser. Crystallisation is typically carried out from the solution, where a slow-moving propeller circulates the suspension of crystals within the crystalliser. The basic design allows larger crystals to sediment in the vessel before being removed whilst fines are recirculated with feed or removed via heating. Due to geometric limitations, this type of crystalliser is also difficult to scale down.

Evaporative crystallisers are also used in industry when the solubility of a solute is not largely temperature-dependent; in such cases, supersaturation in a system can be achieved by removing the solvent. Salt recovery from seawater is the most common example of evaporative crystallisation, where water is being evaporated by solar radiation [21]. Other types of crystallisers are also available, such as static mixers [108] and Couette-Taylor crystallisers[109]. Couette–Taylor crystallisers have also received attention for continuous crystallisation. Manipulation of the Taylor vortex flow generated in the gap between two rotating co-axial cylinders has been used to control the crystal size distribution, phase transformation, polymorphic form and agglomeration [66-68]. Imping jet and spray drying techniques have also been used to produce small crystals combined with other growth mechanisms and better control the final product size [109].

1.6 Characterisation of continuous oscillatory flow crystallisers

1.6.1 Residence time distribution

Continuous crystallisation platforms must deliver a suitable environment for the generation, suspension and movement of particles whilst maintaining a level of supersaturation sufficient to allow particle growth. As a result, it is essential to understand the mixing and flow profile achieved under typical operating conditions. In any vessel, each element of fluid takes a different route and time to pass through the reactor and the distribution of different times for fluid

elements to pass through the system is called the exit age distribution E, or the Residence Time Distribution (RTD) of the fluid (**Figure 1-17**).

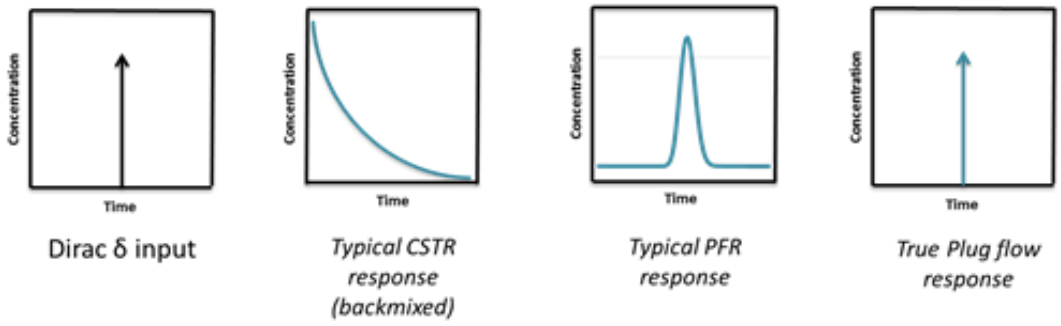

Figure 1-17 Typical tracer concentration responses in different types of reactors. (Adapted from Levenspiel,1962).

The axial dispersion [43] and tanks-in-series [110] models are the most effective methods for estimating RTD in a non-ideal platform [95]. The difference between these models is that the dispersion model considers the reactor whole, and any deviation from plug flow is due to diffusion [95]. On the other hand, the tanks-in-series model divides the reactor into compartments, and the number of compartments determines the deviation from plug flow [95]. Stonestreet *et al.* studied the interaction of oscillatory flow and net flow components on the RTD performance in a laboratory-scale baffled tube reactor [82]. This investigation has shown that using the tanks-in-series model is viable and useful for characterising the RTD behaviour in baffled tubes subjected to oscillatory flow [82]. Dickens *et al.* investigated the effect of oscillatory flow on the RTD in a 2 mm I.D. baffled tube, 0.7 m long. This study concluded that oscillation amplitude profoundly affects the dispersion characteristics compared to the frequency [83]. Howes and Mackley reported dispersion characteristics in a 2.5 m long, 51 mm I.D. baffled tube. They concluded that for fixed Re_n and Re_o values in the range of $500 \leq Re_o \leq 700$, the dispersion reached a minimum value and approached plug flow behaviour [84]. Ni *et al.* investigated the RTD behaviour in a tube and concluded that axial dispersion is directly proportional to Re_o. [85]. Smith *et al.* investigated the scale-up of oscillatory flow mixing in baffled tubes through axial dispersion. They

concluded that the axial dispersion is a function of tube diameter if the values of net flow Reynolds number, oscillatory Reynolds number and Strouhal number are kept constant. They also showed that the fluid mechanics and axial dispersion is similar in single and multi-orifice baffle designs [86]. Liu *et al.* conducted a comparative study between the stirred tank and oscillatory flow reactor. They concluded that the RTDs, for both liquid and solid, were more uniform in the OBR, which indicates the potential advantage of oscillatory mixing over traditional MSMPR's continuous processes [97].

Kacker *et al.* studied the RTD of liquid and solid in an oscillatory flow crystalliser. They concluded that for the processes with fast kinetics, precise knowledge of residence time helps have good control over the process. Hence, plug flow can ensure product quality in terms of particle uniformity if good control over nucleation and growth of crystals is achieved [111]. These studies demonstrate that oscillatory mixing has a definite and quantifiable effect on RTD.

1.6.2 Computational Fluid Dynamics

Computational fluid dynamics (CFD) uses numerical analysis and data structures to analyse and solve problems in processing environments. Several CFD simulations have been performed to understand velocity and shear conditions in oscillatory flow reactors. CFD models, particularly large eddy simulation (LES) models, study flow behaviour, e.g. the shear rate in crystallisers [112-114]. Jian et al. analysed velocity fields and concluded that the velocity ratios of axial to radial velocity components in the oscillatory baffled crystalliser largely depend on the column diameter [115].

Manninen *et al.* compared CFD for moving baffle and moving fluid oscillation environments by employing the axial dispersion coefficient and the ratio of axial and transverse velocities in a CFD simulation and demonstrated that the average shear rate in moving baffle environments is 4 to 11 % higher than that in moving fluid mixing for non-Newtonian fluids. Due to this, the average viscosity in a moving baffle is around 2 to 8 % lower than that in moving Fluid [116]. The important characteristic of moving baffles is that there are no

stagnant regions in the baffle corners and no high viscosity regions in non-Newtonian fluids. The axial dispersion coefficient in moving baffle environments is 10–17 % larger than that of moving fluid ones in non-Newtonian cases. The increase is caused by different mixing properties in moving fluid in the laminar regime. The baffle movement has a minor effect on water as the flow is turbulent, and the mixing is controlled by turbulent eddies [116].

Ni *et al.* showed a 3-D numerical simulation of oscillatory flow with flow pattern and velocity vectors in a baffled column. They validated the results with experimental observations using digital particle image velocimetry measurements [117]. Chew *et al.* demonstrated a comparison of oscillatory flow and stirred tank reactor conditions in terms of shear rate. They concluded that the volume-averaged shear rate in oscillatory vessels was one order of magnitude larger than that of stirred tank reactor and concluded that the particles spend most of their time in the high shear rate regions in oscillatory vessels, whilst in a stirred tank, particles spend considerable time in lower shear rate regions [73]. These studies show that oscillatory mixing with baffles can increase mixing intensity and improve crystallisation performance control [73, 74, 102, 115, 118-123].

1.6.3 Heat Transfer

Heat transfer is a further important factor dictating the effectiveness of platform performance. Uniform mixing and higher surface areas for heat transfer lead to better control over the crystallisation process parameters. For example, when cooling crystallisation procedures are implemented, heat transfer characteristics will dictate the rate at which supersaturation is generated. Poor heat transfer leads to temperature gradients resulting in supersaturation gradients within the bulk solution, potentially impacting processes including nucleation and growth. Conversely, if rapid heat transfer processes occur, care is needed to control bulk supersaturation levels to prevent large supersaturation spikes and associated nucleation events. Mackley *et al*. demonstrated heat transfer enhancement due to oscillatory flow by a factor of

10-30 [99-104]. Mackley *et al*. further concluded that baffles and oscillatory flow enhance mixing in the radial direction. This radial component ensures rapid fluid movement between the tube wall and the inter baffle region, improving convective heat transfer [100]. Mackley and Stonestreet demonstrated that oscillatory mixing with the low net flow could result in a 30-fold improvement in the Nusselt number due to convective heat transfer behaviour [100]. Chen *et al.* investigated the effect of baffle width and the distance between the baffle and the wall on the local heat transfer due to oscillatory flow. They concluded that the local heat transfer coefficient decreases with an increase in the baffle-wall gap for small baffle widths [101].

1.7 Particle engineering

Particle engineering (PE) involves designing and controlling particle and bulk property attributes [124]. PE in pharmaceutical applications is typically concerned with obtaining the optimal particle size, PSD, morphology and surface characteristics. These properties are often important in improving bioavailability (e.g. PSD) and homogeneity (e.g. content uniformity) for oral solid dosage drugs. However, manufacturability is also important with particle impacts on a flow, such as sticking and compaction processes [124].

In **Figure 1-18**, the schematic shows the link between API properties (mechanical, crystal size and shape, PSD, surface energy) and drug product attributes (processing, performance and shelf life), which can be manipulated by PE [124]. Historically, PSD has been considered one of the API's important physical properties. Usually, a PE approach can be implemented either by constructive approaches (size enlargement by crystallisation, spherical

agglomeration, etc.) or destructive approaches (size reduction by milling, micronisation, etc.) [124].

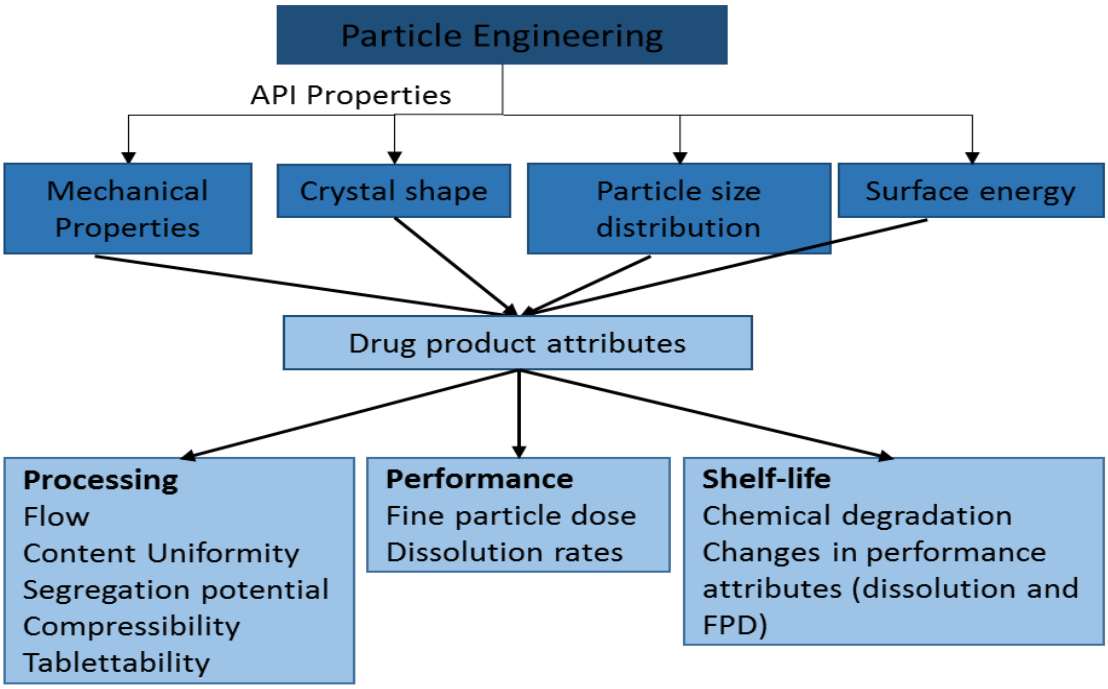

Figure 1-18 The link between particle engineering, key active pharmaceutical ingredient properties, and drug product attributes (adapted from Ticehurst 2015).

1.7.1 Spherical Crystallisation

In recent years, one emerging technology that has received considerable attention, at least in academia, is spherical crystallisation (SC) [125-129]. Spherical crystallisation is a novel PE technique in which crystallisation and agglomeration can be carried out simultaneously to transform single crystals directly into a compacted spherical form [130]. Spherical agglomeration (SA) is one of the more flexible SC methods to produce spherical agglomerates. It usually requires a simpler solvent system and can be carried out simultaneously during or post crystallisation [131]. SA has been demonstrated to improve the downstream API manufacturability of needle-like crystals (e.g. salicylic acid, Benzoic acid, Tolbutamide, Mefenamic acid, Cefotaxime, Fenofibrate, etc.) with low bulk density and poor flowability by agglomerating them into spherical particles in the range of 500 to 2000 µm[125-129, 132].

Due to improved flowability, these agglomerates are suitable for direct compression compared to non-agglomerated crystals. Quasi-emulsion solvent diffusion (QESD), neutralisation and ammonia diffusion are other [125-129] methods explained in Chapter 7. **Figure 1-19 (A)** shows a typical sequence of unit operations involved in pharmaceutical manufacturing to produce a solid dosage form. The SC technique helps in minimising downstream operations, i.e. milling, granulation and blending, by controlling the particle nucleation and agglomeration process within the crystallisation steps, as shown in **Figure 1-19(B)**. Typically, tablets are the most widely used dosage form in pharmaceuticals. The most economical solution to prepare tablets is via direct compression of particles, which results in fewer unit operations, reduced space, less processing time, lower energy consumption and lower labour costs [133].

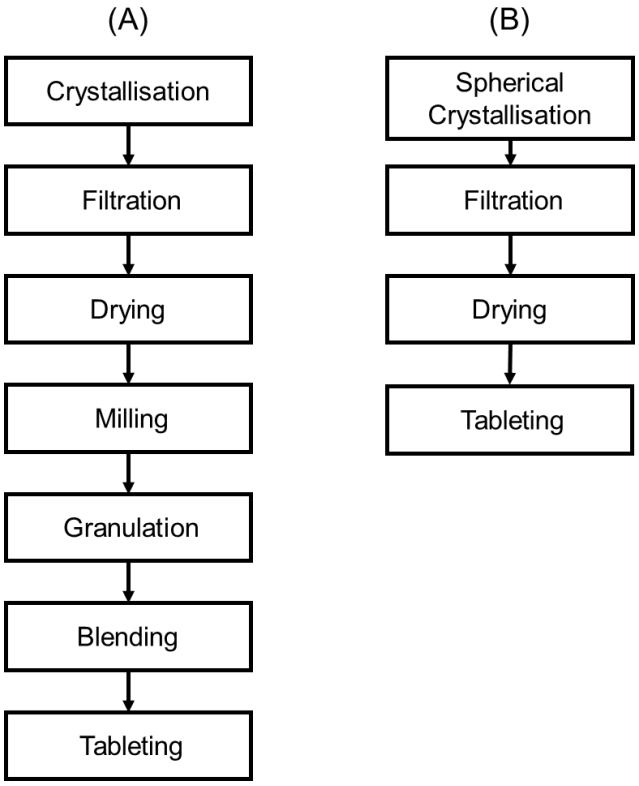

*Figure 1-19 (A) list of the typical process operations involved in pharmaceutical manufacturing. (B) Process intensification by implementing a SA process (adapted from [*133*]).*

Kawashima *et al*. reported improved bulk density, compatibility, and flowability properties of salicylic acid agglomerates to needle-like single crystals [134]. Jbilou *et al.* concluded that the compressibility of ibuprofen agglomerates improves drastically compared to single crystals due to the isotropic texture of the agglomerates [135]. Maghsoodi demonstrated agglomerated carbamazepine tablets with greater tensile strength than single crystals due to stronger bonding during compression of agglomerated crystals than in single crystal tablets [136]. Pitt *et al.* reviewed the understanding of the controlling process parameters and identified the rate processes that control agglomerate attributes. They also examined the modelling approaches taken in the literature to optimise the design of SA [129].

Orlewski *et al.* demonstrated the experimental technique for controlling the size of benzoic acid spherical agglomerates using toluene as the bridging liquid. The bridging liquid was injected into the crystal suspension via a capillary to control the bridging liquid droplets' initial size. Results showed a clear correlation between the initial droplet size and the agglomerate size [137].

Subero *et al.* performed agglomeration in a suspension of salicylic acid. They visualised the immersion mechanism in the vessel when the particle size is smaller than the bridging liquid droplet size [132]. Peña *et al,* published a number of articles on understanding the agglomeration mechanisms of benzoic acid spherical crystallisation. The relationship between bridging liquid, droplet size and primary crystal size determines whether the agglomeration process will follow an immersive or distributive mechanism which depends on the size ratio of the primary crystal and BL droplet size. When the particle's size is bigger than the BL droplet size, the nucleation takes place by a distribution mechanism, where the BL droplets are covered by the primary crystals, which leads to the formation of agglomerates with an irregular shape and a looser structure. When the particles are smaller than the BL droplet, nucleation occurs by an immersion mechanism. During this mechanism, The primary crystals impact against the surface of the BL droplet and enter the

droplet until the droplet's internal volume is saturated with primary crystals. This leads to the formation of agglomerates with a narrower particle size distribution, a more spherical shape, and a denser structure. The immersion route is favourable to achieve better control over final agglomerate size as primary crystals are trapped inside the droplet and how this affects the sizes, the powder flows, and powder compression properties of formed agglomerates. [58, 138, 139]. Peña *et al.* performed continuous spherical crystallisation of benzoic acid in a COBC [58] and a two-stage MSMPR system [59] to demonstrate that the transition from batch to continuous SA should be straightforward, feasible, and the critical operating parameters remain the same for both.

Pal *et al*. constructed the population balance framework to explain the droplets and crystals within the droplets. They highlighted the importance of controlling the droplet size within the SA process to control the agglomerates' size and improve the bioavailability of the product agglomerates [133].

1.7.2 Wet Milling

Mechanical manipulation (milling) of particles post growth with the objective of size reduction is an approach that has been used in the pharmaceutical (and other) industries for many decades. Although particle size is traditionally considered the major targeted result at the end of the milling, changes in the particle shape and surface properties are becoming increasingly recognised due to these processes, as exemplified by the growing number of publications in this field [140]. Problematic particle habits (such as needles) are typically subjected to dry milling after crystallisation to improve processabilities downstream, such as flowability and compactibility [141]. In theory, milling will break particles across the longest axis, reducing needle length whilst preserving width.

Recently High Shear wet mill (HSWM) is increasingly being employed in pharmaceutical manufacturing as a particle engineering technique. The reduction in particle size in HSWM is due to the extremely high shear and turbulence created via the rotor and stator arrangement [140]. Isothermal high

shear wet milling (HSWM) is an emerging technology that, if incorporated into the final API stage, should result in no yield loss, require no handling of dry material, and can be performed so that crystal form changes can be avoided. Wet milling of a liquid medium is becoming increasingly favourable in the pharmaceutical industry, mainly due to the potential for eliminating the need for a separate processing step [142]. This saves considerable time and cost.

1.8 Process Analytical Technology (PAT)

Process analytical technology is a now established approach for designing, analysing, and controlling manufacturing processes through real-time measurements to ensure predefined product quality, thereby avoiding out of specification material through active manipulation of the process [143]. Various PAT tools and techniques are available: (1) In-line methods are probe-based techniques in direct contact with the process fluid, e.g. monitoring temperature using thermocouples, UV or FBRM. (2) Off-line measurements are where the sample is removed, isolated and analysed close to the process stream, e.g. HPLC, XRPD analysis.

Several studies report using PAT and associated applications to monitor continuous crystallisers [63, 144-146]. Kouglous *et al.* demonstrated the use of Focused Beam Reflectance Measurement (FBRM) for real-time monitoring of the steady-state operation of a single-stage continuous MSMPR crystallisation process. More recently, Powell *et al.* have used Raman, UV-vis, PVM and FBRM to investigate methods to minimise the early onset of fouling in a continuous crystallisation of paracetamol using an integrated PAT array multivariate method [147]. Many investigators have reported problems such as encrustation on vessel walls [12], blockage of transfer lines[24, 43], particle settling [145], and difficulties in adopting PAT on small scale plug flow crystallisers. These problems present significant developmental challenges to implementing continuous crystallisation processes at an industrial scale [146, 148].

In-line tools are increasingly being implemented to monitor reactions and crystallisations in real-time. In crystallisation, FTIR [149] and UV-vis [57] probes can be used to monitor the solution concentration over time. A Raman probe can monitor changes in the solid state from of a substance by observing subtle changes in the spectrum. PAT tools can also help with steady-state monitoring in continuous crystallisation [43, 64, 110].

1.8.1 In-line measurements

1.8.1.1 UV spectroscopy

Analysis of the solution phase using attenuated total reflection ultraviolet (ATR-UV) spectroscopy is a proven technique for monitoring a crystallisation process. This technique has been used widely in crystallisation processes for solution concentration monitoring [150], polymorphic identification [151], MSZW detection [152] and residence time distribution [57, 88, 97]. UV can also implement a feedback control system to maintain a supersaturation within the MSZW [153], thereby gaining further control over the crystallisation process.

1.8.1.2 Attenuated Total Reflectance - Fourier Transform Infrared (ATR-FTIR) Spectroscopy

Inline Fourier transform infrared spectroscopy (FTIR) is a technique for measuring the infrared spectra of a solution. This occurs through infrared light from an FTIR spectrometer absorbed in specific frequencies related to the functional groups' vibrational bond energies in the solute molecules. This method can obtain data over a wide spectral range, making it suitable for different compounds, this technique can also be used in conjunction with other concentration monitoring techniques [110], providing concentration feedback to control crystal attributes [57, 149].

1.8.1.3 Focused Beam Reflective Measurement

Focused beam reflectance measurement (FBRM) provides real-time particle size measurements, The instrument consists of a focused laser beam rotating at a constant rate through a set of rotating optics at a fixed velocity (2 $m.s^{-1}$) scanning across any particle which enters the scanning zone [154]. A

schematic diagram of an FBRM probe is shown in Figure 1-20. As the light emitted by the laser hits a particle, a sensor records the light, which scatters back to the probe, the collected data is referred to as a chord length of a particle. It is defined as the distance of the path the beam follows as it moves from one edge of a particle to another, producing the chord length distribution (CLD).

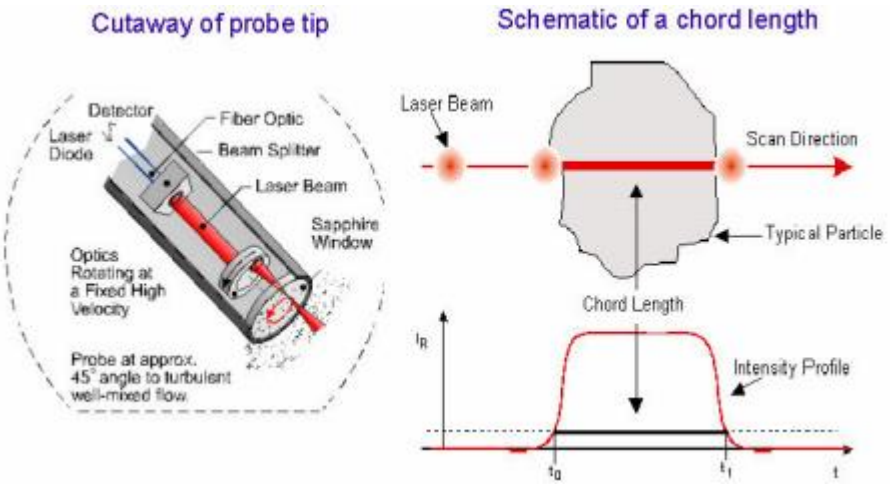

Figure 1-20 FBRM measurements: FBRM probe tip (left) and chord length measurement (right). Adapted from Dr Jorg, 2005 [155].

This length and count-based technique is also sensitive to small particles, making it suitable for detecting dissolution and nucleation phenomena in crystallisation. FBRM has also been widely used in characterising continuous crystallisers for solid residence time distribution studies [97, 111] and to monitor steady-state operation [110].

1.8.1.4 Particle vision measurement

Particle vision measurement (PVM) is based on a high-resolution inline video microscope that visualises particles moving in a slurry suspension [156]. PVM captures images of the in-process phenomena in real-time, capturing quantitative information such as size and crystal behaviour and qualitative information like change in morphological form during nucleation [157]. The PVM sensor captures images of particles using size-independent laser beams to which images are recorded via light scattering backwards and transferred to a camera [158]. Ahmed *et al.* incorporated a PVM probe for the in-depth

understanding of seed PCM crystallisation using a high shear wet milling process [140].

1.8.2 Off-line measurements

1.8.2.1 Particle size analysis

A Malvern Morphology G3 (Malvern Instruments Ltd, Malvern, UK) is a static automated microscopy-based imaging technique for offline particle size and shape analysis.

Another common technique used for PSD measurement is laser diffraction. The MasterSizer (Malvern Instruments Ltd, Malvern, UK) can determine the particle size offline using laser diffraction. The PSD is measured by the angular variation in the intensity of light scattered as a laser beam passes through a dispersed particulate sample [159]. The angular scattering intensity data is then analysed to calculate the size of the particles responsible for creating the scattering pattern through the Mie theory of light scattering [159].

1.8.2.2 Scanning Electron Microscopy

Scanning Electron Microscopy (SEM) is an electron microscope-based technique. The region of interest is scanned with a focused beam of electrons at high magnifications to identify crystal properties, e.g. surface characteristics. SEM offers a powerful imaging capability to investigate from the micron-scale to a few nanometers [160]. SEM scans highly focused electron beams over a surface to create images. The beams interact with the sample producing various signals that can be used to obtain information about the surface topography and composition of the particulate material. **Figure 1-21** displays an example of different polymorphs of N-acyl hydrazone exhibiting plate-like and needle-like morphologies, which can be easily captured by SEM [161].

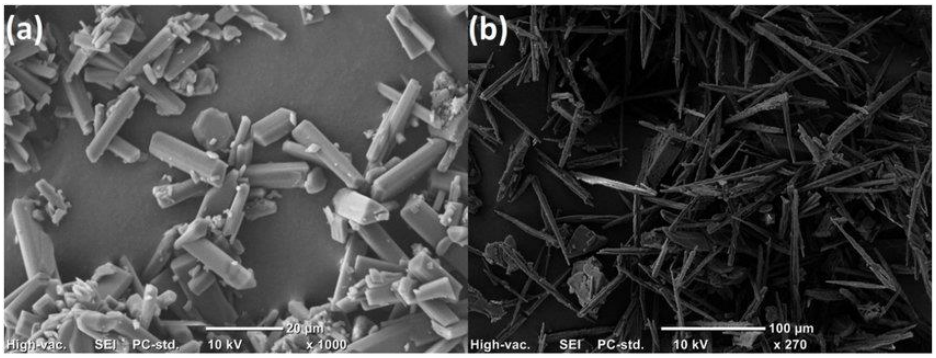

Figure 1-21 SEM images of N-acyl hydrazone crystals exhibiting (a) plate shapes with relatively smooth surfaces and (b) crystals exhibiting needle-like shapes (adapted from Isadora et al.,2018).

1.8.2.3 X-ray

X-ray powder diffraction is a qualitative and quantitative analytical technique used to characterise bulk materials. It provides information on the structural characteristics of single-phase microcrystalline materials, mixtures, and other multi-component systems. When the materials under study are already identified, their individual "fingerprint" patterns can identify the different forms and identify if further components are present in the studied mixture. **Figure 1-22** shows lactose's different forms (alpha lactose monohydrate and beta-lactose) via fingerprint patterns to identify the manufacturing process which produces the desired polymorphic form [110].

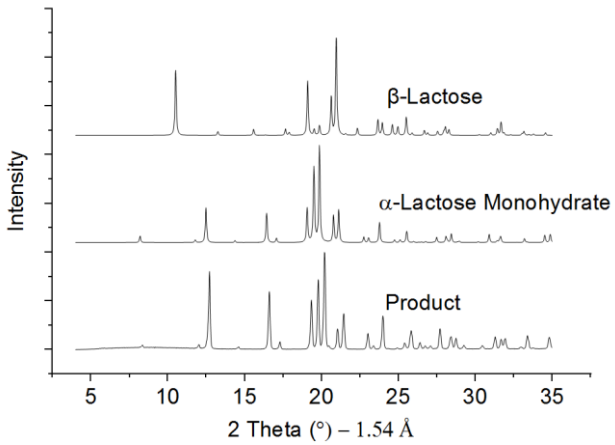

Figure 1-22 An example of the x-ray fingerprint pattern of the different polymorphs of lactose.

In a powder diffraction pattern, reflections are recorded in counts per second as a function of the 2θ angle. Reflections are observed via Bragg's law: nλ= 2d sin θ. Where d is the space between crystallographic planes that have been satisfied for the constructive interference of reflected X-rays.

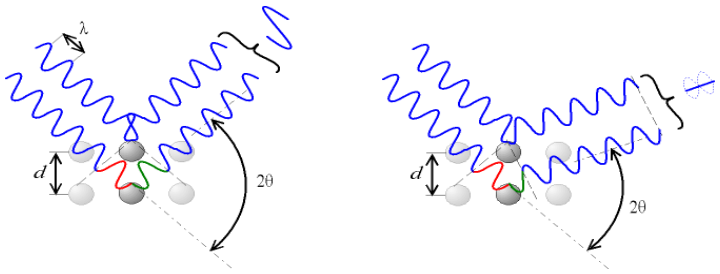

Figure 1-23 The spacing between the reflection planes (d) leads to differences in the diffracted path length of the outgoing radiation, resulting in positions where a detector can measure constructive interference by moving through 2θ. The positions and intensity of these reflections are characteristic of the materials being studied.

1.8.2.4 Powder Rheometry

The flowability of a powder is an important consideration in any pharmaceutical operation involving particle movement as it can significantly affect the material's processability and, ultimately, the final product's content uniformity. However, common methods attempt to measure and quantify powder flow as a single property, such as the angle of repose, flow through an orifice or as a function of the bulk and tapped density (Hausner ratio and Carr's index). The challenge in doing so is that powders are highly functional materials, and flowability cannot be quantified as a discrete property. The powder conditions must be considered, as a fully aerated powder will be far more flowing than loosely packed or consolidated. Some powders are extremely sensitive to external variables, while others are less.

How a powder behaves and responds to external variables may function as the powder's primary particle attributes. These can include particle size, size distribution, shape, surface texture, surface area and mechanical properties (i.e. elasticity, plasticity and brittleness). Considering these attributes and mechanisms of particle interaction, it can then be understood how they can

contribute to powder behaviour by restricting particle movement through friction, mechanical interlocking, inter-particulate forces of cohesion, and liquid bridging. It is, therefore, necessary to determine and understand the effect of the operating conditions. For example, environmental moisture can profoundly affect powder flow; free water at particle surfaces can aid flow by dissipating electrostatic charge and reducing cohesion; however, too much free water can impede powder flow due to the formation of inter-particle liquid bridges. Additionally, the process environment must be considered. The bulk powder is loosely packed at high flow, and cohesive forces dictate particle independence. However, when the powder is more consolidated at low flow conditions, such as in a feeder or hopper, the frictional forces and mechanical interlocking forces dominate as the particles are forced together and the contact points and pressure increase [162].

1.9 Control System Engineering

Process control has always been an important issue in crystallisation and is increasingly important in the context of continuous processes. The potential advantage of continuous crystallisation is that all process parameters (e.g. temperature, residence time, concentration, etc.) are constant once operating in a steady-state condition, making the control of continuous crystallisation easier in principle to control rather than the complex process dynamics involved during a batch crystallisation. Control objectives that need to be considered include maintaining a steady-state, operating under a state of control, start-up conditions, shut-down, changeover, process interruptions and managing fouling [163]. Myerson *et al*. suggested that a well-controlled process takes about five mean residence times from start-up to reach a quasi-steady state and about two times the mean residence time for shut down [163]. The efficient control system can help ensure the segregation of off-spec products during different stages of continuous operation.

Two main control approaches generally applied in continuous crystallisation are model-based and model-free [164]. A schematic summary of the different

control strategies implemented in crystallisation processes is summarised in **Figure 1-24**.

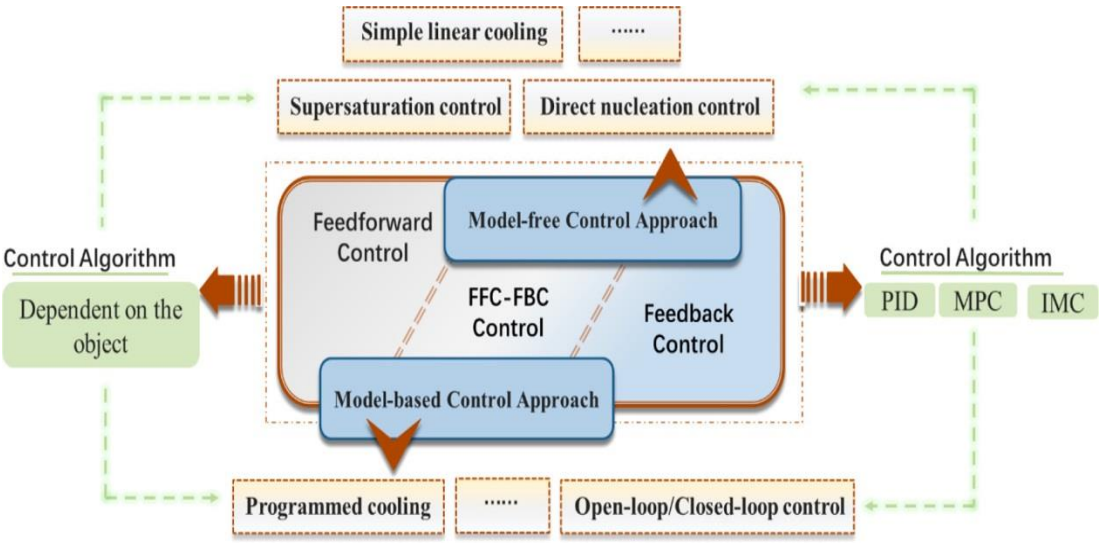

Figure 1-24 Schematic diagram of control-related approaches (adapted from Ma et al. 2020 [23]).

The model-based approach has three main components. (1) The *process model* is used to describe the crystallisation process and predict the product quality; this model usually consists of a series of equations (the population balance equation (PBE), mass balance equation, heat balance equation, solubility expression, and crystallisation kinetic expression). (2) The *observer* is used to estimate whether the system's real state is consistent with the set point. (3) The *optimiser* optimises the operating variables so the system can reach the set point at the lowest cost.

PBE-based models are widely used for modelling crystallisation processes to establish clear and quantitative relationships between variables and characterise key components of a crystallisation process, such as nucleation and growth rates [165]. They are particularly useful for batch and continuous crystallisers for modelling and characterising the PSD evolution in the crystalliser, one of the most important critical quality attributes (CQAs) of the drug substance [133, 165]. **Table 1-2** summarises the various numerical

methods implemented to solve the generic PBEs in the crystallisation process and their associated advantages and disadvantages.

The model-free approach relies on the direct use of in-line PAT (as described in **section 1.8**) with the combination of proportional-integral-derivative (PID) control, model predictive control (MPC), or an internal model control (IMC) control approach [23]. Due to the advancement of in-line PAT, measurement of solution concentration [166, 167], detection of the polymorphic form [168], particle count [166] and temperature control [149] have made it more straightforward to implement advanced control strategies through model-free approaches.

In both the model-based and model-free approaches, two types of control strategies are implemented: feedforward is the manipulation of variables in response to pre-empt disturbances from upstream (pro-active), whereas feedback is a manipulation of variables after measuring a disturbance downstream (reactive). The kinetic parameters required to build these models can be estimated using a sequential parameter estimation approach. Various crystallisation phenomena (i.e. growth, nucleation, agglomeration and breakage) can be estimated individually via isothermal desupersaturation experiments. The data from this experimentation can be used to build dynamic models using a commercial platform like gPROMS FormulatedProducts (developed by Siemens Process System Engineering) with built-in PBEs. Perez-Calvo *et al.* have demonstrated a sequential parameter estimation approach for the determination of primary and secondary nucleation kinetics, growth and agglomeration in batch cooling crystallisation on an industrial API compound by implementing a numerical method in gPROMS to solve the PBE with a high-resolution finite volume scheme with a flux limiting function (HRFVS-FL) solution approach [169].

Table 1-2 Comparison of different numerical methods to solve the PBEs ([170])

Advantages	Disadvantages	Remarks	Reference
Standard method of moments (SMOM)			
• Simple and computationally efficient • Moment transformation is possible for size-independent growth and nucleation	• Closure problem in the case of size-dependent growth, aggregation and breakage. • Cannot retrieve the complete PSD	• It can be used in a simple crystallisation model when growth and nucleation are considered but cannot be used for PSD retrieval.	[39, 171]
Numerical non-linear model reduction approaches: method of characteristics (MOCH) and quadrature method of moments (QMOM)			
• Computationally efficient. Moment transformation is possible for size-dependent growth, aggregation and breakage.	• It gives the coarse approximation of PSD but cannot retrieve the full PSD. • Considers growth and nucleation only	• It cannot be used to develop a model-based control strategy for shaping the PSD as it cannot retrieve the complete distribution.	[133, 172-176]
Direct numerical solution approaches finite-element method (FEM), finite-volume method (FVM), discretised population balances (DPB)			
Provides a universal framework for the solution of generic PBEs.	Computationally inefficient since the solution of integrals is required.	Not an attractive option for model-based optimisation and control.	[169, 177]
Dynamic Monte Carlo simulation (DMC)			
Provides information about the history of each particle in the population.	Computationally inefficient.	The technique is time-consuming and is not an attractive option for online control.	[176, 177]

1.10 Workflow approach for the design of a crystallisation process

More than 70% of active pharmaceutical ingredients (APIs) in the development pipeline exhibit poor manufacturability (e.g. isolation, flowability, tabletability), posing major challenges in producing a consistent product with desired performance. Crystallisation is a key operation in isolating most pharmaceuticals and has been demonstrated as a critical process for improving the drug's manufacturability. While basic design principles for crystallisation are known, such as the fundamental mechanisms of crystal nucleation and growth, applying these in pharmaceutical development with the associated constraints on time and materials is challenging. As a result, decisions made on aspects of the process may embroil development stages both on the drug substance (DS) and the drug product (DP) side.

Brown *et al.* have established a systematic workflow methodology that enables rapid crystallisation process development based on process understanding. At the epicentre of this methodology is the deployment of *in-silico* assisted solvent selection (for the selection of solvents optimising yield and productivity) using miniaturisation platforms (Crystal16/Crystalline) [150]. The aim, methodology, key decisions and output at each stage are defined. A case study is presented demonstrating the successful application of the workflow for the rapid design of processes to produce kilo quantities of product with distinct, specified attributes suited to the pharmaceutical development environment. This work concludes with a vision for future workflow applications in continuous manufacturing development to achieve a rapid performance-based design of pharmaceuticals. A detailed approach to this workflow is summarised in **Figure 1-25**. The main objective in establishing this workflow approach is to use the minimum amount of material and time to design and scale up an industrially relevant crystallisation process. This workflow considers the properties of crystals required in downstream processing. It is used as an objective for designing a process, connecting upstream and downstream

processes and dealing with the drug product's operational and performance challenges.

Figure 1-25 Workflow for seeded continuous crystallisation. Adapted from Brown et al. [150].

Chapter 2. Aims & Objectives

This research focused on implementing PI's key domains (space, time and function) to achieve desired critical material attributes (CMA's) and throughput. The first part of the thesis deals with developing a novel platform to address operational challenges related to existing continuous platforms. The second part of the thesis deals with establishing a robust mechanistic model to dial a particle size of a well-known excipient to overcome challenges related to size and throughput. In the third part of the thesis, a novel approach is developed to engineer particles to reduce several process steps in the downstream processing.

Chapter 4: Design and Characterisation of a Cascade Moving Baffled Oscillatory Crystalliser (CMBOC)

Aim: Designing, building & characterising a lab-scale continuous crystallisation platform.

The overall aim of this research is to implement PI's space and time domain to build, design, characterise, and assess a novel continuous crystallisation platform and investigate its performance on crystal systems using oscillatory mixing. The developed platform needs to have ease of use and the potential benefits over traditional technologies for effective control of particle attributes. The platform should have the potential to be applied in research and development and in manufacturing applications, where well-controlled process conditions are required.

Objectives:

Design and construct a continuous crystallisation R & D platform that uses less material than the conventional platforms and delivers precise control over critical quality attributes (e.g. purity, form, shape, size and yield) and ease of operation, extended operation at steady-state, and afford opportunities for real-time monitoring and control.

Identification of the operating domain in terms of oscillatory conditions within a CMBOC and successive characterisation of the resulting flow performance under this operating space is also a key deliverable of the research presented

in this thesis, which includes developing and validating a method for measuring and characterising the residence time distribution (RTD) behaviour for both liquid and slurry and heat transfer, which are the key parameters that affect the crystallisation process.

1. Assessment of the platform's suitability for continuous crystallisation operation with model compound (i.e. Lactose, paracetamol). The purpose of working with the model compound was to gain experience in using the platform, setting up a system, reproducing existing results obtained previously to gain confidence in the system and laboratory practices and access the on and off-line analytical techniques to provide meaningful results.
2. Another objective of the platform is to integrate automation to provide an interface for automated experimental operations to utilise feedback responses from in-line apparatus, including thermocouples, FBRM and IR probes, to achieve the desired particle attributes such as polymorph control, PSD, yield and purity.

Chapter 5: Control system engineering- Lactose Population Balance Equation modelling

Aim: Develop an integrated continuous crystallisation process in a CMBOC by applying a crystallisation population equation using a sequential parameter estimation approach.

The main aim of this section is to utilise the effect of the unique hydrodynamic behaviour of CMBOC and the key operating region (residence time, mixing and heat transfer) identified in chapter 4 will be implemented to perform crystallisation process to achieve targeted crystal attributes (yield size and narrow PSD) by evaluating nucleation and growth phenomena through developing a mechanistic model of a common pharmaceutical compound to integrate machine learning into real-world scenarios.

Objectives:

1. The main objective of this work is to exploit the advantage of CMBOC to access its effect on different crystallisation phenomena by developing a PBE model of a compound for the crystallisation process, which can be used to control the key rate processes to achieve desired outcomes and, therefore, can be used to predict product attributes against changes to the process conditions.
2. Develop a process understanding by identifying primary nucleation, secondary nucleation and growth parameters by following the sequential parameter approach in a batch oscillatory crystalliser and then applying it to convert the batch process to the continuous process to dial a particle size for primary and secondary nucleation scenarios.
3. Validate the model by applying the condition to the continuous manufacturing of lactose in multi-stage CMBOC.

Chapter 6: Particle engineering- Size controlled spherical agglomeration of benzoic acid

Aim: Apply particle engineering technique to a develop a methodology to produce size-tuneable spherical agglomerates by implementing PI's function domain (Size enlargement, HSWM) and time domain (continuous operation).

As this research progressed, it was identified that there is a gap in the method to produce smaller size spherical agglomerates (<500 μm) with tuneable properties (dissolution rate, compressibility, flow property, porosity) suitable for direct compression. Current pharmaceutical API manufacturing requires multiple unit operations to produce tablets, which is time-consuming and less cost-effective than would be achieved by direct compression.

Spherical agglomeration provides a way to improve the filtration, drying and flowability of crystals into easily handled spherical particles that enable the removal of some of the unit operations (typically: milling, wet granulation and drying) for direct compression route. Recent studies have suggested the possibility of controlling the size of the produced agglomerates by controlling

the size of the formed droplets; however, none of the reported studies has addressed small agglomerate formation. The range produced in the best cases was between 500-2500 μm, which is unsuitable for direct compression with excipients [138, 178].

Objectives:

1. The main objective of this work was to develop a systematic approach to producing size-tuneable spherical agglomerates suitable for direct compression.
2. Another important objective of this work was to develop a method to produce a smaller size bridging liquid droplet, which in turn aid in producing smaller size agglomerates which are of similar size of excipient and filler to enable uniform blending for direct compression.
3. Understand the effect of key process variables (mixing, bridging liquid amount, bridging liquid droplet size, residence time, temperature etc.) on final spherical agglomerates attributes.
4. Understand the key rate processes involved in the spherical agglomeration process and apply learning to convert batch process to continuous spherical agglomeration process.

Chapter 3. Materials & Methods

3.1 Materials

The list of materials used during this research is summarised in **Table 3-1**. Deionised water was available in the laboratory from a Millipore water purification unit.

Table 3-1 List of materials used during this research

Material	CAS number	Source
α-Lactose monohydrate, ≥99%	5989-81-1	VWR
Paracetamol, ≥99%	103-90-2	*Sigma Aldrich*
Sodium benzoate, ≥99%	532-32-1	*Sigma Aldrich*
Benzoic acid, ≥99.5%	65-85-0	*Sigma Aldrich*
Poly vinyl chloride (PVC)	9002-86-2	VWR
Ethanol, ≥99.5%	64-17-5	VWR
Chloroform ≥99.4%	67-66-3	VWR
Isopropanol, ≥99.7 %	67-63-0	VWR

Lactose is a disaccharide of glucose and galactose with two isomeric forms, α and β, that interconvert by mutarotation and exist at equilibrium in solution. [179]. Lactose is a white crystalline solid and has the molecular formula $C_{12}H_{22}O_{11}$. It has a molar mass of 342.297 g.mol^{-1}, a density of 1.525 g.cm^{-3}, and a Melting point of 202°C. Lactose is widely used as an excipient in pharmaceutical products, particularly tablets and inhaled formulations [180].

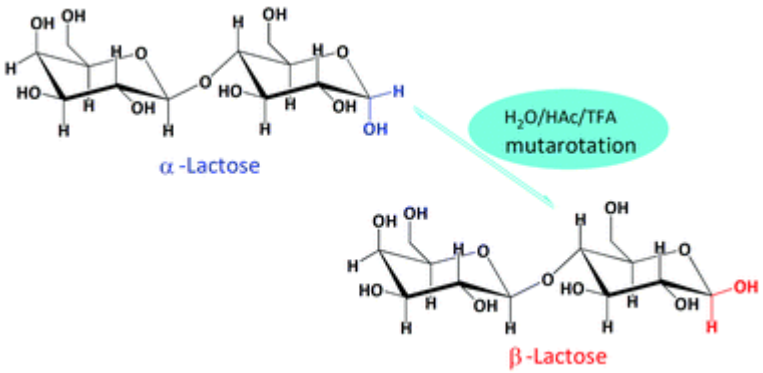

Figure 3-1 lactose mutarotation in aqueous solution [179]

Mutarotation plays an important role in the solubility of lactose. The amount and rate at which lactose will dissolve depend on the form of the input material. β-lactose is more soluble and dissolves faster than ALM. The ALM dissolution process occurs in two stages; if an excess amount of ALM is put into solution, the initial solubility will be reached quickly. As mutarotation occurs and conversion of ALM to β-Lactose proceeds, more ALM will dissolve until the equilibrium ratio is achieved [181]. The mutarotation kinetics governs the dissolution process. Dissolved ALM concentration governs the growth rate of ALM, and the presence of β-lactose suppresses the solubility of ALM. For these reasons, it is important to add mutarotation kinetics in the solubility model to predict the growth kinetics of ALM. The equilibrium ratio of β-lactose to α-lactose was shown to decrease with increasing temperature from 1.64 at 60 °C to 1.36 at 100 °C [181].

Paracetamol (PCM), also called acetaminophen, is widely used as an analgesic and antipyretic and has been studied extensively from a process point of view [182-184]. PCM is a colourless crystalline solid and has the molecular formula $C_8H_9NO_2$. It has a molar mass of 151.165 $g.mol^{-1}$, a density of 1.263 $g.cm^{-3}$, and a Melting point of 249.2°C. Extensive work has been carried out on the monitoring and production in batch[182], with a few studies conducted on the continuous crystallisation of PCM in both MSMPR and PFR platforms [184-187].

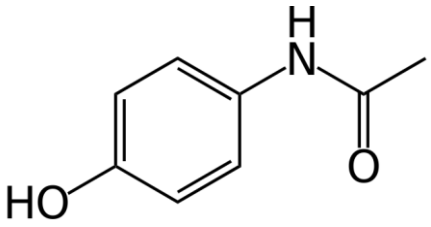

Figure 3-2 PCM chemical structure.

Benzoic Acid (BA), also called benzene carboxylic acid and phenyl carboxylic acid is a colourless crystalline solid with the molecular formula C_6H_5COOH. It has a molar mass of 122.123 $g.mol^{-1}$, a density of 1.27$g.cm^{-3}$, and a melting point of 122.4°C. BA in pure water's solubility is a 0.0034 $g.g^{-1}$ solution and in ethanol is a 0.584 $g.g^{-1}$ solution at 25°C [188].

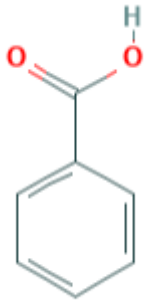

Figure 3-3 Benzoic acid chemical structure.

BA and its salts are used mainly as food preservatives against yeast and mould. BA is also used as a bacteriostatic and bactericidal agent and acts as an antiseptic stimulant. It is also used in cosmetics, resin preparation and plasticisers [188]. BA has been chosen for SAstudy as a test substance because it gives needle-like crystals which are difficult to handle and have poor tabletting properties.

3.2 Methods

3.2.1 Focused Beam Reflectance Measurement

Focused beam reflectance measurement (FBRM) (Mettler Toledo's G400 probe) with iC FBRM software version 4.4 was used for online particle size distribution measurement and monitoring steady-state operation attached to a computer. The signals produced by the FBRM probe can be processed in two different modes: 'Primary' mode and 'Macro' mode. When the 'Primary' mode is used, the particles measured are counted individually, and the 'Macro' mode considers individual particles that constitute an aggregate as a whole. Furthermore, the primary mode is more sensitive to smaller particles (<100 microns), while the Macro mode is more sensitive toward larger particles (>100 microns). Apart from monitoring steady-state operation in Chapters 4, 5 and 6, FBRM has been used in Chapter 4 for solid residence time distribution measurements and in Chapter 6 for in-situ bridging liquid droplet size measurements along with PVM.

3.2.2 Infra-Red Spectroscopy

In-situ FTIR measurements were collected to monitor solution concentration during crystallisation using a Mettle Toledo ReactIR 15 ATR-FTIR probe, connected via a flexible AgX fibre conduit to a ReactIR spectrometer. Mid-IR spectra (650 - 4000 cm^{-1}) were acquired over 16 scans with 8 cm^{-1} resolution. Spectral analysis was performed using iC IR software. Background measurements (air) and a reference solvent spectrum were acquired before sample collections to enable real-time solute concentration and supersaturation monitoring. The calibration method and the multivariate calibration model were performed using GRAMS V9 / AITM (Thermo Fisher Scientific, Renfrew, UK) pre-processing software. ReactIR 15 was used for ALM and PCM case studies to measure steady-state operation in Chapter 4.

3.2.3 Ultraviolet-visible optical transmission spectroscopy

Ultraviolet-visible (UV-vis) optical transmission spectroscopy was performed inline using a UV transflectance probe (5 mm path length) connected to a Carl Zeiss MCS 501 UV spectrometer equipped with a CLD500 deuterium lamp (220 – 620 nm). Using Aspect Plus software, data were acquired at 5-second intervals (190 – 320 nm). UV spectra of sodium benzoate in water were used for RTD studies in Chapter 4.

3.2.4 Particle Vision Measurement

A Mettler Toledo PVM V819 probe (Leicester, UK) was used in Chapters 4 to 6, capturing greyscale images with an image resolution of 1360 x 1024 pixels and pixel size of 0.8 μm equipped with online image acquisition software. A PVM probe was mainly used in Chapter 7 for liquid droplet measurements and understanding the SA process.

3.2.5 Particle size analysis

3.2.5.1 Malvern MasterSizer- laser diffraction technique

Laser diffraction measurements were carried out using a Malvern MasterSizer 3000 system (Malvern Instruments). Powder samples were dispersed in a solution using a HydroMV dispersion unit. A solid sample was added until a laser obscuration of ~8 % was reached. Three measurements were made for

each sample, and the average results were calculated. Laser diffraction measurements were generated with various particle size data. The volume distribution (given in 100 logarithmically spaced size bins from 0.01-10,000 µm) and the d[50] means the particle diameter corresponding to 50 % of the volume distributions were used. Other diameters were used, including the d[10] and d[90], corresponding to 10 % and 90 % of the volume distribution. The span of the PSD was calculated using Equation 3-1.

$$\boldsymbol{Span} = \frac{\boldsymbol{D_{90} - D_{10}}}{\boldsymbol{D_{50}}} \qquad \textbf{Equation 3-1}$$

The MasterSizer instrument was used in in the case study for PCM and ALM for the PSD measurement is in Chapter 4.

3.2.5.2 Malvern Morphology G3- Image analysis technique

Particle size distributions and particle images were collected on a Morphology G3 (Malvern Instruments) using the parameters outlined in **Table 3-2**. For individual scanning of particles, the instrument uses compressed air to aid in dispersing particles onto a glass plate with automated microscopy. Samples were prepared using a high-energy dry dispersion unit requiring 5 - 11 mm^3 of material with a 10x magnification in a size range of 0.5 – 1000 µm. An 11 mm^3 spatula was used to sample a consistent volume of material. The particle size results were reported as Circle Equivalent (CE) diameter with CE10, CE50 and CE90. The test was performed at various dispersion pressures as a means to compare the robustness of the agglomerates. The instrument was used in Chapter 7 for PSD measurements of spherical agglomerates of BA.

Table 3-2: Particle Imaging Method Parameters

Dispersion Pressure	Various
Dispersion Time	20 seconds
Settling Time	60 seconds
Objective Lens	2.5X
Sample Area	5600mm^2
Number of Size Bands	200
Size range	13 µm – 1000µm
Smoothing Factor	11 point Applied
Software	Morphology

3.2.6 X-Ray Powder Diffraction

XRPD data were collected on a Bruker D2 Phaser diffractometer (GX000815) with the following experimental setup: a small quantity (10-50 mg) of the sample was analysed using reflection Bragg-Brentano XRPD, collected on a Bruker D2 Phaser 2nd Gen bench-top diffractometer equipped with θ/θ geometry, with Ni filtered $K_{\alpha 1,2}$ Cu radiation, λ = 1.540596 Å, a line focused. Samples were lightly ground to minimise preferred orientation effects and mounted on a 6-position autosampler. Samples were rotated at 15 rpm throughout data collection to maximise particle sampling and minimise preferred orientation effects. The Bruker D2 Phaser diffractometer instrument was used in the PCM and ALM case study in Chapter 4 and for Benzoic acid polymorph screening in Chapter 7. The parameters are summarised in **Table 3-3**.

Table 3-3: D2 Phaser Operating Parameters

Emission:	
Geometry	Bragg-Brentano reflection θ/θ
Source radiation	Cu $K\alpha_{1,2}$ 1.540596 Å (line focus)
Operating Voltage	30 kV
Operating Current	10 mA
Monochromator	None
Optics	0.2 mm Anti-divergence slit
Sample:	
Treatment	Lightly Ground / as supplied
Stage	6 sample auto changer carousel
Rotation	15 rotations per minute
Sample Holder	Silicon single crystal sample ring
Temperature	Ambient
Detection:	
Optics	2.5° Axial Soller Slits, Ni low-beta filter - 1.56% absorption, Secondary slit size 9.5mm, 4.16° detector opening
Detector	LynxEye 1D Detector

3.2.7 Optical Microscopy

Optical microscopy was used to gain an approximate size and shape of agglomerate in each product and assess if spherical agglomeration had been completed or if any single crystals remained. Images were obtained using a

Leica DM6000 M fixed stage microscope with a bright field and darkfield illumination. Microscopy was used for particle visualisation in Chapters 4, 5, and 6.

3.2.8 Scanning Electron Microscopy

SEM analysis was performed on dried crystals to visualise the agglomerate habit directly. Samples were added to aluminium stubs with sticky carbon tabs and sputter-coated with a 20 nm gold layer to minimise charging in the SEM. Samples were then placed under a vacuum for 2 minutes before transferring to the SEM for analysis. A Hitachi TM4000Plus SEM was operated at beam voltage 10000eV, probe current setting 2, standard vacuum level and with data collected in backscattered electron mode at magnifications of 50x, 250x, 500x and 1000x. SEM images were acquired for experimental Chapters 4, 5, and 6.

3.2.9 Powder Rheometry

Powder rheology was performed by FT4 Freeman Technology, and Data Analysis v4 in FT4 software standard methodology of Stability and Variable Flow Rate and Compressibility and data analysis. As the precision blade moves through the powder sample (25 ml volume), both vertical and rotational resistances are measured in the form of force and torque, respectively. The FT4 produces graphs for torque and force plotted against the distance travelled. Work can then be calculated as the combined resistance of torque and force multiplied by the distance travelled. It is possible to derive the energy gradient, the blade's energy to travel 1 mm through the powder bed. FT4 Powder Rheometer characterised the powder flow properties of the resulting agglomerates. The FT4 uses a blade that rotates while moving down and up through a particle bed at a defined helix angle and speed. The instrument then measures the torque, force, and height as it traverses through the particle bed. Given the blade’s ability to condition the particle bed through gentle clockwise slicing flow patterns, every test starts in a homogeneous, low-stress packing state. This conditioning process makes the FT4 ideal for comparative studies since all samples have similar starting conditions. Actual flow studies occurred under a counter-clockwise aggressive flow pattern. For compressibility, a

vented piston was used to apply force on the particle bed. The flow properties studied include compression percentage (CPS), stability index (SI), flow rate index (FRI), surface energy (SE), basic flowability energy (BFE), and bulk density. The porosity, ε, of the final agglomerates was calculated by:

$$\varepsilon = 1 - \left(\rho_{agg}/\rho\right) \qquad \textbf{Equation 3-2}$$

Where ρ_{agg} is the density of the spherical agglomerates (g.cm^{-3}) and ρ, the true density of the benzoic acid (g.cm^{-3}), powder rheology measurements were performed on benzoic acid spherical agglomerates in experimental Chapter 7.

Chapter 4. Design and Characterisation of a Cascade Moving Baffled Oscillatory Crystalliser (CMBOC)

4.1 Introduction

The potential opportunities for continuous crystallisation to play a bigger role in the purification and particle engineering of pharmaceuticals and other molecular solids and the range of available continuous process technologies have been reviewed in the Introduction (see Section 1.5.3). Oscillatory flow mixing has been widely developed and investigated as a process intensification technology to achieve efficient and controlled mixing in tubular reactors [189]. The first conception of the oscillatory flow reactor was proposed by Mackley in 1989 [74]. There are essentially two modes of operation for oscillatory mixing: moving baffle (MB), where baffles are oscillated within the vessel [75-78] and moving fluid, where baffles are fixed, and the fluid has oscillated [77, 79]. Examples are displayed in **Figure 4-1**. An oscillating piston or bellows may be used for moving fluid setups to oscillate the fluid [190]. The production of eddies generates the mixing in this crystalliser. As the piston or the baffles move through the solution, eddies are created on either side, depending on whether the baffles/fluid moves up or down. The constant production of eddies allows efficient and uniform mixing throughout the system. When considering a continuous operation, the system should be operated such that the maximum oscillatory velocity is at least double the velocity of the fluid flowing through the tube [74]. This means the flow is always fully reversing with the fluid interaction at the baffles. The mixing generated in the zones between successive baffles is then uniform, and the tube itself can behave as a series of well-mixed tanks-in-series [74]. Importantly, mixing is independent of the throughput velocity. It is possible to have a low net flow velocity but maintain good mixing and near plug-flow performance by controlling the oscillatory conditions in a small footprint device.

Oscillatory flow allows uniform mixing conditions to be achieved in the vessel, giving uniform temperature and concentration profiles which have been shown to lead to higher quality crystals and significantly more reproducible results when compared to a stirred tank operating at a similar power density [80]. Whereas scaling up a process in a stirred tank remains non-trivial, partly due to the mixing gradients often found in large-scale stirred tanks, the geometric rules for scale-up of OFRs have been clearly defined [22].

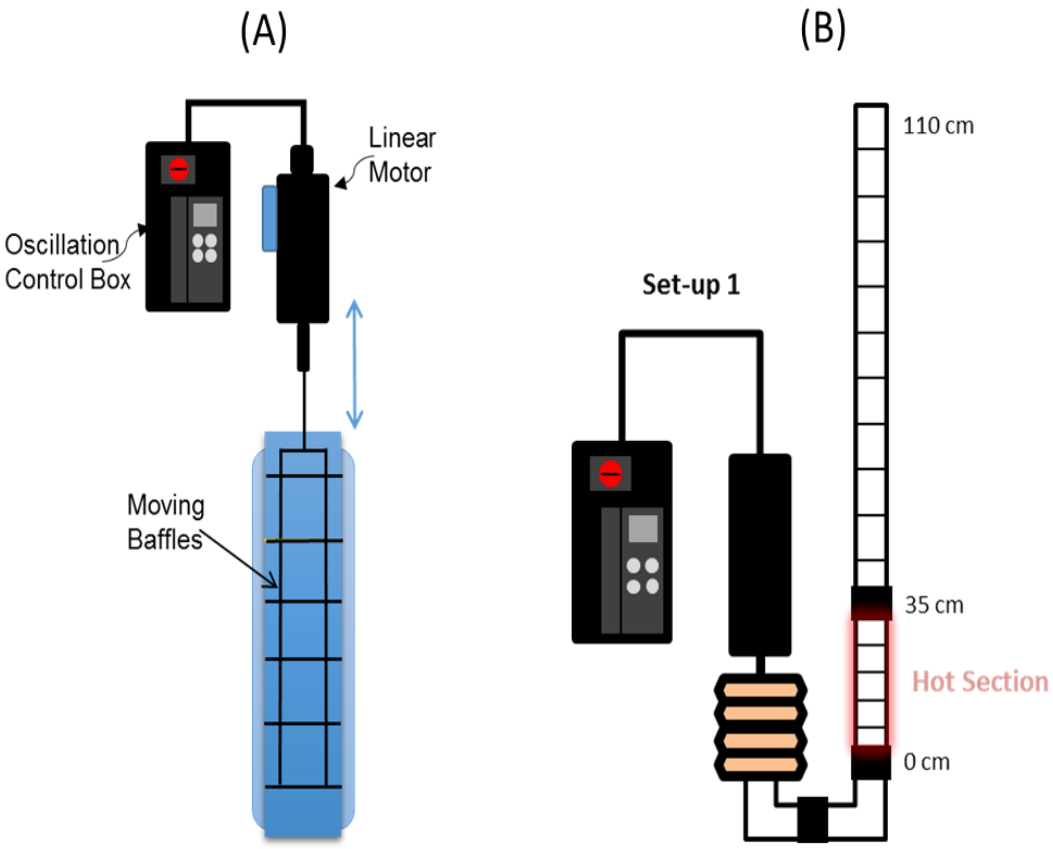

Figure 4-1(A) Moving Baffle (B) Moving Fluid Oscillating crystallisers (adapted from Briggs et al., 2015).

4.1.1 Oscillatory mixing mechanism

The mechanism of oscillatory mixing in the vessel can be understood with the help of **Figure 4-2,** considering sharp-edged baffles placed transverse to an oscillating and fully reversing flow. The oscillation motion is periodic and fully reversing and separates the flow into two half-cycles where each flow accelerates and decelerates according to a sinusoidal velocity-time function [117]. At the start of the downward stroke (**Figure 4-2(A)**), vortex rings form downstream of the baffles; at the end of the stroke, the maximum oscillatory flow velocity is reached, and at that moment, the flow decelerates subsequently, the vortices are swept into the bulk (**Figure 4-2(B)**). On the upward stroke (**Figure 4-2(C)**), the stages are reversed, with vortices and deceleration occurring on the opposite side of the baffle (**Figure 4-2(D)**). This repeating vortex development cycle creates uniform mixing in each inter-baffled zone and across the entire oscillating vessel's different regions or baffled zones [117].

This unique mixing effect is usually achieved by either pulsing fluid or oscillating the baffles in a tube. Changing the combination of frequency and amplitude allows control over eddy generation, which provides access to a range of operating conditions to effect optimal process control [83, 191-195].

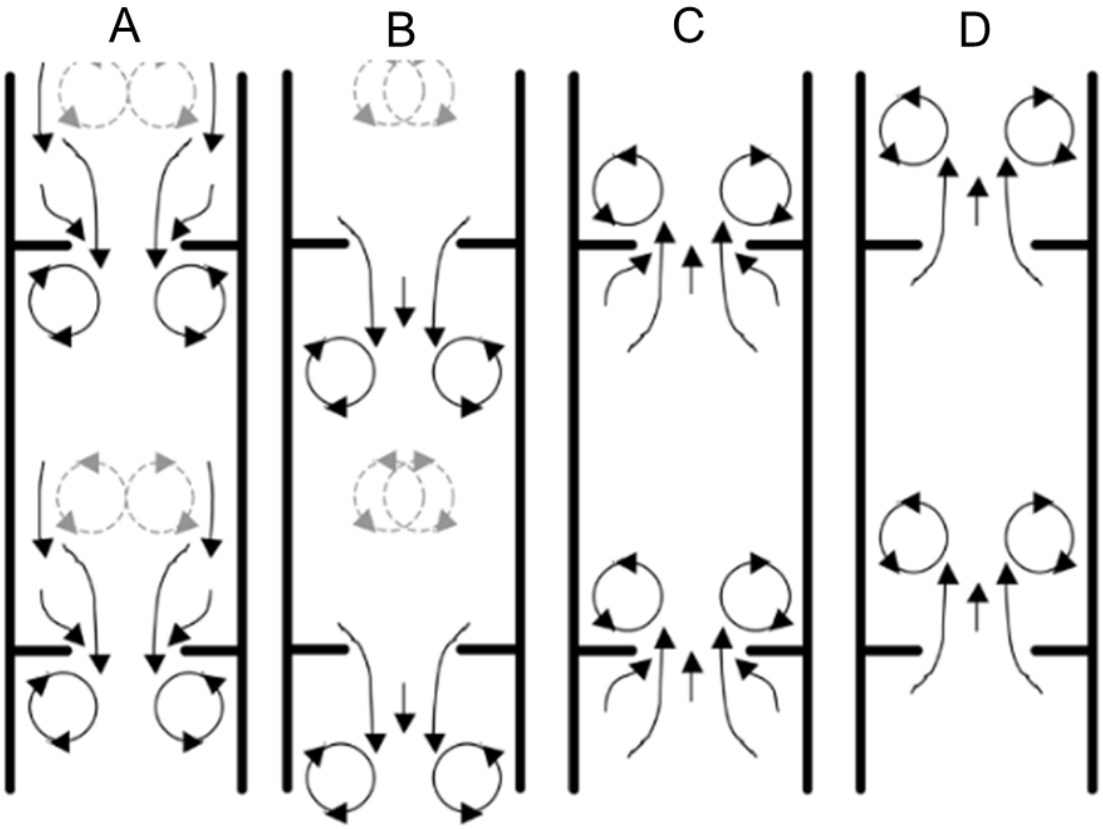

*Figure 4-2 Mixing mechanism in an COBC (A) At the start of downstroke (B) At the maximum point in the downstroke (C) At the start of upstroke (D) At the maximum point in the upstroke. Adapted from Ni 2003 [*117*].*

PFRs are generally favoured for fast processes with short residence times and can achieve uniform mixing and heat transfer, which is often critical to achieving a well-controlled precipitation process. For slower processes, such as crystallisation, a very long plug flow crystalliser is usually required to meet the longer residence time requirements and satisfy the flow rates required to achieve (near) plug flow. However, unlike conventional tubular PFR crystallisers, Oscillatory flow allows longer residence times to be achieved in a shorter reactor whilst maintaining close to plug flow conditions as turbulent

mixing is controlled by the oscillatory conditions and decoupled from the net flow rate [43, 81-86].

The oscillatory flow allows more uniform mixing conditions in the solution and, in doing so can produce higher quality crystals and significantly more reproducible results when compared to a conventional stirred tank [80].The benefits of using oscillatory mixing over a stirred tank extend to scale up, the scaling-up process of the stirred tank is extremely difficult. Mixing gradients are often found on a large scale within the stirred tank and the mixing cannot be linearly scaled-up [22].

Another important consideration in designing a continuous crystalliser is its suitability for operating different crystallisation processes, including antisolvent, cooling, combined antisolvent cooling, and reactive or pH-controlled crystallisations [13, 69]. Each crystallisation type requires a means of control over particular process parameters. For example, a smooth temperature profile and efficient heat transfer are required in cooling crystallisation (essential for dealing with narrow MSZW processes). A controlled mixing components of is often required for antisolvent and pH-controlled crystallisation. Thus for maximum utility, a crystalliser will ideally support different methods of realising supersaturation control via flexible addition points for antisolvent or buffers and control of different temperature profiles and offering ease of setup, use and cleaning [70]. Yiging C. Liu *et al.* showed that the moving baffle crystallisers, operating as a single-stage MSMPR in continuous mode, can produce narrower product particle size distributions than a single-stage continuously operated CSTR [97, 98]. This raises the possibility of combining multiple moving baffled crystallisers as a multi-vessel cascade reactor.

Therefore, the innovative CMBOC configuration has several potential benefits that include handling high solid loadings via control of oscillatory conditions. Compared with a stirred tank, more uniform mixing is achieved by distributing the moving baffles uniformly throughout each vessel [73, 94]. Importantly, the scale-up of this crystalliser setup, as with other oscillatory baffled crystallisers, follows well-defined rules maintaining a consistent baffle to orifice ratio and baffle spacing as the size of the reactor changes [81, 95, 96].

Oscillatory flow crystalliser design principles are governed by three dimensionless quantities, namely: (i) the oscillatory Reynolds number, Re_0, (**Equation 4-1**) *which* describe the intensity of mixing applied to the tube, (ii) the Strouhal number, *St*, (**Equation 4-2**) defining the ratio of the vessel column diameter to the oscillation amplitude and (iii) the velocity ratio, ψ, which is a measure of the degree of plug flow [196].

$$\boldsymbol{Re_0 = \frac{2\pi\omega x_0 \rho d}{\mu}} \qquad \textbf{Equation 4-1}$$

$$\boldsymbol{St = \frac{d}{4\pi x_0}} \qquad \textbf{Equation 4-2}$$

Where ω is the frequency of oscillation (Hz), x_0 is the centre-to-peak amplitude of oscillation (m), ρ is the fluid density (kg.m^{-3}), d is the internal diameter of the tube (m), and μ is the fluid viscosity (cp).

In a tubular reactor, the turbulence region begins at around Re = 2000, while in oscillatory flows, turbulent flow begins at as low as Re_0 = 50 [82]. At Re_0 = 100, the system exhibits plug flow characteristics where vortices are generated symmetrically, known as a soft mixing regime. At Re_0 >300, symmetry gets broken down, and flow becomes more turbulent. *St* measures the effective eddy propagation inside the baffle cavities [197, 198].

When considering a continuous operation, where the external flow is also present, the net flow Reynolds number, Re_n, is calculated as follows:

$$Re_n = \frac{ud\rho}{\mu} \qquad \textbf{Equation 4-3}$$

Where u is the mean velocity through the tube (m.s^{-1}).

The ratio of Re_n and Re_0 can be defined as the velocity ratio, ψ, defined as:

$$\psi = \frac{Re_0}{Re_n} \qquad \textbf{Equation 4-4}$$

For a process to be operating under plug flow, the velocity ratio should be greater than 1 so that the maximum oscillation velocity is always higher than the net flow velocity through the tube; however, values in the range of 2 - 12

have been optimum for plug-flow operation [199]. Therefore, when designing a continuous operation, the net flow rate would be fixed to govern the required mean residence time and then the appropriate oscillatory conditions selected ($\psi > 1$) to dominate the mixing.[199]

Another important parameter to consider in designing an oscillatory reactor is the baffle geometry (**Figure 4-3**). The baffle spacing, *L(m)*, is the distance between two baffles which has a significant influence on the vortex formation and is most commonly kept at 1.5 times the vessel diameter, *d*, to achieve adequate mixing over a wide range of oscillation frequencies and amplitudes [74, 200].

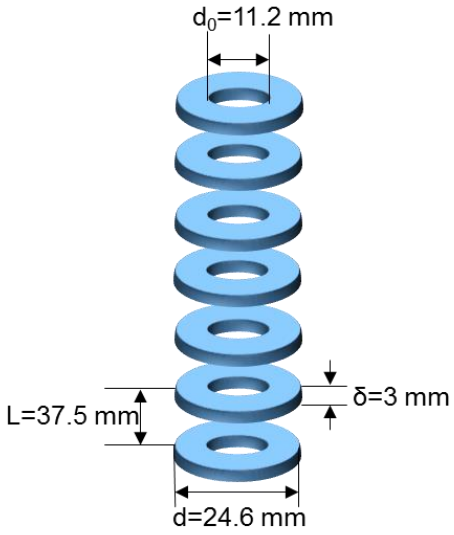

Figure 4-3 Schematic illustrating the baffle dimensions as used in this research.

The baffle open cross-sectional area, *α,* is generally standardised at 0.25 [201, 202], which relates to the orifice diameter, d_0, half the value of the tube diameter. Ni *et al.* studied the effect of α (ranging from 0.11 to 0.51) on mixing time and found that the lowest value tested ($\alpha = 0.11$) displayed the best mixing and, therefore, required shorter mixing times [203]. This has been supported by oil-water dispersion studies, where the smallest orifice diameter (0.22) achieved complete oil dispersion in the dispersing medium at the lowest minimum oscillation frequency tested. This was attributed to more power being applied to the system by oscillatory flow resulting in more intense mixing [195]. The

thickness of the baffle, δ = 3 mm, was identified as the optimal value for reactors of volume up to 5L [204, 205].

$$\mathrm{L} = 1.5\mathrm{d} \qquad \textbf{Equation 4-5}$$

$$\alpha = \left(\frac{d_0}{d}\right)^2 \qquad \textbf{Equation 4-6}$$

During the scale-up of a CMBOC, the baffle spacing, *L* and the open baffle area, *α,* are kept constant as these parameters control the formation of vortices resulting in uniform mixing [204].

To compare the mixing potential of an OBR to a traditional STR, the system's power density (Equation 5-7) can be used as the basis for comparison. The powder density value for a PBR can be defined as:

$$\frac{P}{V} = \frac{2\rho N_b}{3\pi C_D^2}\left(\frac{1-\alpha^2}{\alpha^2}\right) x_0^3 (2\pi f)^3 \qquad \textbf{Equation 4-7}$$

Where N_b is the number of baffles per unit length (m^{-1}), ρ is the fluid density ($kg.m^{-3}$), α is the ratio of baffle orifice area to tube cross-sectional area, x_0 amplitude of oscillation from the centre to peak (m), *f* is the frequency of oscillation (Hz). C_D is the orifice discharge coefficient of the baffles (typically taken as 0.7).

The key parameters and dimensionless groups describing the design operation and scale-up of a CMBOC are summarised in Table 4-1.

These principles have been used to develop a CMBOC platform concept, characterise the platform's key heat transfer and mixing performance and assess its ability to deliver consistent, controllable continuous crystallisation of two example molecular solids, alpha-lactose monohydrate (ALM) and paracetamol (PCM), to control sold form and particle size and span.

Table 4-1 Summary of the geometrical and operational parameters required for the design and operation of a CMBOC.

Parameter	Symbol	Unit
Baffle diameter	d	mm
Baffle orifice Diameter	d_0	mm
Baffle Spacing	L	mm
Baffle Thickness	δ	mm
Oscillation Amplitude	x_0	mm
Oscillation Frequency	ω	Hz
Velocity	u	$m^{2} \cdot s^{-1}$
Dimensionless numbers		
Baffle Open Area	α	-
Oscillatory Reynolds Number	Re_o	-
Net Flow Reynolds Number	Re_n	-
Velocity Ratio	ψ	-
Strouhal Number	St	-

4.1.2 CMBOC design

CSTR and PFR reactor design principles have been described elsewhere (**Section 1.2.4**). This section focuses on CSTR based crystalliser design and specifically on the development of the CMBOC concept. In considering the design and operation of a CSTR based continuous crystalliser, the important factors include the means of control over crystal generation (nucleation), crystal growth, and assuring appropriate velocity is maintained to suspend crystals and avoid settling and to achieve a consistent flow of the crystal suspension from one stage to the next. For multi-vessel or cascade configurations, the total number of stages required in a continuous synthesis or crystallisation is decided based on the process kinetics, the required yield and the degree of back mixing acceptable to achieve good process performance [206]. In practice, CSTRs are often used in cascades of 3 to 4 connected reactor vessels as this provides reasonable operating volume whilst separating process stages into discrete control volumes to manage temperature and/or supersaturation profiles

efficiently, reduces back mixing whilst minimising the complexity and expense of equipment requirements that adding additional CSTR stages adds. Single-stage CSTRs are characterised by severe back mixing of the process liquid, leading to broad residence time distributions and potentially wide particle size distributions [97]. Adopting configurations that combine a cascade of multiple CSTRs allows a narrower residence time distribution with significantly reduced back mixing. In theory, approaching plug flow behaviour as substantially more CSTRs are added to the cascade. The Tanks-in-Series model can describe this effect on mixing behaviour, which relates the total dispersion to the total number of theoretical CSTR stages (more details in **section 4.3.1)**.

To assess the feasibility of the CMBOC platform, a four-stage platform was designed and configured to achieve reasonable mixing, scale and residence times to be suitable for crystallisation. This prototype design aimed to establish, in the first instance, a working continuous crystallisation platform that can be tested with known processes (Alpha lactose monohydrate (ALM) and Paracetamol (PCM)). Characterising the platform's operational considerations and performance concerning liquid and slurry flow [111], residence time distribution; particle suspension and slurry transfer efficiency; heat transfer and temperature control; maximum solids loading tolerated and effective introduction of feedstock. To enable efficient and sparing use of materials during the initial testing, the volume of each vessel was kept to 120 ml, giving a total reactor volume of 480 ml and a mean residence time range of 20-120 mins with an operating temperature range of 0-100^{o}C.

The second part of the design deals with transferring material from one stage to the next. A key challenge in developing any cascade reactor is to connect the individual vessels in series to allow continuous operation. To begin with, it was decided to use a glass baffled U bend to connect one column to the next for continuous transfer, as shown in **Figure 4-4(A).** In this setup, the oscillation was provided only in vertical sections and baffles, whilst the suspension in U bends was stationary. During initial testing, this baffled design led to sedimentation due to insufficient mixing. Therefore, flexible PTFE tubing was decided to connect individual vessel stages. The design of the outlet from each vessel was also assessed. An initial downward-facing outlet led to the

accumulation of solids near the port **Figure 4-4(B).** So an upward angle was selected for the test bed as it was shown to provide smoother slurry transfer (**Figure 4-4(C))**.

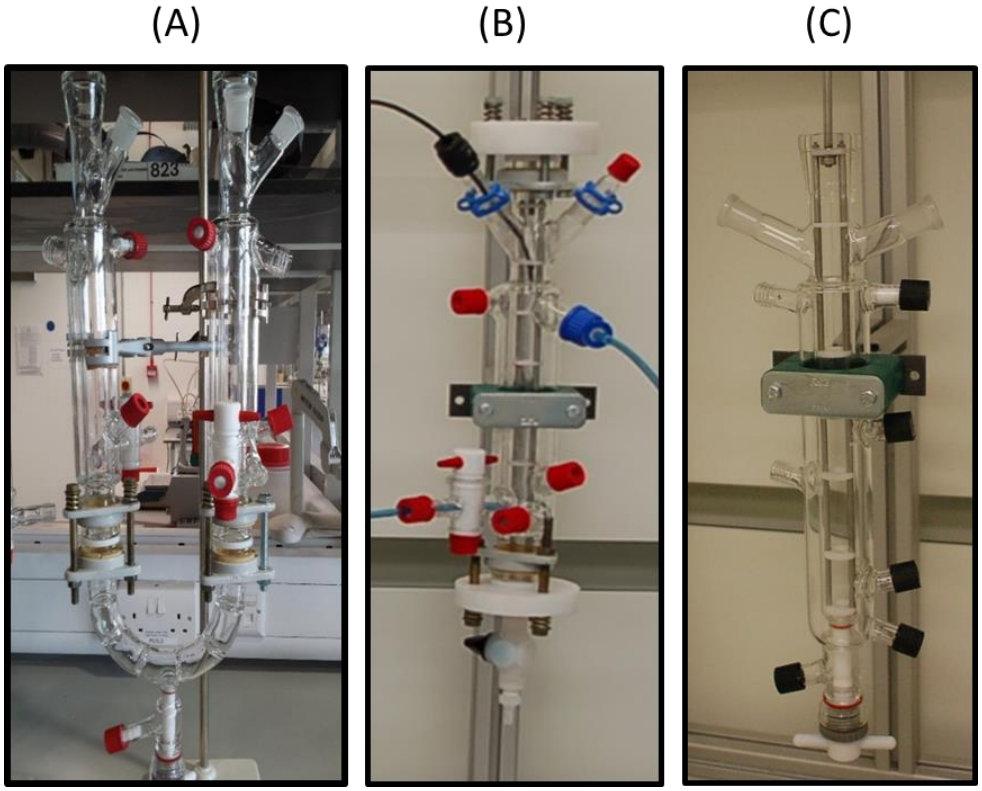

Figure 4-4 Prototype designs for (A) U-bend transfer line with fixed baffles in the bends, (B) outlet with downward angle (C) Final design with the outlet at an upward angle.

Several different transfer strategies were considered for continuous slurry transfer between vessels, taking care to minimise the risk of affecting the product crystal attributes. Gravity transfer was ruled out due to the single oscillator construction that would have made the vessel alignment challenging and the risk of particle sedimentation in the transfer line when operating with lower flow rates [206]. Continuous feed transfer between cascade vessels can be controlled by positive or negative pressure [207] or pumps directly [97]. Pump transfer was deliberately avoided in this setup to minimise the attrition of crystals due to the mechanical force exerted by the moving parts whilst in operation. Therefore, pressure transfer was selected and implemented. The benefit of positive pressure transfer is that crystals are not exposed to damaging mechanical forces [207].

4.1.2.1 Operational Challenges

The feed inlet at the bottom and outlet at the top was finalised to avoid any short-circuiting and also to avoid the effect of gravity on suspended crystals. The pressure required to transfer the slurry between the vessel was tested during the preliminary test. Nitrogen gas was used to generate pressure inside the vessel. Pressure between 0.02 to 0.5 bar was tested to find out the effect of pressure on the slurry transfer. Results showed that the pressure required to run the CMBOC is in the range of 0.02 to 0.05 bar. Any positive pressure above 0.05 bar showed an excess amount of nitrogen travelling through each vessel and generating nitrogen bubbles inside each vessel before finally escaping into the collection vessel at the end. Although it did not hamper the overall operation, it affected the total volume of the vessel.

Sealing the vessel at the point of the moving rod, which connects the linear motor and baffles assembly, was a challenge to facilitate the pressure transfer between vessels. The initial design was incorporated by using the standard O-ring seal, which was not effectively sealing the system. After the initial failure of airtight the system with the help of a standard O-ring, more sophisticated spring-energised seals were implemented, which were supplied by (Alconbury Weston ltd, UK) A spring-energized seal uses a spring to provide a uniform load throughout the circumference of the seal and prevent any leakage due to moving parts.

Another challenge was to overcome to carefully position of PAT port. Unlike the conventional STR or COBC, where not many moving parts are within the vessel, CMBOC contains baffle string which oscillates throughout the area of vessel volume, which makes it hard to insert any PAT probes without obstructing the moving baffles. To overcome this challenge, in the final design of CMBOC, two PAT ports were placed right in the centre of the two baffles, which restricted the maximum amount of oscillation that can be achieved while using the PAT probe to 30 mm (peak to peak). However, due to the diameter of the vessel (25mm id), using an amplitude of more than 1.5 times the vessel diameter is not recommended as it will increase the back mixing as well hinder the full eddy propagation.

After these initial design and prototype testing experiments, the CMBOC setup constructed for this project comprised four jacketed borosilicate glass vessels with an internal diameter of 25 mm and a height of 220 mm, giving a working volume of 120 mL in each vessel. The vessels are mounted on an aluminium frame. A seven-baffle element is present in each vessel to effect mixing. The acetal O-ring baffles have an outer diameter of 24.6 mm, an orifice diameter of 11.2 mm and a thickness of 3 mm, giving a tight fit between the moving baffle and the inner vessel wall. Baffles were spaced at 37.5 mm using stainless steel spacers. These details were based on the optimal design principles for adequate oscillatory mixing [199, 208]. The platform was airtight using a mechanical seal around the moving baffle connecting rod to achieve pressure transfer operation. The oscillatory baffle motion across all the CMBOC stages was provided employing a single linear motor (Copley Controls Corporation) held by an aluminium frame above the CMBOC (**Figure 4-5**). A control box was used to enable the linear motor operation over the frequency range of 0-5 Hz and amplitudes of 0-30 mm (peak-peak). The pressure was generated using a nitrogen gas feed automatically regulated to achieve the target pressure. Transfer lines between stages were made of jacketed 10 mm I.D. PTFE flexible tubing minimises heat loss and the risk of uncontrolled fouling due to local cooling during operation.

Two ports are available in the middle of each vessel to incorporate PAT probes for process monitoring. Both ports are positioned between two moving baffles to avoid breakage or interference of the equipment with any measured signal. A further three ports are positioned at the top of each vessel to serve as inlets, outlets, sampling and/or addition ports. A drain port was also installed at the bottom of each vessel for easy cleaning. Thus, the CMBOC design provides three different ways to configure the inlet and the outlet of transfer between vessels: (1) feed introduced at the top and removed from the bottom; (2) feed introduced at the bottom and removed from the top or (3) both inlet and outlets positioned at the top. The CMBOC multi-stage platform was configured for option (2), i.e. feed transfer from the top of each stage to the bottom of the next, thus minimising the risk of short-circuiting the fluid between inlet and outlet [97].

Each vessel is connected to a temperature circulator to maintain vessel temperatures at the target values.

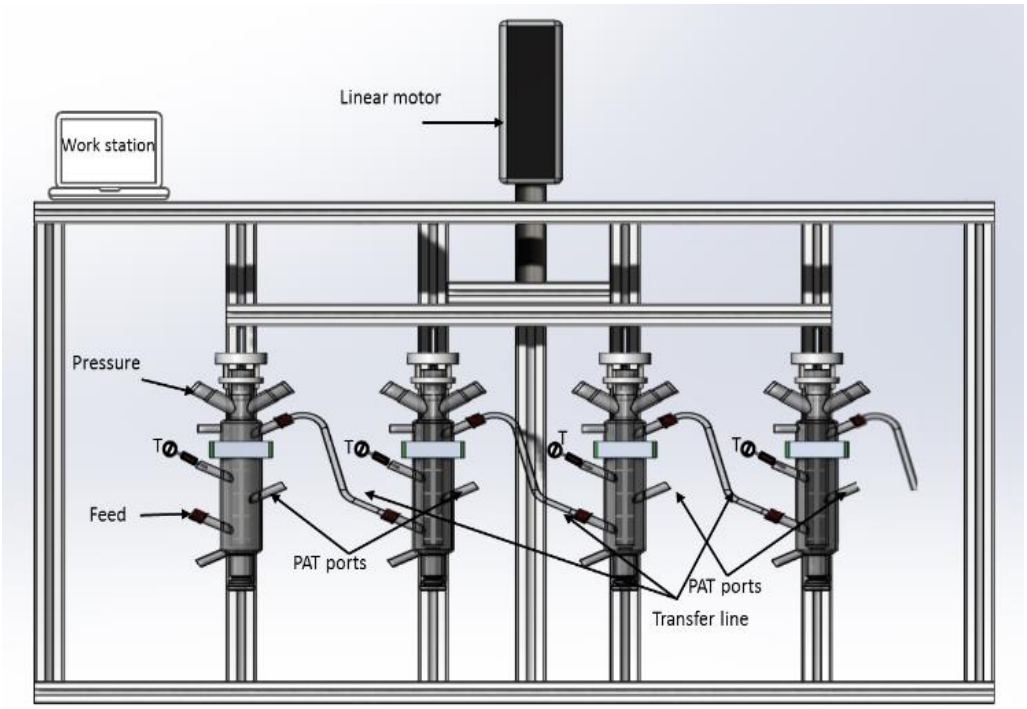

Figure 4-5 Schematic Cascade of Moving Baffle Oscillatory Crystalliser set up with pressure transfer line.

4.2 Crystallisation operational parameter control

The pumps (Watson Marlow, 520Du) for feed and seed transfer to the first vessel, circulators (Lauda Ecogold 620), pressure regulators, linear motor (Copley Motors) and thermocouples were interfaced with a PharmaMV control system (Perceptive Engineering Limited, version V7) [209] with the interface shown in **Figure 4-6.** The PharmaMV Advanced Process Control (APC) platform also provides an integrated control environment for equipment automation, integrates PAT, aligns time-series data collection, and automates the setup and control of actuators and sensors to enable monitoring of processes they run. The platform also manages the archival of process data to allow retrospective analyses. Integrating the APC controller is a benefit of enabling real-time model predictive control via PAT-enabled closed-loop operation. Therefore, this can allow the implementation of hierarchical

controllers, for example, temperature, concentration, and direct control over particle attributes. This is possible where attributes can be measured directly, such as crystal size, using the FBRM signal to monitor fit against the control objective with the APC adjusting process conditions to achieve the selected target particle size [149].

Here an APC system was configured to operate with the CMBOC platform to develop a model of predictive temperature control as part of the initial platform evaluation case studies. The methodology used to develop the APC and further details on the control methodology, models and algorithms used in modelling the process and effecting control against objective set points are described elsewhere [149].

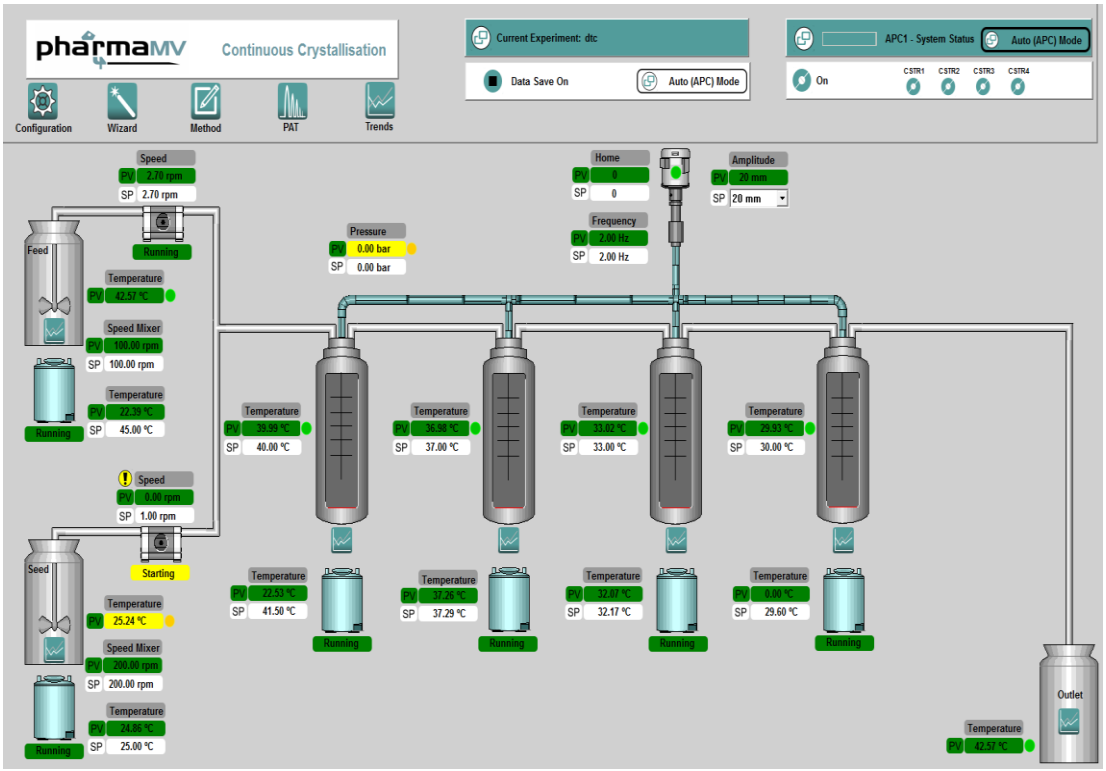

Figure 4-6 PharmaMV interface showing the basic platform configuration and sensor values.

4.2.1 Model Predictive Temperature Control on the CMBOC

This project developed a temperature controller to allow rapid setup and real-time control over the temperature profile used in the case studies. A series of step tests were conducted to develop a model predictive controller that can set

the circulator temperature settings required to achieve the target values and respond to any perturbations in process conditions to maintain the set point.

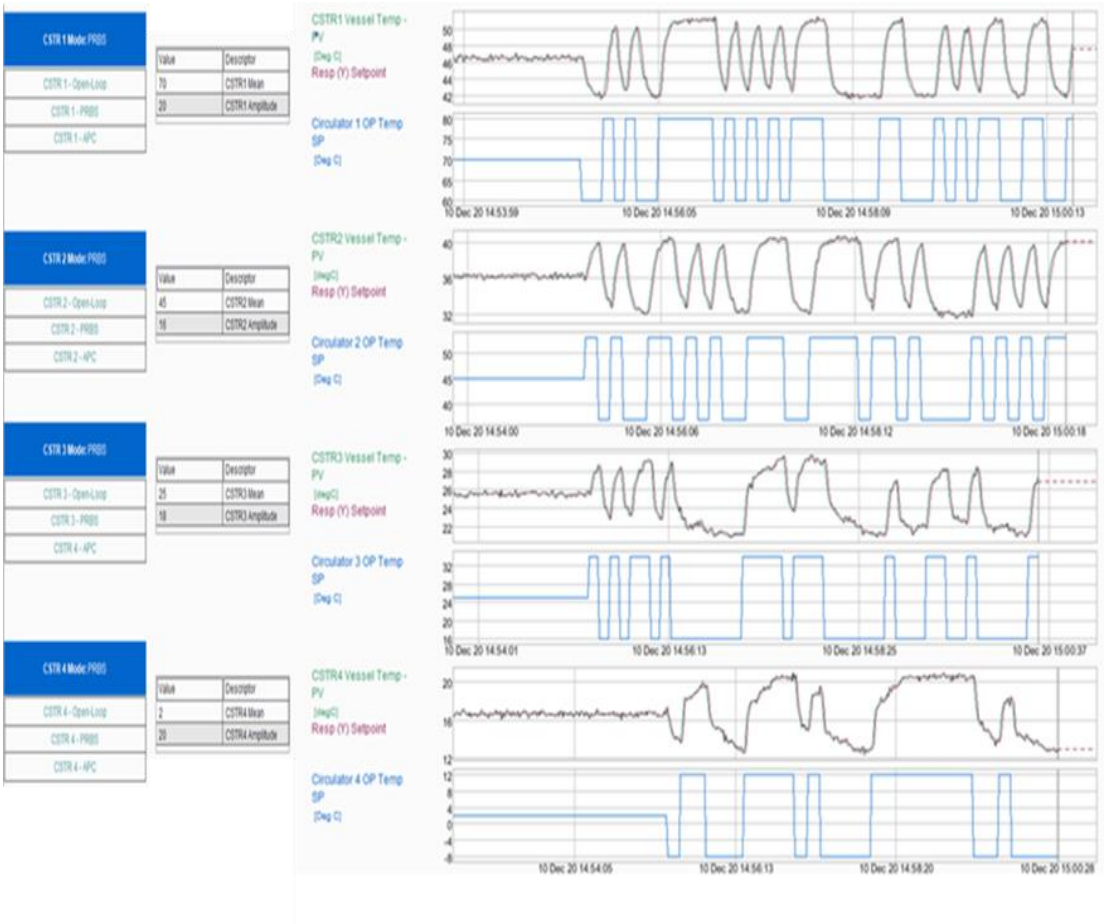

Figure 4-7 An example of the PRBS step tests carried out on each vessel and their responses to build the APC model. Circulator temperature is assumed to be the same as jacket temperature, and flow rates were kept constant at 10mL.min^{-1}.The blue line is the circulator set point, and the black line is the vessel temperature.

Pseudo-Random Binary Sequence (PRBS) tests were applied to the circulator temperatures to provide experimental data describing the system response and informing the development of the temperature model. PRBS allows statistically rich data to be obtained automatically [210], and when used on multiple actuators, the experimentation time can be reduced [210]. **Figure 4-7** shows such a training dataset where PRBS was applied. During the test, the vessel circulator temperatures were varied in the range of 10-80 °C using step sizes of 15 to 20 °C, and the subsequent response in the corresponding vessel temperature was measured. The temperature model was built using data

across this temperature range and from different feed (water) flow rate ranges of 5 to 20ml.min^{-1}.

In reactor temperature profile control, multivariate control schemes such as APC offer several benefits over manual control. This is especially true for crystallisation, where faster temperature change response and avoidance of temperature overshoots are necessary and complex relationships between process inputs, conditions, and outputs. This type of control could be extended for the CMOBC to include additional levels of control over saturation and PSD by integrating UV and FBRM in future.

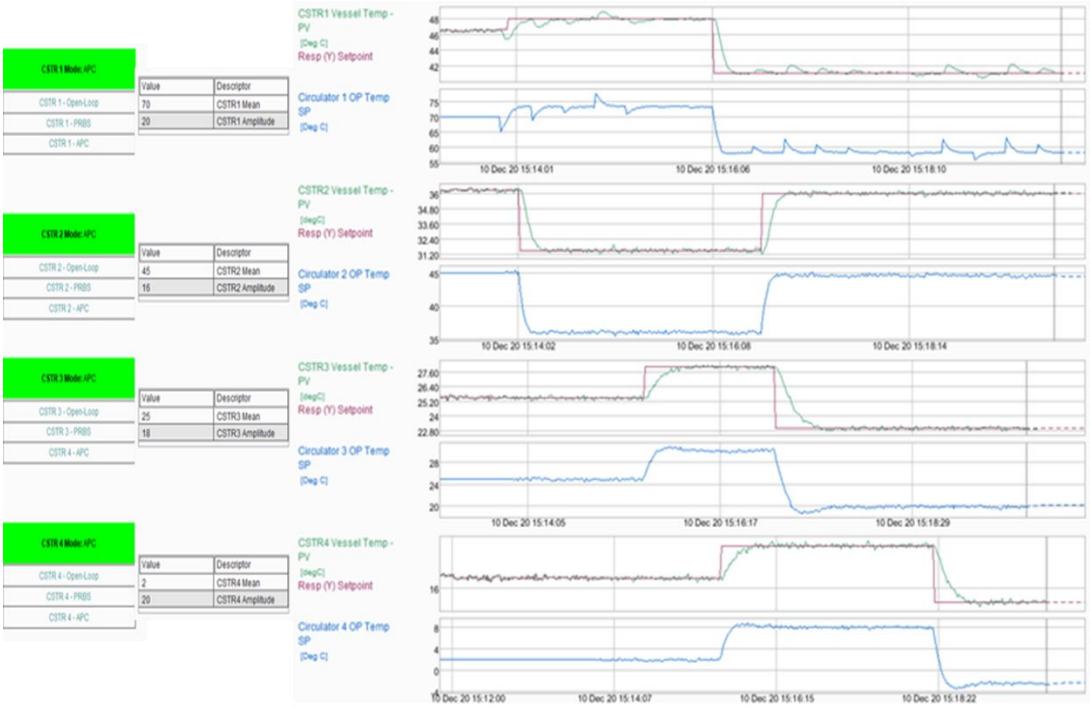

Figure 4-8 An example of the APC control on CMBOC Vessel temperature's quick response to the change in circulator temperature. The blue line is the circulator set point, the green line is the actual vessel temperature, and the red line is the vessel set point.

Figure 4-8 shows the close correspondence between the set point temperature for each vessel and the actual temperature with the APC active. Vessel temperature is maintained with a maximum deviation of ±0.5 °C. Changes in target temperature are achieved between 3 and 6 min from the set point change, depending on the magnitude of the temperature change selected (5 –

20 ^{o}C respectively in this case). This demonstrates that the APC system effectively controls the four circulators and the interactions between them and the process fluid and provides accurate and responsive control over the temperature profile applied across the 4 stages of the CMBOC. Note that the model has been extended for 5 stages, although we restricted it to using four CMBOC stages in this work.

4.3 Characterisation of CMBOC

Understanding the mixing and flow profile achieved under typical operating conditions in a continuous flow platform is essential. OFRs have been extensively studied and characterised as PFRs for continuous processes, reviewed extensively in **Section 2.5.**

MSMPRs remain the most widely utilised platform for continuous crystallisation research due to familiarity with the operation and control of existing batch equipment. These have been successfully operated at a range of scales from 1 – 10 L [14]. However, some recognised disadvantages of MSMPRs include localised high shear near the impeller or agitator, non-uniform thermal control and nonlinear process scalability [13, 71]. Crystal product quality can be particularly sensitive to the shear rate distribution during crystallisation [72, 73]. Chew *et al.* investigated the shear rate distribution and flow patterns in a stirred tank and a single-stage moving oscillatory baffle crystalliser (MBOC) using computational fluid dynamics (CFD) [73]. They showed that in an MBOC, particles spend most of their time in the high shear regions whilst the MSMPR particles reside mainly in regions of low shear. This affects the uniformity of growth, purification, attrition, and agglomeration observed in the product [32, 80, 97].

In this study, a novel four-stage of CMBOC is characterised in detail for the mixing and heat transfer performance during continuous operation. The suitability of the system for crystal and particle engineering applications and extended continuous operation at a laboratory scale is also investigated for two molecular crystal systems.

4.3.1 Residence time distribution

In any vessel, each element of fluid takes a different route and time to pass through the reactor and the distribution of different times for fluid elements to pass through the system is called the exit age distribution E, or the Residence Time Distribution (RTD) of the fluid **(Figure 4-9)** which has a unit of time^{-1}.

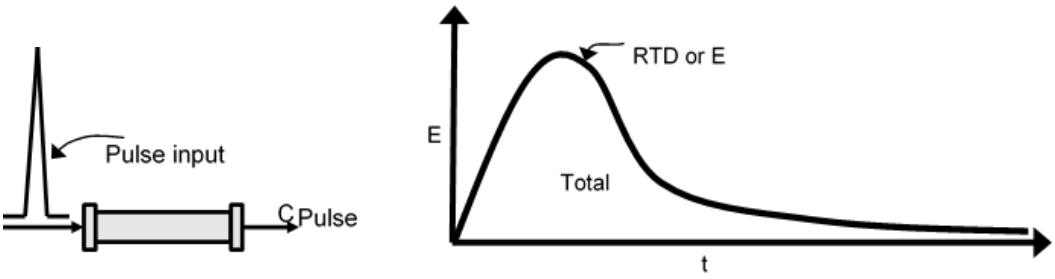

Figure 4-9 (left) Pulse input representation (right) Exit age distribution curve E

The axial dispersion and tanks-in-series models are the most effective methods of estimating RTD in a non-ideal platform [95]. These models have been widely applied to characterise many types of continuous reactors. The principles and methods are summarised below and described elsewhere [82, 95, 211].

Unlike conventional tubular reactors in which the turbulent net flow causes mixing, the mixing achieved in an oscillatory flow reactor is mainly obtained by fluid oscillations. Therefore, the RTD within the device can be tuned by both the net flow rate and the oscillation. This study performed the experiments by applying the tanks-in-series model with 'perfect pulse tracer' experiments over a wide range of oscillatory conditions and net flow rates in the four-stage CMBOC. The experimental tracer injection procedure lasts only 3-5 s compared to the average residence time of 20 to 90 min in the CMBOC; hence the tracer injection profile is assumed to be perfect, i.e. infinite and narrow with no dispersion.

The measured tracer concentration profiles at different locations can estimate the vessel dispersion number [111]. The E curve can be calculated for the vessel of volume V (m^3) with a net flow of Q ($m^3.s^{-1}$) of the primary fluid and the tracer unit injected as the perfect pulse by recording the concentration vs time profile of the tracer leaving the vessel. Each pulse can be evaluated independently. The simplest way to study the dispersion of the injected pulse at the exit of the CMBOC is to analyse the variance of dispersion, σ^2 of the

measured signal (g.L^{-1}). In this work, we have studied both the liquid RTD using concentration and the solid RTD from the number of particles from the mean residence time t_m or θ (s). The mean residence time is defined as τ, calculated from experimental data using **Equation 4-8**.

$$\tau = \frac{\sum Citi\Delta ti}{\sum Ci\Delta ti} = \frac{V}{\mathrm{Q}} \qquad \textbf{Equation 4-8}$$

V (m^{-3}) is the vessel volume, and Q (m^3.s^{-1}) is the flow rate of the bulk phase in CMBOC. The exit age distribution E can be calculated by merely dividing the concentration of the tracer pulse by area. The expressions used to calculate σ^2, the measure of variance or spread of the experimental tracer curve, and t_m are shown in **Equation 4-9** and **Equation 4-10,** respectively.

$$\sigma^2 = \frac{\sum ti^2 Ci\Delta ti}{\sum Ci\Delta ti} - \tau^2 \qquad \textbf{Equation 4-9}$$

Where Ci is the concentration of tracer at i, time interval, Δti= difference between each time interval, ti is the time from the injection of tracer, and τ is the mean residence time. An ideal reactor will yield σ^2 of 1 and ideal plug, flow produces a completely uniform RTD. The smaller the variance, the narrower/ more uniform the RTD profile, and the more consistent the end-product is likely to be.

t_m, The dimensionless experimental mean residence time in all tanks can be calculated as follows:

$$t_m \text{or } \theta = \frac{\bar{t}}{\tau} \qquad \textbf{Equation 4-10}$$

Where $\bar{t}$ is the experimentally measured mean residence time, and τ is the theoretical mean residence time. In a true continuous process, regardless of idealness, t_m should be equal to one. When $t_m > 1$ indicates potential stagnant areas or 'dead zones'. When $t_m < 1$, it suggests possible bypassing issues.

Then, the tanks-in-series-model **Equation 5-11** for a closed vessel was fitted to the system to the normalised RTD profiles.

$$E_\theta = \frac{N(N\theta)^{N-1}}{(N-1)!} e^{-N\theta}$$ **Equation 4-11**

Where τ is the meantime of passage when the curve passes by the exit, θ is dimensionless time-based on the mean residence time in all tanks, E_θ exit age distribution function, and N is the number of tanks. Residence time distribution can be represented by the residence time distribution function (E-curve) which is the normalised concentration profile (***Figure* 4-10**).

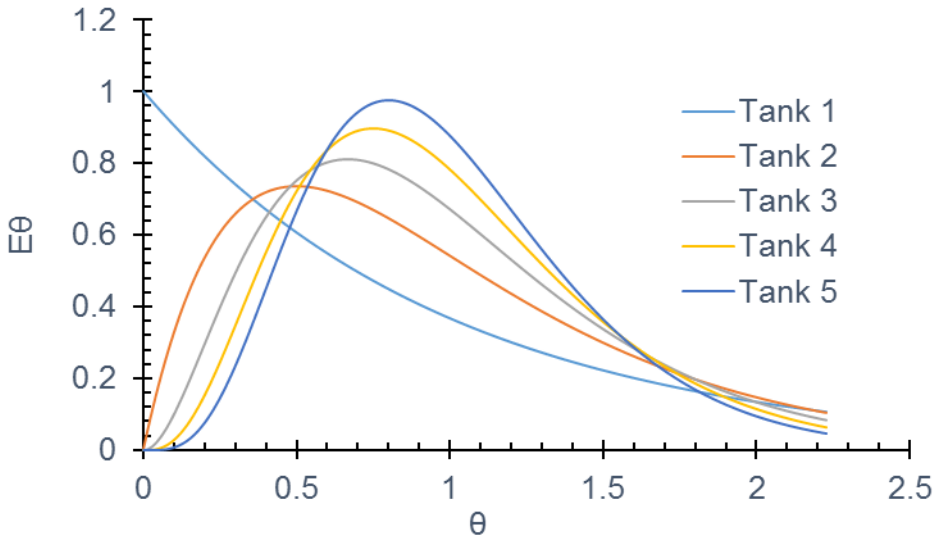

Figure 4-10 Theoretical tank-in-series curve for Eθ, exit age distribution vs dimensionless time θ derived for 5 tank-in-series.

4.3.1.1 Residence time distribution (liquid) method

The Liquid RTD experiments were performed by applying the tanks-in-series model to 'perfect pulse' tracer experiments over a wide range of oscillatory conditions and flow rates. Sodium benzoate was used as a tracer material for the liquid RTD experiments. The λ_{max} for the Sodium Benzoate was determined at 226 nm (see **Figure 4-11**) using a UV transflectance probe with a path length of 5 mm.

A calibration UV curve for that is shown in **Figure 4-12** with an R^2 value of 0.9988, corresponding to an excellent linear response fit to the data. The deionised water was used as a main flow for the experimental work. Data were acquired using a UV transflectance probe connected via fibre optics to a UV

analyser (see section 3.2.3). Different concentrations of sodium benzoate were tested to develop a calibration model for the concentration conversion. The aim was to select the wavelength where the measured A value for the maximum concentration used never exceeds 1 AU to maintain the linearity required by the Beer Lamber Law. The sodium benzoate's detection limit was determined as 2.501 x 10^{-6} g.L^{-1} (signal: noise, 3:1).

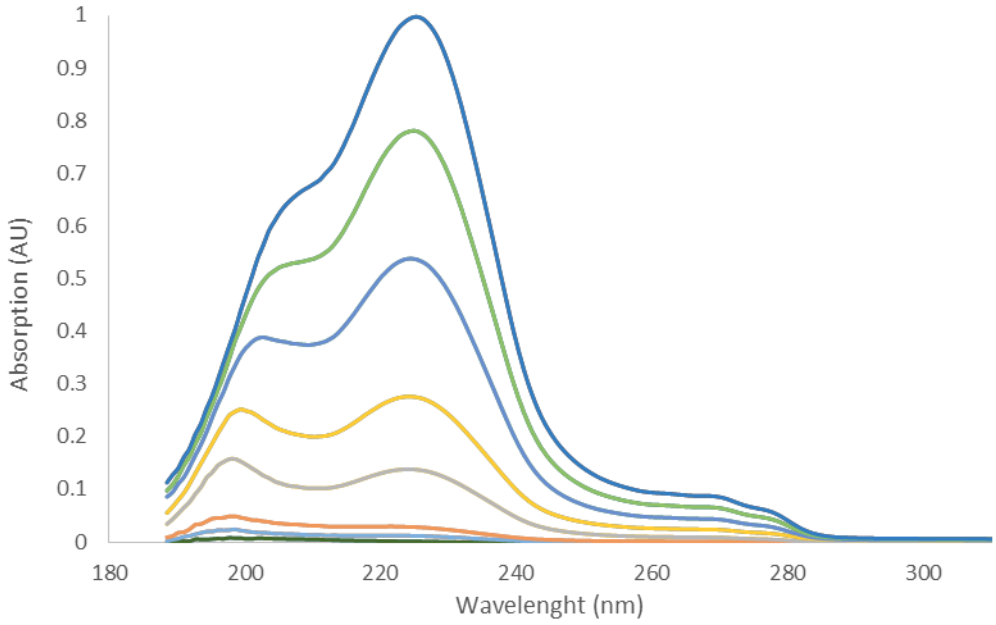

Figure 4-11 Example of a typical response from UV transflectance spectrometer.

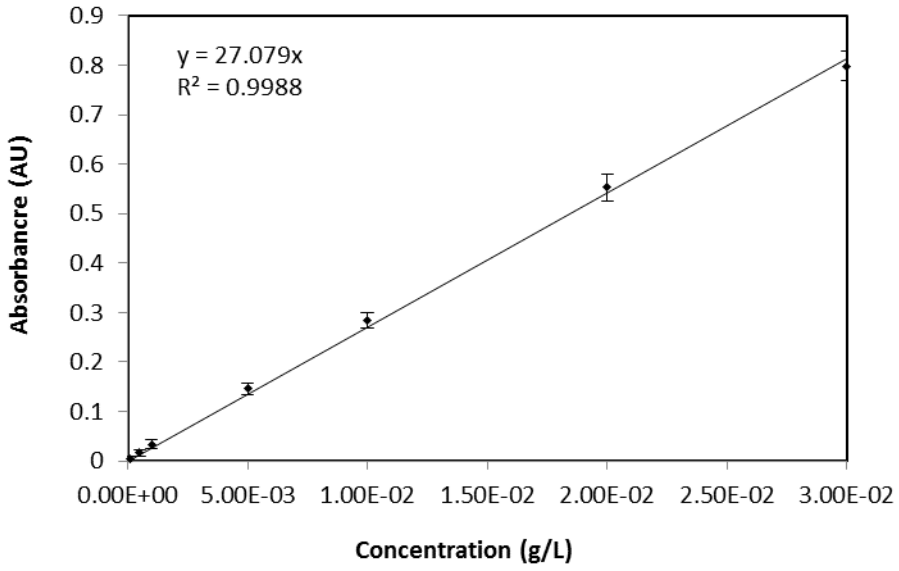

Figure 4-12 UV spectrometer calibration of sodium benzoate at 226 nm

The optimal volume and concentration for the tracer were determined to be 3ml of 0.5g.L-1 aqueous sodium benzoate from the experiments. The tracer was instantaneously injected via syringe and needle connected to the port via a septum on the first vessel (see **Figure 4-13**). UV transflectance probes were positioned in the 2nd and 4th reactor on subsequent runs via GL18 ports to measure the concentration response during the liquid RTD studies.

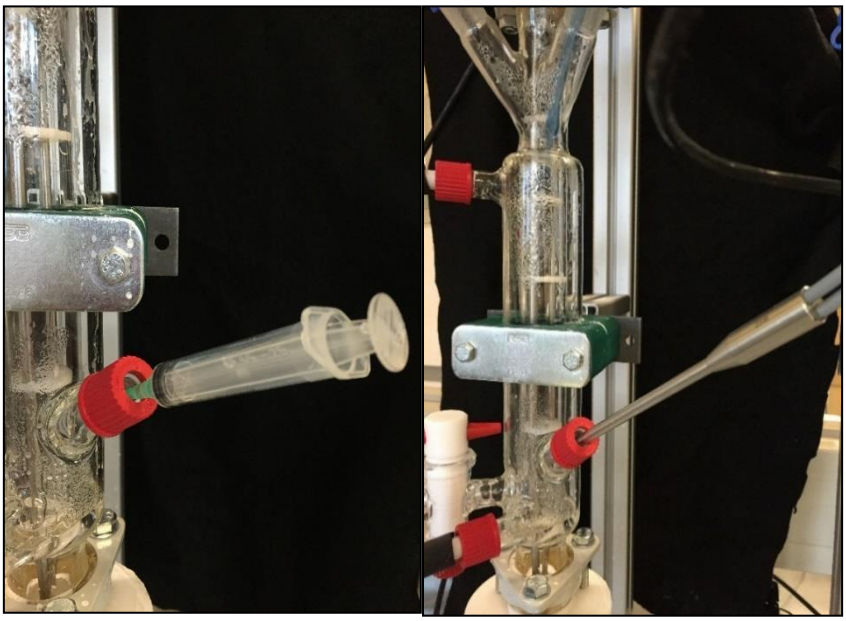

Figure 4-13 the photograph of the CMBOC setup showing the tracer injection port in vessel 1 (left) and the UV transflectance probe in vessel 4(Right) in CMOBC for Liquid RTD studies.

4.3.1.2 Residence time distribution (solids) method

Given the aim of assessing the platform's suitability to run continuous crystallisations, the mixing and flow performance of the platform was also assessed for slurries to ensure no hold-ups or bypass of particles occurred. An FBRM based method was used to investigate the mean RTD for solids following Kacker *et al*.,[111]. A series of experiments were conducted to find the optimum amount of tracer particles injection detectible with an FBRM. The tracer amount injected in vessel 1 and the FBRM response were measured in vessels 1 and 4. The iC FBRM software [156] was used to record the data from the FBRM probe. In principle, FBRM is a calibration-free tool that directly gives a

quantitative measure of the number of particles in the system. [111] Since a constant net flow ensured that the pulse of the tracer particles passed across the small focus region of the FBRM probe, clear detection of the pulse from the start to the end could be made. For the solid RTD studies, the pulse of 3 ml of 10 wt% polystyrene particles (density 1.055 $g.cm^{-3}$) in water with a mean size of 90 µm was injected into the first vessel via syringe. The use of mono-sized and virtually neutrally buoyant particles to track the solid RTD does not fully represent the behaviour of distribution of crystals during prolonged operation which can be assessed in future. FBRM probes positioned in the first and fourth vessels were used to measure the response of the total count of tracer particles passing through the platform over time. Since the injection procedure lasts only for 3-5 s compared to the average residence time of 20 to 90 min in the CMBOC, the tracer injection can be assumed to be a pulse. Because the shot of tracer injected is immediately dispersed by the flow oscillation present at the time of injection, justifying the assumption of the pulse injection.

The measured tracer FBRM profiles can then be used to calculate the dispersion coefficient using the tank-in-series model. Each pulse can be evaluated independently, and the simplest way to study the dispersion of the injected pulse at the exit of the CMBOC is to analyse the variance of dispersion σ^2 of the measured particle count from the mean residence time θ (s) for the polystyrene bead tracer systems. An example of a typical FBRM total count trend positioned in the 4^{th} vessel via a GL18 port to track the solid tracer journey during the solid RTD studies has shown in **Figure 4-14**.

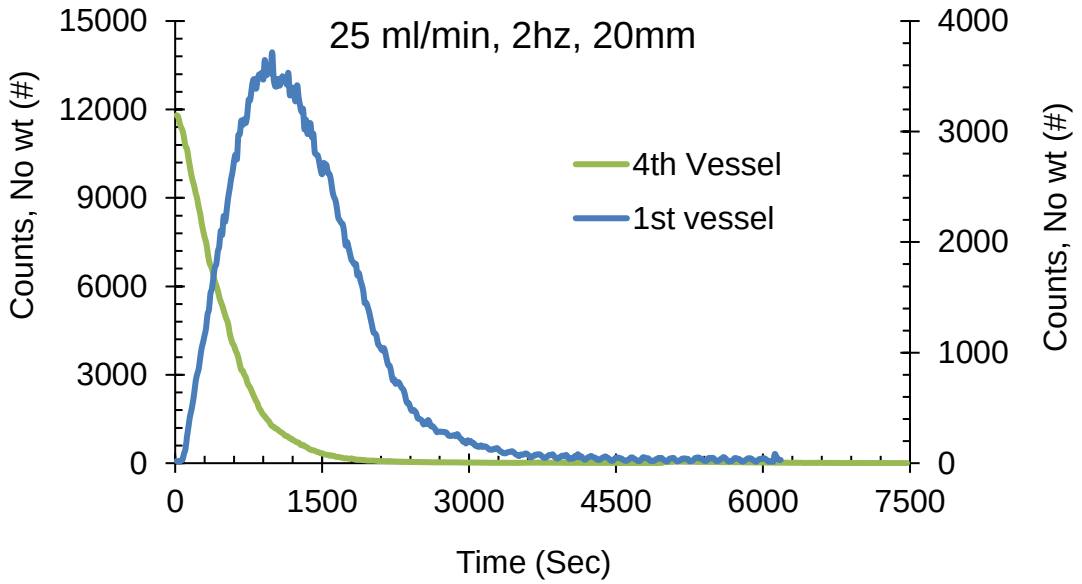

Figure 4-14 Typical FBRM total count trend for Solid RTD measurement in 1st and 4th vessel of CMBOC while operating the CMBOC at 25 ml.min-1flow rate and 2 Hz and 20 mm oscillation condition.

4.3.2 Heat transfer characterisation

Heat transfer behaviour was investigated in a single-stage CMBOC. Heat transfer enhancement due to oscillatory flow by a factor of 10-30 has been reported previously [99-104]. This work focuses on understanding the natural convective heat transfer characteristics under relevant oscillatory conditions for the specific geometry of this platform. The method to determine the overall heat transfer coefficient, h, for oscillatory flow in baffled tubes was adapted from Stephens *et al.* [102]. This is based on the correlation between the Nusselt number, Nu_t and the net, Re_n and oscillatory flow, and Re_o, Reynolds numbers reported by Brunold *et al.* [74]. The experiment was carried out in the same way as for a shell and tube heat exchanger [102], where fluid flow maintains a constant temperature through the shell side, which in turn cools or heats the fixed mass of fluid on the tube side. In turn, the tube-side Nusselt number can be calculated from the temperature variation of the tube side fluid. The overall heat transfer coefficient contains contributions from the shell-side heat transfer coefficient, the coefficient due to heat transfer across the wall separating the tube and the shell, and the tube side heat transfer coefficient. This relation is given by:

$$\frac{1}{h} = \frac{1}{h_t} + \frac{r_i ln(r_o/r_i)}{k_w} + \frac{r_i}{r_o h_s}$$ **Equation 4-12**

A non-steady-state heat balance for a fixed mass of fluid in a tube is given as:

$$\frac{Aht}{mC_p} = \ln\left(\frac{T_i - T_w}{T - T_w}\right)$$ **Equation 4-13**

where m (0.12 Kg) is the mass of fluid in the tube which is being cooled, A (0.0173 m^2) in the area of the heat transfer surface, C_p (4181 $J.kg^{-1}K^{-1}$) is the specific heat capacity of the tube-side fluid, h_t is the tube-side heat transfer coefficient, T is the time-varying temperature of the tube-side fluid, T_i is the initial tube-side temperature, T_w is the temperature of the shell-side fluid which remains constant, and t is the elapsed time. This can be rearranged to

$$ln(T - T_w) = -\frac{Ah_t}{mC_p} + ln(T_i - T_w)$$ **Equation 4-14**

It can be seen that a graph of $-ln(T\text{-}T_w)$ against *t* should give a straight line of slope Ah/mC_p and intercept $-ln(T_i\text{-}T_w)$. The overall heat transfer coefficient can then be determined from the slope of the graph, as shown in **Figure 4-15**. Where h_t is the tube-side heat transfer coefficient, h_s (510.69 $W.m^{-2}K$) is the shell-side heat transfer coefficient that will remain constant for all the experiments. k_w (0.8 $W.m^{-1}K^{-1}$) is the conductivity of the tube wall, and r_i and r_o are the inner and outer radius of the tube wall curvature, respectively.

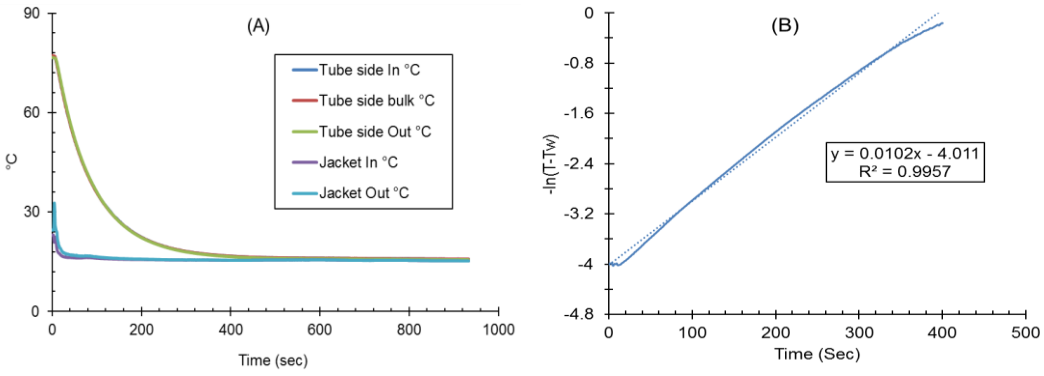

Figure 4-15 (A) Example of typical temperature profile and (B) Typical response of –ln(T-Tw) against t gives a straight line of slope Ah/mCp.

For the equation to be used in this form, the overall heat transfer coefficient must be related to the inner radius of the tube wall curvature, so the heat

transfer area term should refer to the area inside the tube wall. The tube-side heat transfer coefficient can then be determined from:

$$Nu_t = \frac{h_t D_i}{k_t}$$ **Equation 4-15**

Where k_t (0.6 $W.m^{-1}K^{-1}$) is the conductivity of the fluid in the tube.

For all the experiments, the shell-side fluid was tap water at the mains pressure at a constant flow rate of 0.0833 $kg.s^{-1}$. While 120 g of tap water was filled in the vessel, which was heated to 80 ^oC before the start of each experiment.

Table 4-2 summarises all the parameters used for heat transfer calculations.

Parameter	Value	Units
Shell-side diameter	0.055	m
Wall thickness	0.002	m
Vessel diameter	0.025	m
Shell-side equivalent diameter, de	0.017	m
Shell-side flow rate, Q	0.083	$Kg.s^{-1}$
Shell-side cross-section, A	0.001	m^{-2}
Shell-side mass velocity	83.21	$Kg.m^{-2}s^{-1}$
Shell-side Re	1414	
Cp of water	4180	$J.kg^{-1}K^{-1}$
The conductivity of the fluid in the tube, k_f	0.6	$W.m^{-1}K^{-1}$
Shell side Nusselt number, Nu	14.46	
Shell-side heat transfer coefficient, h_s	510	$W.m^{-2}K^{-1}$
The conductivity of the tube wall, K_w	0.8	$W.m^{-1}K^{-1}$

4.4 Result and discussion

This study aimed to characterise the RTD behaviour of CMBOC for a range of operating conditions and to develop a correlation between the RTD behaviour of the system against the net flow and oscillatory conditions. The effect of frequency and amplitude was investigated for four net flow rates corresponding to Re_o. The experiments were performed by applying the tanks-in-series model over a range of oscillatory frequencies (1–3 Hz), and amplitudes (5–20 mm) were also investigated with a net flow through the CMBOC cascade ranging from 1–30 mL.min−1. **Table 4-3** and **Table 4-4** for the liquid and solid RTDs

respectively summarise the results of all the operating conditions and their effect on the final RTD of the system.

4.4.1 Residence time distribution (Liquid)

The data presented for liquid tracer experiments were examined using a tank-in-series model to understand the effect of oscillation parameters and flow rates on the RTD.

The dimensionless experimental mean residence time, t_m, and variance of dispersion, σ^2, were calculated against the Re_o, which is used here to define the mixing intensity in the CMBOC. Smaller variance values correspond to a more uniform and narrower RTD and are expected to deliver a more consistent product. Fluid oscillation is coupled with the net flow, σ^2 is affected by three parameters: oscillation frequency, amplitude, and net flow rate [212]. The tanks-in-series model for the liquid RTD was applied for two and four-vessel cascade arrangements. Under all the investigated conditions, a good fit was obtained between the experimental data and the theoretical liquid RTD. It also shows a good fit of the theoretical tank-in-series model RTD with experimental conditions, as shown in **Figure 4-16**.

Table 4-3 Experimental details and results from liquid RTD measured in 2nd vessel and 4th vessel, while the tracer injected in 1st vessel.

					2nd Vessel				4th Vessel			
Exp No.	Flow rate (mL/min)	ω (Hz)	x_0 (mm)	Re_o	T(min)	$\bar{t}$ (min)	t_m	σ^2	T (min)	$\bar{t}$ (min)	t_m	σ^2
1	5	2	10	1568	48.0	49.8	1.04	0.21	96.0	95.0	0.99	0.12
2	25	2	10	1568	9.6	9.2	0.95	0.20	19.2	20.4	1.06	0.16
3	5	3	10	2351	48.0	49.9	1.04	0.21	96.0	84.5	0.88	0.10
4	25	3	10	2351	9.6	10.4	1.08	0.22	19.2	20.9	1.09	0.11
5	5	2	20	3135	48.0	51.4	1.07	0.25	96.0	96.2	1.00	0.12
6	25	2	20	3135	9.6	8.9	0.92	0.20	19.2	17.9	0.93	0.11
7	5	3	20	4703	48.0	49.9	1.04	0.20	96.0	92.2	0.96	0.12
8	25	3	20	4703	9.6	9.1	0.95	0.21	19.2	19.2	1.00	0.10
9	1	2.5	15	2939	240.0	228.0	0.95	0.26	480.0	423.0	0.88	0.09
10	29	2.5	15	2939	8.3	8.6	1.04	0.21	16.6	16.6	1.01	0.15
11	15	1.8	15	2116	16.0	16.4	1.02	0.23	32.0	26.3	0.82	0.05
12	15	3.2	15	3762	16.0	17.0	1.06	0.24	32.0	29.3	0.92	0.12
13	15	2.5	8	1568	16.0	16.3	1.02	0.21	32.0	31.9	1.00	0.13
14	15	2.5	22	4311	16.0	18.0	1.13	0.14	32.0	34.8	1.09	0.15
15	15	2.5	15	2939	16.0	16.9	1.06	0.21	32.0	30.8	0.96	0.01
16	15	2.5	15	2939	16.0	16.9	1.06	0.21	32.0	33.8	1.06	0.12
17	15	2.5	15	2939	16.0	13.6	0.85	0.21	32.0	32.4	1.01	0.12

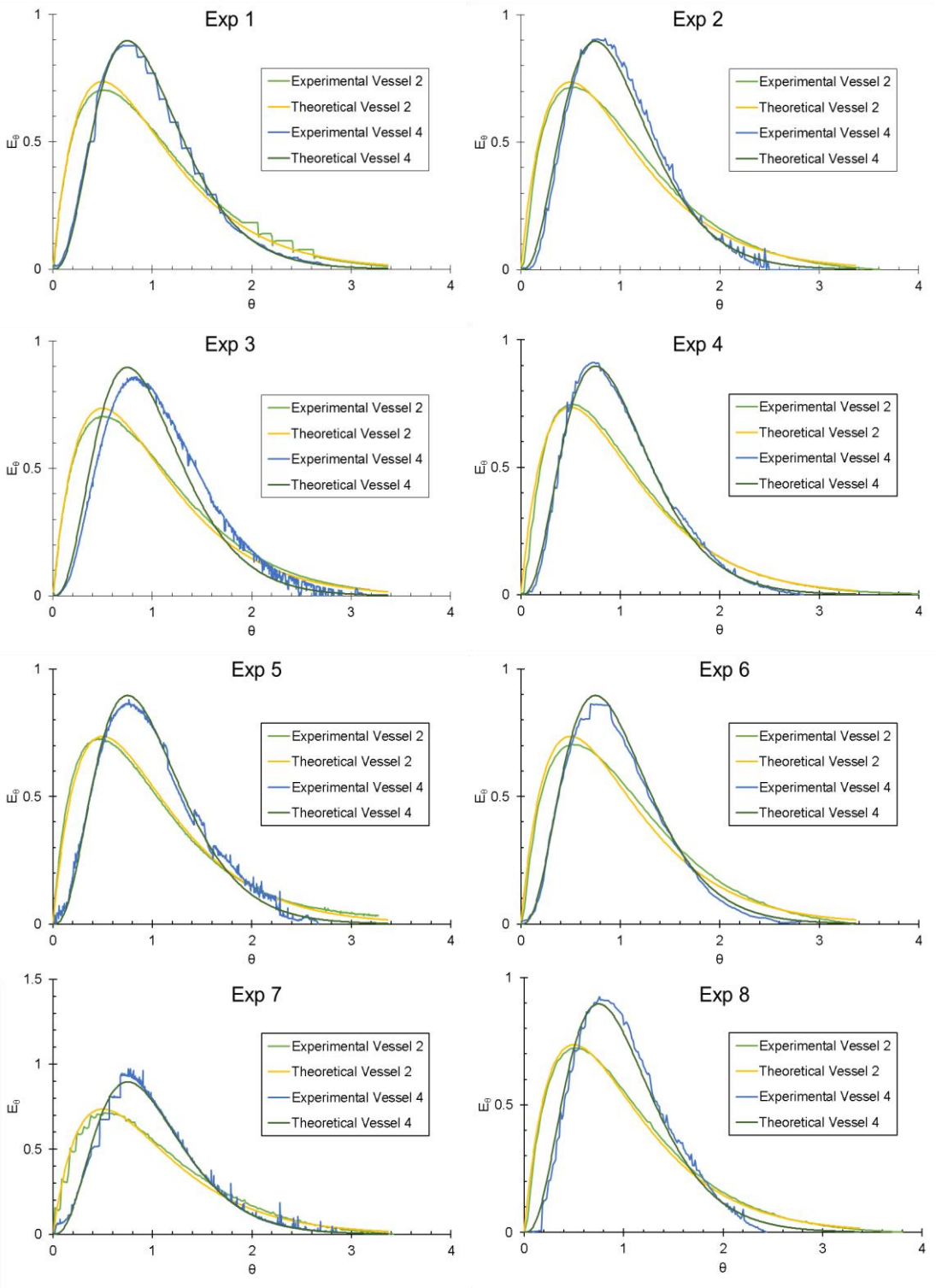

Figure 4-16 Experimental and Theoretical Tanks-in-series model responses for liquid RTD in 2nd and 4th Vessel of CMBOC. The details of the operating condition of each experiment are summarised in Table 4-3.

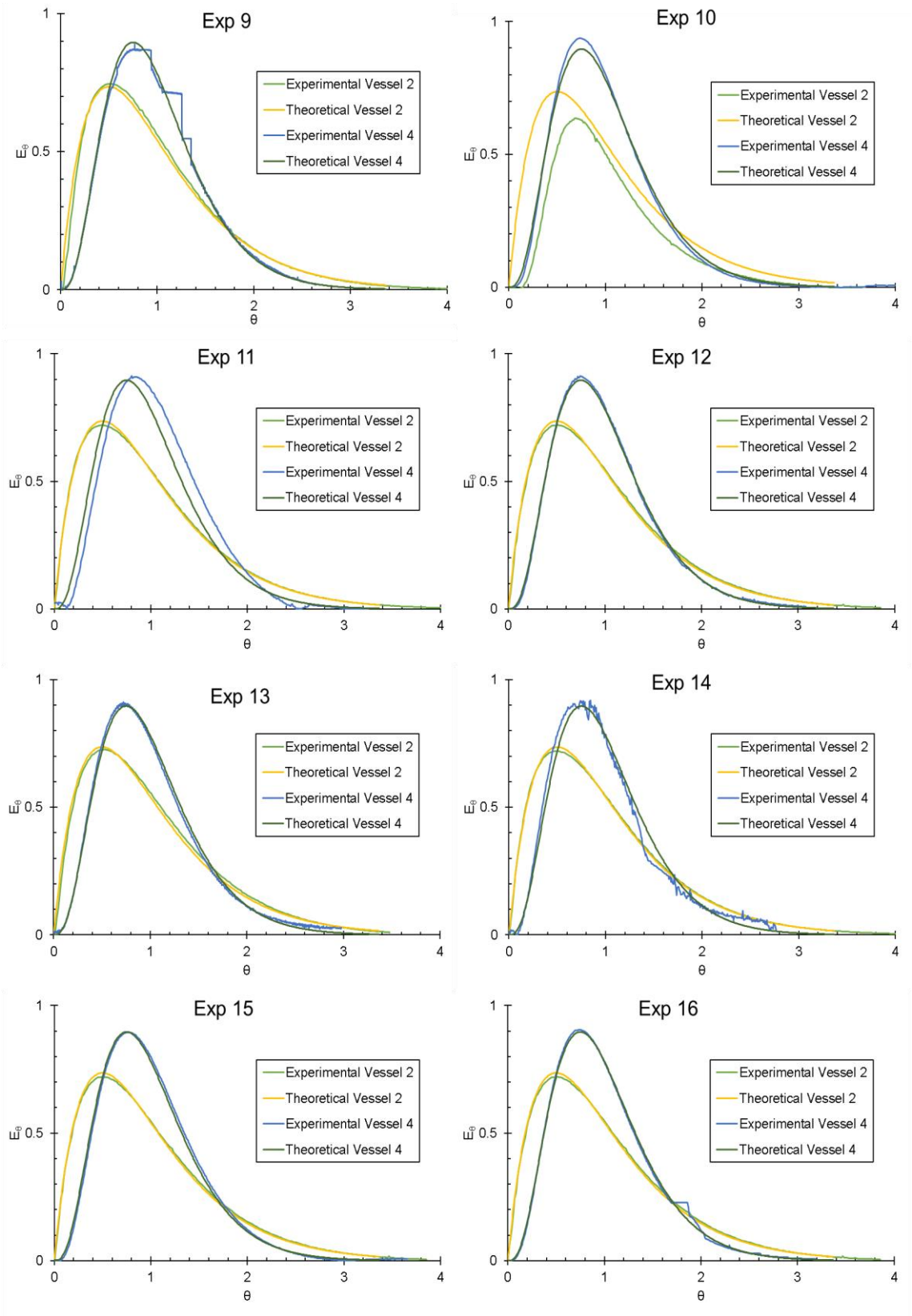

Figure 4-16 Continued…

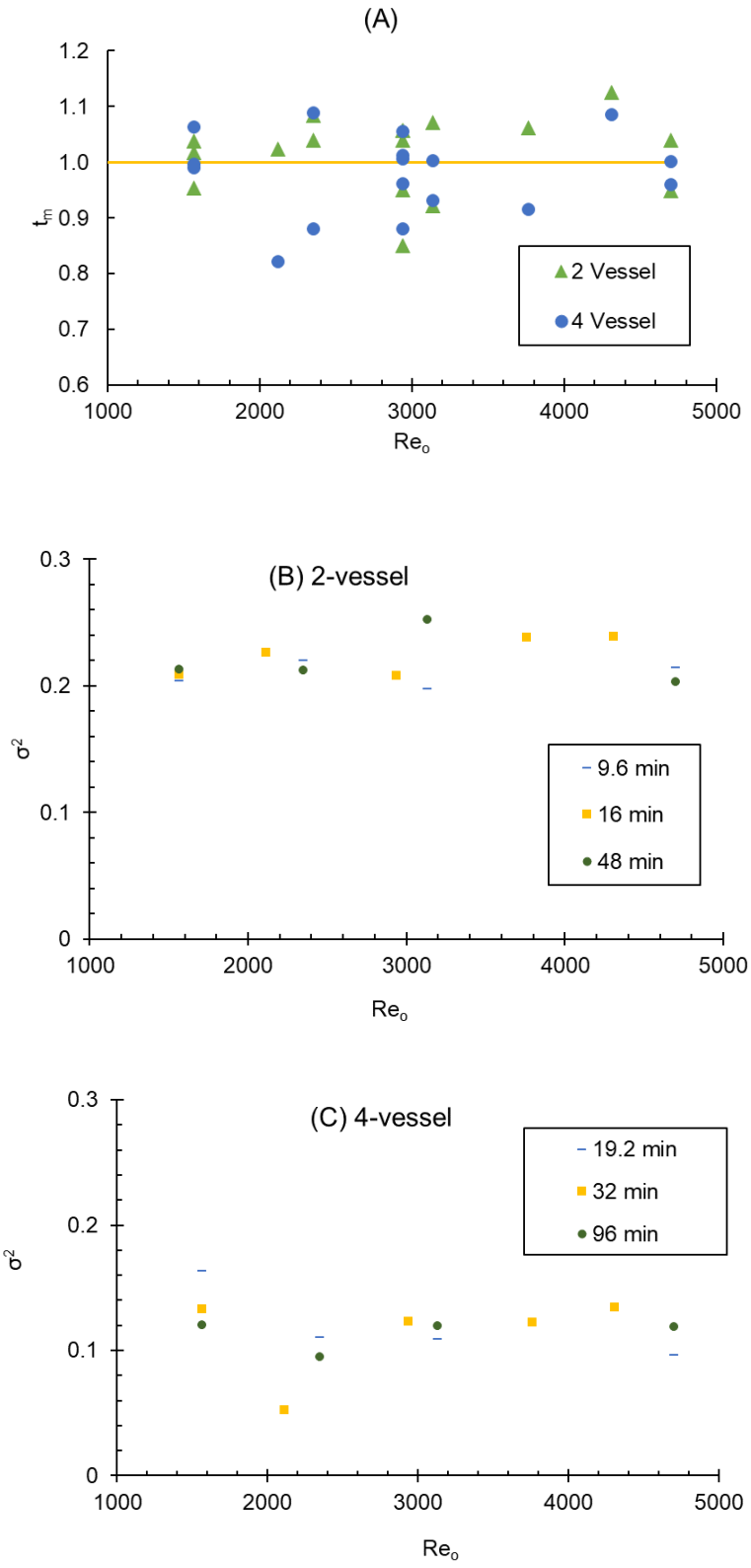

Figure 4-17 Liquid RTD study results (A) Plot of mean residence time, t_m vs Re_o *(B) variance of dispersion, σ^2 vs Re_o in 2nd vessel (c) variance of dispersion, σ^2 vs* Re_o *in 4 th vessel*

The liquid RTD was assessed in 2nd and 4th -vessel. The selection of the number of vessels for a specific process depends on several factors. For example, in crystallisation processes, the number of stages can be selected based on supersaturation limits and the required final yield [213]. For both vessel configurations tested here, the experimental mean residence time, t_m, was very close to the theoretical mean residence time, T (Figure 4-17 (A)). These results indicate an excellent overall mixing performance with no significant dead volumes or short-circuiting. For the two vessel arrangement (Figure 4-17 (A)), σ^2 was higher (average ~0.2) compared to the value obtained from the 4th vessel (Figure 4-17 (A))(average ~0.1) as expected.

4.4.2 Residence time distribution (Solid)

The mixing and flow performance was also assessed for slurries to assess the platform's suitability to run continuous crystallisations. The tanks-in-series model reasonably fits the experimental RTD and theoretical RTD for lower to moderate frequencies and net flow rates (1-2 Hz and 5-20 mL.min^{-1}, see **Figure 4-18)**. However, a more significant deviation from the theoretical RTD has been observed at higher frequencies and a high net flow rate (3Hz and 25 mL.min^{-1}).

This indicates an operating window for effective mixing conditions with slurries based on the current geometry of the platform. Operation outside of this range (<2000 Re_o, > 20 mL.min^{-1}) will lead to short-circuiting and dead zone formation. The system will no longer be close to an ideal mixing regime and impact the consistency and quality of the product.

A similar trend is observed for the mean residence time, t_m, as discussed in the liquid RTD section above. Results related to the increase in variance, σ^2, on moving from 1st vessel (average ~0.4) (**Figure 4-19 (B)**) to 4th vessels (average ~0.2) (**Figure 4-19 (A))** were similar to those observed for the liquid RTD. The σ^2 value for solids was almost double that of the liquid only RTD. This is in line with similar results reported elsewhere for solid RTDs [116, 214].

This increase in variance is ascribed to the non-Newtonian behaviour of the suspension of particles compared to a solution not accounted for in the tanks-in-series model [116]. Another important factor for the increase in variance

comes from the method used to inject the tracer pulse. A potential deviation from the model theory is that the slurry pulse was injected over ca. 10 sec compared to the liquid RTD pulse that was able to be injected near instantaneously.

Table 4-4 Experimental details and results for Solid RTD measured in 1st and 4th vessel while solid tracer injected in 1st vessel

					1st Vessel				4th Vessel			
Exp No	**flow rate (mL/min)**	**ω (Hz)**	**x_0 (mm)**	**Re_o**	**$\bar{T}$ (min)**	**$\bar{t}$ (min)**	**t_m**	**σ^2**	**$\bar{T}$ (min)**	**$\bar{t}$ (min)**	**t_m**	**σ^2**
1	5	2	20	3135	24.0	31.2	1.3	0.5	96.0	53.5	0.6	0.2
2	25	2	20	3135	4.8	10.8	2.3	0.5	19.2	19.6	1.0	0.2
3	5	2.5	10	1960	24.0	14.6	0.6	0.8	96.0	48.8	0.5	0.2
4	25	2.5	10	1960	4.8	6.0	1.3	0.4	19.2	18.2	0.9	0.2
5	5	3	10	2351	24.0	13.8	0.6	0.3	96.0	49.8	0.5	0.2
6	25	3	10	2351	4.8	5.1	1.1	0.4	19.2	17.3	0.9	0.2
7	5	2	10	1568	24.0	11.6	0.5	0.4	96.0	40.8	0.4	0.3
8	25	2	10	1568	4.8	4.2	0.9	0.4	19.2	18.0	0.9	0.4
9	5	2.5	20	3919	24.0	8.1	0.3	1.0	96.0	31.0	0.3	0.2
10	25	2.5	20	3919	4.8	3.0	0.6	0.5	19.2	20.3	1.1	0.5
11	5	3	20	4703	24.0	6.6	0.3	0.4	96.0	23.8	0.2	0.2
12	25	3	20	4703	4.8	3.3	0.7	0.5	19.2	13.1	0.7	0.5
13	15	2.5	10	1960	8.0	7.3	0.9	0.4	32.0	21.6	0.7	0.2
14	15	2.5	10	1960	8.0	7.1	0.9	0.4	32.0	22.0	0.7	0.2
15	15	2.5	10	1960	8.0	7.4	0.9	0.4	32.0	23.3	0.7	0.2
16	12	3	20	4703	10.0	3.9	0.4	0.6	40.0	13.5	0.3	0.4

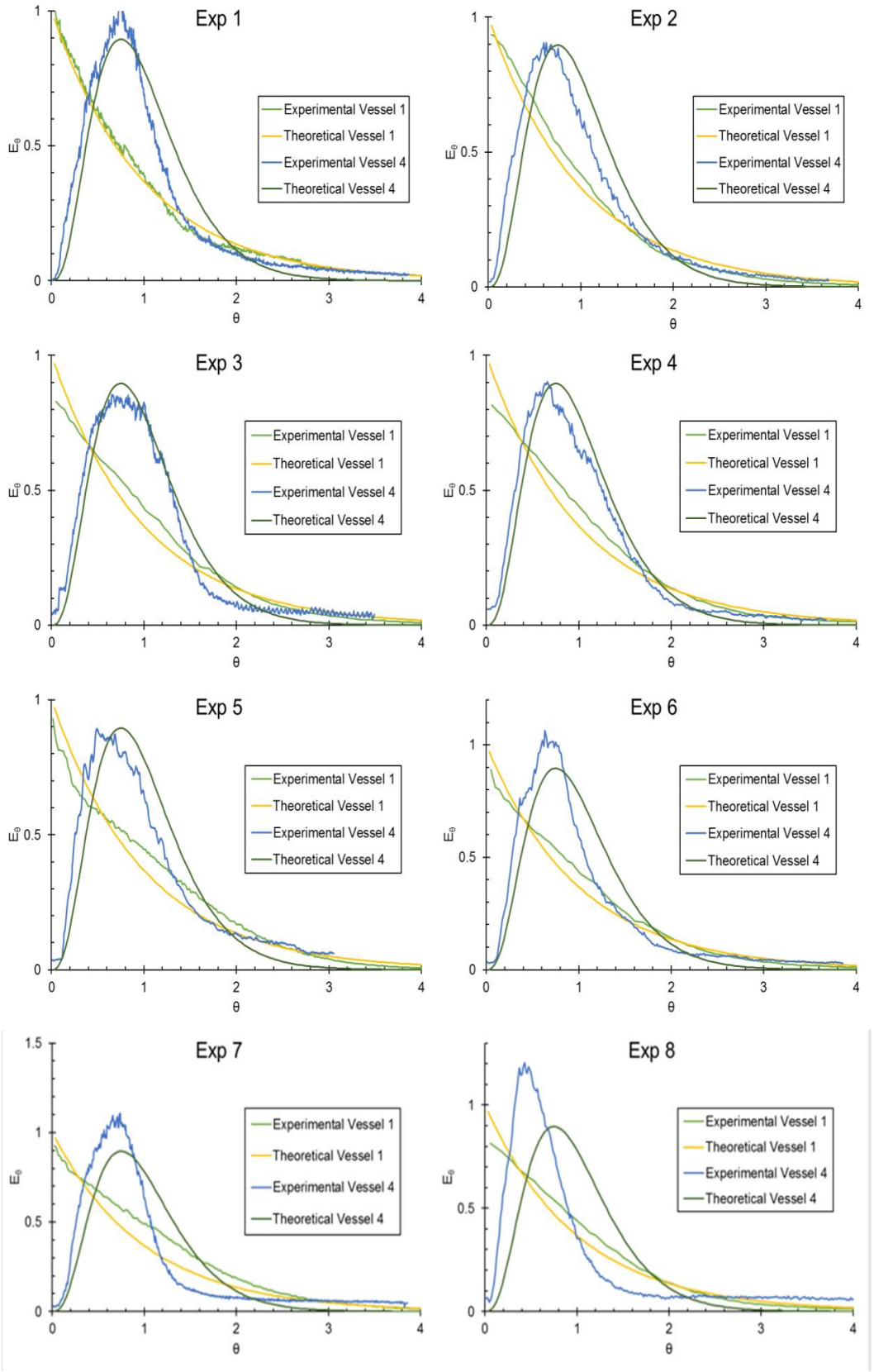

Figure 4-18 Experimental and Theoretical Tanks-in-series model responses for solid RTD in 1st and 4th Vessel of CMBOC.The details of operating condition of each experiments are summarised in Table 4-4.

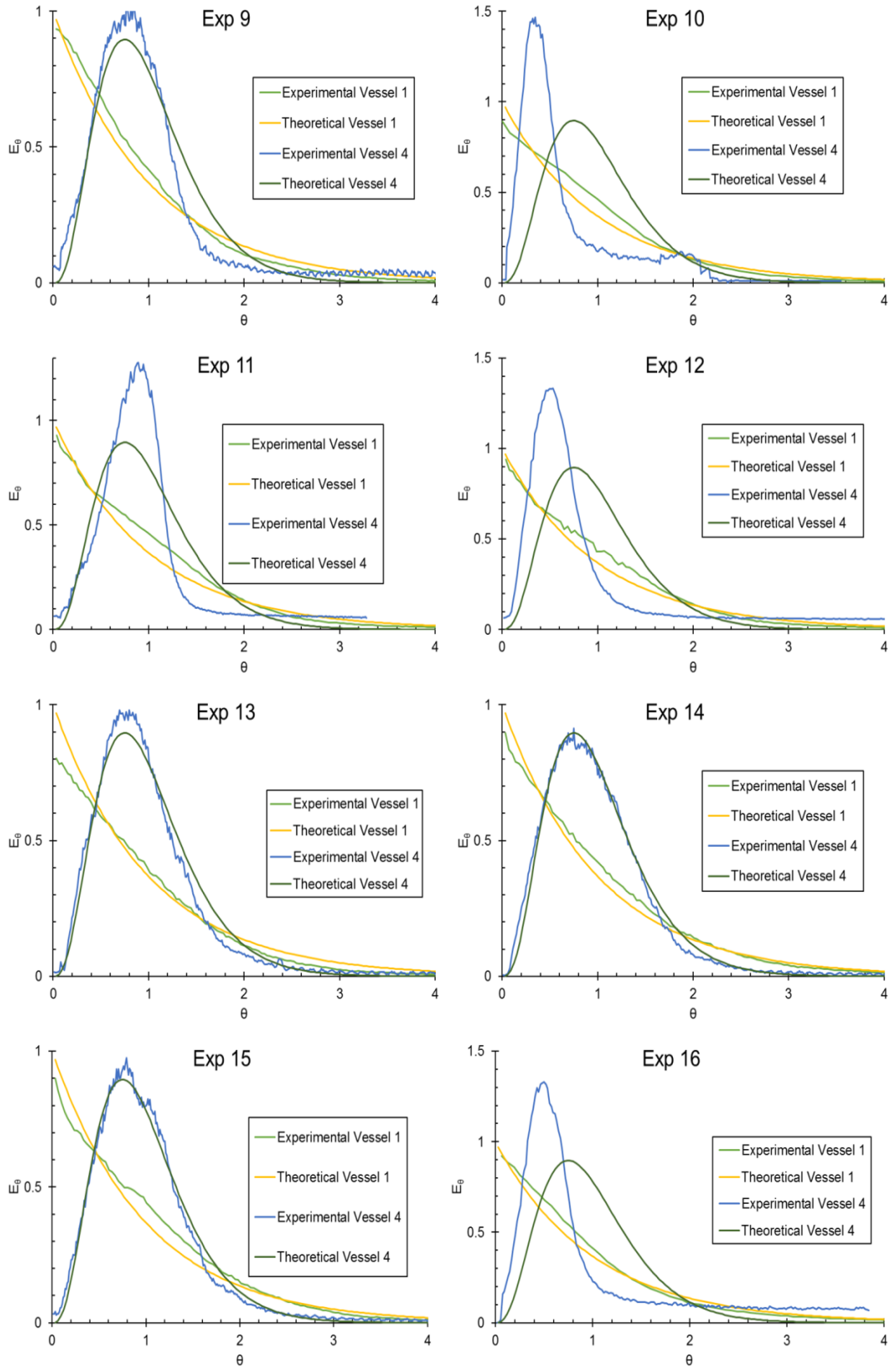

Figure 4-18 Continued...

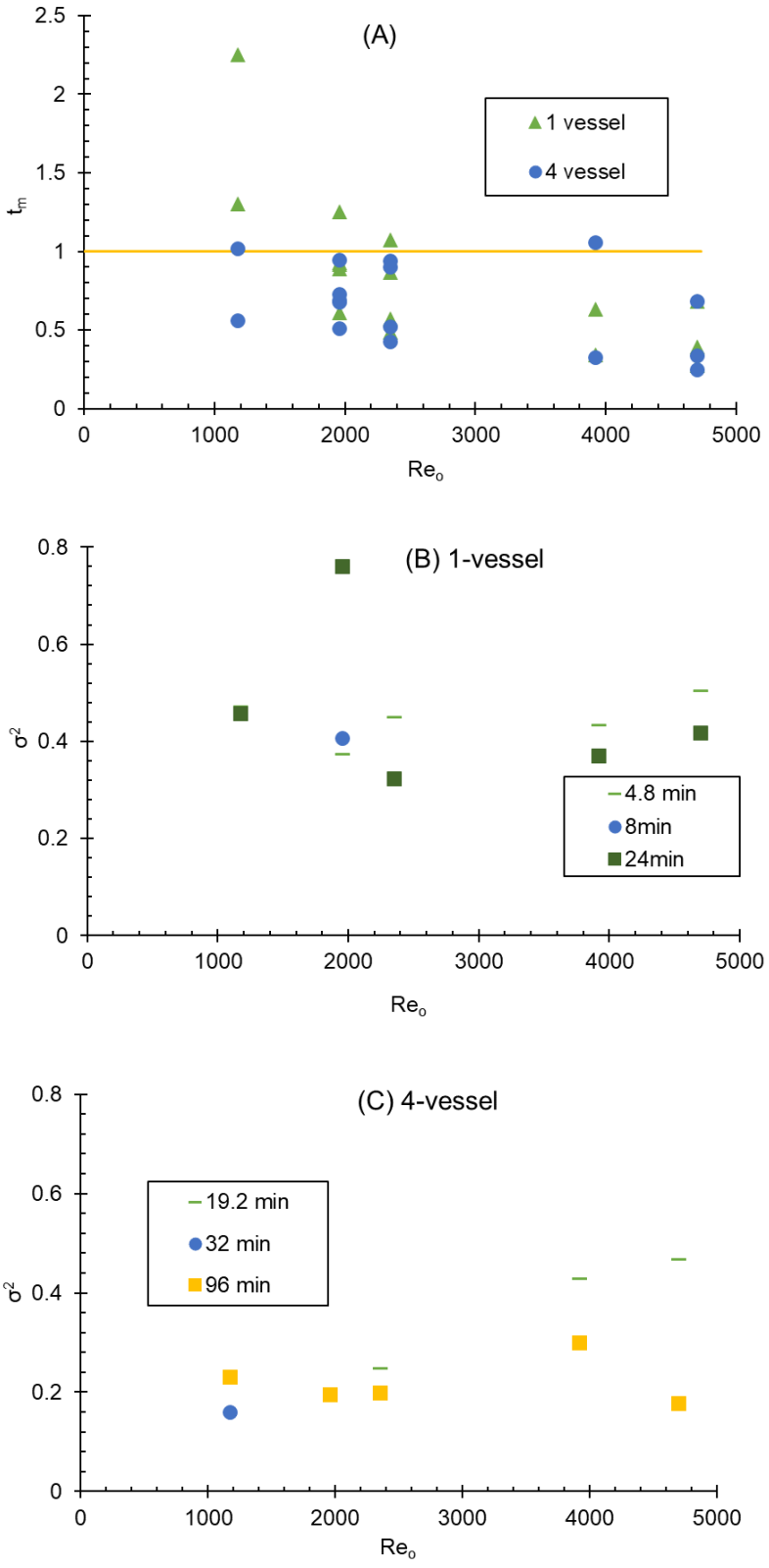

Figure 4-19 Solid RTD study results (A) Plot of mean residence time, t_m vs Re_o (B) variance of dispersion, σ^2 vs Re_o in the 1st vessel (c) variance of dispersion, σ^2 vs Re_o in the 4th vessel.

4.4.3 Heat transfer

The heat transfer coefficient increased consistently with increasing oscillatory Reynolds number, Re_o (

Figure 4-20**)**. These results are consistent with previously published data on the heat transfer performance of an MBOC [102]. Stephens *et al.* investigated the heat transfer performance of oscillatory flow crystalliser with fixed baffles and with moving baffle arrangements. Comparing the heat transfer coefficient in these geometries with a stirred tank reactor based on similar power densities indicated that comparable heat transfer coefficients to the STC are achievable in these reactors at very low Re_o values [102]. It has been reported that the heat transfer performance of a batch MBOC is similar to a continuous tubular crystalliser operating under turbulent regimes [102]. Adding net flow on top of oscillatory flow further enhances the heat transfer performance.

CMBOC and tubular crystallisers have higher surface-to-volume ratios than CSTR, making them more efficient in providing uniform heat transfer performance with minimal disturbances [215, 216]. The heat transfer characterisation indicates that this system can effectively deal with processes where temperature control is crucial for achieving desired product specifications, e.g. controlled supersaturation and heat removal in exothermic reactions.

Table 4-5 Heat transfer calculation experimental conditions.

Sr No	ω (Hz)	x0 (mm)	Re_o	h_t (W/m^{2}K)	h_s (W/m^{2}K)	h (W/m^{2}K)	Nu_t
1	2.5	20	3919	1099	511	293	46
2	0.5	20	784	665	511	249	28
3	0	0	0.0	464	511	215	19
4	3	5	1176	952	511	282	39
5	1.5	10	1176	952	511	282	39
6	0.8	20	1254	920	511	279	38

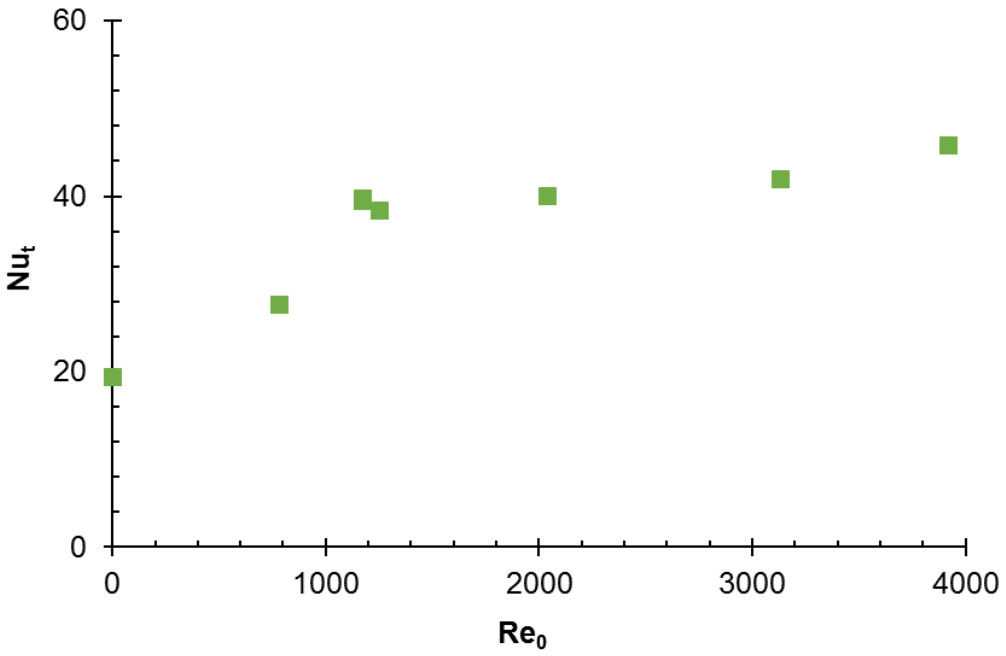

Figure 4-20 Effect of oscillatory Reynolds number on the tube side Nusselt number, Nu_t

4.5 Platform assessment for continuous crystallisation

The platform was specifically designed to support the requirements of performing continuous operations such as mixing, synthesis and crystallisation. Having determined the heat transfer characteristics and the liquid and the slurry mixing performance, the CMBOC platform was evaluated by performing the continuous crystallisation of two different APIs, ALM and PCM, that require residence times (RT) of 90 and 20 min, respectively hence testing a wide range of operating conditions for the CMOBC platform.

4.5.1 Continuous cooling Crystallisation of ALM

ALM is widely used as an excipient in pharmaceutical products, particularly tablets and inhaled formulations [180]. The crystallisation of lactose has been studied extensively, where it can be used to control purity, form control, particle size, and shape [181, 217-220].

Industrial challenges include delivering specific particle size distributions to avoid reliance on secondary processes such as sieving and achieving high

product yields. Hence, the aim was to achieve a narrow particle size distribution span (target, 1.2 – 1.6) without compromising yield (target = min 60%). Operating parameters, including cooling profile, RT, and seed loading for the continuous crystallisation, were selected using a lactose crystallisation model. The model development for ALM is described in detail in Chapter 6. For this case study, a basic model was developed from data collected following a sequential parameter estimation approach [169] in a batch MBOC. (More details about the model can be found in Chapter 6). A 90 min mean RT for a four-stage CMBOC was required to achieve the specific target d[50]= 65 µm with an overall yield of 60%. The target yield was based on the commercially reported yield for ALM [181, 219]. Oscillatory conditions were selected based on the RTD results presented above. A frequency of 2 Hz and amplitude of 20 mm was used to minimise axial dispersion at a net flow rate of 4.4 $g.min^{-1}$.

The saturated aqueous seed slurry at 55 °C with a D[50] =32 µm and a span of 1.1 was introduced continuously at 0.62 g.min-1 to maintain a seed loading of 1% entering in the first vessel at a supersaturation of 1.4. The solution concentration and the time for crystallisation to achieve steady-state were monitored using an ATR mid-IR probe (ReactIR15) in the second vessel and FBRM in the fourth vessel (trends shown in

Figure 4-22). Steady-state was achieved by the end of the third RT, and the system was operated for a further 7 RT after approaching the steady state. The process start-up from an empty platform involved pumping a saturated aqueous feed solution (46.7 wt %) at 70 ˚C into the first vessel. Initially, temperature control was achieved by controlling all the jacket temperatures at 70 ˚C, and once all the vessels were filled with feed, the temperature in each vessel was controlled using a feedback APC temperature controller with vessel set point temperatures of 55, 44, 37 and 20 ˚C, for 1 to 4 vessels respectively (

Figure 4-21). Product from the final stage was analysed at the end of each RT using laser diffraction, XRPD and microscopy.

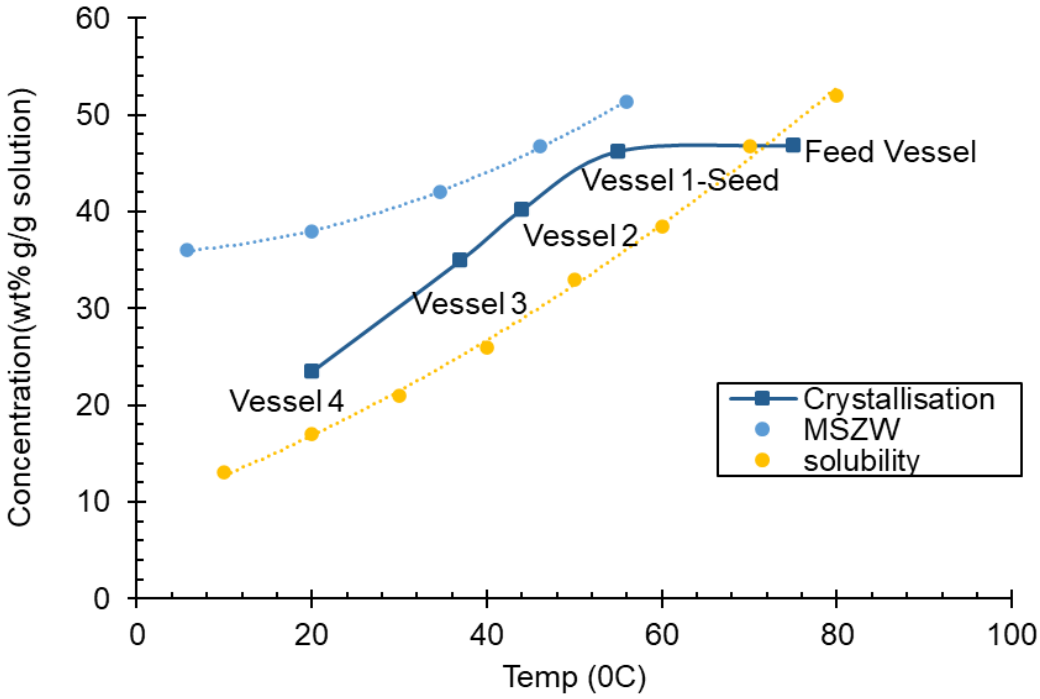

Figure 4-21 Concentration in feed vessel and in each vessel during ALM continuous cooling crystallisation of 4-stage CMBOC

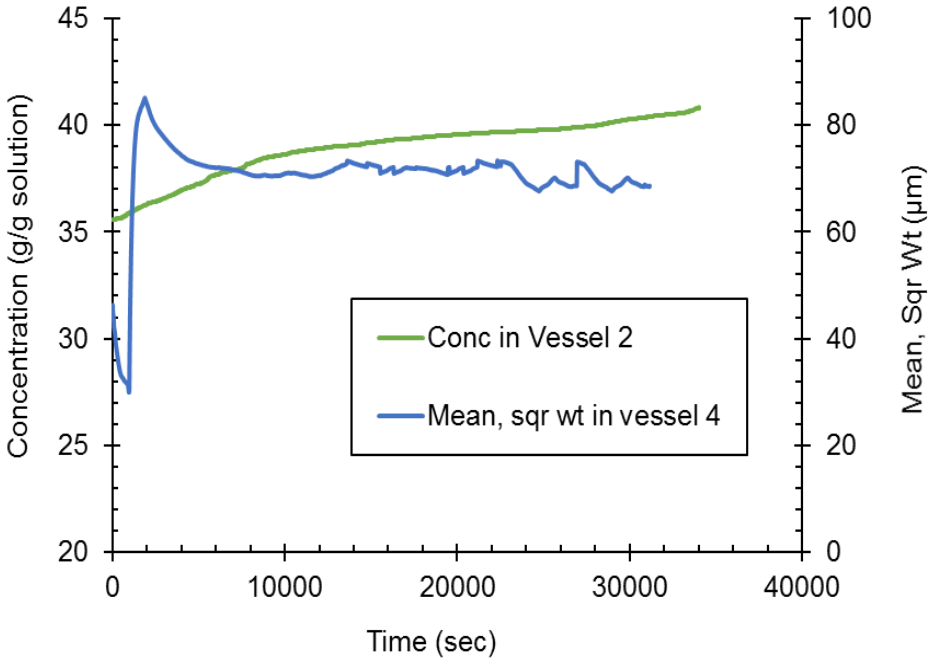

Figure 4-22 FBRM mean square weight trend in 2nd vessel and infrared spectroscopic data in 4th vessel for ALM crystallisation case study.

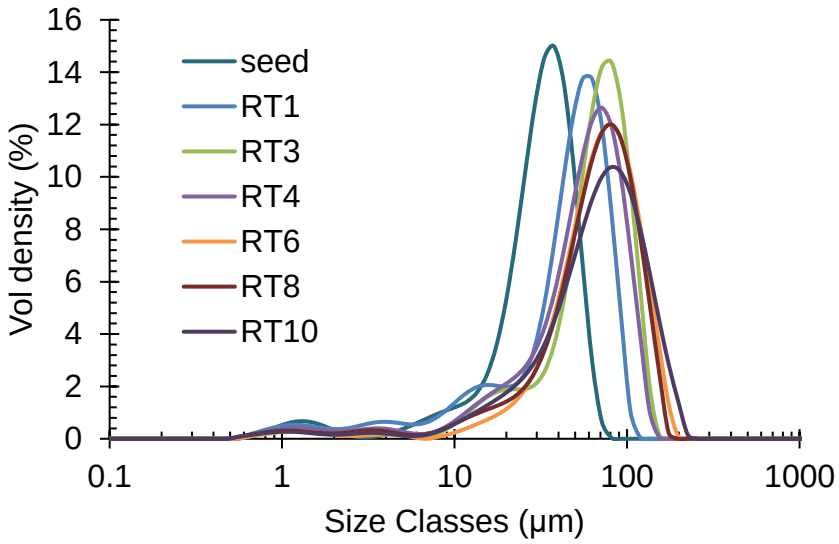

Figure 4-23 shows the evolution of the PSD as volume density vs size at different residence times.

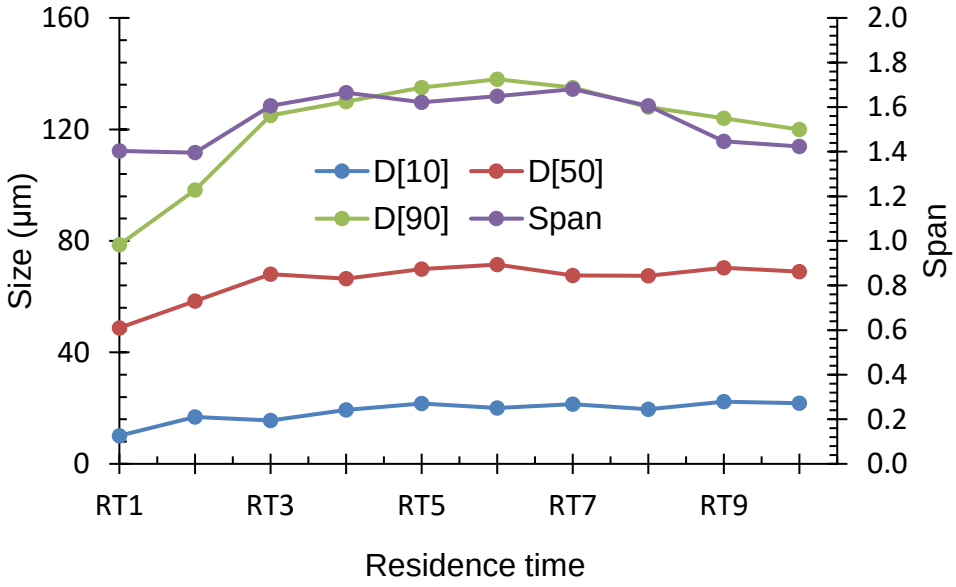

Figure 4-24 Comparison of D[10], D[50], D[90] and span at different residence time for ALM showing approaching the steady state of the process.

The product PSD was consistent from the third RT onwards, indicating steady-state operation. During the process, no signs of fouling or blockages were observed in the transfer lines. Crystals obtained from the CMBOC had a narrow PSD with D50 = 65 ± 5µm and a span of 1.4 ± 0.2 and were non-

agglomerated (**Figure 4-23** and **Figure 4-24**) with the expected well-defined 'tomahawk' shape as shown in the microscopic image in **Figure 4-25** [221, 222]. Crystal form was confirmed using the XRPD sample taken from the bulk product and was of the target non-hydrate form, as shown in **Figure 4-26**. An overall yield of 70% of ALM was achieved. By comparison, commercially available lactose shows a bimodal distribution with a particle span greater than 2 [181].

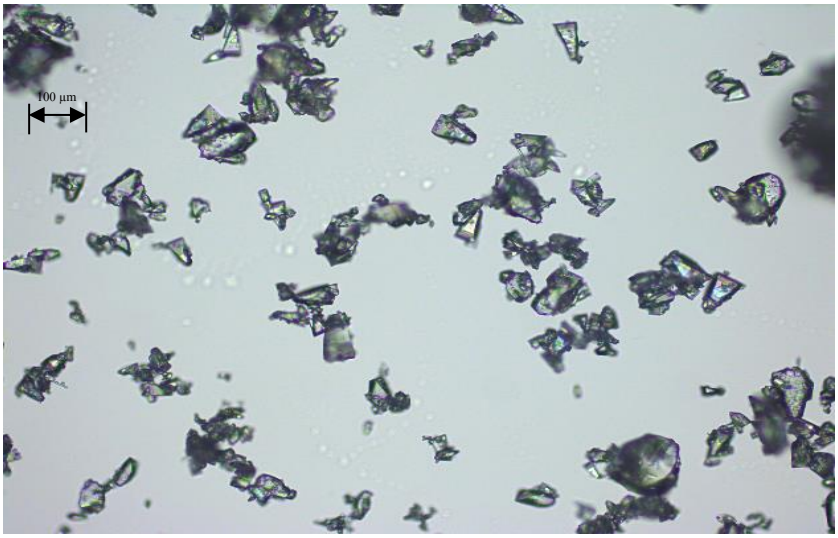

Figure 4-25 *Microscopic* image conforming the *tomahawk shape of ALM crystals product.*

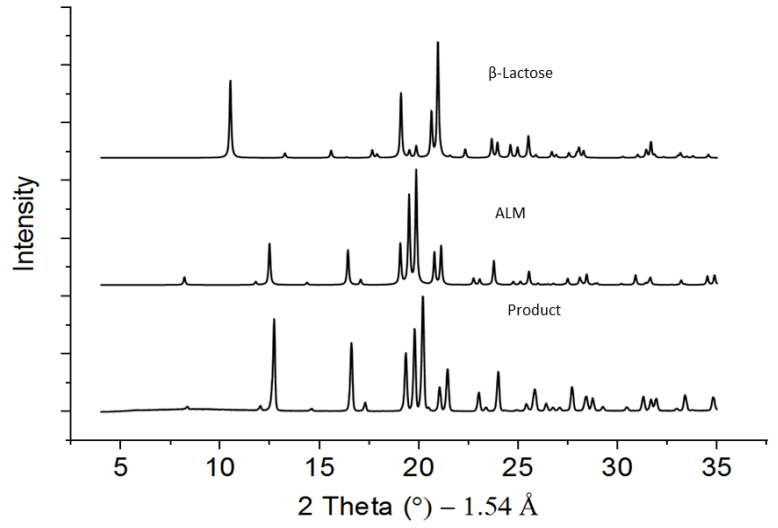

Figure 4-26 X-ray powder diffraction patterns for ALM, β-Lactose and Product

4.5.2 Continuous cooling crystallisation of PCM

PCM is widely used as an analgesic and antipyretic and has been studied extensively from a process point of view [182-184]. Extensive work has been carried out on the monitoring and production of PCM in batch crystalliser [182]. A few studies have been conducted on PCM's continuous crystallisation in MSMPR and PFR platforms [184-187].

Several reports have shown fouling problems and blockages of transfer lines during the continuous crystallisation of PCM [183]. This case study aimed to investigate the feasibility of this platform in performing continuous crystallisation of PCM to deliver form and size control whilst avoiding fouling and agglomeration. The successful operation was expected based on the uniform mixing and narrow shear distribution in the CMBOC, leading to a less agglomerated product [116]. Crystallisation conditions were selected from preliminary work conducted by Brown *et al.* to develop a seeded cooling continuous crystallisation workflow [150].

PCM crystallisation was performed for five RT, where one RT was 20 min. A frequency of 2 Hz and amplitude of 20 mm was used as the oscillatory conditions for effective mixing at the feed flow rate of 18 $g.min^{-1}$. The feed solution concentration of 34.1 g/kg solvent in 60:40 volume of water: isopropanol system. The saturated seed slurry with a d[50] =287 µm was introduced continuously into the first vessel at a flow rate of 5 $g.min^{-1}$ with a seed loading of 10 wt. % where the temperature was set to achieve a supersaturation ratio of 1.38. The feed vessel was kept at 50 °C, and a linear temperature profile was established by maintaining the temperature of four stages at 40, 30, 20 and 10 °C, respectively (**Figure 4-27**). Initially, temperature control was achieved by controlling all the jacket temperatures at 45 °C. Once all the vessels were filled with feed, the temperature in each vessel was controlled using a feedback APC temperature controller.

The process was observed to be approaching steady-state by the third RT, which was monitored using offline PSD measurement and an In-line FBRM probe positioned in 1st and 4th vessel, as shown in **Figure 4-28**. FBRM placed

in vessel 1st vessel showed upward trend in steady-state during the crystallisation.

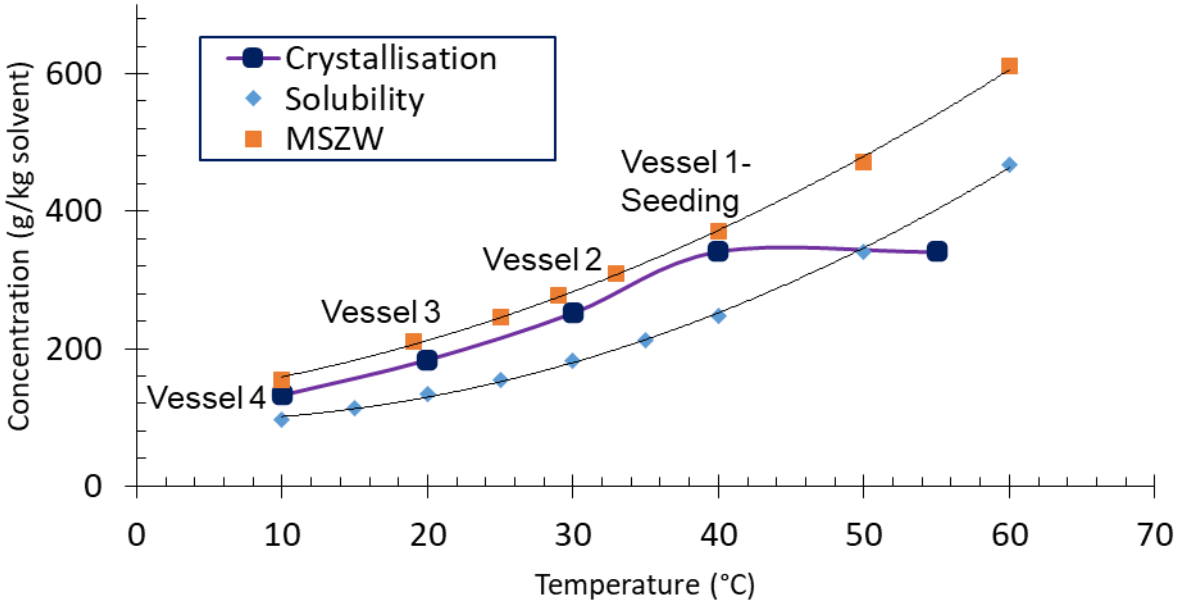

Figure 4-27 Concentration profile in each vessel during PCM continuous cooling crystallisation in 4 stage CMBOC.

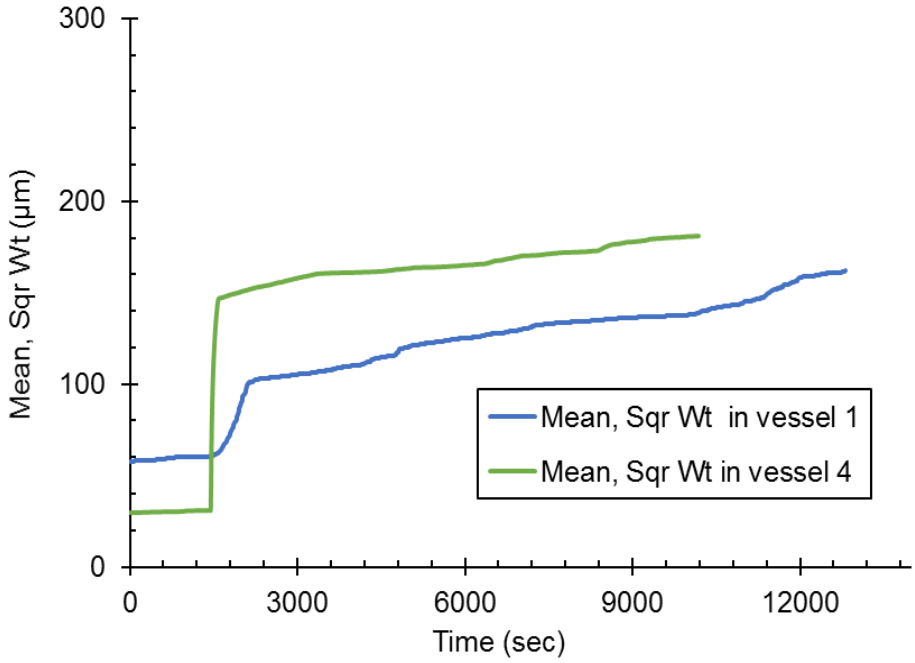

Figure 4-28 FBRM mean square weight trend measured in 1st vessel and 4th vessel for the PCM case study.

The PSD was also consistent by the third RT with a measured d[50] =398 ± 20 µm and a span of 1.5 ± 0.2, shown in **Figure 4-29**. The product was non-agglomerated and well-defined prismatic crystal shapes, as shown in **Figure 4-30**.

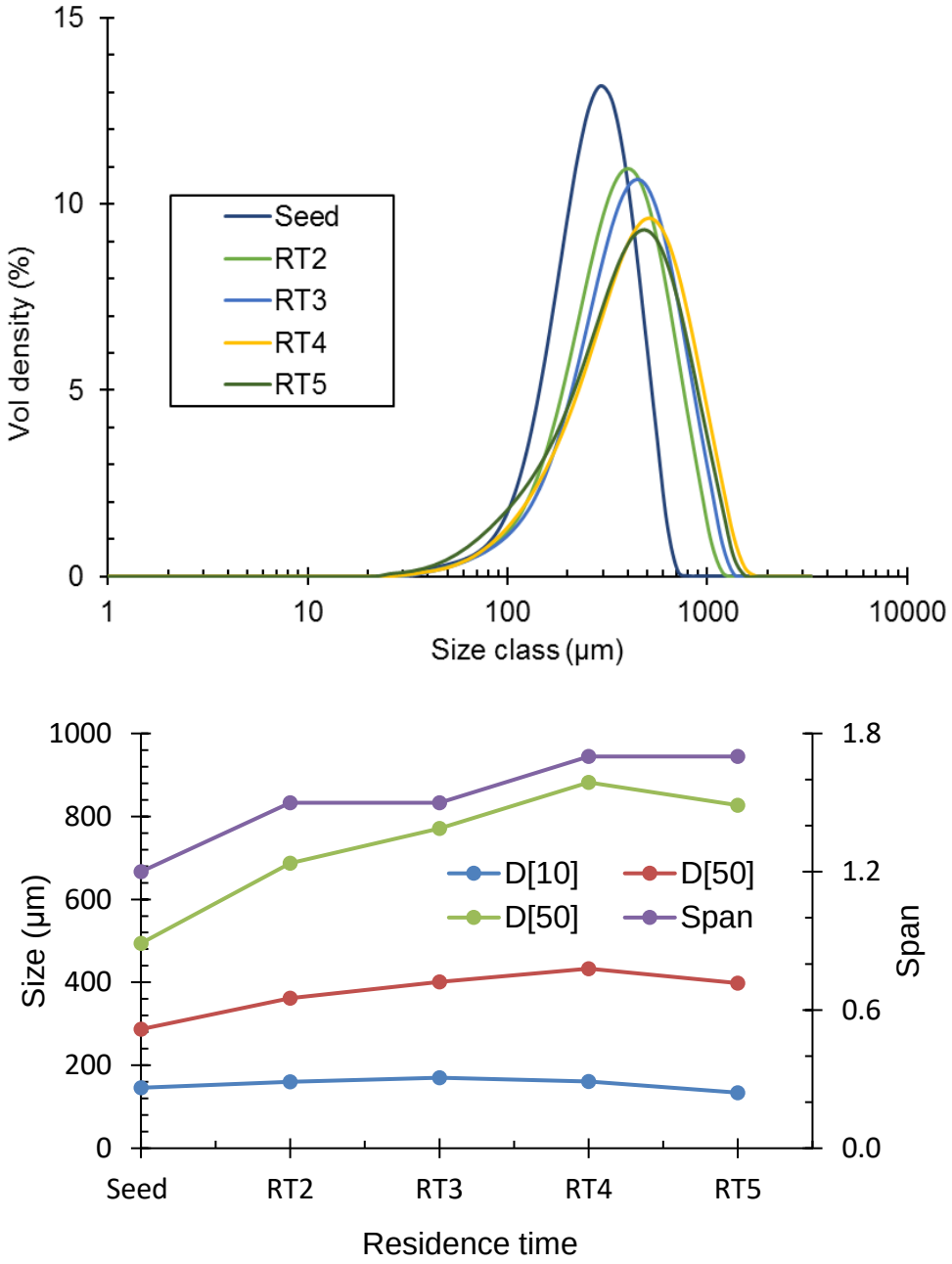

Figure 4-29 Evolution of PSD measurement at different residence time of PCM product

An average thermodynamically achievable yield of 85% was achieved with no evidence of fouling in the vessels and no blockage of the transfer lines

observed. The crystals obtained at the end of the process were confirmed to be the target form I PCM, as shown in **Figure 4-31**.

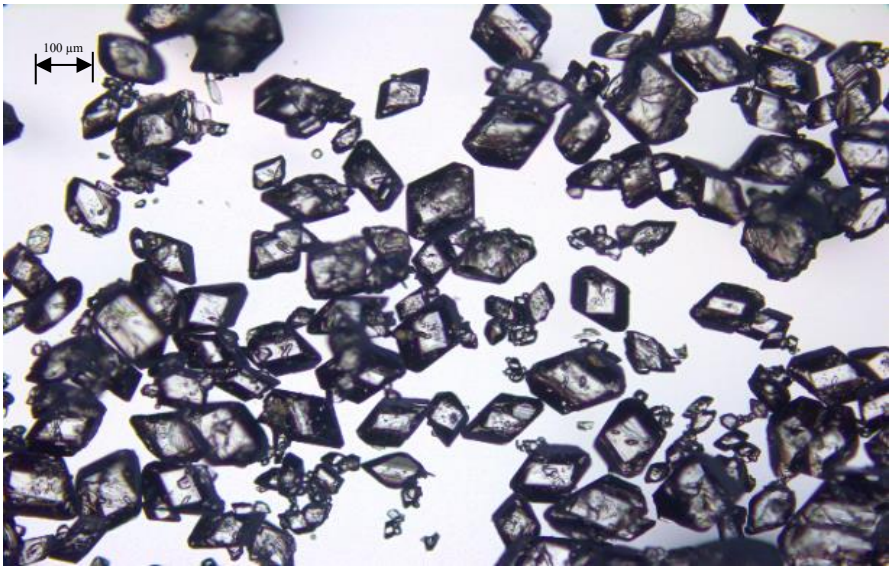

Figure 4-30 Microscopic image of the PCM product.

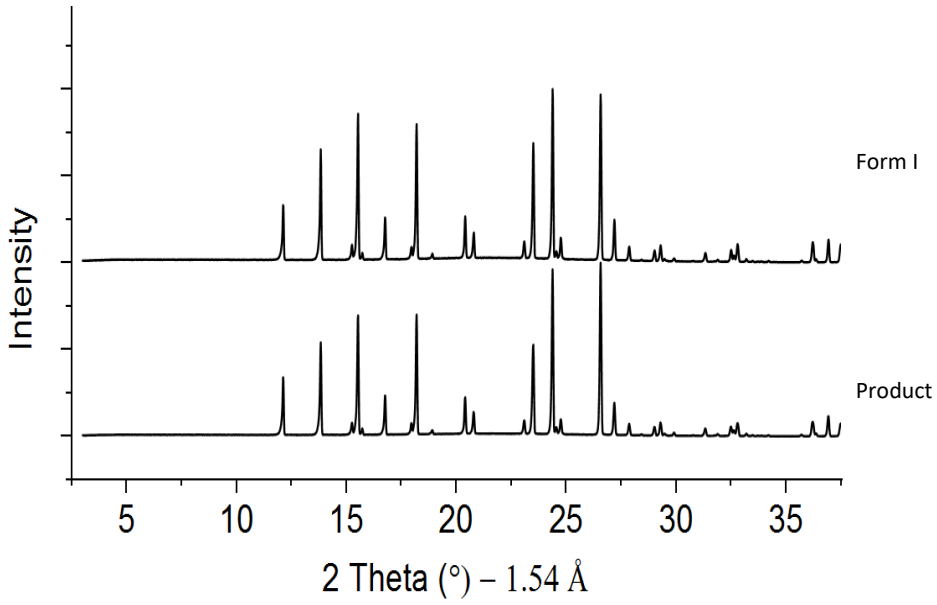

Figure 4-31 X-ray powder diffraction patterns for PCM product.

Based on the total RT, the change in median particle size, and the achieved yield, an experimentally measured overall average growth rate of 8.90×10^{-8} $m.s^{-1}$ was estimated, which was calculated from **Equation 4-16** [21]. This is comparable to experimentally measured values of 0.67 to

2.56x10^{-8} m.s^{-1} were previously reported in a similar solvent system [223] and are within the range (3.47 to 18.08x10^{-8} m.s^{-1}) of values estimated for a size-dependent growth model [223]. The overall growth rate, G, (m.s^{-1}) in terms of mass deposited per unit time per unit area of crystal surface by measuring the mass deposition on a known mass of sized seed crystals under controlled conditions can be calculated as,

$$G = \frac{M_i^{\frac{1}{3}} - M_f^{\frac{1}{3}}}{(\alpha \rho N)^{\frac{1}{3}} * t}$$ **Equation 4-16**

Where M_i and M_f are the initial and final crystal masses (5.86E-07 and 6.17E-05Kg), respectively, N is the number of individual crystals (1.35E+06), α is their volume shape factor (0.886), ρ is their density (1243 kg m^{-3}), and t is the time (1200 s).

4.6 Operational considerations of the CMBOC

Several operational benefits were identified for the CMBOC based on the two continuous crystallisations performed. The crystallisation start-up procedure, as with other multi-vessel cascade setups, is very efficient as the system can be started by introducing feed and seed flow to the first vessel at time zero with the entire platform initially empty. The process has approached the steady state after the third RTs from time zero. Start-up with empty vessels is possible in a CSTR assembly, but the dead volume is higher in a CSTR than in a CMBOC before it reaches the mixing point due to the format of the baffle insert. The inlet and outlet points for process streams are designed in such a way to avoid dead volumes and short-circuiting, and the RTD studies confirm this. The vessel design also allows for the flexible incorporation of PAT tools. These sensors can be fully integrated into a control system such as APC to provide closed-loop feedback control development and execution [57, 149]. Pressure-induced slurry transfer between stages helped minimize issues related to transfer line blockages [224] and breakage [150] of crystals which were also evidenced from the microscopy images of crystals (**Figure 4-30**). The system maintained particle suspension at a solid loading of over 30%, significantly

higher than is typically achievable for PFRs (~20%) [64, 81]. In moving fluid oscillatory baffled crystallisers, oscillation dampening is a significant issue due to the presence of gas or the extended length of the crystalliser. The CMBOC, therefore, offers the advantage of continuous operation without any dampening due to gas or from using an extended number of stages. Longer mean RTs can be easily accommodated by reducing flow rates and increasing vessel volume. Further flexibility could be achieved by introducing individual motors to control the oscillation conditions in each vessel, which may be beneficial, for example, in controlling the size of agglomerate in SA processing [59, 129, 137].

4.7 Summary

This work presents the development of the CMBOC cascade and its characterisation in mixing, heat transfer, solid and liquid flows. The operability and platform performance were assessed by performing two continuous crystallisations for ALM and PCM. The system was run for up to 10 RT in these tests without any operational issues, and the target process outcomes in terms of crystal form, particle size, and yield were achieved consistently. The key actuator and sensor components of this novel crystalliser platform have been automated with data stream integrated using an APC system to ease set up of equipment and ancillaries (heater chillers and linear motor pumps, and pressure controller) for process start-up and to precisely control all the operating parameters in the crystalliser during operation.

For a broad range of conditions, experimental RTD was consistent with theoretical RTD from a tanks-in-series model, showing efficient and well-mixed mixing performance. More deviation in solid RTD was observed compared to liquid RTD and deviation reduction in 1st vessel to 4th vessel.

This predictable performance allows for ease of process design. The system was also characterised by heat transfer performance, and it was revealed that the oscillatory conditions significantly contribute to the enhanced heat transfer performance of the platform. It can be concluded from the outcomes of the crystallisation operations that this platform can deal with several challenges

related to continuous crystallisation, such as fouling and operating at higher solid loadings. An additional benefit of this platform includes achieving narrow PSDs and lower agglomeration. No evidence of significant attrition was observed during these studies.

Chapter 5. Control system engineering- Lactose Population Balance Equation modelling

5.1 Introduction

5.1.1 Population Balance Equation (PBE)

In industrial crystallisation processes, it is important to achieve the final crystalline product's desired properties, including dissolution behaviour, flow, bioavailability, or filterability and do so consistently. These crystalline properties are directly affected by solid characteristics such as the PSD, crystal shape, polymorphic form and crystal purity. Another important requirement for an industrial crystallisation process is to meet the desired throughput. A balance between the desired product properties and high throughput and yield can be possible using model-based control and optimisation strategies. Hence, a well-characterised, validated process model that accurately describes the crystallisation process can be a great asset in delivering efficient and robust process performance [164, 169].

The major challenge in developing a crystallisation process is to meet the desired objectives of size, yield, purity, polymorphic form and shape. There are many approaches to achieve these objectives, such as model-based, empirical or predictive design approaches [164, 169]. However, it is always difficult to achieve all the desired objectives using these approaches. The PBE modelling framework is a versatile approach that can consider all these properties and is becoming an increasingly widely used approach for developing and designing high-performance crystallisation processes [159].

In most cases, the PSD determines the product quality since many physical properties of the crystalline product are closely related to the size distribution of crystallites produced from the process conditions. The PSD heavily influences the efficiency of downstream processes such as filtration and drying, e.g. where large variations in fines composition can significantly impact cake resistance. Furthermore, the dynamics of the crystallisation process can only be captured if the PSD is considered. PSD changes may occur over time in a crystalliser due to several physical processes such as nucleation, growth, dissolution, breakage and attrition (**Figure 5-1**). The PBE form a framework for the dynamic modelling of crystallisation based on explicit consideration of these rate processes' effect on the resultant PSD and yield. The PBE

describes a first interaction between the population of solid crystals, classified by their size L, and a second ageless population of solute molecules of the constituent in a liquid phase. The equation models the birth, growth and death of crystals, as well as breakage and attrition.

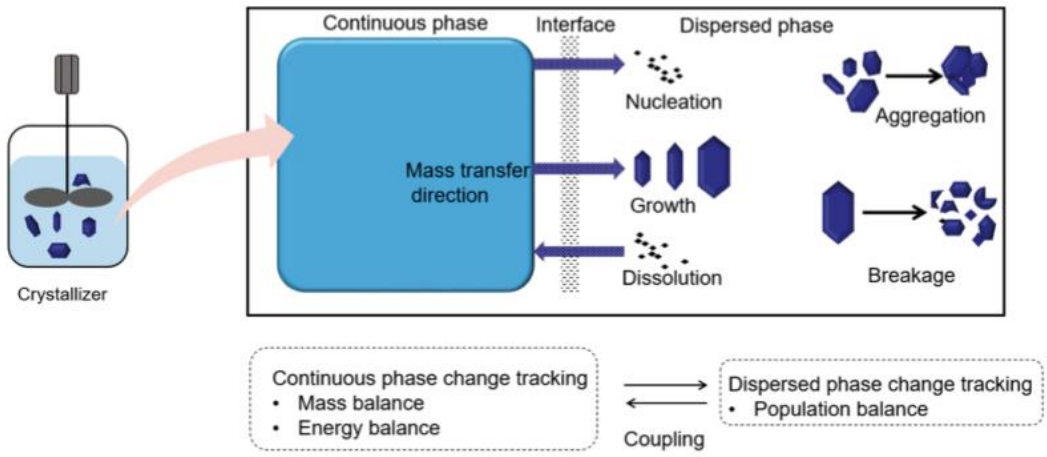

Figure 5-1 Physical processes involved in crystallisation, adapted from Myerson et al.2015 [163]

Table 5-1 Physical processes are discussed in detail in the literature review (section 1.8). This table describes general empirical semi-empirical models describing these processes.

Physical Process	Mechanism	Model equations	Remarks
Nucleation	Homogenous nucleation	$B = k_b exp\left[\frac{-16\pi {\sigma_s}^3 v^2}{3k^3T^3 ln^2(s)}\right]$	
	Heterogeneous nucleation	$B = k_b exp\left[\frac{-16\pi {\sigma_s}^3 v^2 f(\varphi)}{3k^3T^3 ln^2(s)}\right]$	Extra factor f(φ) is to consider foreign surface effects
	Two-step nucleation	$B = \frac{k_2 c_1 T\ exp\left(-\frac{\Delta G^*_2}{k_B T}\right)}{\eta(C_1, T)\left[1 + \frac{U_1}{U_0} exp\left(-\frac{\Delta G^0_c}{k_B T}\right)\right]}$	Two-step nucleation rate model.
	Primary/ secondary nucleation	$B = k_b \sigma^b$ $B = k_b \sigma^b \mu_2$	Commonly used nucleation expression
Growth	Size independent growth	$G = k_g \sigma^g$	Commonly used growth expression
	Temperature-dependent	$G = k_g \sigma^g exp\left(-\frac{E_g}{RT}\right)$	Semi-empirical model
	Size-dependent growth	$G = k_g \sigma^g (1 + \Upsilon L)^p$	Size-dependent model
	Power-law size dependent	$G = k_g \sigma^g L^p$	Size-dependent model
	Size independent dissolution	$G = k_d \sigma^g$	Commonly used dissolution expression
	Size independent dissolution	$G = k_d C_s \sigma$	Dissolution mechanism is controlled by mass transfer

Breakage (functions)	Power-law	λ^k	
	Exponential	$exp(k\lambda)$	
	Tangent hyperbolic	$\frac{1}{2}[\tan h[k(\lambda - L_{crit})] + 1]$	
Agglomeration (Kernels)	Brownian motion	$(L+\lambda)^2$	
	Sum	$L^3 + \lambda^3$	
	Hydrodynamic	$(L+\lambda)^3$	
	Differential force	$(L+\lambda)^2 \lvert L-\lambda \rvert^2$	

B = Nucleation rate (#.m^3.s^{-1})

σ_s=interfacial tension; (J. m^{-2}))

μ_2: second moment

V=molecular volume (m^3)

K=Boltzmann constant K_b = Nucleation rate constant (#.m^3.s^{-1})

G =Growth rate ($m.s^{-1}$)

k_g = Growth rate constant ($m.s^{-1}$), Υ= Parameter of size dependent growth rate model, m^{-1}

K_d = mass transfer coefficient

L, λ= crystal length (µm)

5.1.2 Modelling MSMPR crystallisers

The MSMPR reactor is the most commonly used continuous crystallisation platform and is an analogue of the CSTR with similar modelling assumptions, namely:

- continuous steady flow, steady-state operation
- perfect mixing of around Vessel
- no classification of crystals
- uniform degree of supersaturation
- crystal growth rate independent of crystal size
- uniform temperature
- mother liquor in equilibrium with the crystals
- crystal size distribution is uniform in the crystalliser and equal to that in magma

In the case of PBE of cooling crystallisation in the MSMPR, the state variables modelled are the system volume (V, ml), solute concentration (C, $g.cm^{-3}$), crystalliser temperature (t, ^0C), coolant temperature and the PSD [29]. The crystalliser mass balance, describing the mass accumulation in the MSMPR, can be written as:

$$\frac{d(V\rho)}{dt} = F_f\rho_f - F\rho \qquad \textbf{Equation 5-1}$$

The initial condition V(t = 0) = V_0 gives the volume of suspended crystals and solvent with dissolved solute (m^3) being initially in the crystalliser; subscript f stands for the feed stream, F_f ($m^3.s^{-1}$) is the feed flowrate and F ($m^3.s^{-1}$) is the output flow rate and ρ (kg m^{-3}) is the density. The component balance equation for the crystallising compound, taking into account the liquid-solid mass transfer generated by nucleation (B – with constant nuclei size L_n) and growth (G, $m.s^{-1}$), as well as the impact of feeding and evacuation streams, is:

$$\frac{d(Vc)}{dt} = -Vk_v\rho_c\left[BL_n{}^3 + 3G\int_0^{L_{max}} L^2 n(L,t)dL\right] + F_f c_f - Fc \qquad \textbf{Equation 5-2}$$

The initial condition c(t=0) = C_0 is for the initial concentration (g.cm^{-3}), ρ_c is the crystal density(g.cm^{-3}), and k_V is the volumetric shape factor of the crystal, which is a shape-specific constant, used to relate the crystal volume (V_c)(cm^3) to the linear crystal size as:

$$v_c = K_v L^3 \qquad \textit{Equation 5-3}$$

Crystallisation is associated with releasing the latent heat of crystallisation (ΔH_c). Hence, the heat of crystallisation must be included in the energy balance describing the process. Due to the homogeneous temperature field MSMPR assumption [21], it is considered that the whole mass of suspension absorbs the heat of crystallisation. The energy balance takes into account the impact of feeding and evacuation streams, the heat exchange between the crystalliser slurry and coolant as well as the heat of crystallisation:

$$\frac{d(V\rho c_p T)}{dt} = -\Delta H_c V \rho_c k_v \left[B L_n^{\,3} + 3G \int_0^{L_{max}} L^{\,2} n(L,t) dL\right] + F_f \rho_f c_{p,f} T_f - F\rho c_p T - UA(T - T_{cool}) \qquad \textit{Equation 5-4}$$

Where C_p (J.kg^{-1}.K^{-1}) denotes the specific heat capacity of the slurry, T (°C) is the temperature, and UA (J.s^{-1}.K^{-1}) is the product of the overall heat transfer coefficient and heat transfer area. The energy balance of the coolant, assuming constant coolant volume, takes the form:

$$\frac{dT_{cool}}{dt} = \frac{T_{cool,i} - T_{cool}}{\tau_{cool}} + \frac{UA}{V_{cool}\,\rho_{cool} C_{p,cool}} (T - T_{cool}) \qquad \textit{Equation 5-5}$$

Subject to the T(t = 0) = T_0 and T_{cool}(t = 0) = $T_{cool,0}$ initial conditions, which are the jacket and crystalliser temperatures at the initial moment of time.

For the description of particle population, the monovarietal population density function (often referred to as PSD) is used n(L,t) (# m^{-} m^{-3}), which gives the number of crystals within the (L, L + dL) size range at the time, t, moment (at time t) in the unit volume of suspension. The PSD is governed by the PBE, which, assuming nucleation with constant nuclei size, growth, breakage and agglomeration mechanisms, takes the form:

$$\frac{\partial[Vn(L,t)]}{\partial t} + V\frac{\partial[Gn(L,t)]}{\partial L} = V\left[B\delta(L-L_n) + B_{agg} - D_{agg} + B_{bre} - D_{bre}\right] + F_f n_f(L,t) - Fn(L,t)$$ ***Equation 5-6***

With n(L,t = 0) = $n_{0(}$L) initial, and $\lim_{L\to\infty}$n(L,t) = 0 boundary conditions. The initial condition gives the initial size distribution in the crystalliser (seeds), whereas the boundary condition states that the crystals have a finite size. n_f(L,t) denotes the PSD in the feeding stream: 0 if the crystalliser is fed with liquid only, but n_f(L,t) can represent a continuous seeding PSD of an upstream crystalliser. B_{agg} and B_{bre} are birth (source) functions which describe the production rate of new crystals of size L by agglomeration and breakage. D_{agg} and D_{bre} stand for death (sink) functions for the consumption rate of crystals of size L by agglomeration and breakage. The first section of this Chapter describes the commonly used nucleation, growth and breakage functions. Further assumptions can be made to simplify the model depending on the requirements of a specific process application [150].

5.1.3 Lactose modelling

Specifically, this Chapter sets out to develop a model for the lactose crystallisation process, which is used to build a mechanistic understanding of the key rate processes controlling the process outcomes and, therefore, can be used to predict product attributes against changes to the process conditions. Furthermore, the PBE model developed will be used to design a continuous crystallisation process to achieve desired product attributes (i.e. unimodal size distribution with higher yield (>60%) and size in the range of 50-70 µm).

Mutarotation plays an important role in the solubility of lactose. The amount and rate at which lactose will dissolve depend on the form of the input material. β-lactose is more soluble and dissolves faster than ALM. The ALM dissolution process occurs in two stages; if an excess amount of ALM is put into the solution, the initial solubility will be reached quickly. As mutarotation occurs and conversion of ALM to β-Lactose proceeds, more ALM will dissolve until the equilibrium ratio is achieved [181]. The mutarotation kinetics governs the dissolution process. Dissolved ALM concentration governs the growth rate of

ALM, and the presence of β-lactose suppresses the solubility of ALM. For these reasons, it is important to add mutarotation kinetics in the solubility model to predict the growth kinetics of ALM. The equilibrium ratio of β-lactose to α-lactose was shown to decrease with increasing temperature from 1.64 at 60 °C to 1.36 at 100 °C [181].

5.2 Experimental setup

5.2.1 Modelling platform

The modelling platform selected for this work is gPROMS FormulatedProducts 1.3. The numerical method implemented in this software to solve the PBE is the high-resolution finite volume scheme with flux-limited function (HRFVS-FL), which is described in detail elsewhere [225, 226].

A vessel model was built in software using an MSMPR unit operation configured as a batch mode in the flowsheet models (**Figure 5-2**). The crystallisation slurry employed a well-mixed single compartment that assumes that the mixing time is much lower than the time scales of nucleation, growth, and agglomeration. Under this assumption, the energy dissipation from the stirrer can be averaged over the whole crystalliser. Hence, the mechanism for particle formation can be assumed to be independent of the position within the crystalliser [227]. Other assumptions state that the liquid and solid phases in bulk are in thermal and mechanical equilibrium, with the same temperature and pressure. Time variant controls for the model included the mass of crystals in the slurry and solution composition, which was retrieved from experimental concentration profiles from the IR probe. PSD data from the Malvern Master sizer for the initial seed input and the product was used for the PSD location parameter. Temperature profiles (TC) were input as piecewise linear (An option to provide desired temperature setpoints for a temperature profile) with four control intervals approximated from the supersaturation control experiments.

The concentration data (IR calibration model -Inline concentration measurement) and the crystal size distribution measurements (laser diffraction size analysis approach) were used to estimate the kinetic model parameters

and validate the model. In addition, the microscopic images were used to obtain qualitative information about the crystallisation phenomena in each experiment, such as crystal morphology, size, shape, attrition and degree of agglomeration. Physical properties such as molecular weight, density, solubility, etc., were configured in the global specifications module within the software. Mutarotation equilibrium and kinetic information were taken from elsewhere [181, 228] and implemented using a reaction model in the software.

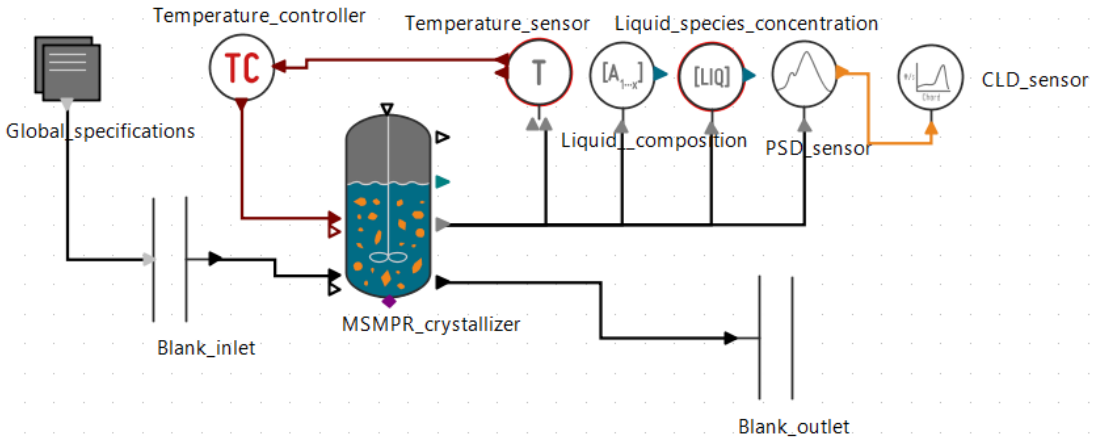

Figure 5-2 Schematic flowsheet model used to describe the batch crystallisation of ALM in water solution for parameter estimation. Typical experimental inputs include process temperature controller (TC), solution concentration (A), particle size measurements (offline data by laser diffraction) (PSD sensor) with selected kinetic models and operating conditions in the crystalliser MSMPR unit.

5.2.2 Experimental setup

A batch reactor setup for parameter estimation consisted of a 220 ml jacketed glass Moving Baffle Oscillatory Crystalliser. The vessel temperature is controlled using a (Lauda HE20) circulator connected to the jacket. A side port at the top is used to introduce the feed solution, and there are two more ports for introducing analytical process tools. Mixing is achieved by oscillating the string of baffles with the help of a linear motor, which can provide oscillation in the range of 0-10 Hz frequency and 0-40 mm amplitude via the Xenox control box. A thermocouple (type K) (from top) and FBRM probe were inserted from the side to monitor temperature and particle dynamics, respectively. A react IR (inserted from the top) is used for in situ, real-time concentration monitoring

(Figure 5-3). At the end of each experiment, the slurry was filtered using a lab-scale Buchner funnel, washed with two times ethanol, and dried overnight in a vacuum oven.

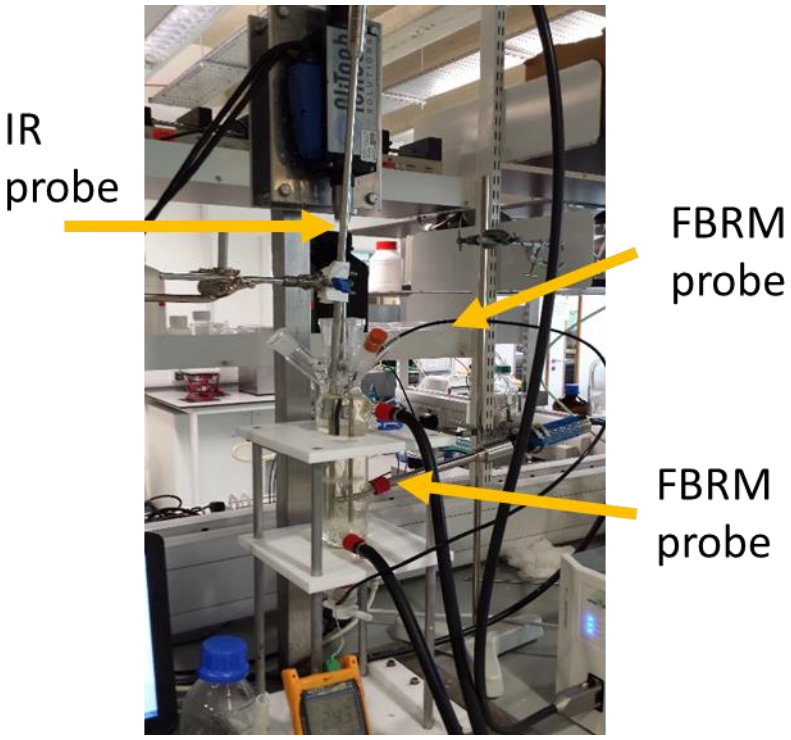

Figure 5-3 200ml batch Moving Baffle Oscillatory Crystalliser setup used for parameter estimation experiments

The 5-Stage CMBOC continuous experiment set up for seeded and unseeded model validation experiments consists of four 120 ml jacketed vessels similar to the setup used in Chapter 4 for platform characterisation and assessment. In addition, a 220 ml MBOC vessel was added to achieve the required residence time (**Figure 5-4**). Oscillation is provided to this fifth vessel by a separate linear motor. PharmaMV APC systems were used to control the temperature of the circulator, the flow rate of the feed and seed pump and the pressure actuator to control the transfer between each vessel in the cascade. All vessels have thermocouples inserted into them to monitor the temperature. The FBRM and IR were connected in vessels 3 and 4 for in situ, real-time steady-state operation and concentration monitoring. At the end of the trial, the product slurry was filtered in a 10 L agitated Nutsche filter, washed twice

with two times of cake height with ethanol and dried overnight in a vacuum oven.

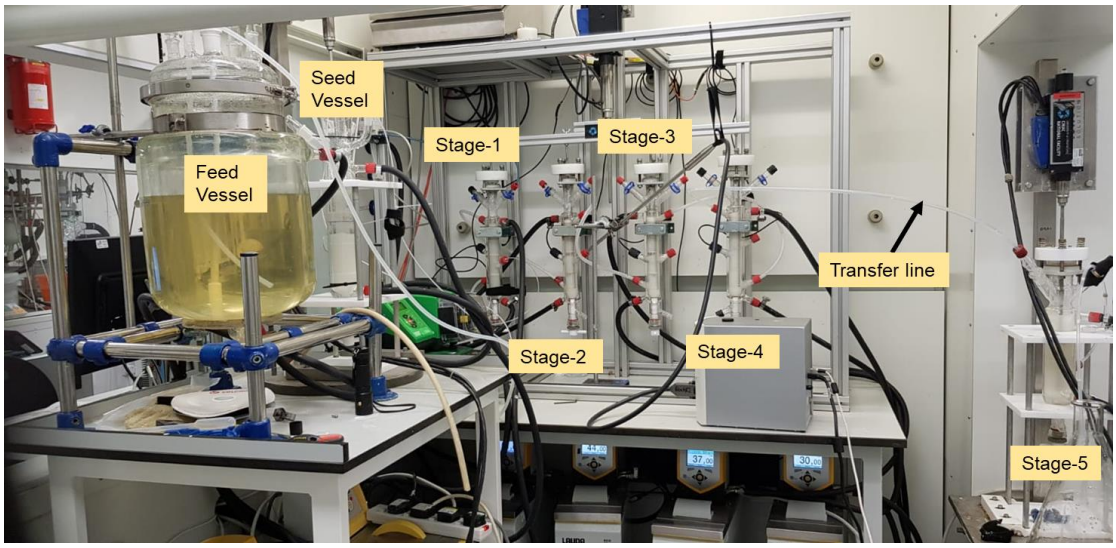

Figure 5-4 Setup of 5-stage CMBOC used for seeded ALM model validation experiments. 5th stage is added addition to four existing stage to accommodate longer residence time according to model.

5.2.3 IR calibration model for lactose concentration

To develop a calibration model, a range of concentrations was prepared. IR spectra were collected using a ReactIR 15 (Mettle Toledo) ATR-FTIR probe for each concentration at a specific temperature range (from the solubility temperature to the temperature where the system nucleated). The temperature-dependent solubility of ALM and MSZW were determined in the same experiment. Several multivariate analysis techniques were used to develop calibration models; however, due to mutarotation in lactose solution, these calibration models were unsuitable for accurately predicting ALM concentrations. It was challenging to accurately determine total lactose concentration during the crystallisation due to changes in peak area over time due to mutarotation in solution [229]. Therefore, a simple approach was applied where a calibration plot was generated by plotting the peak area of lactose against concentration. A polynomial fit was used to predict

concentration. This calibration model was validated with a maximum 1% error in prediction. Validation was performed by assessing IR spectra of a solution of known concentration, and then the error was estimated by comparing predicted concentration vs actual concentration. An equilibrium solubility model equation considering mutarotation kinetics [181] was used to estimate alpha lactose content in the solution at equilibrium.

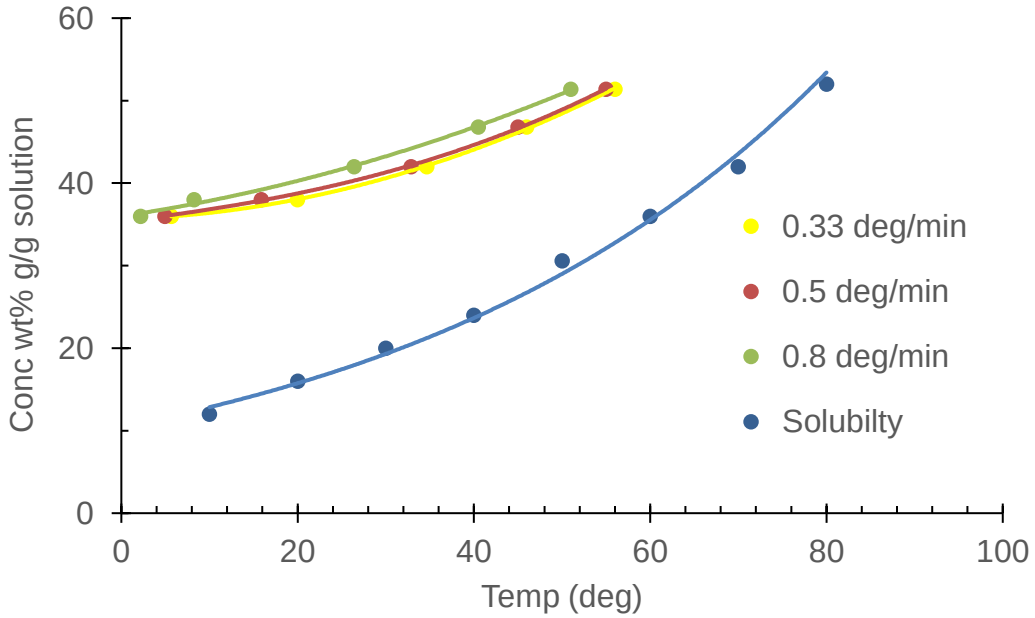

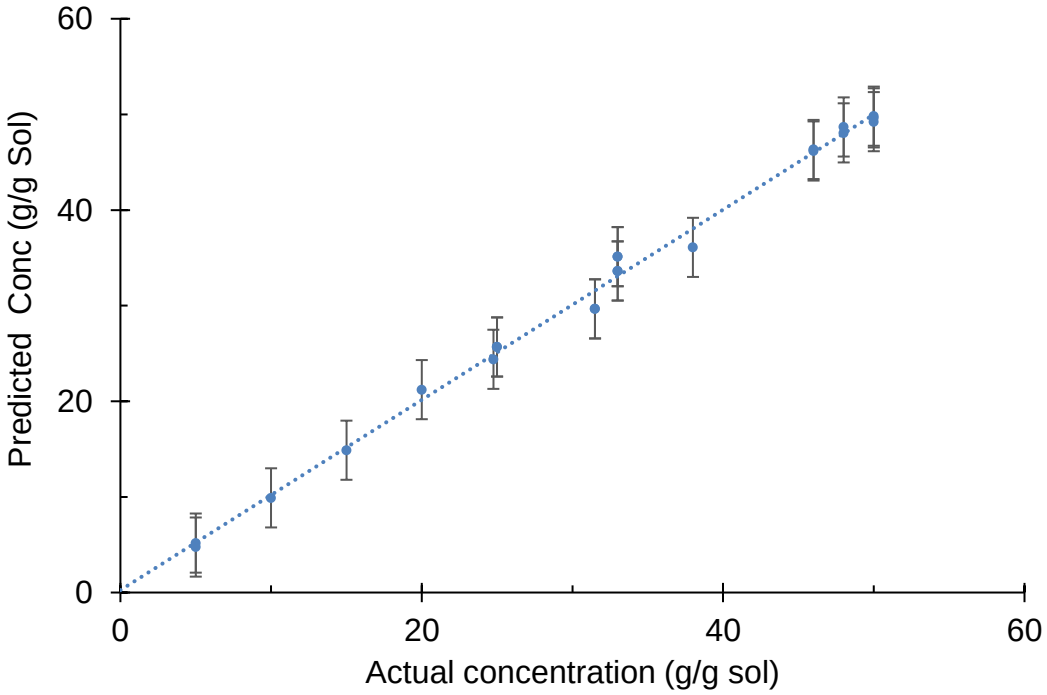

Figure 5-5 (Top) MSZW of ALM in MBOC at different cooling rates. (Bottom) A total lactose concentration calibration plot was generated by simply plotting the peak area of lactose against concentration, and a polynomial fit was used to predict concentration.

5.2.4 Sequential parameter estimation modelling approach

A sequential approach to parameter estimation was undertaken to allow for the best estimation of kinetic parameters. Whilst it is impossible to decouple all crystallisation mechanisms completely, this approach involves designing experiments to enhance a specific mechanism to allow its parameters to be estimated. This is based on methodologies presented by Kramer et al. [169]. In total, 13 experiments were performed to build the PBE of crystallisation of API in gPROMS, accounting for primary nucleation, crystal growth and attrition by secondary nucleation: Two isothermal dissolution experiments (for bulk diffusion terms), eight-seeded isothermal desupersaturation experiments (for surface integration terms) and three unseeded isothermal desupersaturation experiments (for nucleation terms) were performed. All the experimental conditions were summarised in **Table 5-2**.

5.2.4.1 Primary nucleation

A range of experiments was designed to estimate lactose crystallisation nucleation and growth kinetics. Primary nucleation experiments were designed to cover a range of concentrations and cooling rates (**Table 5-2**).

A solution of fixed concentration was cooled at various cooling rates (0.3 to 0.8°C.min^{-1}) to estimate primary nucleation kinetics. Power law expression (**Equation 5-7**) was used to estimate nucleation kinetics.

A further distinction can be made between homogeneous and heterogeneous primary nucleation, corresponding to situations without and with the presence of particulate matter (e.g. dust particles) that can facilitate the primary nucleation process. In practice, some particulate matter is always present, i.e. homogeneous primary nucleation is rarely observed. The only difference is the order of magnitude of the pre-exponential factor in the rate expression from the modelling perspective.

The empirical power-law expression is used where relative supersaturation is employed to describe the level of supersaturation present in the solution, as follows:

$$\boldsymbol{J_{prim} = k_n \left(\frac{\Delta C}{\rho_c}\right)^n exp\left(\frac{-E_{A,n}}{RT}\right)} \qquad \textbf{Equation 5-7}$$

Where k_n is nucleation rate constant (#/m^3.s), n is order of nucleation, ΔC absolute supersaturation (kg.m^{-3} solution), ρ_c crystal density (kg.m^{-1}) and $E_{A,n}$ activation energy for nucleation (J.mol^{-1}). Primary nucleation rate expressions contain two parameters that need to be estimated from experimental data: the nucleation rate constant and the nucleation order.

5.2.4.2 Growth kinetic

For growth kinetics, empirical power-law expression was used. The crystal growth and dissolution rate expressions contain three parameters that need to be estimated from experimental data: the growth/dissolution rate constant, the activation energy for crystal growth/dissolution, and the growth/dissolution order.

The overall crystal growth rate, R_G, which is the rate of mass deposition onto the crystal over time, is expressed as

$$\boldsymbol{R_G = K_G A (C_b - C^*)^g} \qquad \textbf{Equation 5-8}$$

where k_G is the growth rate coefficient, A is the crystal surface area (m^2), C_b (g.cm^{-3}) is the solute concentration in the bulk solution, and C^* (g.cm^{-3}) is the equilibrium solute concentration, and g is the overall growth order.

The crystal growth process involves two separate steps, which are considered to occur in series. First, the solute is transported to the solid-liquid interface; then, it integrates into the crystal lattice. Each step has a different driving force and a different rate associated with it. Thus, **Equation 5-8** can be broken up into two steps: [230]

$$\boldsymbol{R_G = K_d A (C_b - C_I)} \qquad \textbf{Equation 5-9}$$

$$\boldsymbol{R_G = K_r A(C_I - C^*)^r}$$ **Equation 5-10**

Equation 5-9 represents the rate of mass transfer, where k_d is the mass transfer rate coefficient and C_I (g.cm^{-3}), is the concentration at the solid-liquid interface. **Equation 5-10** represents the rate of integration, where k_r is the integration rate coefficient, and r is the integration rate order.

When the rate of mass transfer is slower than the integration rate (i.e., the mass transfer step offers more resistance), the growth process is considered to be "mass transfer controlled" and $k_d \ll k_r$. When the integration step offers more resistance, the growth process is "integration controlled," and $k_r \ll k_d$. In the case of integration-controlled growth, the concentration at the interface, C_I (g.cm^{-3}), will approach the bulk concentration, C_b, (g.cm^{-3}), and The overall crystal growth rate, R_G can be approximated as

$$\boldsymbol{R_G = K_r A(C_b - C^*)^r}$$ **Equation 5-11**

The Damköhler number, Da, is often used to compare the relative contribution of each step:

$$\boldsymbol{Da = \frac{K_d (C_b - C^*)^{r-1}}{k_r}}$$ **Equation 5-12**

Thus, growth is mass transfer controlled when Da is large, and growth is integration controlled when Da is small. Experiments were designed in such a way to address both mechanisms [231].

The empirical power-law expressions utilised in gPROMS to describe crystal growth and dissolution rate kinetics are similar to the expression employed in the two-step model for the surface integration step. Where the level of supersaturation is described by the absolute supersaturation as follows:

$$G = k_g \, exp\left(\frac{-E_{A,g}}{RT}\right)\left(\frac{\Delta c}{\rho_c}\right)^g$$ ***Equation 5-13***

Where $k_g$is proportional factor for surface integration (m.s^{-1}), $E_{A,g}$ is activation energy for surface integration (J.mol^{-1}), R is gas constant (J.mol^{-1}.K^{-1}), T is the absolute temperature (K), ΔC absolute supersaturation (kg.m^{-3} solution), ρ_c Crystal density (kg.m^{-3}) and g is supersaturation dependent on surface integration rate.

The crystal growth and dissolution rate expressions contain three parameters that need to be estimated from experimental data: the growth rate constant, the activation energy for crystal growth and the growth order. The concentration profile between the addition of the seed crystals and dissolution of seed, as well as the PSD of the seeds were used for parameter estimation.

5.2.4.3 Secondary nucleation

After the growth rate parameters are estimated, it would be possible to conduct a similar estimation for secondary nucleation kinetics based on the attrition between crystal and impeller collisions. Again, power-law expressions were used for secondary nucleation rate estimation. Similar to the growth estimation, experiments were designed such that secondary nucleation should be enhanced compared to other mechanisms. As with the growth estimation experiments, only the concentration profile was used to estimate parameters as the product PSD could be subject to agglomeration.

$$\boldsymbol{J_{Sec} = exp\ (ln\ k_n)\left(\frac{\Delta c}{\rho_c}\right)^n exp\ \left(\frac{-E_{A,n}}{RT}\right)\varepsilon^a \varphi^b} \qquad \textit{Equation 5-14}$$

Where K_n is nucleation rate constant (#.m^{-3}.s^{-1}), n is the order of nucleation, $E_{A,n,}$ is the activation energy for nucleation (J.mol^{-1}), ε is the energy dissipation rate (m^2.s^{-3}), *a* is the energy dissipation rate order, and *b* is the surface area order.

The secondary nucleation rate expressions contain five parameters that need to be estimated from experimental data: the nucleation rate constant, order of nucleation, the activation energy for nucleation, energy dissipation rate order and slurry density order.

After model development, the supersaturation control experiments were imported into the gPROMS, where the concentration profile by ReactIR and quantified by the previously developed calibration model (**Section 5.2.3**), temperature and PSD (measured at the batch end) were saved. On the successful inputs of the batch experimental data, a group of kinetic parameters (Table 5.3) could be estimated using the model validation entity in estimate parameter mode. Several initial guesses for lower and upper bounds for the crystallisation kinetic parameters were usually necessary to obtain a good agreement between model predictions and experimental measurements.

Table 5-2 Experimental conditions for a sequential approach to parameter estimation.

Crystallisation phenomenon	Exp No	Conc wt % g/g solution	T_{sat} (°C)	T seed (°C)	SS at seed addition	Seed (wt %)	Seed size (µm)	Cooling
Volume diffusion (growth)	1	24.75	40	63	0.66	-	4	Isothermal
	2	24.75	40	63	0.66	-	40	Isothermal
Surface integration (growth)	3	38	63.55	40	1.6	10	4	Isothermal
	4	38	63.55	47	1.4	10	4	Isothermal
	5	25	40	20	1.66	10	4	Isothermal
	6	31.5	52	35	1.4	10	4	Isothermal
	7	38	63.55	40	1.4	2	4	Isothermal
Secondary nucleation (Attrition)	8	33	63.55	42	1.66	2	90	Isothermal
	9	38	63.55	42	1.66	2	90	Isothermal
	10	33	63.55	42	1.66	2	130	Isothermal
Primary nucleation	11	46	80	unseeded				0.5 °C/min (80-20 °C)
	12	38	63.55	unseeded				0.3 ^{0}C /min (62-10 °C)
	13	42	70	unseeded				0.3 ^{0}C /min (72-10 °C)

5.3 Result and discussion

5.3.1 Growth Kinetics

For volume diffusion experiments, an undersaturated solution was prepared to create negative supersaturation, and then ALM was added to make it saturated while monitoring the concentration profile.

Experiments were designed to measure the surface integration component of growth as seeded crystallisations covering a range of driving forces (S = 1.4 – 1.66). The seed size and mixing conditions were kept constant for all the growth experiments, and higher seed loading was used to avoid attrition and maximise growth.

The IR calibration model determined the concentration profile with time for each experiment, which was reduced to 6-8 samples depending on the length of the experiment. For growth parameter estimation, the concentration profile was used to fit against the model. A comparison of the experimental and model fitted concentrations are shown in **Figure 5-6.**

Overall, reasonably good agreements are obtained between the measured and the predicted data (**Table 5-3)** for the solute concentration and crystal size distribution. The volume diffusion experiment obtained a reasonably good fit (X^2 of 1.63321, considerably lower than X^2 Critical 26.2962). Uncertainties in the crystal size distribution may relate to the non-spherical and non-uniform crystal shape for the laser diffraction measurement and using a single characteristic size for the one-dimensional population balance model.

The growth of lactose crystals depends on the degree of supersaturation and starting concentration. The driving force for growth is insufficient at lower supersaturations, leading to secondary nucleation). Predicted PSD deviates from the experimental PSD in experiments 6 and 7 (**Figure 5-7)** due to increased secondary nucleation rate. The secondary nucleation rate becomes dominant with a higher starting concentration as well. Results from the growth model also indicate an increase in growth rate with the increase in supersaturation. The growth rate for lactose in this platform was 0.37-0.49, $\mu m.m^{-1,}$ slightly higher than the reported growth rates for ALM(0.3 -0.39

μm.m^{-1}). This increase in growth rate is due to uniform shear distribution and enhanced mass transfer due to mixing in CMBOC with the comparable operating condition with STR [181].

Table 5-3 Estimated growth parameters from the sequential parameter estimation experiments.

Parameter	Value	Symbol
Growth rate constant (m.s^{-1})	6.95e-8	k_g
Supersaturation order	1.5	g
Effective diffusivity correction	0.003	α
X^2 Critical	26.3	
X^2	1.6	

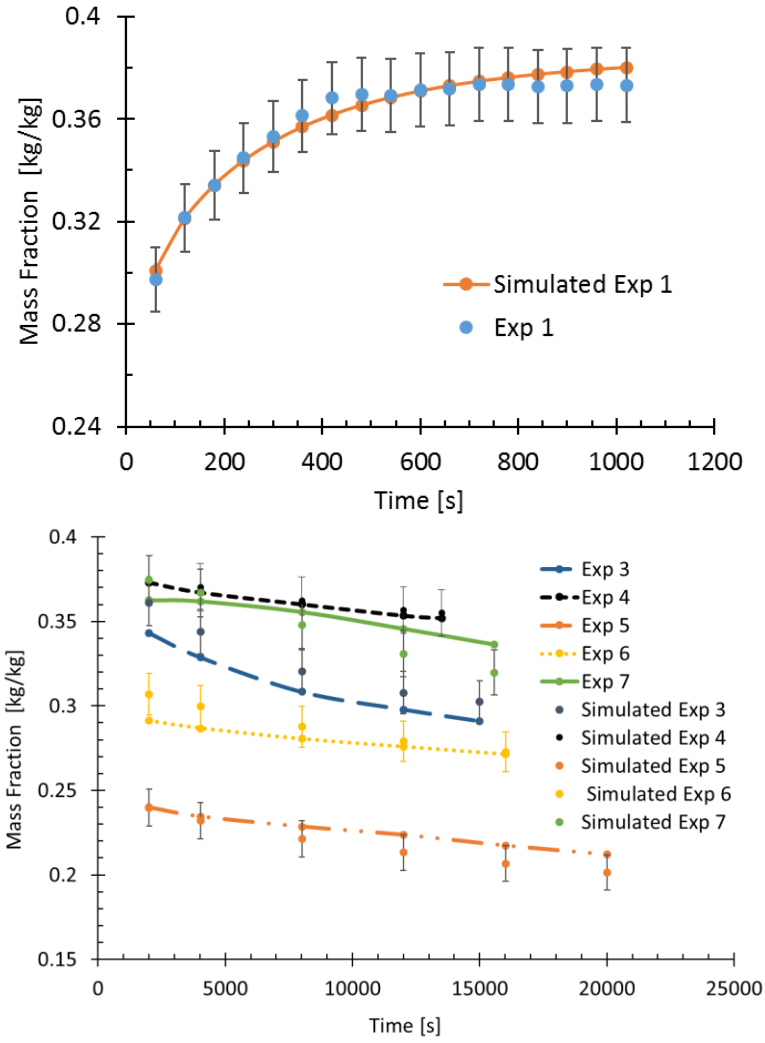

Figure 5-6 Experimental and predicted concentration profile for (Top) volume diffusion (bottom) and surface integration experiments.

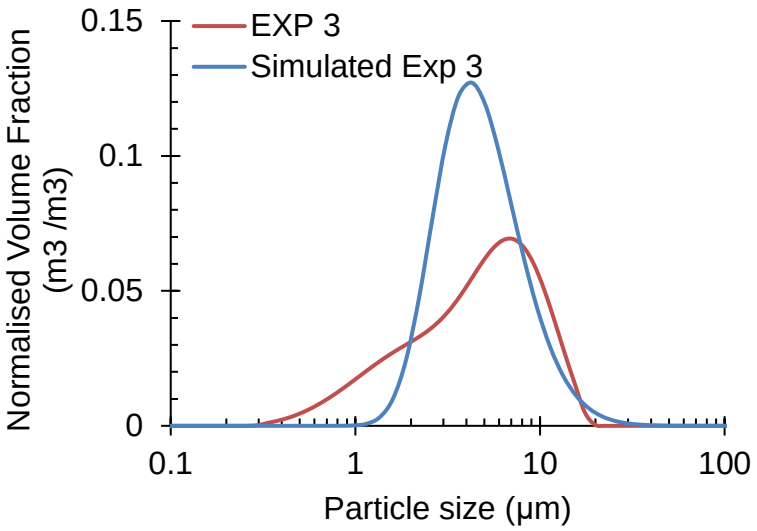
0.15
0.1
0.05
0
0.1
1
10
100
Normalised Volume Fraction (m3 /m3)
Particle size (µm)
EXP 3
Simulated Exp 3

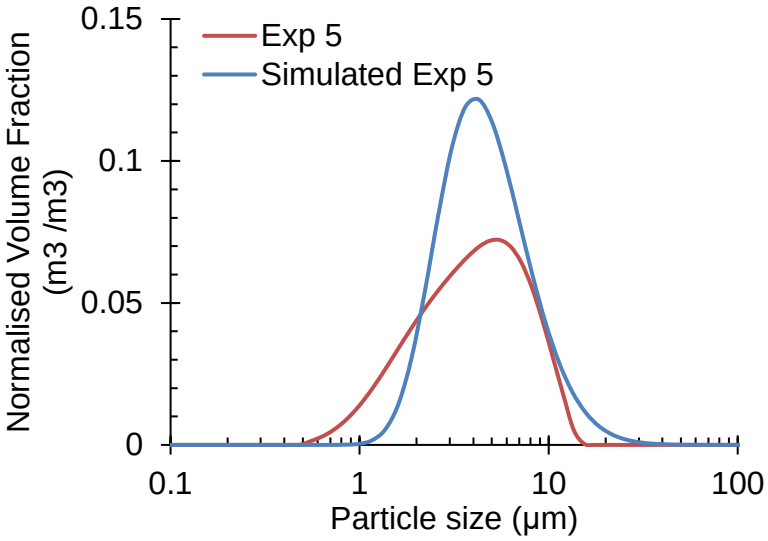
0.15
0.1
0.05
0
0.1
1
10
100
Normalised Volume Fraction (m3 /m3)
Particle size (µm)
Exp 5
Simulated Exp 5

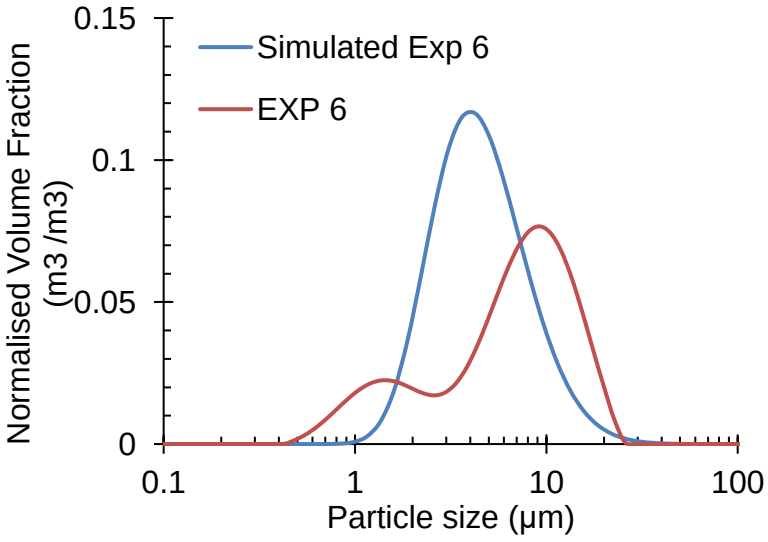
0.15
0.1
0.05
0
0.1
1
10
100
Normalised Volume Fraction (m3 /m3)
Particle size (µm)
Simulated Exp 6
EXP 6

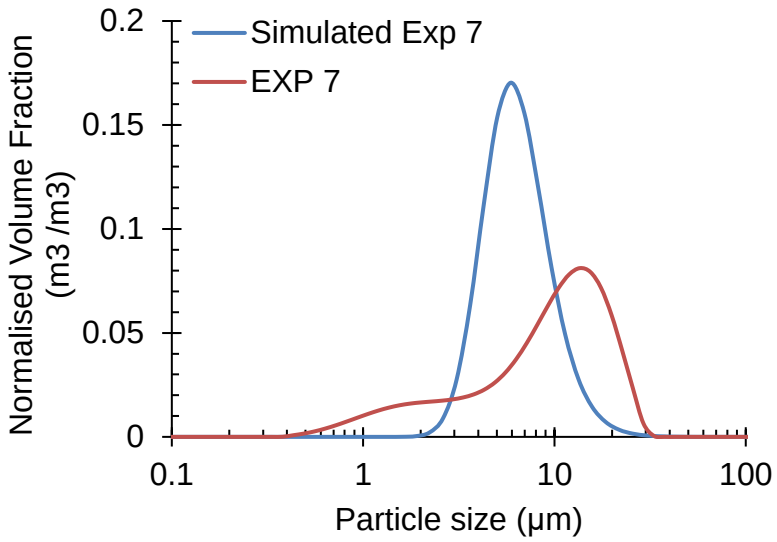

Figure 5-7 Experimental and predicted PSD from the estimated kinetic parameters in growth-only experiments.

5.3.2 Secondary nucleation

The growth rate parameter estimation applied growth boundaries (**Table 5-4)** to estimate kinetic parameters for secondary nucleation. Experiments were specifically designed to enhance secondary nucleation. Isothermal desaturation experiments were performed to estimate secondary nucleation parameters using Power-law kinetics. A good fit (X^2 of 4.10 lower than the X^2 critical of 23.68) was obtained for the concentration data (**Figure 5-8**). The secondary nucleation rate is not dominant in the boundaries of investigated crystallisation range. The system will be subjected to secondary nucleation within these boundaries due to attrition if the crystal size is above 67 µm. Supersaturation order dictates that within evaluation limits, secondary nucleation is not very dominant due to the tighter shear distribution as described in chapter 4 compared to an STR where you get localised high shear occurs close to impeller. The experimental data observed the slight deviation in simulated PSD (**Figure 5-9**). This might be due to the secondary nucleation parameters were estimated considering only attrition based phenomena, however, there might be some secondary nucleation due to supersaturation level in tune generating fines in experimentally measured PSD. To minimise secondary nucleation, a higher surface area is required for growth (surface

integration controlled process). Higher seed loading leads to more growth and less secondary nucleation and supersaturation is consumed for growth avoiding secondary nucleation. Based on the experimental boundaries, solutions at less than 0.38 g g^{-1} lactose are relatively stable to secondary nucleation within the experimental conditions investigated. Tight monitoring is required when the solution concentration is high to control secondary nucleation in a crystallisation process. However, when the concentration drops close to 0.30 g g^{-1}, the level of secondary nucleation can be controlled simply by staying out of the labile zone.

Table 5-4 Estimated secondary nucleation parameters from the sequential parameter estimation experiments.

Parameter	**Value**	**Symbol**
nucleation rate constant (#.m^{-3}.s^{-1})	23.7	k_n
Order of nucleation [-]	0.	n
Activation energy (J.mol^{-1})	1645	$E_{A,n}$
Size above which crystal undergoes attrition (µm)	67	L_{min}
Surface area order [-]	0.001	b
Energy dissipation rate order [-]	0.5	a
X^2 Critical	23.7	
X^2 value	4.1	

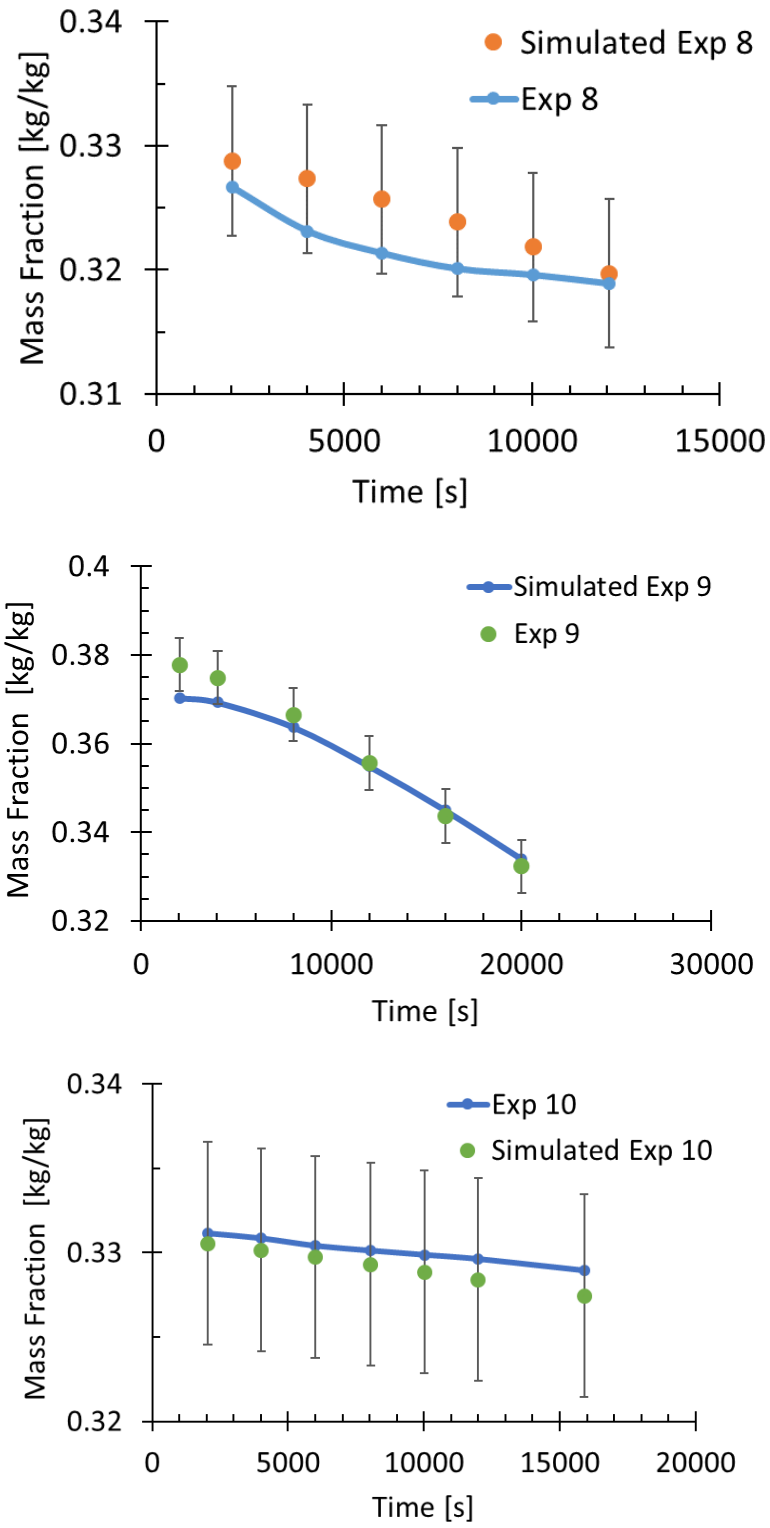

Figure 5-8 Experimental and simulated concentration profiles for parameter estimation experiments designed to estimate secondary nucleation and attrition

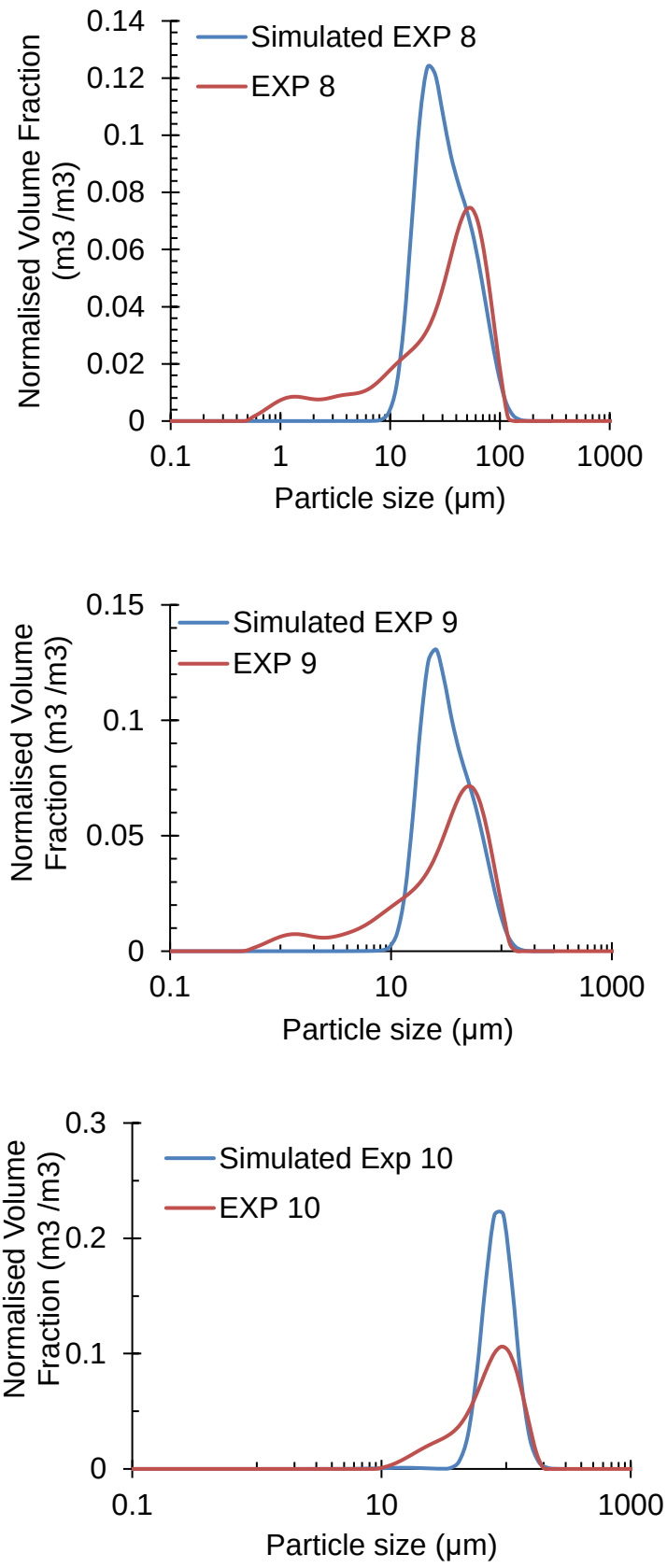

Figure 5-9 Experimental and predicted PSD from the estimated kinetic parameters in the secondary nucleation and attrition model.

5.3.3 Primary nucleation

A number of starting concentrations and cooling profiles were chosen to estimate primary nucleation kinetic parameters. A good fit was obtained using the power law kinetics model in gPROMS against experimental concentration data yielding the parameter estimates (**Figure 5-10)**. The primary nucleation rate was higher for higher concentrations, further confirmed with the estimated super saturation order from the primary nucleation model. Estimated parameters for primary nucleation were used to fit PSD data. A good fit was obtained for predicted PSD against experimental PSD data (**Figure 5-11**). A close fit to PSD data dictates that a higher surface area (uncontrolled primary nucleation) pushes the system to growth only by minimising secondary nucleation. A noticeable reduction in fine particles was observed by providing a higher surface area for growth.

Table 5-5 Estimated primary nucleation parameters using power law kinetics

Parameter	Value	Symbol
Rate constant (log ($\#.m^{-3}.s^{-1}$)	38.8	k_n
Supersaturation order	7.1	n
χ^2-critical	26.3	
χ^2-value (95%)	7.0	

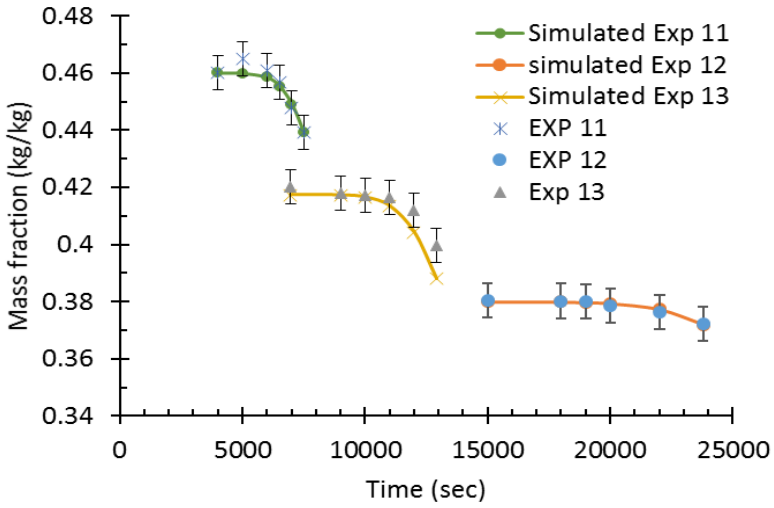

Figure 5-10 Experimental and simulated concentration profiles for parameter estimation experiments designed to estimate primary nucleation.

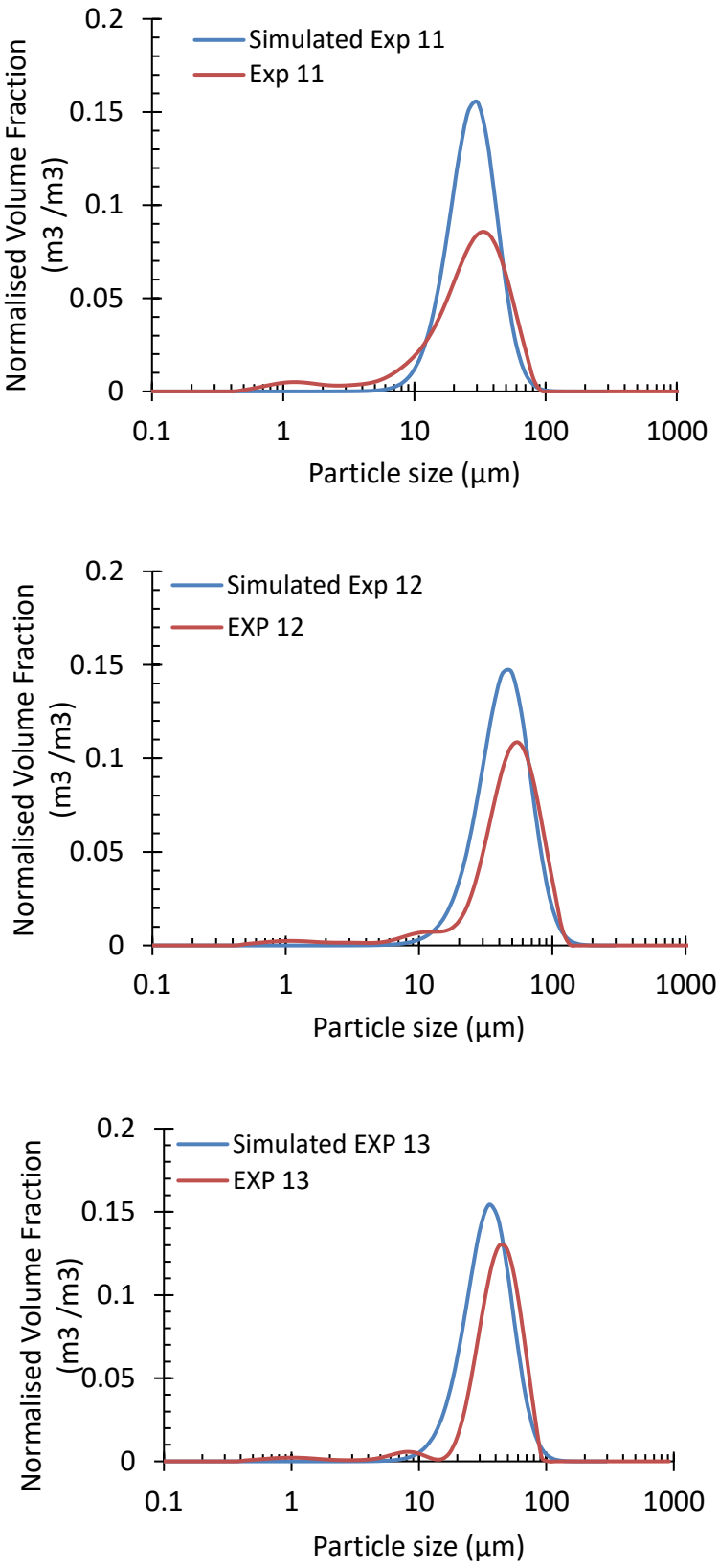

Figure 5-11 Experimental and predicted PSD from the estimated kinetic parameters in primary nucleation experiments.

5.3.4 Model validation on continuous crystallisation in 5-stage CMBOC

5.3.4.1 Optimisation

The model developed and parameterised from the batch process was used to design a continuous process. So far, designing a continuous process from a batch is still a challenge. However, a good mechanistic model can assist in the design of a robust continuous process. Dynamic optimisation (using CVP_SS solver) was used to design the required continuous process. Conditions to develop an optimised process are summarised in Table 5-6.

The attainable region approach previously used in the design of chemical reactor networks and separation systems is applied to the crystallisation processes to identify attainable regions in a diagram of mean product particle size vs total process residence time [232]. The target objective for the continuous crystallisation was >90% yield for ALM and a total lactose yield of >40%. Constraints in the process were the residence time (<4 hr) and temperature range (5-70 °C). An optimisation tool was run to maximise or minimise the mean size of the product by varying the residence time while keeping the yield above 90 or 80%. The final output from these optimisation runs was used to develop an operating region (**Figure 5-12**) for the continuous crystallisation process in terms of final product size and residence time.

Table 5-6 Process optimisation conditions to develop continuous crystallisation process with desired outputs (Yield, Size)

Parameter	**value**
Total residence time	120-240 min
Mass flow rate	2-12 $g.min^{-1}$
Operating Temperature range	5-70 °C
ALM Yield required	Region 1>90% Region 2 >80%
Total lactose yield required	Region 1 >40%, Region 2 >30%

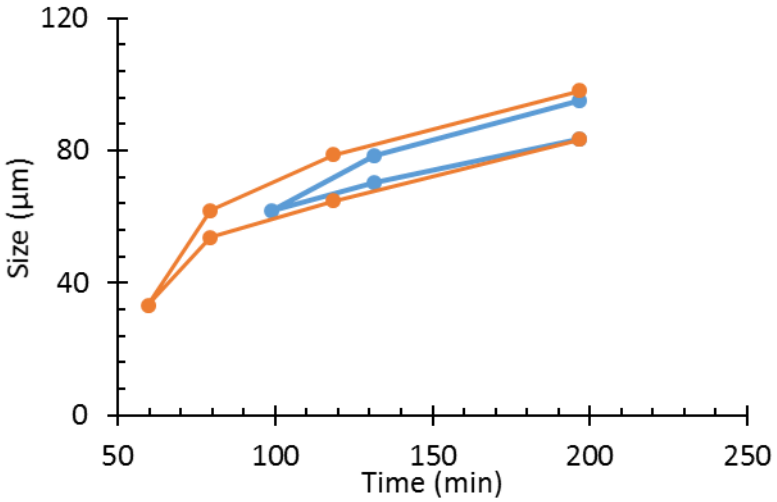

Figure 5-12 Attainable mean sizes from continuous crystallisation with a constraint on final yield of ALM. (Blue region for >90 yields, Orange region for >80 Yield)

Operating parameters for the 5-stage continuous crystallisation validation experiments, including cooling profile, residence time, feed flow rate and seed loading, were derived from the attainable region developed by running the process optimisation tool in gPROMS. These conditions are summarised in **Table 5-7** and **Table 5-8**.

Table 5-7 Operating condition for model validation experiments.

Condition	**Unit**	**Unseeded Experiment**	**Seeded Experiment**
Concertation	(g/g solvent)	46.8	46.8
Feed flow-rate	(g/min)	6.15	10
Seed flow-rate	(g/min)	--	1.66
Seed Loading	(%)	--	1%
seed size	(µm)	--	32
One Residence time	(min)	114	60
No of residence time (system run)		5	10
Target particle size	(µm)	70	51.48
Total volume	(ml)	700	700
Mixing	Oscillation	2Hz, 20mm	

Table 5-8 cooling profiles for 5-stage model validation experiments.

	Cooling profile (°C)	
Vessel	**Unseeded Experiment**	**Seeded Experiment**
1	33	50
2	33	44
3	30	37
4	5	30
5	5	20

5.3.4.2 Seeded 5-stage CMBOC model validation

Validation of the crystallisation mechanisms and kinetic parameters estimated from batch experiments were considered using continuous crystallisation experiments conducted in a 5-stage CMBOC crystalliser.

A 60 min mean RT for a five-stage CMBOC was required to achieve the specific target d[50]= 51 µm with an overall yield of 60%. The target yield was based on the commercially reported yield for ALM [181, 219]. Oscillatory conditions were selected based on the RTD results presented in Chapter 4 to minimise axial dispersion at a net flow rate. The saturated aqueous seed slurry at 55 °C with a d[50] =32 µm and a span of 1.1 was introduced continuously at 1.66 $g.min^{-1}$ to maintain a seed loading of 1% in the first vessel at a supersaturation of 1.4. The solution concentration and the time for crystallisation to achieve steady-state were monitored using an ATR mid-IR probe (ReactIR15) in the fourth vessel and FBRM in the third vessel (trends shown in **Figure 5-16.**

The process was operated for 10 hr under the specified conditions (**Table 5-7),** and the experimental PSD was plotted against the model predicted PSD values. A good fit of experimental to model PSD data was observed for stages 1 to 4. Stage 5 experimental PSD deviated from the model predicted PSD

(**Figure 5-15**). A tail in the small crystal size range was attributed to secondary nucleation, which occurred under high supersaturation (1.66) towards the end of the crystallisation and during the presence of large crystals (hence decreasing the surface area of growth). It was confirmed from the model and experiments that the growth rate decreases with the decrease in supersaturation and surface area for growth. Thus, the deviation from the model predicted values is likely due to the lower surface area available for growth leading to secondary nucleation.

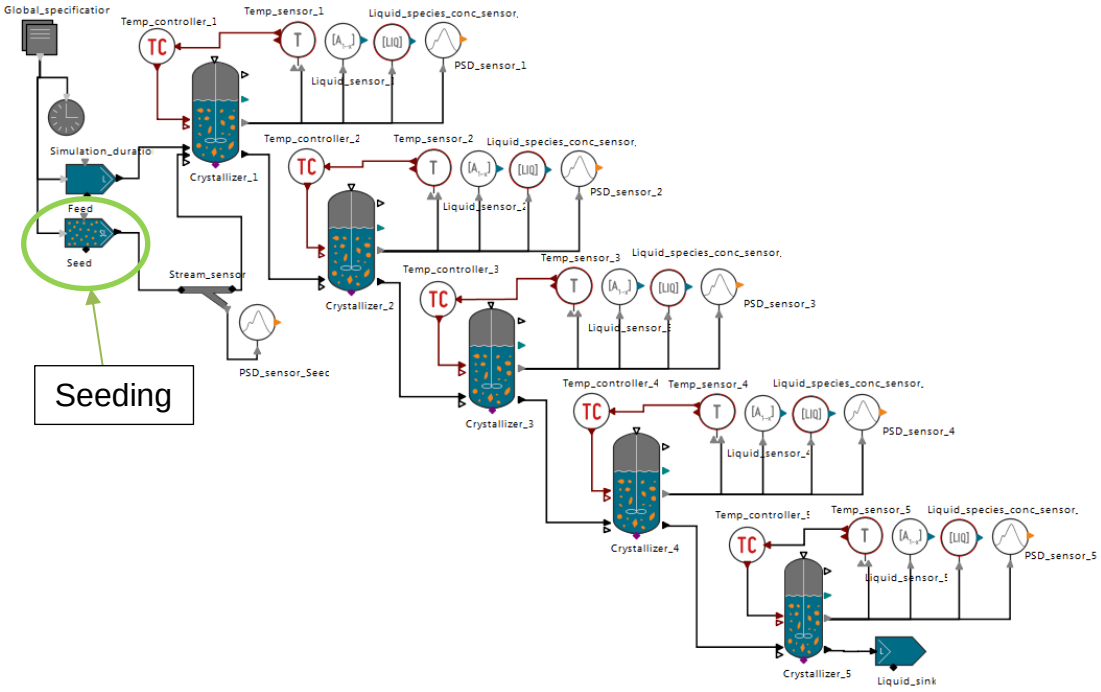

Figure 5-13 Continuous 5-Stage CMBOC primary nucleation model flowsheet

The estimated parameters were further utilised to design a continuous crystallisation process (seeded and unseeded) aiming to “dial-up” target particle size and deliver the required material attribute directly. Predictions from the models were validated against the product collected from the continuous trial. Reasonably good agreements were obtained between the experimental measurements and model predictions (simulated 51.48 µm vs measured 55.40±7 µm at different RT) within the defined model boundaries and uncertainties. Moreover, specific advantages of the moving baffle arrangement were demonstrated through the experiments and simulation.

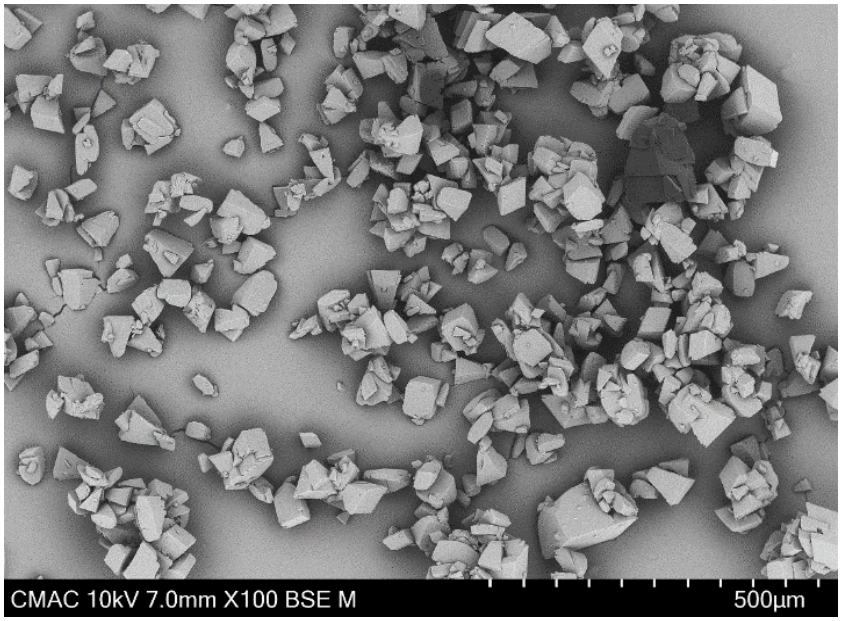

Figure 5-14 SEM images of ALM product from 5-stage CMBOC seeded continuous crystallisation validation experiment.

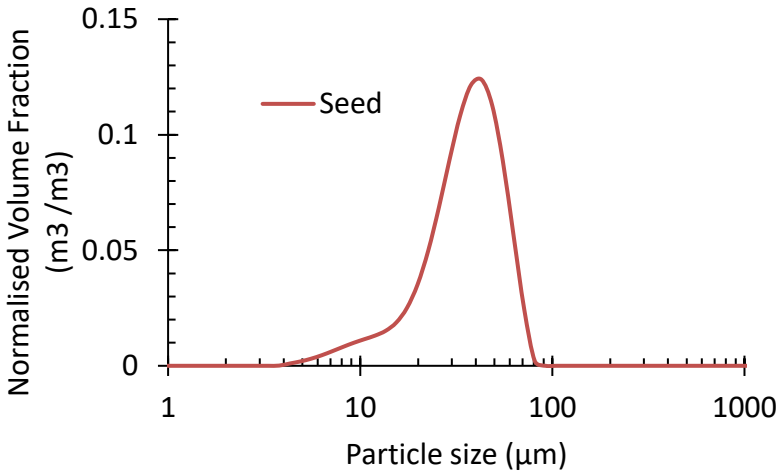

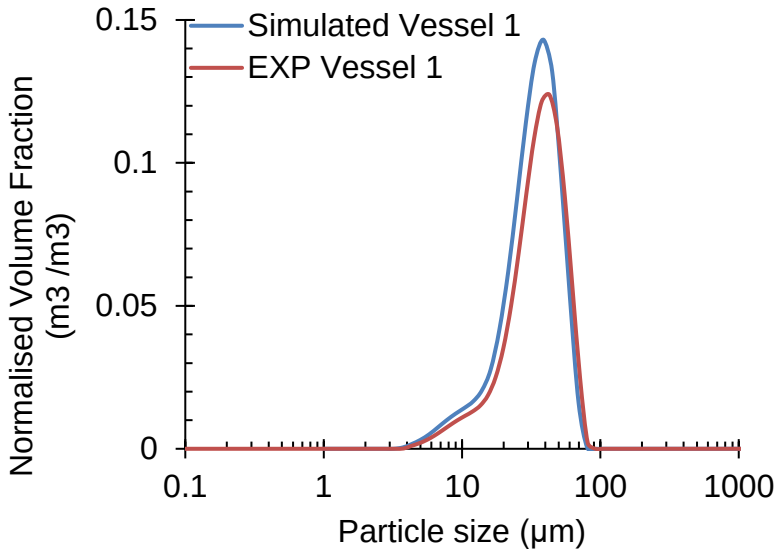
Simulated Vessel 1
EXP Vessel 1
Normalised Volume Fraction (m3 /m3)
0.15
0.1
0.05
0
0.1
1
10
100
1000
Particle size (μm)

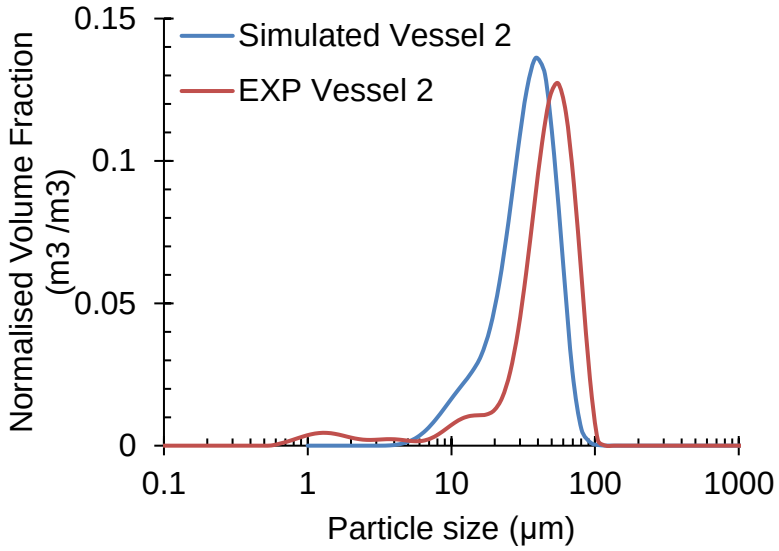
Simulated Vessel 2
EXP Vessel 2
Normalised Volume Fraction (m3 /m3)
0.15
0.1
0.05
0
0.1
1
10
100
1000
Particle size (μm)

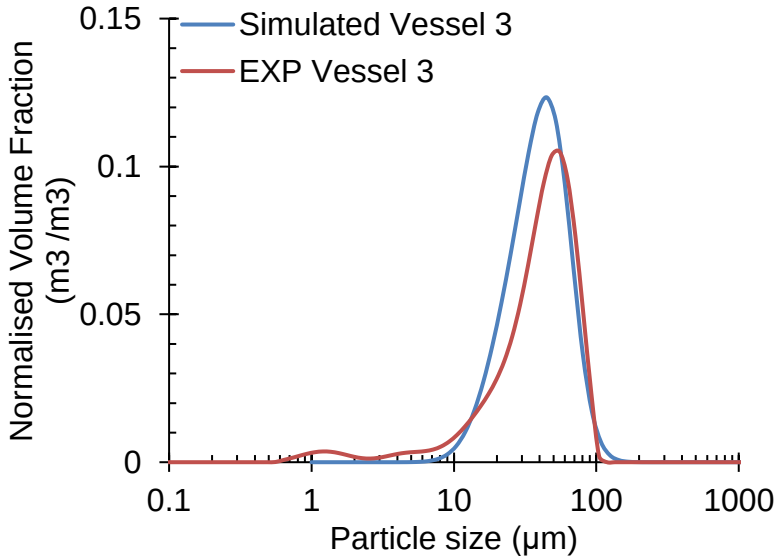
Simulated Vessel 3
EXP Vessel 3
Normalised Volume Fraction (m3 /m3)
0.15
0.1
0.05
0
0.1
1
10
100
1000
Particle size (μm)

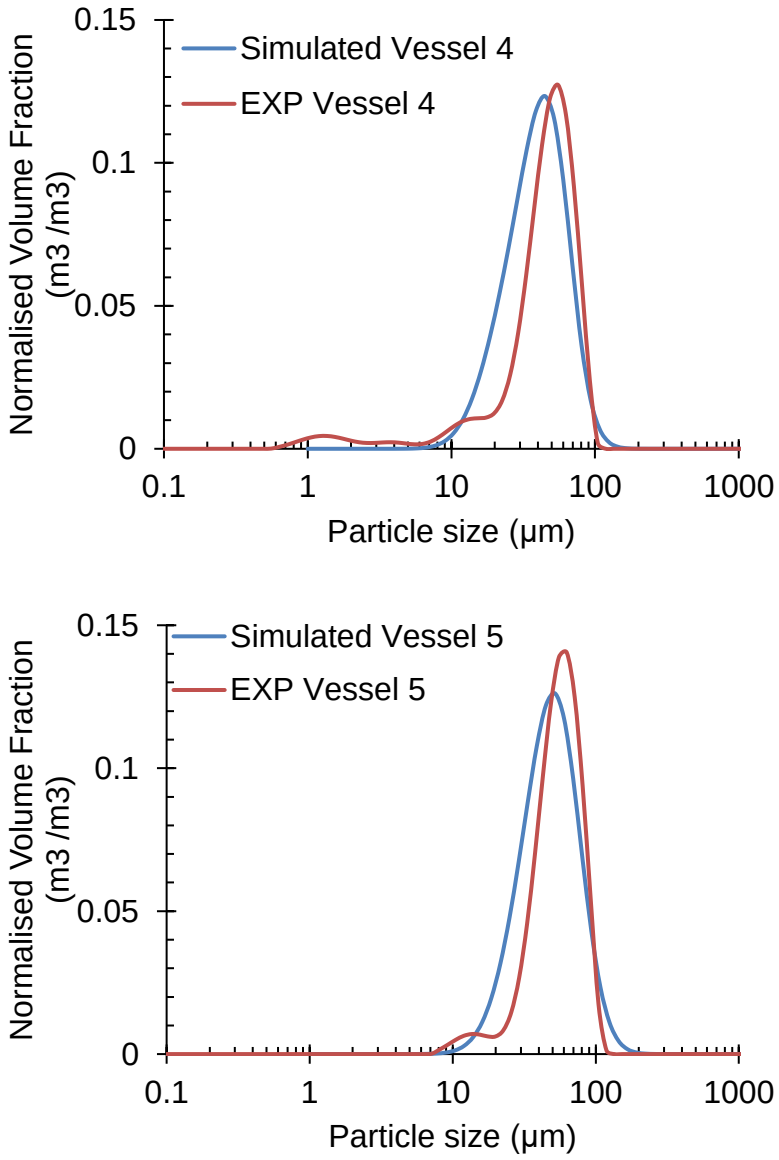

Figure 5-15 PSD of initial seed and comparison of actual versus simulated PSD of each of the vessels.

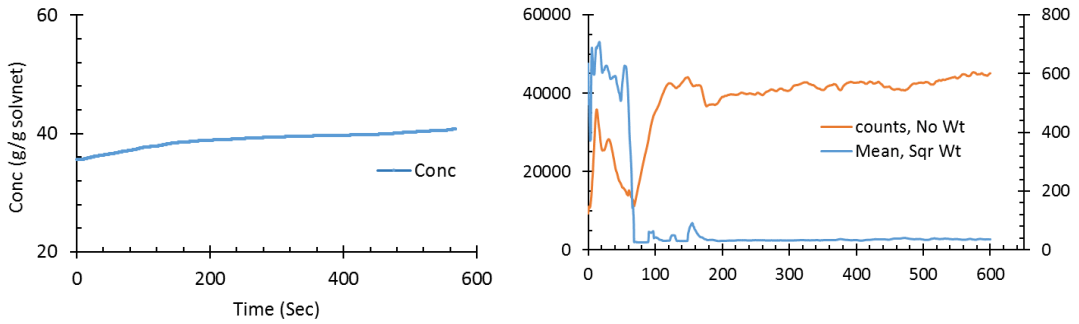

Figure 5-16 (left) Concentration profile in 4th vessel and (Right) FBRM trend in 3rd Vessel showing approaching steady-state after 2 RT.

Table 5-9 experimentally measured PSD and solid recovery after each residence time.

Experimental					
RT	Solid recovery	D[10]	D[50]	D[90]	Span
	(%)	(μm)			
Simulated		27.1	51.5	90.4	1.2
1	63.13	12.1	38.1	60.3	1.3
2	65.33	11.9	38.9	67.2	1.4
4	63.74	14.4	43.1	72.8	1.4
6	64.87	16.3	47.7	74.0	1.2
8	65.13	31.9	55.4	83.0	0.9

5.3.4.3 Primary nucleation 5-stage CMBOC model validation

The unseeded continuous crystallisation process was designed to target a final mean particle size of 70 μm to assess whether the process could be operated without seeding. Primary nucleation and growth kinetics from

Table 5-5 was used to optimise the unseeded continuous crystallisation process. Flowsheet for 5 stages continuous crystallisation process is shown in **Figure 5-17,** with nucleation taking place in stage 1. FBRM data showed steady state was achieved after 3rd RT and maintained throughout each stage of the process for 5 RT. No wash-out effect was observed in the process that would indicate sufficient nucleation was achieved and that the system remained steady throughout the run once the condition was achieved. A dip in IR data after around 6hr was observed during the process operation due to fouling of the probe. The probe was removed for cleaning and then replaced and reached the desired set point again (**Figure 5-18** Bottom). Temperature control was precise, and at all targets, set points were maintained within $\pm$ 0.5 ^{o}C throughout the run (**Figure 5-18** Top). The temperature in each vessel was controlled using model predictive control using PharmaMV control software

(**section 4.4.1**). The final results showed a close agreement with the simulated results. The mean product size predicted for each stage was close to the actual PSD. PSD data for residence times in each vessel dictates that the steady state was approached from the third residence time, and particle span was reduced when the system approached a steady-state (**Figure 5-19**). Nice tomahawk shape unagglomerated ALM product is also visible in the SEM image in ***Figure 5-20*****.**

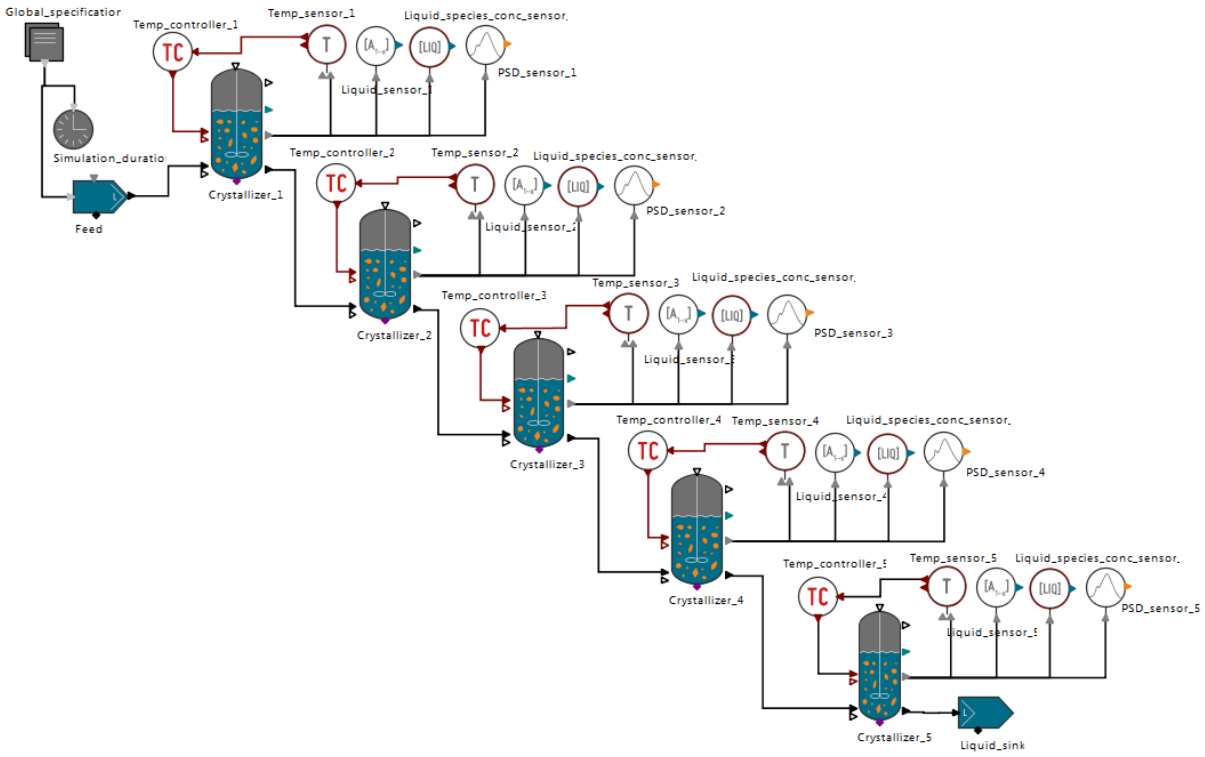

Figure 5-17 Continuous 5-Stage CMBOC primary nucleation model flowsheet in gPROMS.

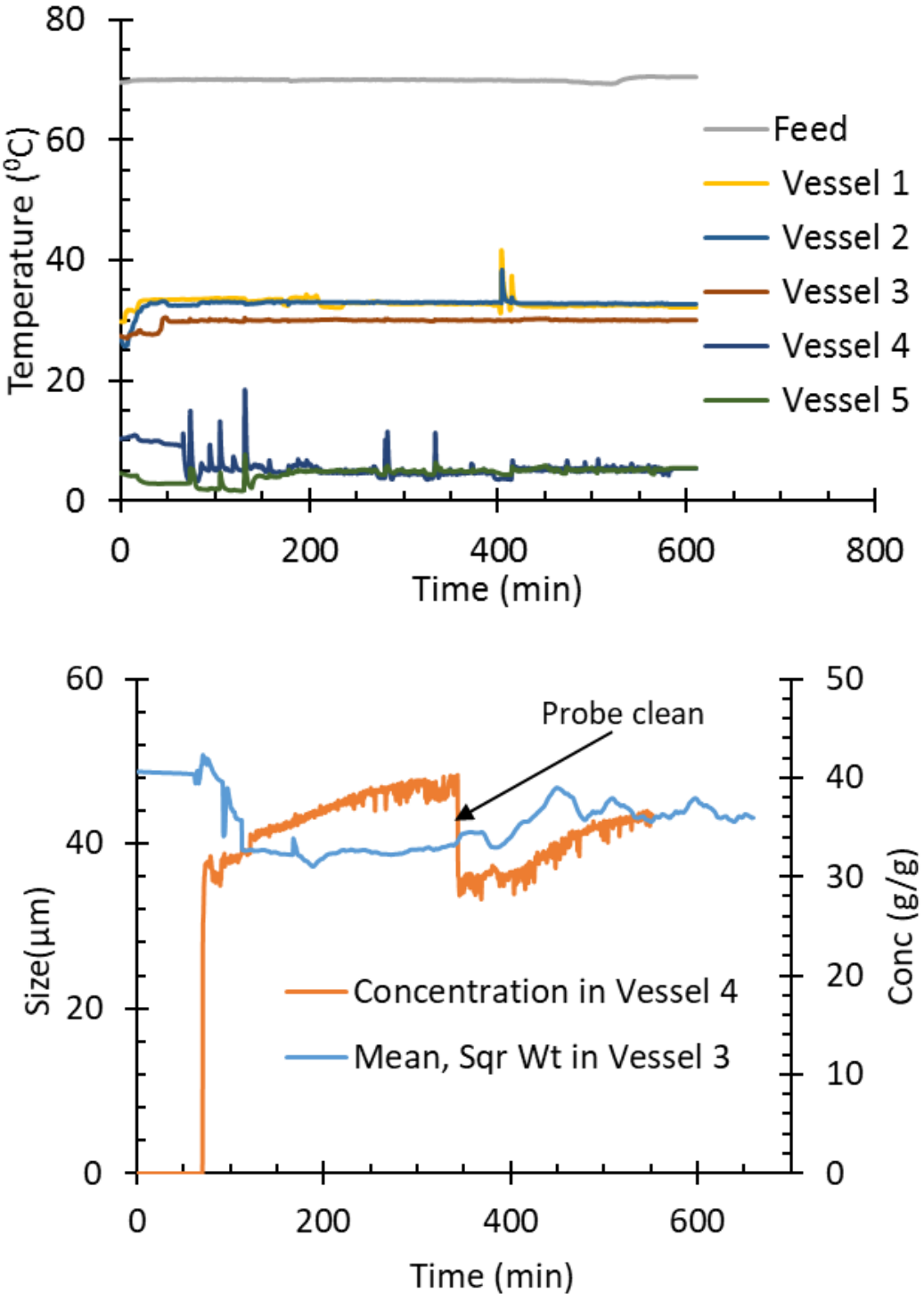

Figure 5-18 Top) Temperature profile over a whole run showing consistent operation. (Bottom) The concentration profile measured in the 4th vessel and FBRM trend from the 3rd vessel shows approaching steady-state operation after the third residence time.

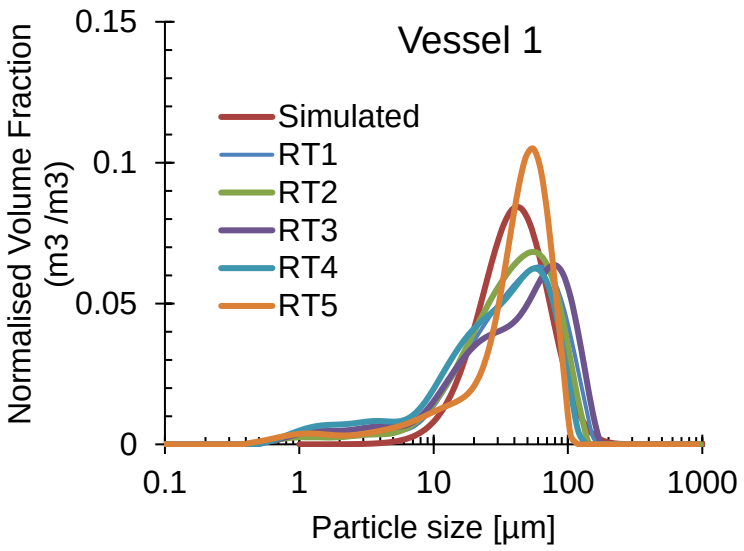
Vessel 1
Normalised Volume Fraction (m3 /m3)
0.15
0.1
0.05
0
Simulated
RT1
RT2
RT3
RT4
RT5
0.1
1
10
100
1000
Particle size [µm]

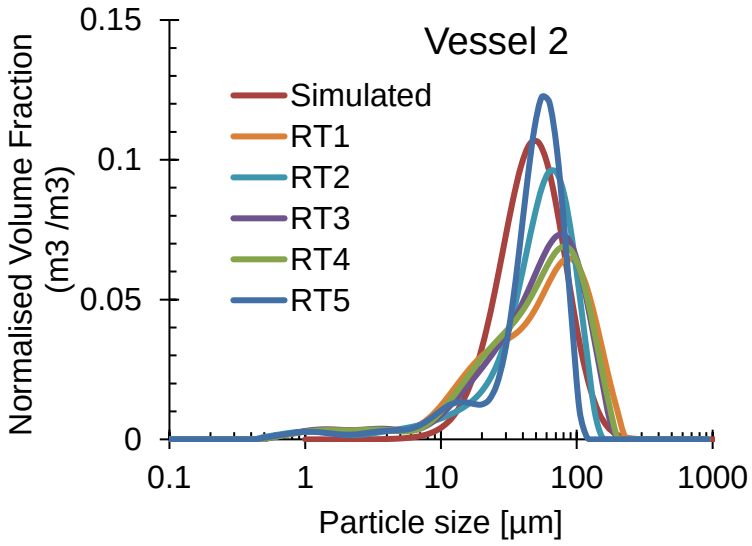
Vessel 2
Normalised Volume Fraction (m3 /m3)
0.15
0.1
0.05
0
Simulated
RT1
RT2
RT3
RT4
RT5
0.1
1
10
100
1000
Particle size [µm]

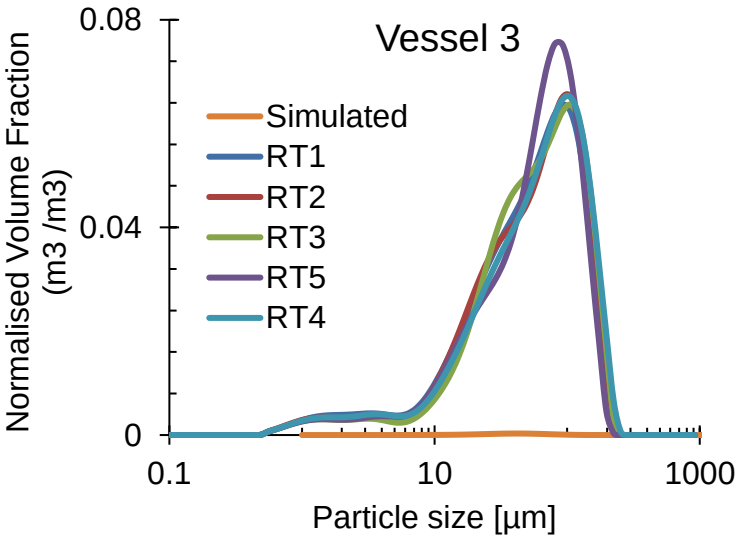
Vessel 3
Normalised Volume Fraction (m3 /m3)
0.08
0.04
0
Simulated
RT1
RT2
RT3
RT5
RT4
0.1
10
1000
Particle size [µm]

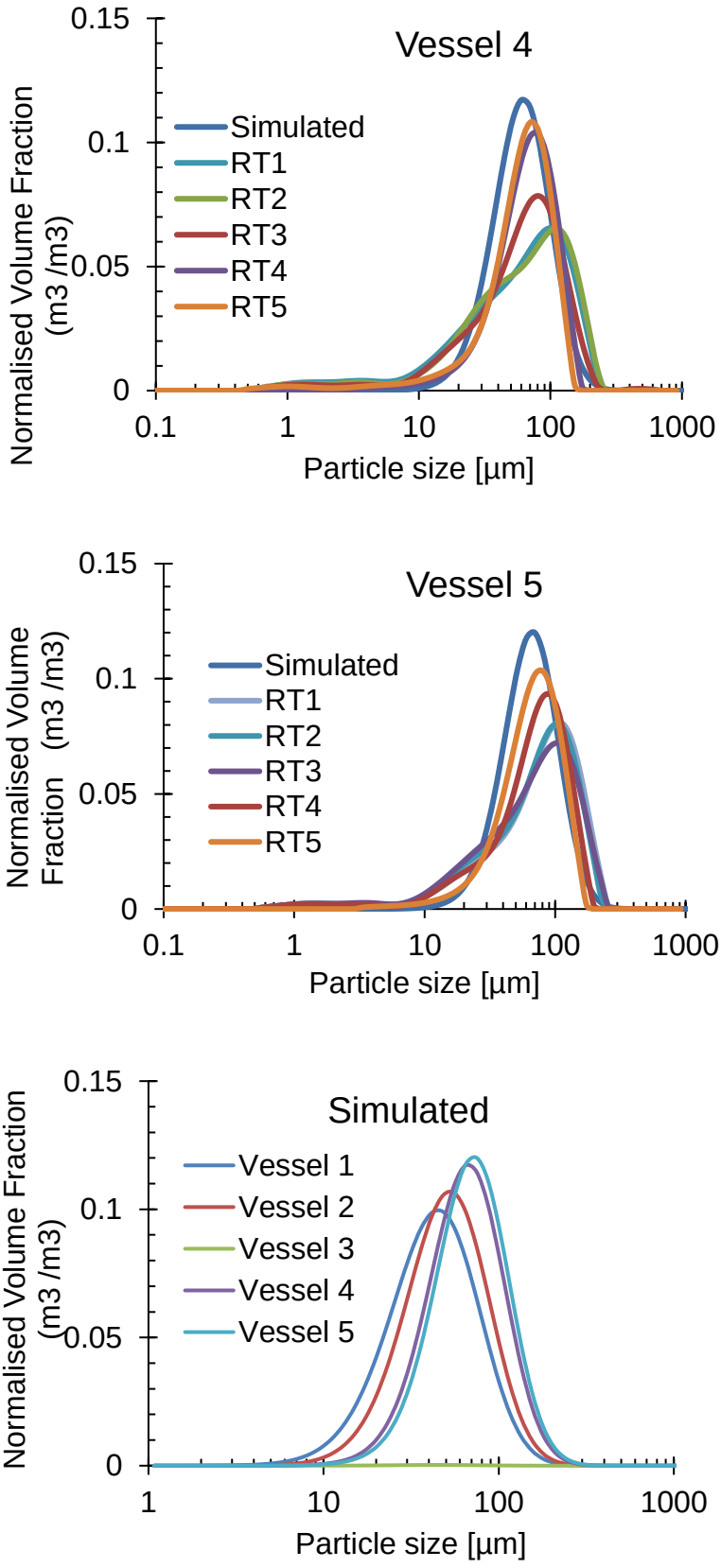

Figure 5-19 comparisons of actual versus simulated PSD of the different vessels after each residence time.

Table 5-10 Simulated PSD and concentration at each vessel for unseeded crystallisation experiment.

Simulated					
Vessel	**Conc**	**D[10]**	**D[50]**	**D[90]**	**Span**
	(g/g)	**(μm)**			
1	0.46	18.61	42.30	86.27	1.60
2	0.45	23.48	50.05	97.78	1.48
3	0.43	28.02	57.11	108.16	1.40
4	0.41	32.52	64.52	119.42	1.35
5	0.37	35.45	69.29	126.39	1.31

Table 5-11 experimentally measured PSD at each vessel for the unseeded crystallisation experiment.

Experimental					
Vessel	**Solid recovery**	**D[10]**	**D[50]**	**D[90]**	**Span**
	(%)	**(μm)**			
1		9.02	43.7	74	1.486
2		13.5	50.4	79.4	1.308
3		12.9	61.3	127	1.86
4		24.2	62.8	106	1.296
5	65.53	20.2	71.4	129	1.53

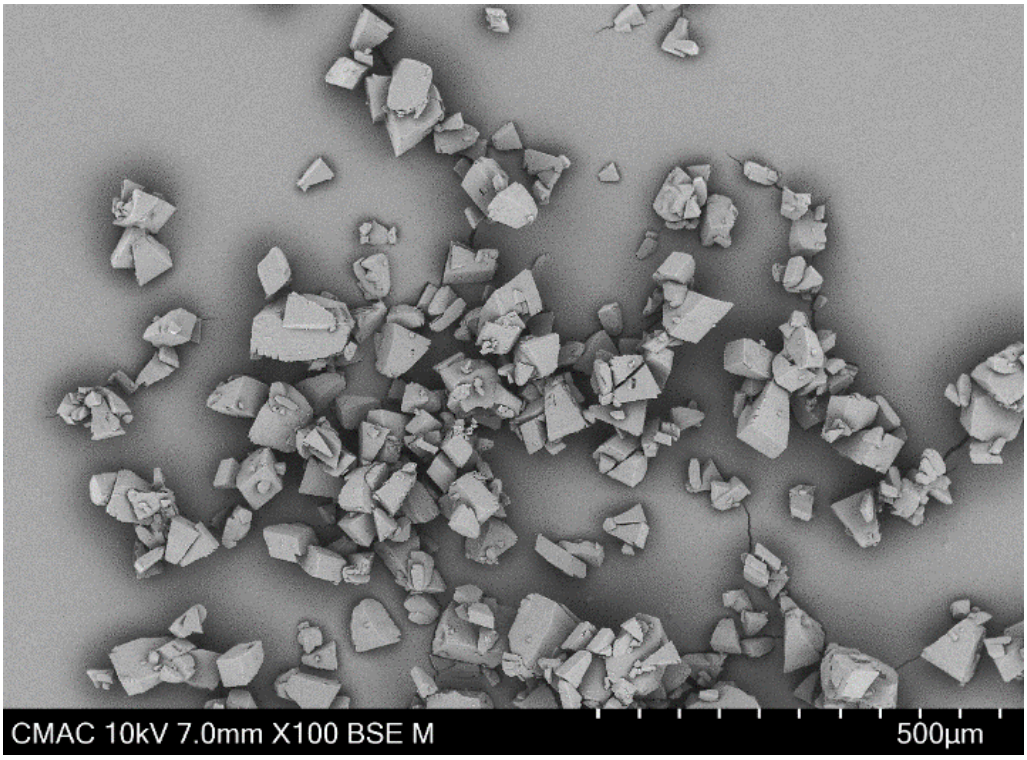

Figure 5-20 SEM images of ALM crystal product from 5-stage CMBOC primary nucleation validation experiments.

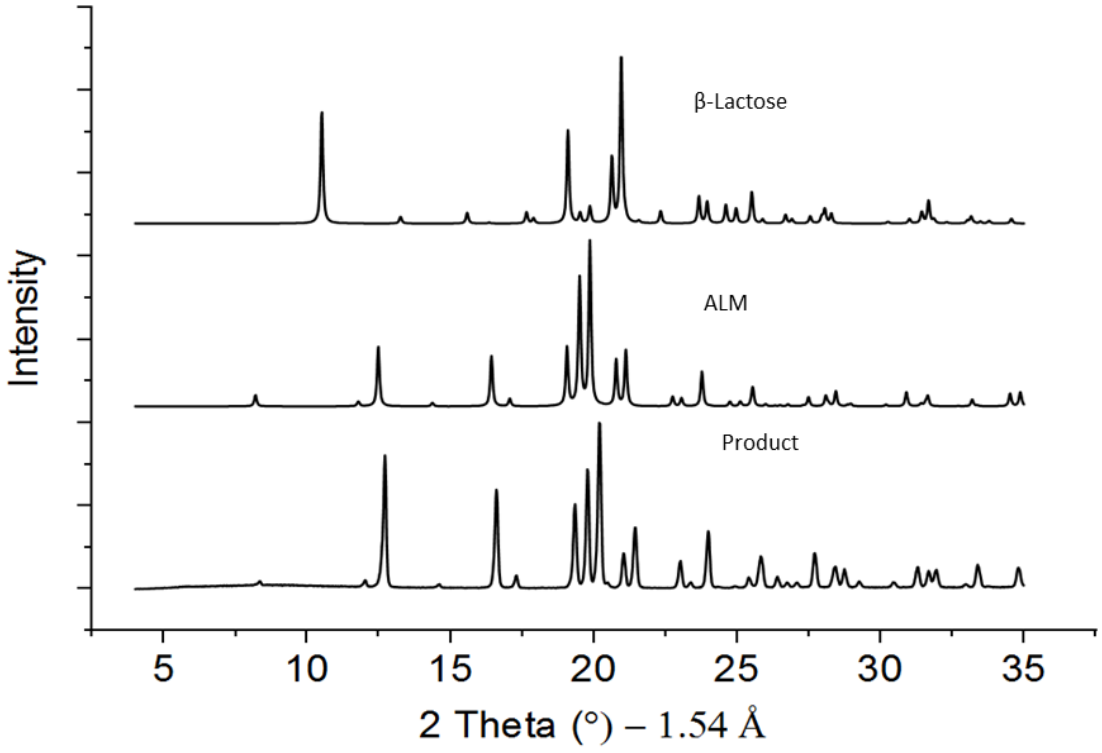

Figure 5-21 X-ray powder diffraction patterns for ALM, β-Lactose and Product

5.4 Operational consideration during a lactose modelling

There are a range of approaches and models available in literature. However, choosing the right model for the specific compound is always challenging and mostly based on the researchers preference. There is always a compromise between accuracy and effort required to build a specific model. Here in this work I have chosen the sequential parameter approach. In which different crystallisation phenomena were parameterised sequentially in isolation as practically as possible. However, due to the complexity of the lactose system there were some limitations in the design of experiments and validating model above certain boundaries due to which growth and secondary nucleation kinetics were observed overlapping during the experiments. There are always measurement errors during the isolation of product for off-line analysis (PSD measurement) above room temperature. which can also effects the accuracy of the model. However, the measurement errors such as size analysis from the mastersizer cannot be avoided which in turn impact the model outcomes and its validation to an extent. Most of the time there are parameters in the model which are highly correlated that can also have affect on model accuracy. To avoid this there is a need to design experimental plan by implementing DOE approach to narrow the operating boundaries to develop the model.

5.5 Summary

This chapter optimises the continuous lactose crystallisation process in a CMBOC by developing a crystallisation population balance model using a sequential parameter estimation approach. The modelling platform used for this investigation was gPROMS. A set of experiments were performed in a batch crystalliser to estimate primary and secondary nucleation and growth. One important factor implemented during model development was the mutarotation of alpha to β-Lactose in the solution phase. Due to mutarotation, the actual alpha lactose concentration is significantly lower than the total lactose concentration. It is very important to estimate the rate of mutarotation to design and implement a cooling crystallisation process for alpha lactose monohydrate.

An accurate complex solubility model in the solution phase was implemented in gPROMS considering lactose mutarotation. Then nucleation and growth parameters were successfully estimated based on actual alpha lactose concentration in the solution. These estimated parameters were utilised in designing a continuous crystallisation process (seeded and unseeded) aiming to dial a particle size. Predictions from the models were validated against the product collected from the continuous trial. The experimental measurements and model predictions within the defined model boundaries and uncertainties were obtained with good statistical agreements ($\pm$5 µm between simulated and experimental measured mean size). Moreover, the advantage of the moving baffle arrangement in transferring the kinetic model from a batch to a continuous process was proved through experiments and simulation.

Chapter 6. Particle Engineering- Size controlled spherical agglomeration of benzoic acid

6.1 Introduction

Spherical agglomeration (SA) is a process whereby simultaneous precipitation and agglomeration or agglomeration of particles in suspension (post-crystallisation) take place, resulting in the formation of spherical particles. This can lead to improvements in bulk powder properties compared to non-agglomerated or neat powder. Therefore, this technique presents excellent opportunities as a particle engineering approach for APIs with suboptimal or challenging attributes, for example, a particle that crystallises in a needle-like morphology [129]. By applying a SA step to such particles, improvements in important material attributes can be achieved, including higher bulk density and better flow properties to enable easier filtration or downstream processing. In addition, due to their shape control, i.e. moving from the high aspect ratio of primary particles to spherical agglomerates, enhancing their bulk properties and Mechanical properties can also be modified as particle microstructure altered from the pure, monolithic crystal lattice, e.g. enabling compaction can also provide benefits through dissolution rates and bioavailability behaviour [233, 234].

The terms spherical crystallisation (SC) and spherical agglomeration (SA) are often used interchangeably, although SC covers a number of different methodologies to produce spherical agglomerates. For the purposes of this thesis, the SC will be termed as the overall process (i.e. particle formation plus agglomeration steps), and SA is one of the methodologies to produce spherical agglomerates, where the API is crystallised through traditional techniques suspended in a medium, and the SA process is a subsequent step applied to those crystals.

6.1.1 Spherical Crystallisation

The SC method employs suitable solvent and anti-solvent systems for the direct crystallisation of the solid. A miscible anti-solvent is added to an API solution to reduce the material's solubility and create supersaturation. Currently, four common spherical crystallisation methodologies have been reported; Ammonium Diffusion (AD) [235, 236], Neutralisation (NT) [237],

Quasi-Emulsion Solvent Diffusion (QESD) [238, 239], and Spherical agglomeration (SA) [58, 134, 137, 240-243].

6.1.1.1 Ammonia Diffusion

AD is a modified spherical crystallisation technique applicable to amphoteric substances (such as Enoxacin, Norfloxacin), which are only soluble in acidic or alkaline aqueous solutions and insoluble in neutral aqueous solutions and organic solvents. Therefore, agglomerating them using more conventional SC techniques is challenging. In this technique, a binary solvent system of ammonia and water used as solvents. The solid can be dissolved in either water or ammonia; the other is used as an antisolvent, which was selected depending upon the solubility of the solid in that particular solvent. The ammonia water also acts as a bridging liquid in the third solvent's absence [235, 236, 244, 245]. The AD process is divided into three stages [235]. The solid dissolved in ammonia-water is initially precipitated while the droplets collect the crystals (**Figure 6-1 A**). Simultaneously, ammonia in the agglomerate diffuses into the organic solvent (**Figure 6-1 B**). Subsequently, spherical agglomerates are formed (**Figure 6-1 C**).

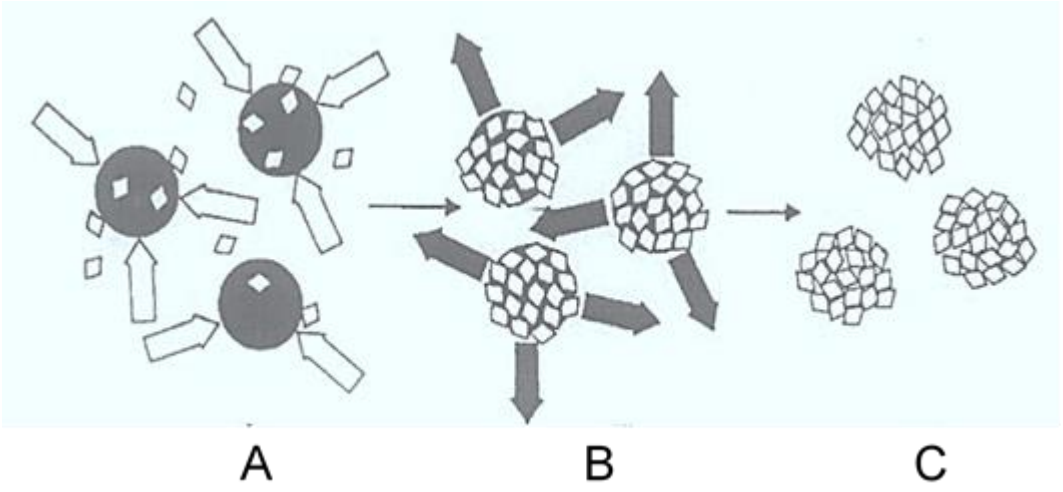

Figure 6-1 Spherical Crystallisation mechanism using the AD method. (A) An invasion of organic solvent in ammonia water droplets (B) diffusion of ammonia from agglomerates to the organic solvent (C) Agglomerated crystals. Adapted from Ueda et al.1990.

Ueda et al. produce spherical agglomerates of the antibacterial drug Enoxacin. Firstly, the 16 % (w/v) Enoxacin was dissolved in ammonia-water solution at 40 °C; then, the solution was poured into a mixture of (80:20) acetone:DCM solution, where the acetone entered the ammonia-water droplets. Subsequently, Enoxacin precipitates out in the droplet while the ammonia diffuses out of the formed agglomerates [235].

Puechagut et al. also demonstrated formation of norfloxacin's agglomerate crystals by dissolving in ammonia-water and then precipitating by adding acetone [236].

6.1.1.2 Neutralisation

In NT, bridging liquid is added to the API solution to form agglomerated particles. This technique involves forming the primary crystals by neutralising a saturated basic solution with acid instead of using a solvent change, i.e. involves reactive crystallisation rather than antisolvent. Sano *et al.* produce spherical agglomerates of the anti-diabetic drug tolbutamide by dissolving it in a sodium hydroxide aqueous solution [233]. The solution is then neutralised by adding hydrochloric acid, leading to Tolbutamide's crystallisation. The ethyl ether (bridging liquid) was added dropwise to bind together the primary crystals and create interparticle bridges to form an agglomerate [233]. Kawashima et al. also reported a neutralisation method by dissolving sodium theophylline monohydrate crystals in ethylenediamine and sodium chloride solution which were added in chloroform and ethanol solvent mixture to produce spherical agglomerates [237].

6.1.1.3 Quasi-Emulsion Solvent Diffusion

QESD is also known as the transient emulsion method. This method requires only two solvents, a solvent and an antisolvent [238]. In the QESD method, the solid and solvent's affinity is stronger than between solvent and anti-solvent. Because of the higher interfacial tension between the solvent and antisolvent, the saturated solution is dispersed into the antisolvent to produce quasi-emulsion droplets [238], neglecting that both pure solvents are miscible [233, 239, 246]. Nocent *et al*. agglomerated salbutamol sulphate in a water-ethyl acetate solvent system (1:10 ratio) with the QESD method [238]. Sano

et al. prepared tolbutamide spherical agglomerates by QESD in a water-DMF solvent system (1:40 ratio), showing a higher dissolution rate and larger specific surface area of the agglomerated product compared with the primary material [239]. As illustrated in **Figure 6-2,** the solvent diffuses gradually out of the emulsion droplets into the outer antisolvent phase during the counter diffusion step, and the antisolvent diffuses into the droplets. The solid then crystallises inside the emulsion droplets due to decreasing solubility of the solid insolvent [246].

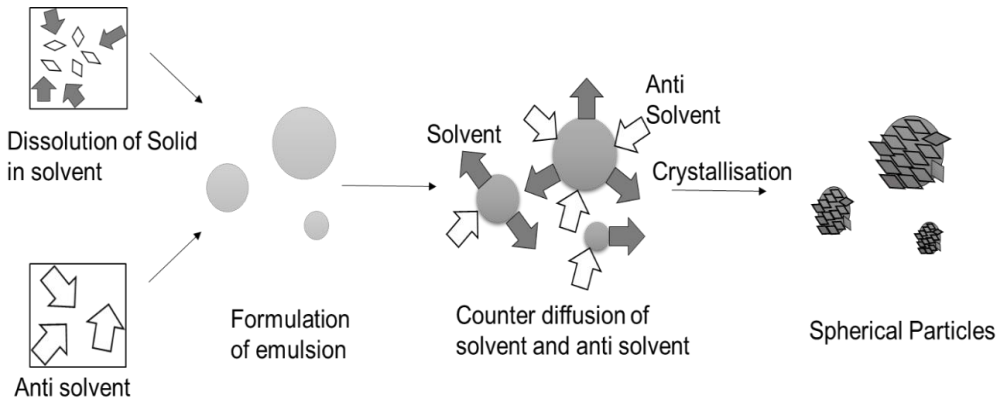

Figure 6-2 The steps involved in QESD spherical agglomeration method Adapted from Mahanty,2010. [246].

6.1.1.4 Spherical Agglomeration

SA can be considered most flexible SC method: it usually requires a more straightforward solvent system than other methods described previously. It can be carried out simultaneously with crystallisation or post-crystallisation [131]. However, selecting the appropriate BL can be difficult, especially considering the potential toxicity of any residual BL in the final agglomerates [129].

SA can help combine several process steps, i.e. synthesis, crystallisation, separation and agglomeration, to simplify the overall process [131, 134, 247]. SA method involves good solvents in which solids dissolve, and then anti-solvents (also called dispersant liquid (DL)) are added to the saturated solution for direct crystallisation. Once a suspension of particles has been achieved (which may also be produced by dispersing existing crystals in the dispersing

liquid), a third solvent bridging liquid (BL) is added to the suspension, aiding the formation of dense, compacted spherical agglomerates. This is achieved via either a distribution or immersion mechanism depending on the relative size of the primary particles and droplets (**Figure 6-3)** [129]. Mechanistically, the SA process can be broken down into several separate processes, many of which may occur simultaneously. SA process steps can be similar to wet granulation, albeit with a lower solid concentration. After adding BL to a suspension of crystals in the DL; wetting, nucleation, consolidation, coalescence and breakage are described below [129, 247-249].

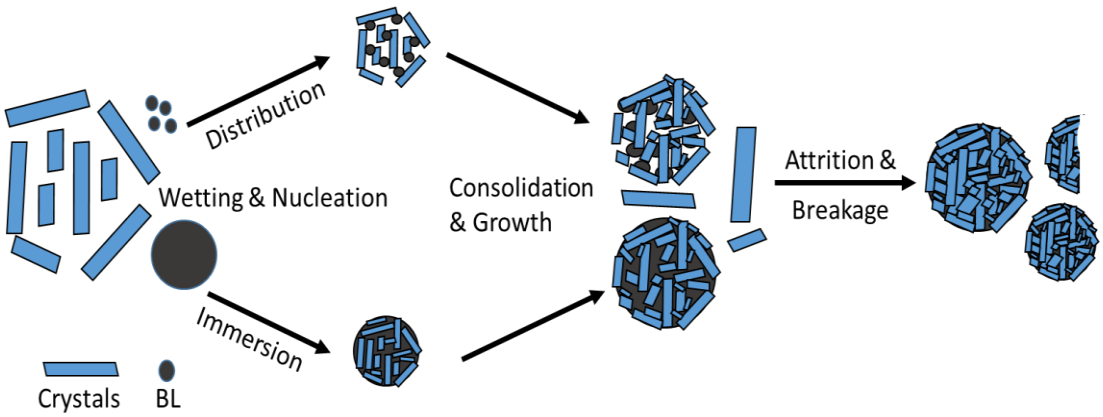

*Figure 6-3 different stages of SA. Adapted from Pitt et al. 2018 [*129*].*

In summary, the formation of agglomerates via the SA method can be described by the following process steps (adapted from Subero *et al.* [132] and Omid *et al*. [250]).

Wetting and nucleation: Similar to wet granulation, different mechanisms have been proposed for the nucleation step: distribution and immersion, which depends on the size ratio of the primary crystal and BL droplet size.

When the particle's size is bigger than the BL droplet size, the nucleation takes place by a distribution mechanism, where the BL droplets are covered by the primary crystals, which leads to the formation of agglomerates with an irregular shape and a looser structure. When the particles are smaller than the BL droplet, nucleation occurs by an immersion mechanism. During this mechanism, The primary crystals impact against the surface of the BL droplet

and enter the droplet until the droplet's internal volume is saturated with primary crystals. This leads to the formation of agglomerates with a narrower particle size distribution, a more spherical shape, and a denser structure. The immersion route is most favourable when you require better control over final agglomerate size as primary crystals are trapped inside the droplet.

Consolidation: The consolidation process occurs following wetting and nucleation, where the forming agglomerate nuclei begin to compact and internally rearrange whilst reducing the porosity by squeezing out the bridging liquid. Subsequently, the robustness of particles increases through the formation of inter-particle bridges. Agglomerates' compaction can also occur due to agglomerate-agglomerate/agglomerate-equipment collisions at a higher stirring rate.

Attrition & Breakage: In the final step, agglomerates' Breakage and attrition may also occur simultaneously to growth due to shear forces and agglomerate-agglomerate/agglomerate-equipment impacts. Eventually, equilibrium is reached where the mean particle size remains constant or may even reduce slightly due to the breakage [129, 248].

Kawashima *et al*. introduced an SA technique into pharmaceutical manufacturing in the early 1980s by forming salicylic acid agglomerates [134]. Several researchers have extensively studied SA for different APIs, including Aminophylline [134], Fenbufen [240], Acetylsalicylic acid [241], Mefenamic acid [242], Benzoic acid [58, 137, 243], Cefotaxime sodium salt [251] and Clopidogrel hydrogen sulfate [252]. In this method, spherical agglomerates are produced and agglomerated simultaneously.

The motivation for this research is to design tuneable spherical agglomerates of benzoic acid (BA) with the SA method to target particles less than 500 µm. In addition, the compaction performance of these agglomerates will be assessed using direct compression studies [188]. It is essential to control the BL droplet size to produce smaller agglomerates [137], for which a novel HSWM approach was implemented and is described in detail in **Section 6.5.2**. BA spherical agglomeration has been well studied previously; however, BA's reported agglomerates size was in the 700-3000 µm range [58, 247, 253]

hence the interest in targeting smaller agglomerates sizes and investigating the factors that control size. These large particles create significant challenges for downstream pharmaceutical processes, where blend and content uniformity are key requirements [58, 59, 137, 188]. Hence the smaller target size of less than 500 µm was selected as a useful target.

6.1.2 Influence of process parameters on spherical agglomeration

It is essential to understand the relationship between input material properties, process conditions and outputs to achieve controllable, predictable and reproducible outcomes for any given process. Several studies have reported the effect of various process parameters on SA that include: mixing rate, [248, 254] residence time,[247, 248, 255] initial crystal size, [254] starting solid concentration, [59, 129, 188] amount of BL [58, 243] and the addition rate of the BL [58, 247]. These parameters influence the productivity and the resultant micrometric properties such as particle size distribution, morphology, compressibility, and product strength.

6.1.2.1 Solvent Selection

The selection of solvents systems is largely driven by empirical approaches to enable each SA process. Chow *et al.* gave some general guidelines to use as a starting point to select solvents and proceed further using different methods, summarised in **Table 6-1**[256]. A general rule of thumb for selecting the BL is that it should not be miscible with the anti-solvent. Meanwhile, anti-solvent and solvent systems should be miscible, and their affinity must be stronger than those between solid and solvent.

Capes and Sutherland demonstrated that the final agglomerate size varied directly with the solid and bridging liquid's interfacial tension ratio to the initial solid particle size [257]. The particles' wettability in the DL and the BL and the interfacial tension between these solvents were similarly considered critical factors [243]. Chen *et al.* recently proposed a design strategy to select the ternary solvent system for cefotaxime sodium, BA, potassium chloride, maltitol and trisodium phosphate SA method based on the Lifshitz-van der Waals acid-

base approach to characterise the wettability of liquid and the interaction among individual crystals [258].

Table 6-1 Solvent selection for the SA method [256].

Solid	**Dispersant liquid**	**Bridging liquid**
Soluble in water	Water-miscible organic solvent	Immiscible organic solvent or salt solutions in high concentration without common ions.
Soluble in organic solvents	Water	Water-immiscible organic solvent
Soluble in water-miscible organic solvents	Saturated aqueous Solution	Organic solvent mixture
Insoluble in water or any organic solvent	Water-immiscible organic solvent	Salt solutions in high concentration without common ions

In SA, crystals are initially clustered together from a mechanistic viewpoint due to surface tension and capillary forces associated with the liquid-liquid interface between the DL and the BL. Thus, interfacial tension is a critical property impacting the performance and outcome of SA [131]. **Figure 6-4** shows a schematic of two spherical particles' kept together by interfacial and capillary forces. Liquid B is the BL, and liquid A is the DL. When the BL efficiently wets the particle surfaces, the contact angle, θ, becomes less than 90 degrees resulting in a curved interface. As a result of this curved surface, the BL side's pressure is less than the pressure on the dispersant liquid side. This pressure difference leads to capillary forces on the particles, pushing them together**.** On the other hand, if the BL is more attracted to the solid surface, the contact angle is lower between the solid and the liquid, facilitating the penetration through capillaries and helping produce agglomerates [259].

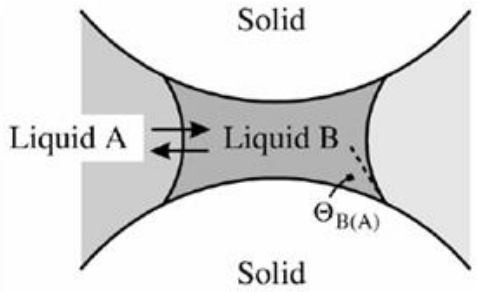

Figure 6-4 Meniscus of liquid phase B and liquid phase A between two-particle surfaces Adapted from Butt and Kappl, 2009 [259].

A concave meniscus occurs when the BL is more attracted to the solid surface than the liquid molecules in the DL. Capillary action acts on a concave meniscus to pull the liquid into the capillaries, increasing the favourable contact area between liquid and solid surfaces. In addition, the direct action of the interfacial tension of the liquid around the periphery of the meniscus contributes to pulling the particles together [259]. Therefore, the BL and the crystallisation solvent's interfacial tension are as important as the solid material's wettability with the BL. Too low an interfacial tension does not lead to SA even if the wettability is good [131]. The relation between pressure difference, interfacial tension and contact angle given by **Equation 6-1** shows that the capillary pressure increases with increasing γ and cos θ [260].

$$\Delta \boldsymbol{P} = \boldsymbol{C_1} \frac{\boldsymbol{1-p}}{\boldsymbol{p}} \frac{\boldsymbol{\gamma}}{\boldsymbol{D}} \boldsymbol{COS\ \theta} \qquad \textbf{Equation 6-1}$$

C_1 is a constant depending on the particles' specific surface areas, p is the agglomerate porosity, D is the mean diameter of the agglomerate, γ is the interfacial tension between the liquids (water and bridging liquid), and θ is the contact angle.

In summary, choosing the right solvent system and to produce stable bridging liquid droplet to perform spherical agglomeration is not always straight forward. Sometimes in preparing the dispersion of bridging liquid can create flocculation, coalescence, flocculation, Ostwald ripening and layer separation. In few instances, stabilisers, wetting agents, ripening inhibitors are often used to increase the stability of droplets [261]. These inhibitors helps in lowering the

interfacial tension between dispersing liquid and bridging liquid and by doing so, induce droplet to break up and also provide stability to formed droplets against coalescence. Using saturated dispersing liquid with the bridging liquid up to its miscibility value before the start of agglomeration process can also helps in accelerating the wetting of the solid and prevent foaming.

6.1.2.2 Amount of Bridging Liquid

The amount of bridging liquid added to the SA system can significantly impact the process. Consequently, it has often been the most influential parameter, along with the BL droplet size affecting the final product attributes [129].

Each solid system requires a different amount of BL to be added. The ratio of BL to the number of solid particles is denoted as the bridging liquid to solid ratio (BSR). The BSR range is highly dependent on the system and tends to be found empirically by scanning varying BL addition volumes to a particle suspension. With increasing BL addition, the primary particles begin to aggregate and agglomerate, eventually reaching an optimal BSR where stable spherical agglomerates are formed. A paste-like material is formed when the BSR exceeds the critical range for agglomerate formation (i.e. too much BL is present) [59, 129]. Only within this critical range is the agglomeration process efficient. Thati and Rasmuson found that agglomerate deformability increases with high BSR, resulting in more energy dissipation during collisions and an increase in agglomeration efficiency, ultimately yielding larger agglomerates [243]. Blandin *et al*. and Subero-Couroyer *et al*. reported that the agglomerated salicylic acid's product size significantly increases from 700 to 2200 µm with a BSR increase from 0.35 to 0.47 [132, 248].

6.1.2.3 Temperature

Kawashima *et al.* studied the effect of temperature on the SA process of salicylic acid in the ethanol-water-chloroform solvent system. They demonstrated that the bulk density of the agglomerates decreases with increasing temperature. The large agglomerates produced at higher temperatures were bulkier, less spherical and loosely compacted in a cylinder resulting in a low bulk density [131]. Work from Thati and Rasmuson showed the effect of temperature on the SA of BA. They concluded that the

agglomerate size and strength increased with a decrease in temperature while the particle shapes also improved with a decrease in temperature. The hypothesis is that solubility is decreased at lower temperatures while supersaturation increases, which affects the higher nucleation rate and subsequent interparticle growth amongst the colliding particles [243].

6.1.2.4 Mixing and Residence Time

The agitation rate of the system during SA can impact a number of aspects of SA formation and directly influence the agglomerates formed through the level of hydrodynamic forces produced [129]. Furthermore, increasing agitation speed promotes agglomerate collisions that could significantly increase agglomerate growth. However, too much agitation can also lead to the disruption of coalescence and the breakage of agglomerates that do form. Consequently, studies investigating the agitation rate effect often report an increase in agglomerate size up to a certain agitation rate, followed by decreased size after this point [188, 262]. Therefore, an optimum agitation rate is often sought to give the desired agglomerate size.

The probability of collisions between crystal particles and BL droplets increases at higher agitation rates (Amaro-Gonzalez and Biscans). However, very high agitation rates can also lead to short contact times, which may impede wetting and coalescence [260].

Agitation rate also influences the BL droplet dispersion and size, increasing agitation rate and giving smaller droplet sizes as more energy is input to the system (Subero-Couroyer *et al.)* [132]. Higher agitation rates may also affect the dispersion of initially formed particles and agglomerates, and too low an agitation rate could lead to flocculation in the absence of a BL [132]. Furthermore, the minimum BSR amount required decreased with the agitation rate, indicating that less BL is required to obtain agglomerates at higher agitation rates. This results in achieving a more homogeneous dispersion of BL in the suspension, improving particle wetting, and yielding more efficient nucleation [263].

Agitation rate has also positively influenced agglomerate porosity and compressive strength. Blandin *et al.* reported that increased stirrer speed led to decreased agglomerate porosity, giving denser agglomerates greater compressive strength [248]. The decrease in agglomerates' porosity with increasing agitation speed has been attributed to higher shear forces aiding the agglomerates' compaction [264]. Compaction and consolidation will also lead to a reduction in agglomerate size [255]. Improved sphericity and flowability with increasing shear rate have also been reported by Usha et al., [265].

As expected, residence time in the process is another important parameter affecting SA product properties. Kawashima *et al.* reported that the size of agglomerates of aminophylline increased gradually with longer residence time and, after a certain time, an equilibrium state was attained [134]. A similar observation was noted by Morishima *et al.* with an increase in agglomerate size with increasing agitation time due to continued coalescence [266]. Blandin *et al.* described changes in salicylic acid agglomerates' porosity decreases as the residence time increases [248]. As the agglomerates grew, their porosity decreased and became more spherical. This was attributed to compaction via agglomerate-agglomerate collisions or agglomerate-vessel collisions due to the system's continued agitation. The compaction process also gives the agglomerates increased compressive strength. Thati and Rasmuson also reported similar observations regarding agglomerate size, sphericity and strength with continued agitation after the completion of feeding in their study on the SA of BA [122]. Morishima *et al.* have also noted an increase in Bucillamine agglomerate density with agitation time [266].

6.1.2.5 Bridging Liquid Droplet Size

The BL droplet size can also significantly affect SA product properties. The droplet size will determine whether the SA process will take the distributive or immersive mechanism route, as mentioned in **Section 6.1.1.4** [129]. Orlewski *et al.* produced benzoic acid spherical agglomerates of varying sizes using toluene as the BL with good reproducibility by injecting the BL into the crystal suspension via a capillary to control the BL droplets size [137]. They have

demonstrated the agglomerate size noticeably decreases with reducing the BL droplet size [137]. Pena *et al*. demonstrated that agglomerate formation depends on particle collisions with BL droplets. Poor mixing prevents uniform BL distribution, causing particle settling, and reduced collision events, resulting in a bimodal PSD. This bimodality results from particles remaining unagglomerated due to reduced collisions, larger particles created due to particle settling, and very large agglomerates generated from over agglomeration due to poor bridging liquid distribution [58]. There is a critical relationship between BL droplet size and crystal size, determining whether the agglomeration occurs via an immersive or distributive mechanism. The mechanism's difference leads to vastly different particle sizes, powder flows, and powder compression properties [138].

6.1.3 Continuous Spherical Agglomeration

Continuous manufacturing has received much attention in the pharmaceutical industry because of its efficiency, economy, better quality control, and relative ease of scale-up [7]. Furthermore, a continuous manufacturing process typically has a smaller volume of material in process at any given time than a similar batch process, providing ease of control over small process volumes whilst creating the need to ensure a steady state or a state of control is achieved and making optimisation and control much easier. Because of these benefits, continuous spherical crystallisation has been explored in the pharmaceutical field to monitor and control process parameters in real-time [127].

Pena *et al.* developed a two-stage continuous MSMPR system to produce Benzoic acid agglomerates, where the two-stage system enables to decoupling of the nucleation and growth rate processes from agglomeration, offering more degrees of freedom to control each mechanism, which in turn provides more control over the agglomerated product with desired biopharmaceutical properties (e.g., morphology, bioavailability, dissolution) and processing performance (e.g., filtering, drying, tabletability) [59]. Similarly, Tahara et al. demonstrated continuous SA of fenofibrate with impurity complexation using a one-stage MSMPR crystalliser via the QESD method.

As a result, they produced spherical agglomerates of 300 μm with improved purity levels from 95.1% to 98.5% [128]. Bos and Zuiderweg also found differences in the size enlargement regime between batch and continuous when using a multi-stage MSMPR [267]. Pena et al. also demonstrated process intensification through continuous spherical crystallisation using COBC to achieve better control over different stages of agglomeration process through a spatially distributed solution, solvent, antisolvent and bridging liquid addition points [58].

6.2 Experimental setup

6.2.1 Solvent Selection

There is a plethora of literature available for BA spherical agglomerate formation. Examples using Ethanol as solvent and water as anti-solvent is the most common, and toluene, chloroform, heptane, and pentane have all been used as BLs [58, 59, 138, 243]. Water is selected as a dispersing fluid since BA has poor aqueous solubility, as shown in **Table 6-2**.

Table 6-2 Benzoic acid solubility measured in water and Ethanol.

Temperature (^{0}C)	Solubility of Benzoic Acid	
	Water (g/g Solvent)	Ethanol (g/g solvent)
5	0.0018	0.127
10	0.0023	0.135
20	0.0035	0.168
30	0.0046	0.198

The initial screening was performed using a small-scale crystallisation platform (Crystalline, Technobis) to identify the optimal range required for BL to deliver strong spherical agglomerates. The system consists of eight independently controlled reactors fitted with 8 mL vials with temperature control and a turbidity detector, cameras for imaging and overhead stirring (**Figure 6-5**).

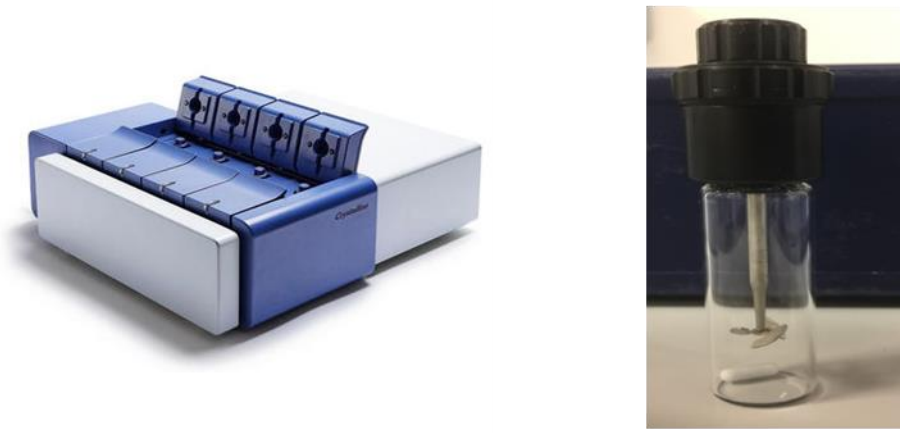

Figure 6-5 Crystalline instrument (left) close-up of an individual 8 ml crystalline vial with the top stirrer (right).

The process protocol for screening experiments is summarised below.

- A suspension of 5% w/w of BA and water (dispersing liquid) was prepared in each vial. The temperature was held constant at 10°C within ±0.1°C.
- Vials were stirred at 1250 rpm using overhead stirrers with a three-blade impeller to ensure efficient mixing. The slurry was stirred for 10 minutes to suspend the BA crystals evenly in water.
- BL was added in 50 µl increments every 10 minutes with a Gilson pipette until a paste was formed.
- This process was monitored by the integrated camera in the crystalline during the addition process to monitor the SA process.

6.2.2 Bridging Liquid Droplet Generation

Next, it is important to identify the practically useful range of BSR and BL droplet size to control the final agglomerates' particle size [137]. Typically, overhead stirring and, in a few cases, the capillary provide stable, uniform-sized droplets for SA processes [129, 248]. However, there is a need to explore the method to generate the droplet in-situ.

This work explored a high shear wet mill (HSWM) as a potentially novel method to control fine BL droplet formation. It is expected that the high-energy

collisions facilitated by the HSWM will produce small droplets of the immiscible BL and promote the efficient wetting of primary crystals and forming of agglomerate nuclei within the HSWM system by circulating the slurry between stirred vessels.

The goal of this work is to understand the influence of BL droplets size on the final agglomerate properties and to understand the interaction between BL droplets and primary crystals by exploiting the advantages offered by HSWM, which enables the generation of a large quantity of uniform BL droplets which size can be carefully tuned by varying the speed of HSWM. It also allows the decoupling of the initial BL addition from other operating parameters, thus enabling a better understanding of the BL's role in the SA process. HSWM is expected to influence the wetting process of primary crystals and the formation of agglomerate nuclei within the BL droplet and also help in stabilising the droplets and reducing the rate of coalescence and break up of droplets, resulting in smaller size agglomerates.

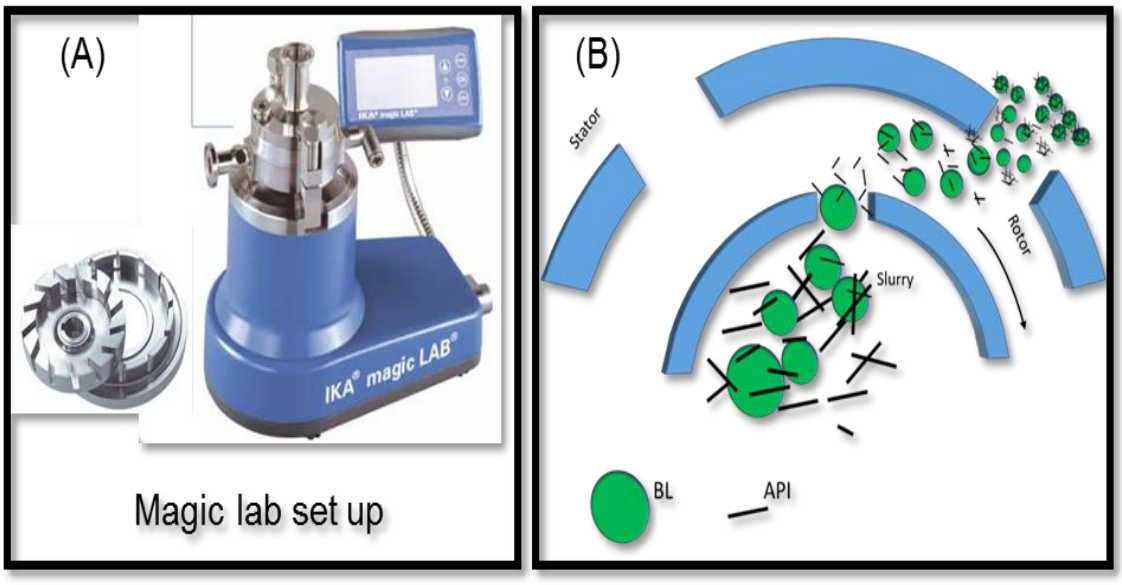

Figure 6-6 (A) HSWM (Magic Lab UTL module, IKA) set up showing single-stage rotor-stator (4M generator). (B) Schematic illustration of BL droplet and API crystal size reduction inside the stator-rotor.

An IKA MagicLab (Module DRS) (**Figure 6-6**) HSWM unit was used for the in-line BL droplet generator. Rotational speeds can be operated between 5000

to 26000 rpm with varying rotor-stator tooth pair configurations. The temperature of the wet mill chamber was cooled by circulating mains water on the jacket side to avoid excess heating due to high-speed rotational speed. The Peristaltic pump (Watson Marlow 620s) circulated the slurry between HSWM and the agglomeration vessel. The circulation flow rate was kept constant to achieve the half volume turnover per minute to make sure bridging liquid is well suspended over the entire volume of dispersing liquid. A particle vision and measurement (PVM) probe and an FBRM in-line PAT probe are incorporated to examine the evaluation of BL droplets. Temperatures of the inlet and outlet of HSWM and vessel bulk were also monitored.

For BL droplet characterisation, Chloroform, toluene and heptane were used with 10% w/w solution concentration as BL and dispersed in water to generate droplets. This is well within the range of BSR required to form BA spherical agglomerates with these BLs [188]. The chord length distribution and particle counts were monitored using an FBRM (Mettler-Toledo Particle Track G400). In-situ images of the process were taken using a particle vision and measurement (PVM) (Mettler-Toledo Particle View V19). The droplet was also generated by only overhead stirring (OHS) only and then compared with the droplets generated with the HSWM setup.

6.2.3 Spherical Agglomeration in 1-L Batch

Process understanding experiments carried out in batch to performed antisolvent crystallisation of BA. A subsequent stage of SA was carried out in a 1L jacketed vessel fitted with a 4-pitch blade impeller and jacket side connected to a water bath circulator (Lauda ECOgold 450) to control the process temperature.

The setup also consists of the FBRM probe to monitor the agglomeration process and a thermocouple for temperature monitoring (**Figure 6-7**). The whole SA process describes below in sub-stages of crystallisation, pre-milling and SA steps. Preliminarily experiments were carried out to optimise setup and find out the experiment's bounds for effective SA (i.e. pre-milling time, BL addition position, milling stage and duration, which are explained in detail along with the final operating condition in the below section.

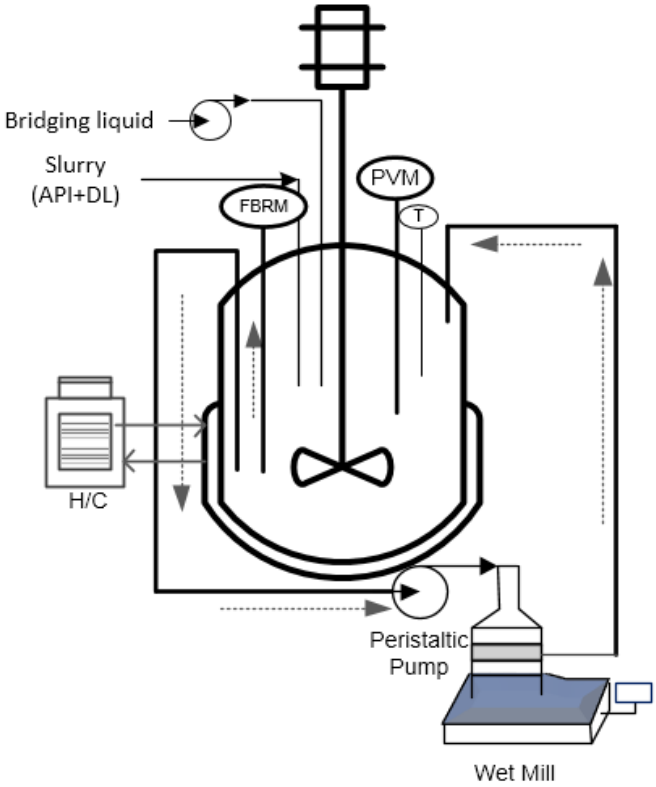

Figure 6-7 Schematic of SA process setup

Crystallisation step:

In all Batch experiments, the feed solution was prepared by dissolving BA (40 g) in ethanol (80 g) to obtain the chosen concentration of 0.5 $g_{solute}/g_{solvent}$ in a 250 ml Duran bottle at 40°C, which was then cooled down to 10 °C in 20 min before the start of each experiment.

Water (800 g) was then charged into a vessel at 10 °C, and the BA feed solution was pumped into the vessel dropwise via the peristaltic pump (Watson Marlow) for over 30 min. As soon as the BA solution entered the vessel, BA precipitated out. The slurry was left to age for a further 30 min after the feed solution addition finished. The overall crystallisation stage time was kept constant at 60min (30 min for BA solution addition and 30 min after hold) for all the experiments. The crystallisation process was carried out for a sufficiently long period to allow the system to desupersaturate and approach equilibrium before agglomeration. The agitation rate was kept at 300 rpm during the crystallisation period.

Pre-milling step:

Prework was carried out to optimise setup and experiment bounds for effective SA to determine the initial pre-milling time.

After the crystallisation stage, The overhead stirring (OHS) was increased to 600 rpm to provide high shear for effective SA. At the same time, the slurry was circulated through the HSWM to reduce the primary particle size, which helped favour the immersion distribution mechanism route for SA.

Spherical Agglomerations step:

The BL addition location is also crucial. A surface addition (low shear region) resulted in more BL consumption than adding the BL in bulk near the agitator (high shear region). It is also important that the BL is kept off the vessel wall to avoid fouling the wall. The BL addition tubing was secured to a thermocouple to ensure BL delivery was away from the vessel wall and entered the system near the agitator and at a similar position in each run to avoid this fouling. The BL was added via a peristaltic pump via 0.8 mm ID PTFE tubing.

HSWM operation was initially planned for the BL addition stage to produce uniform BL droplets and primary agglomerate nuclei formation. However, preliminary experiments demonstrated that keeping the wet mill running even after the wetting and nucleation stage into the consolidation stage helps produce more compact and stronger agglomerates, as visible in (**Figure 6-9)** SEM images. Therefore, one experiment was carried out while running the wet mill for a longer period in the consolidation stage to find the optimum time required for the consolidation stage. As per the FBRM trends shown in **Figure 6-8,** all the scoping experiments had a 15 min hold in this stage. A reduced speed was used to minimise the excessive breakage of newly formed agglomerates. In this consolidation stage, agglomerate goes from light with fluffy surfaces to smooth, more dense particles. During the coalescence stage, HSWM stops and stirring is maintained at 600 rpm for a further 15 minutes; in this stage, compaction due to agglomerate-agglomerate/agglomerate-

equipment collisions is observed, which results in a decrease in agglomerate size and porosity.

BL was added at varied flow rates according to the BSR (0.8, 0.85 and 9), addition time (30 and 60 min) and the wet mill speed varied (10000, 15000 and 20000 rpm) as per the requirements of each experiment.

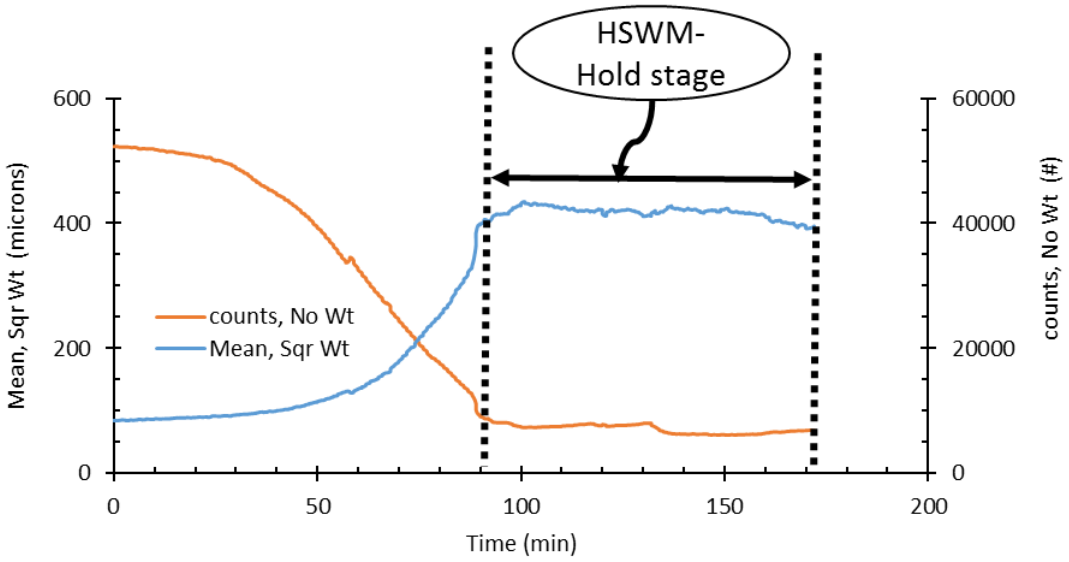

Figure 6-8 FBRM trend in consolidation stage with wet mill running. The holding stage shows the constant size and particle counts during hold(between dashed lines).

Filtration step:

The agglomerates are filtered using a standard lab-scale Büchner funnel setup and dried at 40 ^{0}C. **Figure 6-17** shows the BA particle size distribution of the primary crystals with a mean size of 68 µm with plate-like needle-shaped crystals visible in the microscopic image.

No washing strategy has been implemented as a water wash produced lumps after drying while heptane wash led to breakage of some agglomerates (**Figure 6-10**).

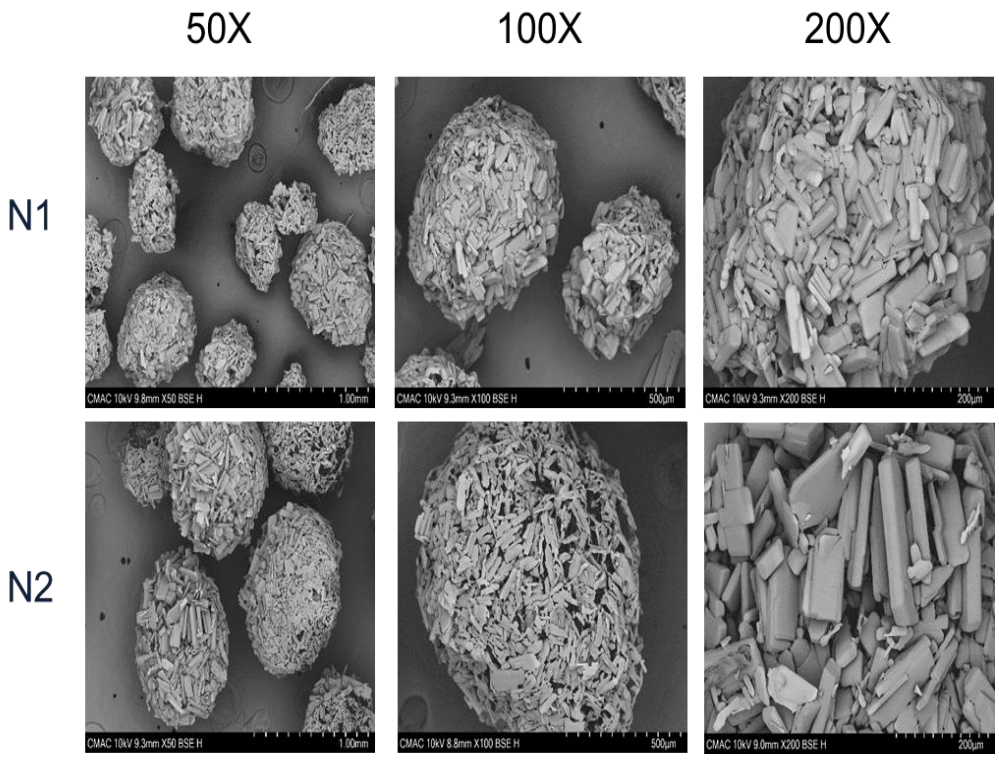

Figure 6-9 SEM images: N1- HSWM in BL addition stage and consolidation stage and N2- HSWM in BL addition stage only.

Figure 6-10 Washing protocol; No wash, Heptane wash and water wash from left to right.

6.2.3.1 Process understanding:

The following section summarises the experimental work conducted to check the influence of key process parameters that affect the product attributes. The effect of BSR, mixing and BL additional time were analysed using MODDE Pro (version 12) from Sartorius to build a multiple linear regression (MLR) model.

For each factors, an individual MLR model was built, and any transformations applied to the response and factors used where tuned to maximise the model fit (R2), future prediction precision (Q2), Model validity and model's reproducibility. The parameters kept constant during these studies are 5 w/w % solid concentration, Chloroform was used as BL and fixed 10 °C vessel temperature. Fourteen experimental conditions were performed with the mixing (10,000, 15,000, 20,000 rpm), Bl addition time (30,45, 60 min) and BSR (0.8, 0.85, 0.9) varied in different experiments. Further, five experiments were performed using only overhead stirring (OHS) mixing (600, 800 rpm) and with BSR (0.8, 0.85, 0.9) to compare the final agglomerates attributes against the agglomerates produced with HSWM.

Table 6-3 Input variables condition for SA experiments with HSWM

Exp Name	Wet mill speed (rpm)	BSR	Addition time (min)
N1	20000	0.8	60
N2	20000	0.8	30
N3	20000	0.9	30
N4	20000	0.9	60
N5	15000	0.8	60
N6	15000	0.85	45
N7	15000	0.8	30
N8	15000	0.8	30
N9	15000	0.9	30
N10	15000	0.9	60
N11	10000	0.8	30
N12	10000	0.8	60
N13	10000	0.9	30
N14	10000	0.9	60

Table 6-4 Input variables condition for SA experiments with only OHS

Exp Name	OHS (rpm)	BSR
E1	600	0.85
E2	600	0.9
E3	600	0.9
E4	800	0.8
E5	800	0.8

6.2.4 Scale-up experiment in 5-L Batch

A batch scale-up experiment was performed in a 5L jacketed vessel with a similar setup described in **Section 6.2.3** to explore the impact of scale on process outcome. Only the HSWM circulation flow rate has increased to keep constant half volume turnover. Agglomerates were filtered and dried before being characterised for agglomerate size and morphology using microscopy and SEM. Agglomerates were also examined for polymorphic form by XRPD and flow characteristics using an FT4 powder rheometer.

6.2.5 Continuous MSMPR experimental setup

The initial research objective was to perform the continuous spherical agglomeration processes to compare the performance of the CMBOC platform against the MSMPR and by doing so it would have given continuity between the thesis chapters. However, as the research progressed the gap in the area to produce in-situ smaller size bridging liquid droplet to target <500 µm spherical agglomerates where identified. And to address that challenge HSWM was incorporated to produce smaller spherical agglomerates. The current CMBOC set up consist of 120 ml volume vessels while the HSWM compartment and circulation tubing connecting between HSWM and the process vessel consumed approx. 120-150 ml volume which makes it quite impractical to operate with current CMBOC setup. Another problem of moving Baffle close to vessel wall with 0.5mm of gap would have crushed the formed agglomerates. In future larger vessel volume and design of baffles with no gap between vessel wall and moving baffle can be implemented to evaluate spherical agglomeration in CMBOC.

The continuous spherical crystallisation experimental setup of the work presented in this section was carried out in a six-stage MSMPR crystalliser. The proposed setup aims to achieve two of the pharmaceutical industry's current major focuses: process intensification and continuous manufacturing. Process intensification occurs through the spherical crystallisation technique, producing spherical particles that can be directly compressed. Continuous manufacturing in the proposed MSMPR setup has the potential, once at a steady state, to deliver consistent control over the process conditions for the

entire process volume and improve efficiency while reducing intermediate products' handling and reducing the number of unit operations in a drug product line. The proposed six-stage MSMPR crystalliser setup also serves as a robust means of controlling the key rate processes, enabling the decoupling of nucleation, growth and agglomeration mechanisms in space and time, each being controlled separately in individual vessels.

The continuous experimental setup (**Figure 6-11**) consists of six jacketed vessels, each fitted with a 4-pitch blade impeller and with the jacket side connected to a water bath circulator (Lauda ECO gold 450) to control the process temperature. An FBRM probe was inserted in stage six to monitor in real-time the agglomeration process, and thermocouples were placed in every vessel for temperature monitoring and control. Peristaltic pumps (Watson Marlow 520D) were used to pump the feed, BL addition and transfer slurry between each vessel. A section of 8 mm internal diameter PTFE tubing was fixed at the required liquid volume level (measure before the experiment) level to maintain a constant volume in each vessel. Two HSWMs (IKA Magic lab UTL-course rotor-stator) were connected to stages 4 and 5 to produce smaller BL droplet generation with half a volume turnover via the pump between the vessel and HSWM. The six-stage MSMPR setup is divided into three stages for crystallisation and three-stage for agglomeration.

In the first two-crystallisation stage, nucleation occurs through the anti-solvent (water) addition and in the third stage, growth happens during hold at 10 °C. Furthermore, the agglomeration stage consists of agglomerate wetting/nucleation (stage-4), where BL is continuously added via a pump, and the growth zone is separated into stage-5 and stage-6. The operating process parameters (volume of each vessel, Residence time, agitation and HSWM speed, feed flow rate, antisolvent and BL addition values) are tabulated in the P&ID diagram in **Figure 6-11**.

At the start of the process, the feed solution was prepared by dissolving BA (350 g) in ethanol (700 g) to obtain the chosen concentration of 0.5 $g_{solute}/g_{solvent}$ in a 1L Duran bottle at 40°C. The dissolved solution was then cooled to 10 °C in 20 minutes and held in the water bath with stirring. This is

then pumped into the first stage at the 2.5 g/min flow rate at the start of the experiment. The water was added at 12.5 g/min to maintain the required 30 min residence time into stage-1 and 2. Stage-3 was just held at 10 °C with OHS to induce growth. During the start-up, in the agglomeration stage (stage-4), starting with at least half the vessel filled with crystallising slurry before BL addition was beneficial. Otherwise, lack of mixing will create big lumps of agglomerates, which are just stuck at the vessel's bottom. To implement this during the run in the stage-4, BL addition was not started until the vessel volume reached 500 g. After that, wet-mill circulation started, and the equivalent BL was added in the aliquot and let run for a few minutes after that the normal continuous run resumed. This way, uninterrupted continuous operation is implemented without any blockage or fouling issue.

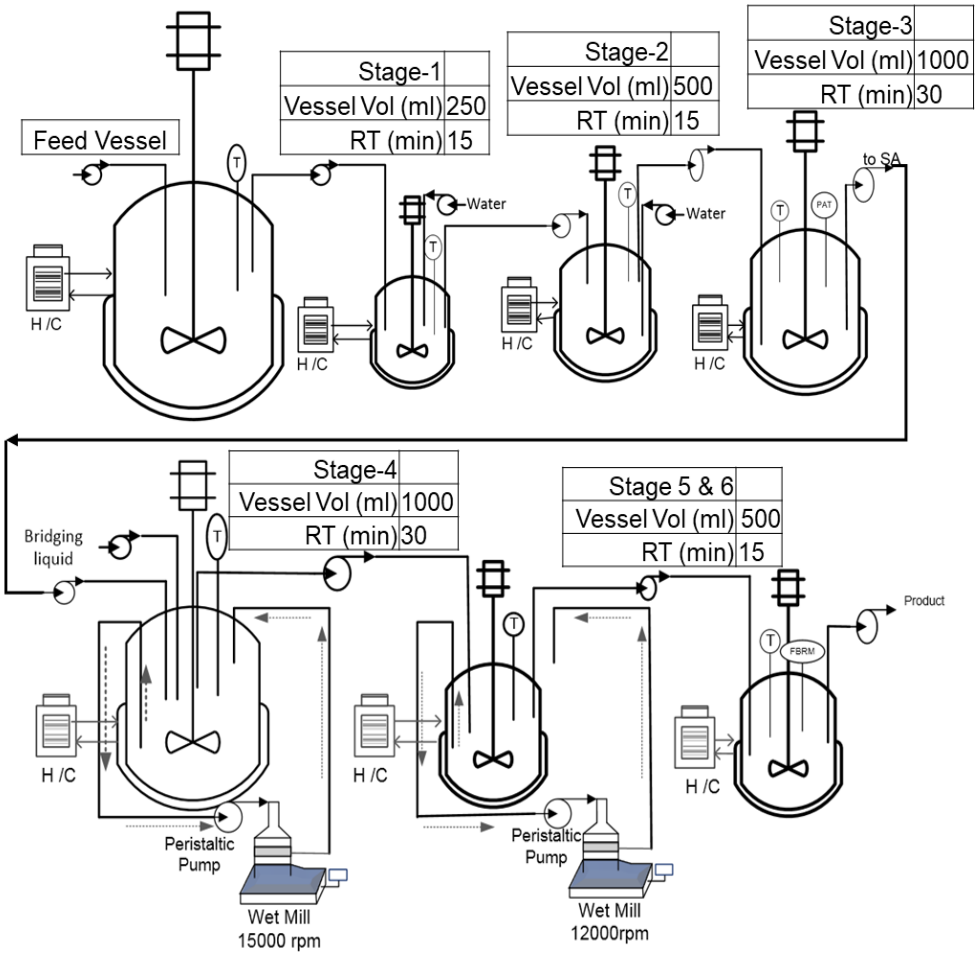

Figure 6-11 P&ID shows the 6-stage MSMPR set-up and operating conditions for the feasibility study on the continuous manufacturing of BA spherical agglomerates. (Above) Crystallisation stages (Below) SA stages

6.3 Result and discussion

6.3.1 Solvent selection

The solvent selection work was performed in the crystalline platform to identify the optimal range required for BL to deliver strong spherical agglomerates.

The ethanol-water solvent system was used as solvent and antisolvent for the BA crystallisation stage chosen from the literature [243]. Work focusing on the screening of BL operating range performed with chloroform, toluene, heptane, ethyl acetate, and diethyl ether, selected based on their immiscibility with water, which helps to form the BL droplet in the DL. These BLs have also been reported previously in the literature for SA of BA generation [58, 59, 137, 188]. No spherical agglomerates were formed from ethyl acetate and diethyl ether even after adding 10 BSR. At the same time, the operating range for the chloroform, toluene and heptane was identified from the Crystalline experiments. Results are summarised below in **Table 6-5**.

Figure 6-12: Images of crystalline vials at different stages of BL addition for Chloroform, water, ethanol solvent system.

Chloroform was then chosen as BL for the SA process. This was on the basis that it yielded consistent compact spherical agglomerates from a wide BSR operating range (0.5-1.5) compared to toluene and heptane, and also, there was the least fouling observed out all the screened BLs.; hence, it was easier to work with to generate a wide range of agglomerates.

Table 6-5 BSR operating range for different BL and water as DL.

Bridging liquid	BSR operating range (g BL/g BA)		
	loose aggregate	Strong agglomerates	Paste
Chloroform	<0.5	0.5 – 1.5	>1.5
Toluene	<0.6	0.6 – 1.1	>1.1
Heptane	<0.8	0.8 -1.3	>1.3
Ethyl acetate	No Agglomerate		
Diethyl ether	No Agglomerate		

6.3.2 Bridging Liquid Droplet Generation

This work aims to create small droplets of BL in the DL. The ratio of BL droplet size to the primary crystal size will determine the agglomeration mechanism (distribution versus immersion). A set of experiments was carried out under the same experimental setup described in **Section 6.2.2.1** on a solute-free basis (i.e., no solid present) with water as DL and chloroform, toluene and heptane as BL. Droplets were generated with OHS only mixing at 600, 800 and 1000 rpm speeds and then compared with different HSWM mixing speeds and configurations with a fixed OHS speed of 600 rpm in the vessel to produce in-line BL droplets. Droplet size monitored by FBRMs means chord length distribution and PVM images.

Table 6-6 summarises the square weighted mean chord length (SWMCL) for different configurations and BLs. Overall, with OHS's only mixing, the droplet was in the range of 112 to 78 µm in size, and the volume percentage of the droplet was around 2 to 4% on a chord length distribution. HSWM has managed to produce a much smaller size of droplet compared to OHS; for example, with chloroform as BL, Droplet size reduces to 30 to 40 µm range with HSWM and volume percentage of the droplet were around 14 to 16% on a chord length distribution (**Figure 6-13**). Droplet images captured by PVM at different mixing conditions display the size range generated with the droplet generation between the OHS and HSWM configuration shown in Figure 6-15.

Table 6-6 Droplet size generated at different OHS speeds and HSWM with the course and fine stator-rotor set up at different rpm.

			Solvent		
			Toluene	Chloroform	Heptane
	Mixing	RPM	FBRMs-SWMCL (µm)		
	OHS only	600	98	92	112
		800	82	86	93
		1000	78	83	87
OHS and HSWM-setup	Coarse rotor-stator	8000	57	40	60
		15000	53	35	57
		20000	47	33	55
		26000	45	30	48
	Fine rotor-stator	8000	61	37	59
		15000	58	33	58
		20000	49	30	44
		26000	43	28	40

In summary, the droplet size is reduced with increased mixing intensity, which will positively affect the agglomeration process's wetting mechanism. An increase in the mixing velocity favours the generation of a bigger number of smaller droplets. Therefore, a higher surface area of BL is available to contact the primary crystals [132].

There is little difference in the mean droplet size generated between course and fine rotor-stator configuration. For instance, when chloroform was used as BL, droplet generated by course configuration at different rpm was 35± 5 µm compared to 30± 5 µm range with fine configuration. However, the process temperature significantly increased (7± 2 °C) using wet mill speed over 20000 rpm for the fine tooth configuration as can be seen in **Figure 6-14 (A)** compares to 3± 2°C rise using the course set up **(Figure 6-14 (B))**. Due to the rise in temperature with the fine rotor-stator which is going to affect the solubility of benzoic acid in the solvents, all the subsequent experiments were

performed using a single course rotor-stator configuration to maintain the temperature of process.

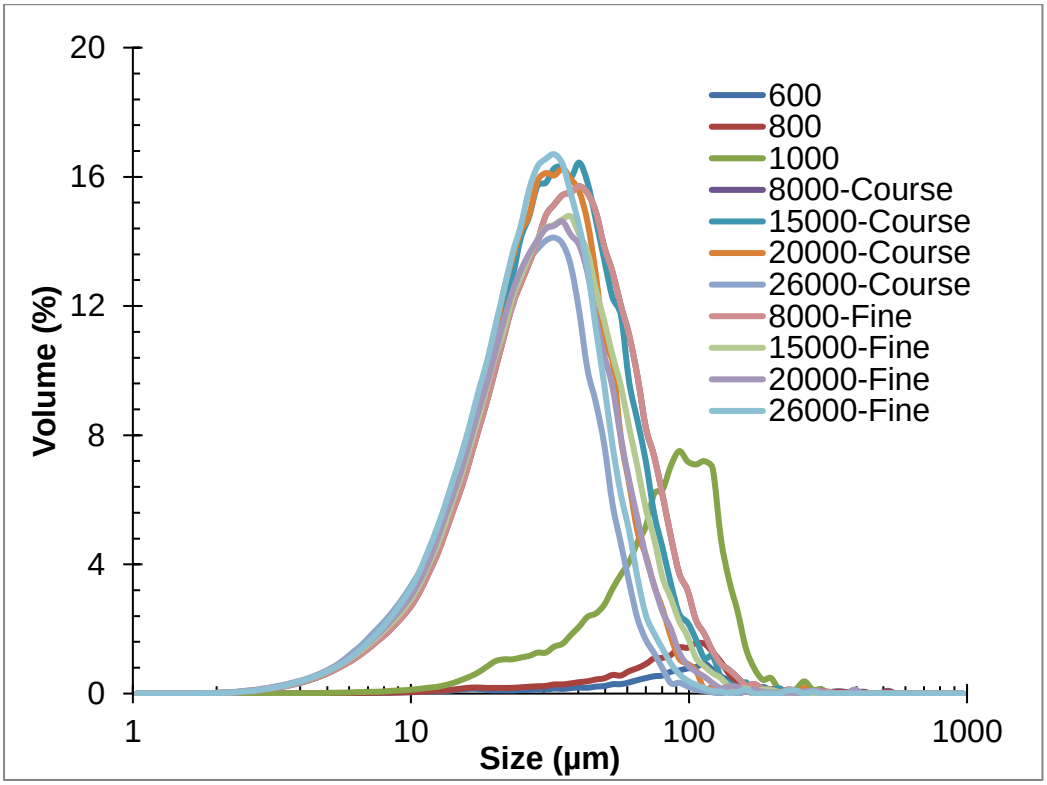

Figure 6-13 Chord length distribution for dispersed BL droplets measured with FBRM of chloroform as BL in the water at different OHS mixing and with HSWM configurations.

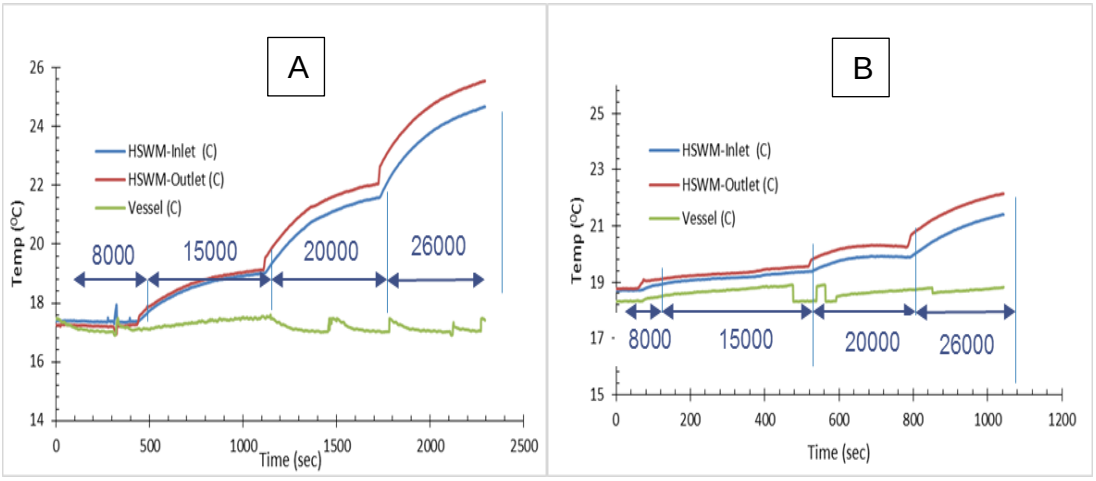

Figure 6-14 Difference in temperature rise in (A) fine rotor-stator configuration and (B) course rotor-stator configuration

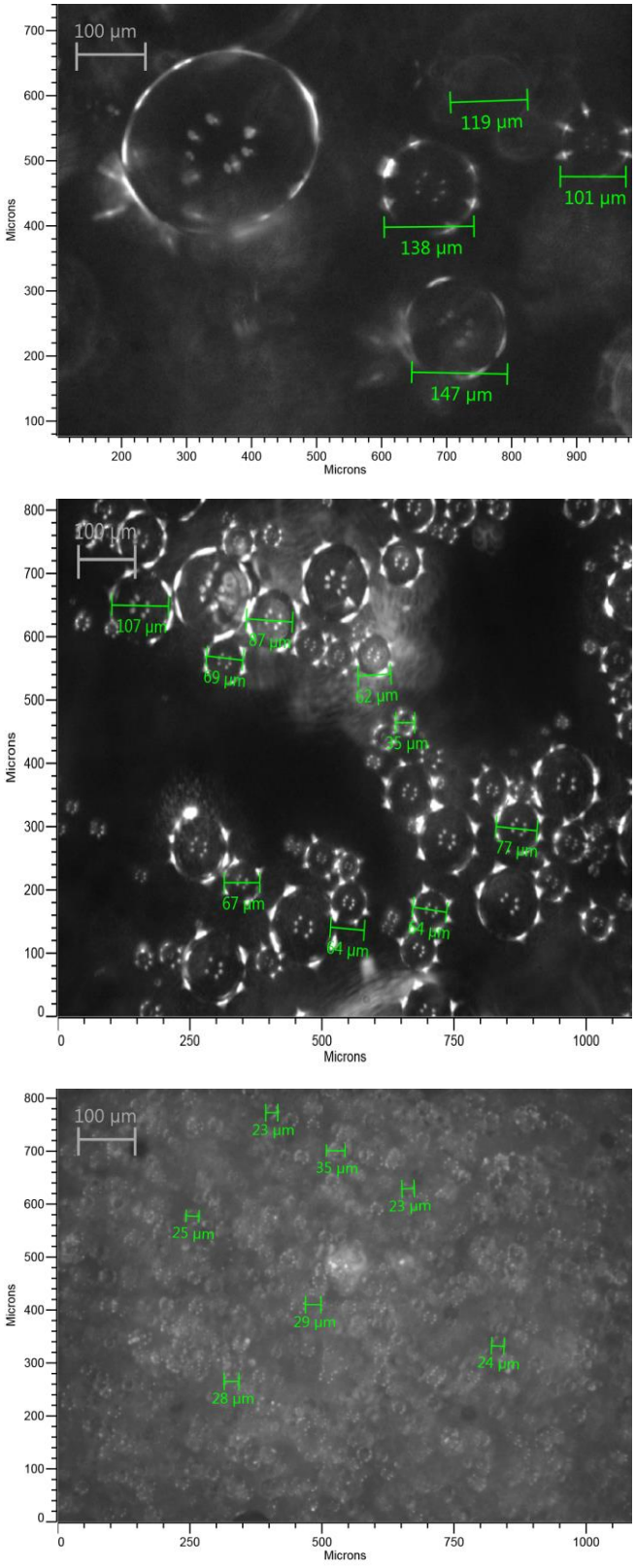

Figure 6-15 PVM images of Chloroform droplets generated in the water at 800 rpm OHS only mixing , with 15000 rpm HSWM and 26000 rpm HSWM speed from Top to Bottom respectively.

6.3.3 Spherical Agglomeration experiments

6.3.3.1 Batch 1 L scale

Several experiments were performed in a 1L jacketed stirred tank vessel to understand the effect of BSR and mixing on the different agglomerates stages. All these observations are apparent in the FBRM trends shown in **Figure 6-16,** which shows the typical FBRM trend of the total number of counts (in orange) and the Mean square weight trend (in blue) to understand the different stages of the SA process of BA which are further elaborated in below in subsections.

These observations agree well with the mechanistic insights reported in the literature [138, 268].

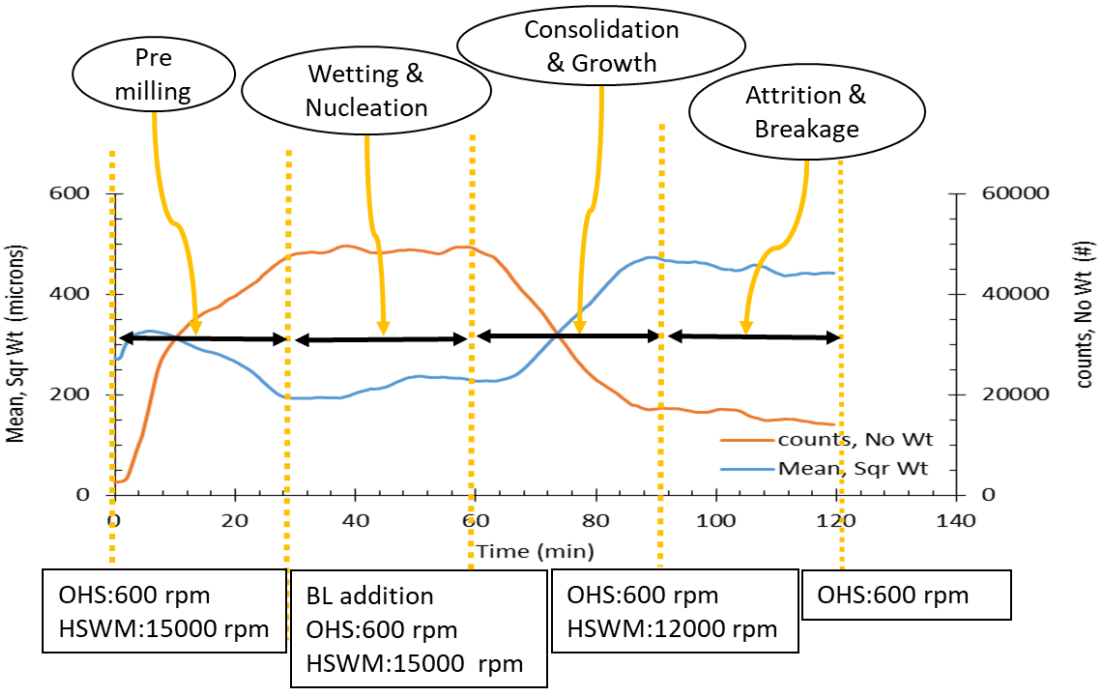

Figure 6-16 FBRM trend of typical spherical agglomeration experiments (Exp-N12) showing different stages of agglomeration process and the mixing parameters of over head steering and HSWM.

Crystallisation stage:

Initially, BA crystallisation was carried out using a reverse antisolvent addition where the ethanolic BA solution is fed to the antisolvent already charged into the vessel. Due to the low solubility of benzoic acid in the water, the high

supersaturation generated leads to fine plate-like crystals of around 60µm precipitate out.

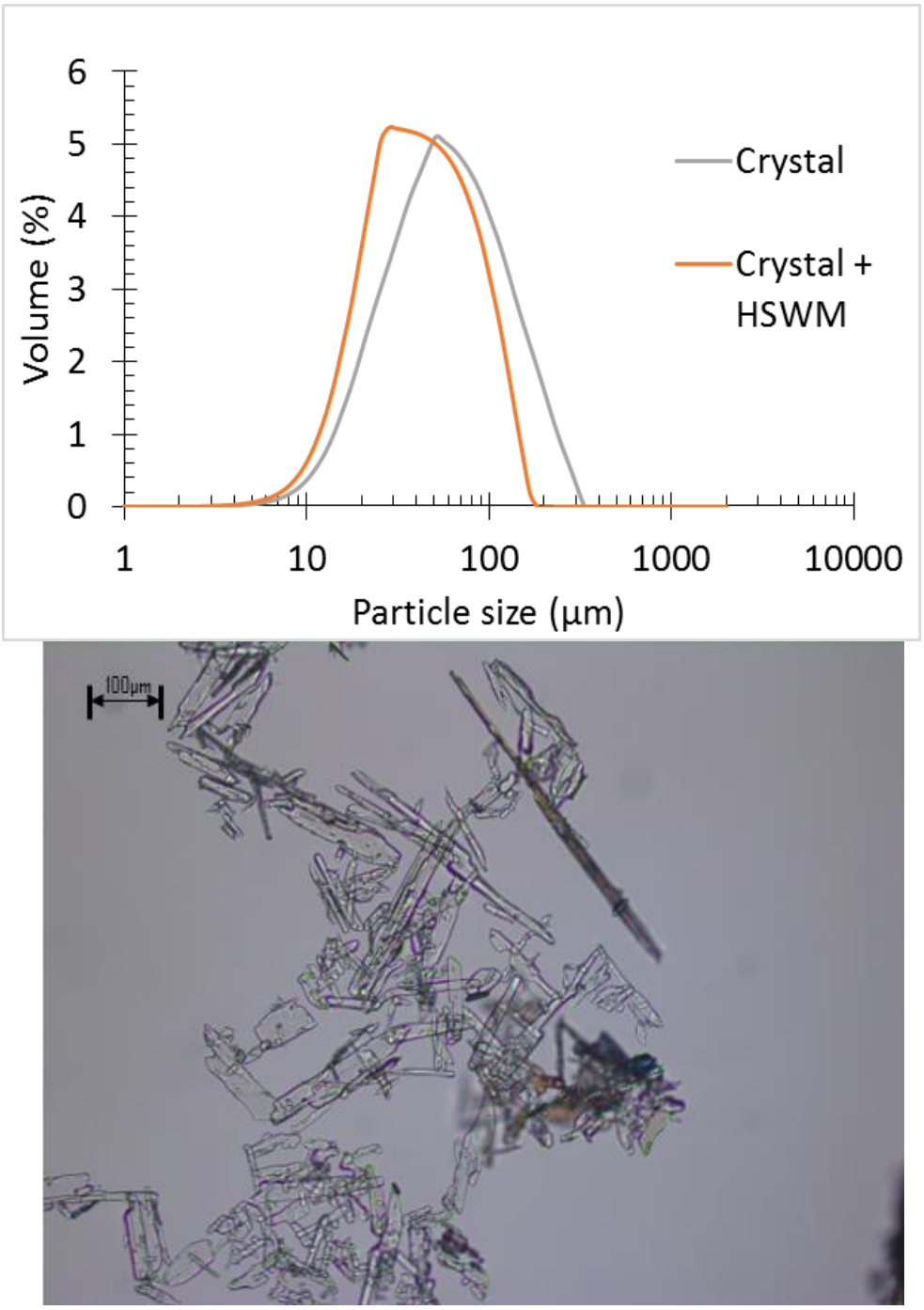

Figure 6-17 (Top) PSD of primary BA crystals before and after the pre-milling and (Bottom) microscopic image of the primary crystals, small needles of BA can be observed.

Pre-milling stage:

Pre-milling time further reduces the primary crystals' size to 35 µm (**Figure 6-17**) with HSWM running at 15000 rpm. The hypothesis was that smaller primary crystals could rearrange and compact more easily during the agglomeration phase than larger ones and induce the immersion mechanism. This can be seen in the FBRM trend in **Figure 6-16,** where total particle count increases and mean square size decrease in the pre-milling stage.

Wetting and nucleation stage:

After the pre-milling stage, the BL is introduced, which induces the wetting and nucleation stage. The high shear mixing imparted by HSWM helps generate a smaller BL droplet size and stabilises the generated droplet by preventing it from coalescing once it's formed. These BL droplets preferentially wet the BA particles, leading to agglomerate nuclei formation; here, not much growth happens, which can be seen in the FBRM trend in **Figure 6-16** (section 2) and PVM images in **Figure 6-18**.

Consolidation and growth stage:

After the initial wetting period, the system went through a consolidation period where the agglomerates became much more compact and started to take their spherical shape as BL diffuses from the agglomerate core to the surface and, ultimately, liberated into the continuous phase of the DL.

In this stage, The reduced HSWM speed also reduces attrition of formed agglomerates, which go from light with fluffy surfaces to smooth, denser particles. It appears consistent with the impact of capillary and interfacial tension forces that govern the formation of the agglomerates described in **Section 6.1.2.5**. Continued agitation beyond the moment of termination of the BL addition contributes to generating the spherical shape and increases agglomerate strength. The crystal morphology of BA (i.e., small plate-like needle crystals) most likely leads to the improved compaction and sphericity observed in the microscope images.

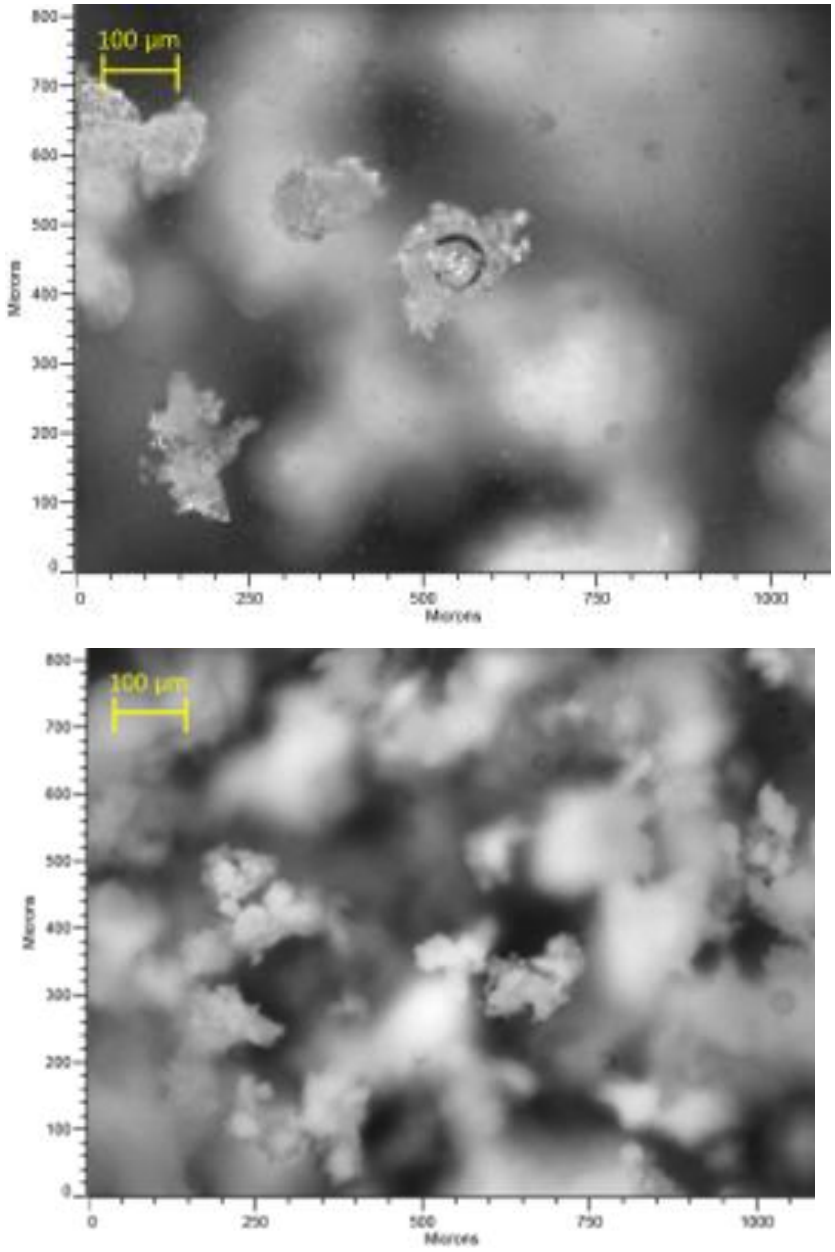

Figure 6-18 PVM image shows the initial wetting and nucleation stage during BA SA.

The agglomeration process immediately undergoes a fast growth period after the wetting and nucleation stage and before a size reduction period, and finally, levelling off at an equilibrium size during the consolidation and coalescences stage (section 3 in **Figure 6-16)**. The initial fast growth period results from the reduced slurry density and bridging liquid dispersion at the onset. The initial particles and bridging liquid added to the system tend to flocculate together into very large agglomerate nuclei due to their limited

availability, reducing dispersion resulting in very large agglomerates (can be seen in **Figure 6-19)**.

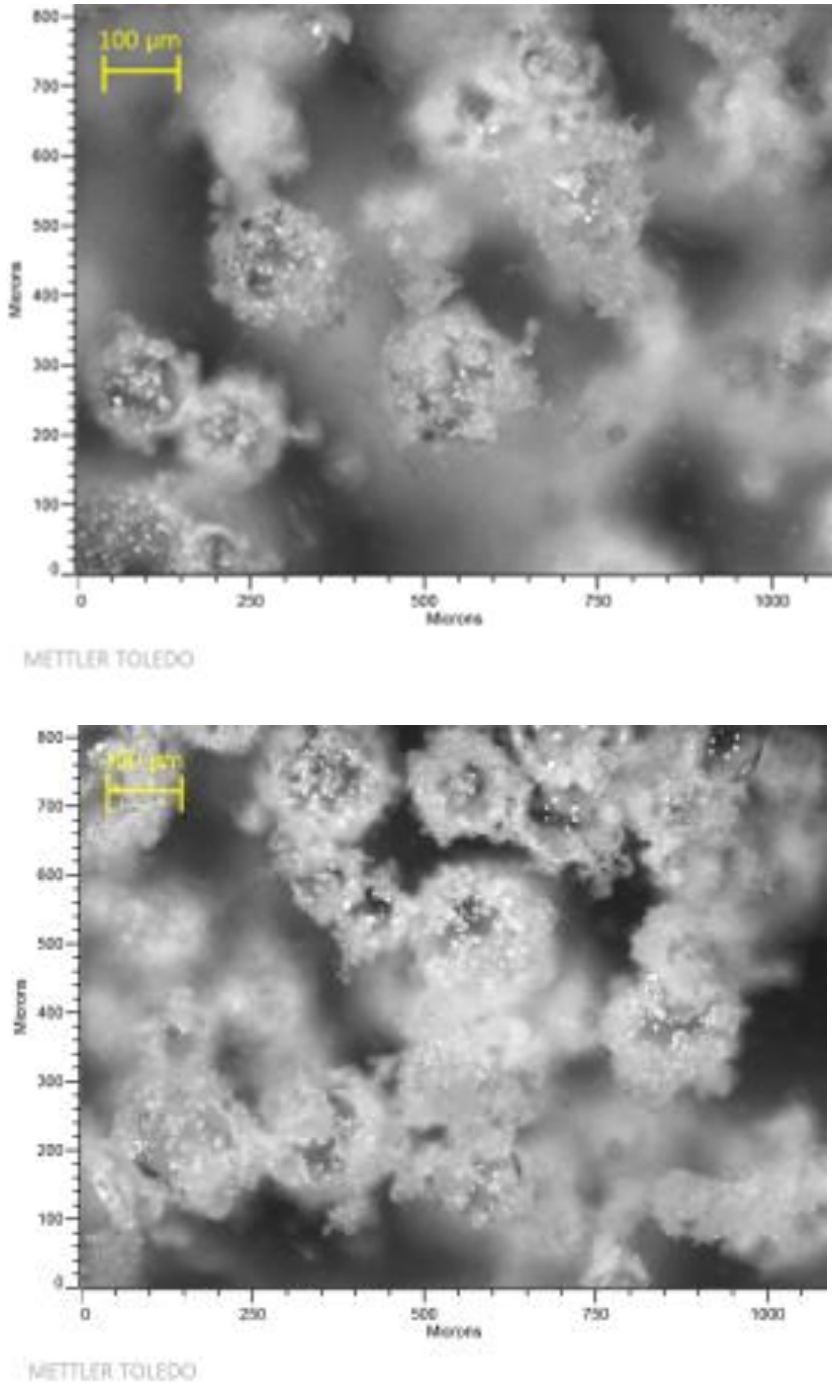

Figure 6-19 *PVM images of consolidation and growth stage of BA agglomeration of multiple agglomerates and the liberation of bridging liquid droplets.*

Breakage and attrition stage:

As the operation continues, the size reduction period is attributed to increased slurry density and increased dispersion of bridging liquid leading to smaller agglomerate nuclei and agglomerates. The balanced addition rate and dispersion of particles and bridging liquid lead to the equilibrium size, i.e. the steady-state. Some breakage and attrition have also been observed due to agglomerate-agglomerate and agglomerate-equipment collisions, which result in a decrease in agglomerate size and porosity which can be seen in section 4 in **Figure 6-16 FBRM** trend and **Figure 6-20**.

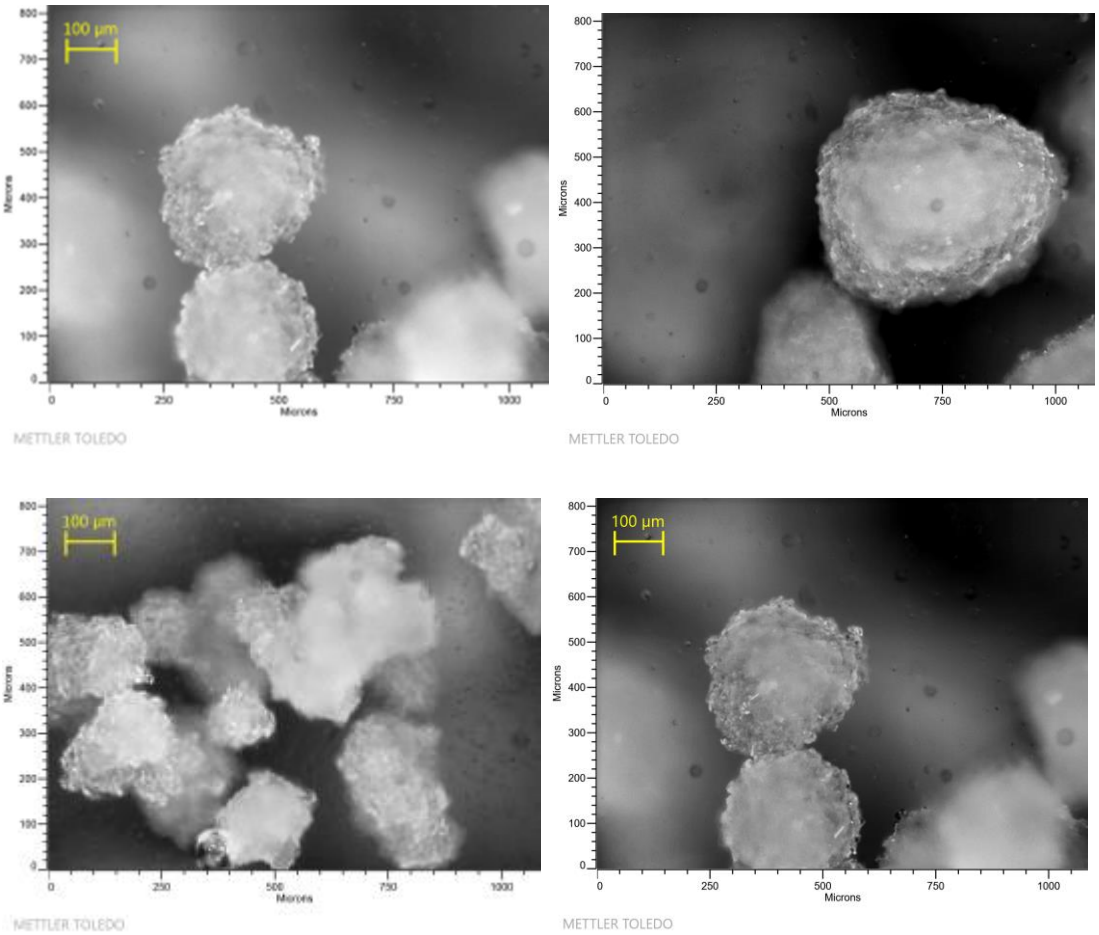

Figure 6-20 *PVM images of growth stage (Top) along with some attrition and breakage (below) of BA agglomeration of multiple agglomerates.*

Table 6-7 and **Table 6-8** summarise experiments operating conditions and agglomerates characterisation in terms of the size and the powder flow properties of the experiments performed with HSWM and only OHS mixing, respectively. The results were analysed using DOE approach by using the MODDE Pro software to evaluate the effect of individual factors.

Table 6-7 summarises of the experiment performed with HSWM.

Exp Name	Wet mill speed	BSR	Time	Mean size	Flow Rate Index	Bulk Density	Compressibility	Stability Index	Surface Energy	Basic flowability energy
Unit	RPM		(min)	(µm)	(FRI)	g/ml	CPS (%)	(SI)	(mJ/g)	BFE (mJ)
Crystal	N/A	N/A	N/A	68	1.36	0.25	22.62	0.72	8.14	201
N1	20000	0.8	60	237	1.07	0.38	5	0.48	4.94	119
N2	20000	0.8	30	265	1.14	0.38	16.14	1.08	5.76	131
N3	20000	0.9	30	275	1.09	0.37	27.83	0.66	6.53	159
N4	20000	0.9	60	363	1.05	0.43	15.1	1.08	5.6	131
N5	15000	0.8	60	384	1.18	0.41	5.4	0.79	3.52	72
N6	15000	0.85	45	593	0.87	0.42	21.33	0.97	4.93	138
N7	15000	0.8	30	405	1.2	0.39	18.3	1.1	5.57	138
N8	15000	0.8	45	461	1.19	0.4	11.99	1.01	4.37	112
N9	15000	0.9	30	597	1.02	0.4	8.54	0.81	4.97	121
N10	15000	0.9	60	673	1.05	0.44	10.17	1.11	5.2	121
N11	10000	0.8	30	689	1.04	0.42	13.42	0.66	4.03	99
N12	10000	0.8	60	730	0.9	0.37	13.4	1.09	6.99	132
N13	10000	0.9	30	693	0.9	0.37	13.4	1.09	6.99	132
N14	10000	0.9	60	736	0.91	0.38	13.36	1.07	6.79	155
5L batch	15000	0.8	30	341	1.15	0.38	9.18	0.85	4.18	92
Continuous	15000	0.8	30	356	1.19	0.42	5.4	0.84	8.91	125

Table 6-8 summary experiment performed with OHS only

Exp Name	OHS	BSR	Mean size	Flow Rate Index	Bulk Density	Compressibility	Stability Index	Surface Energy	Basic flowability energy
Unit	**RPM**		**(µm)**	**(FRI)**	**g/ml**	**CPS (%)**	**(SI)**	**(mJ/g)**	**BFE (mJ)**
Crystal	N/A	N/A	68	1.36	0.25	22.62	0.72	8.14	201
E1	600	0.8	2143	0.99	0.43	8.40	1.07	4.87	198
E2	800	0.9	2033	0.99	0.39	11.79	0.83	4.48	108
E3	600	0.9	2692	0.88	0.41	20.39	1.32	8.06	284
E4	800	0.8	1877	1.22	0.47	4.83	0.72	7.21	296
E5	800	0.8	1825	0.93	0.42	13.71	0.87	4.45	140

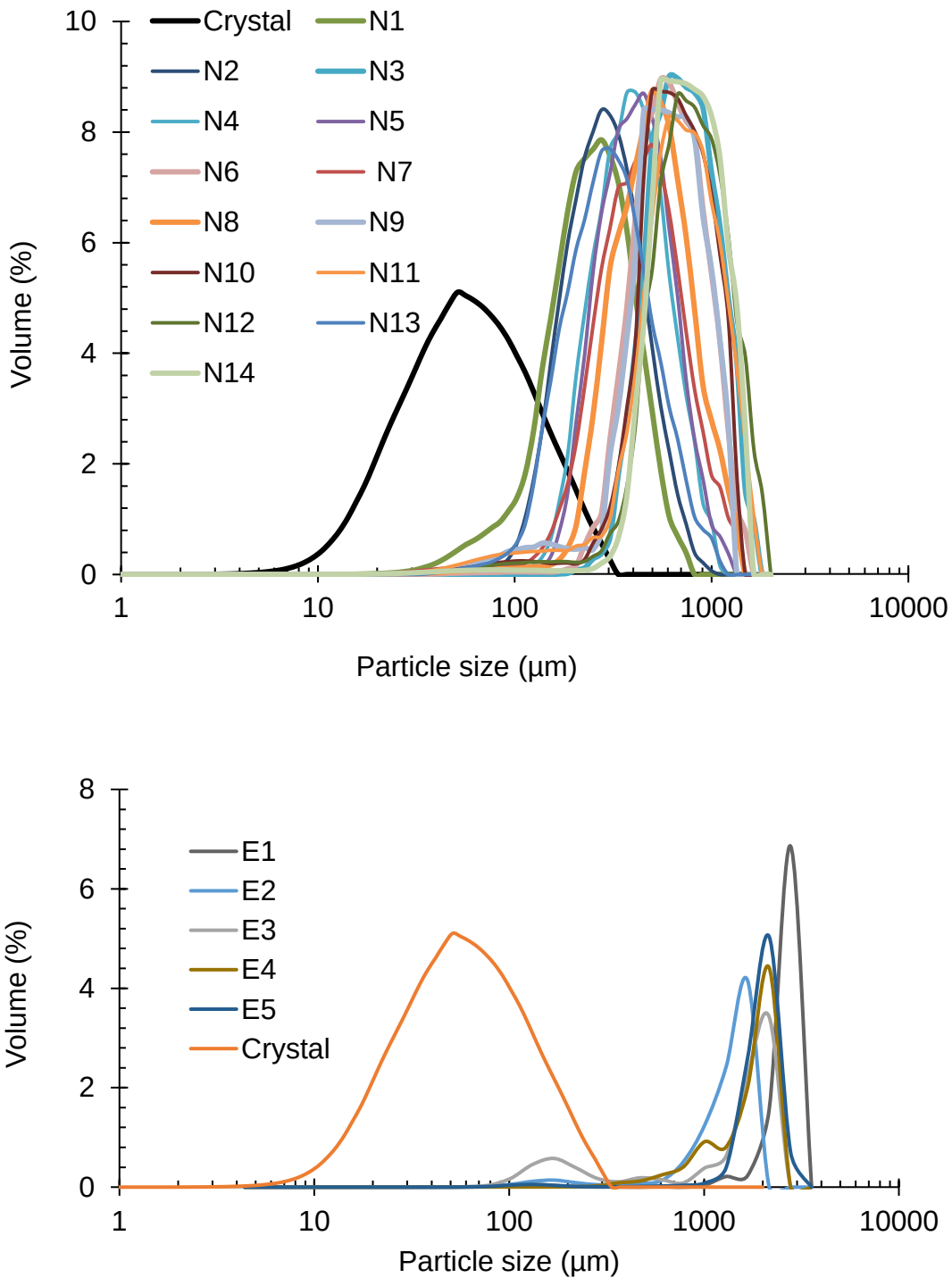

Figure 6-21 PSD of the experiments performed (Top) with HSWM showing mean size of the product (<700 µm) and (Bottom) with OHS only mixing showing the relatively larger size of the agglomerated product (>1800 µm)

Table 6-9 size analysis summary of spherical agglomerates products from all 1-L scale batch expriemnts perfromed with HSWM.

Sample Name	D[10] (µm)	D[50] (µm)	D[90] (µm)	Span
Crystal	26	68	131	1.5
N1	129	237	350	0.9
N2	180	265	410	0.9
N3	184	275	480	1.1
N4	258	363	555	0.8
N5	278	384	551	0.7
N6	418	593	715	0.5
N7	251	405	694	1.1
N8	331	461	729	0.9
N9	420	597	719	0.5
N10	427	673	776	0.5
N11	376	689	894	0.8
N12	490	730	1002	0.7
N13	510	693	873	0.5
N14	560	736	869	0.4

Table 6-10 size analysis summmary of spherical agglomerates products from all 1-L scale batch expriemnts perfromed with Over head stirring only.

Sample Name	D[10] (µm)	D[50] (µm)	D[90] (µm)	Span
Crystal	26	68	131	1.5
E1	1505	2033	2429	0.5
E2	246	2143	2950	1.3
E3	1993	2692	3067	0.4
E4	883	1877	2359	0.8
E5	1149	1825	2975	1.0

The particle size distributions of the agglomerates produced with HSWM mixing and OHS only mixing are given in **Figure 6-21**, **Table 6-9** and **Table 6-10** . The agglomerates produced with HSWM showed a tighter span, with most of the mean size of agglomerates being under 700 µm, and the agglomerates produced with OHS only mixed, showing the relatively larger agglomerated product with a mean size of over 1800 µm. Thus, the BL droplet

generated by OHS only mixing is bigger in size and less quantity than HSWM, resulting in larger size agglomerates for the same range of BSR and addition time, proving the effectiveness of HSWM for the SA process.

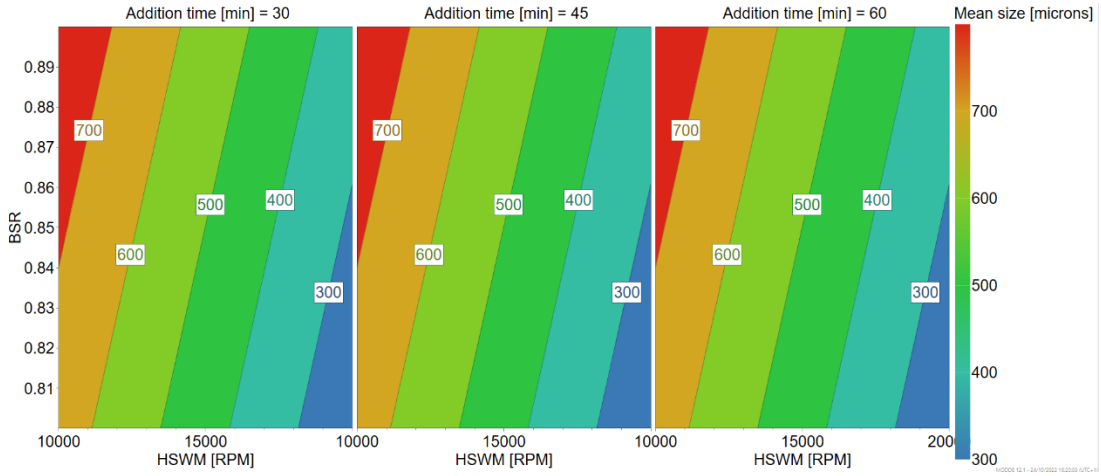

Figure 6-22 showing the effect of process parameters (BSR, mixing and addition time) on produced spherical agglomerates size.

R2 of 0.86 (R2 shows the model fit; with a value grater than 0.5 considered to be good model) Q2 of 0.74 (shows an estimate of the future prediction precision. Q2 greater than 0.5 considered to be good model) model validity 0.5606 (model validity is a test of diverse model problems. Value less than 0.25 indicates statistically significant model problems such as the presence of outliers, an incorrect problems or a transformation problem) reproducibility 0.97 (is the variation of the replicates compared to overall variability. A value greater than 0.5 is considered to be good model) . Overall, The high shear mixing imparted by the wet mill shows negative effect on final the spherical agglomerates size while higher BSR in conjunction with lower HSWM speed shown positive effect on the spherical agglomerates size while addition time does not show any influence on the final spherical agglomerate size. As shown in **Figure 6-22** wet mill speed of 15000 and 20000 rpm produced agglomerates of less than 500 µm compared to around 700 µm with 10000 rpm wet mill speed. No notable corelation was derived from the model about the different factor versus the bulk density which suggest that, any size of

produced spherical agglomerates will have density in the range of 0.4 $g.ml^{-1}$ compare to the 0.25 $g.ml^{-1}$ for the single crystal.

SEM and microscope analysis was performed on the agglomerates product to visualise the BA agglomerates shape and how well it has compacted compared against the HSWM and OHS only mixing are shown in **Figure 6-23** and **Figure 6-24,** respectively. Agglomerates produced with HSWM are in experiments N1 to N14, and agglomerates produced with OHS only mixing are in experiments E1 to E5. Along with the size and shape of agglomerates, porosity and compressibility are also properties of interest for downstream processing due to their effects on other properties like dissolution and compressibility [138]. In **Figure 6-23** the agglomerates produced with HSWM can get increasingly spherical as size increases. The agglomerates appear more compacted at higher BSR with less porous surfaces due to the higher amount of BL, leading to a stronger bond with a single particle which is evident with higher bulk density compared to primary crystals. The rounding effect can also be observed with larger size agglomerates.

The agglomerates produced with OHS only mixing are visibly less smooth, with a rougher surface. The primary particles appear relatively large compared to the agglomerate with the HSWM agglomerates. The reason behind the larger size of agglomerates are due to the BL droplet size is much larger (around 220µm) than the BL droplet produced with HSWM (around 40 µm) along with less shear imparted in OHS only mixing. The particle surface has large boulders with few pore openings at the particle surface. The overall shape remains the same in all agglomerates products from OHS only mixing: rougher, more porous, and less densely packed, giving a more irregular appearance. In summary, the agglomerates produced with HSWM are much more rounded, spherical, compacted and smaller than the agglomerates generated with OHS mixing only, which again proves the effectiveness of using the HSWM for the SA process to produce smaller size agglomerates that can be used for direct compression.

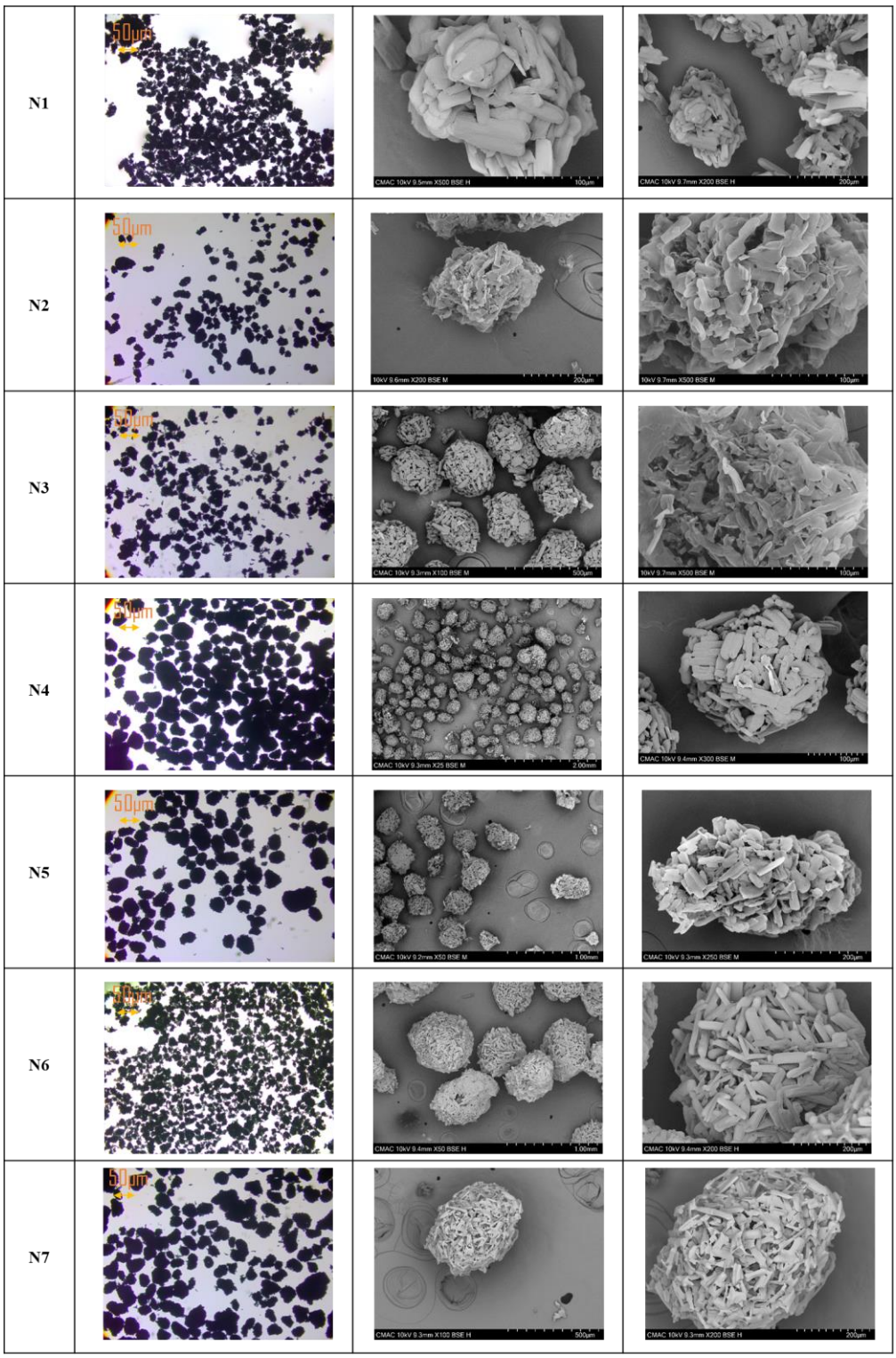

Figure 6-23 microscopes (left column) and SEM images (centre and right column) of spherical agglomerates produced with HSWM mixing. Due to the agglomerate size variation, magnification has not been kept constant. Operating condition of each experiments are detailed in Table 6-7.

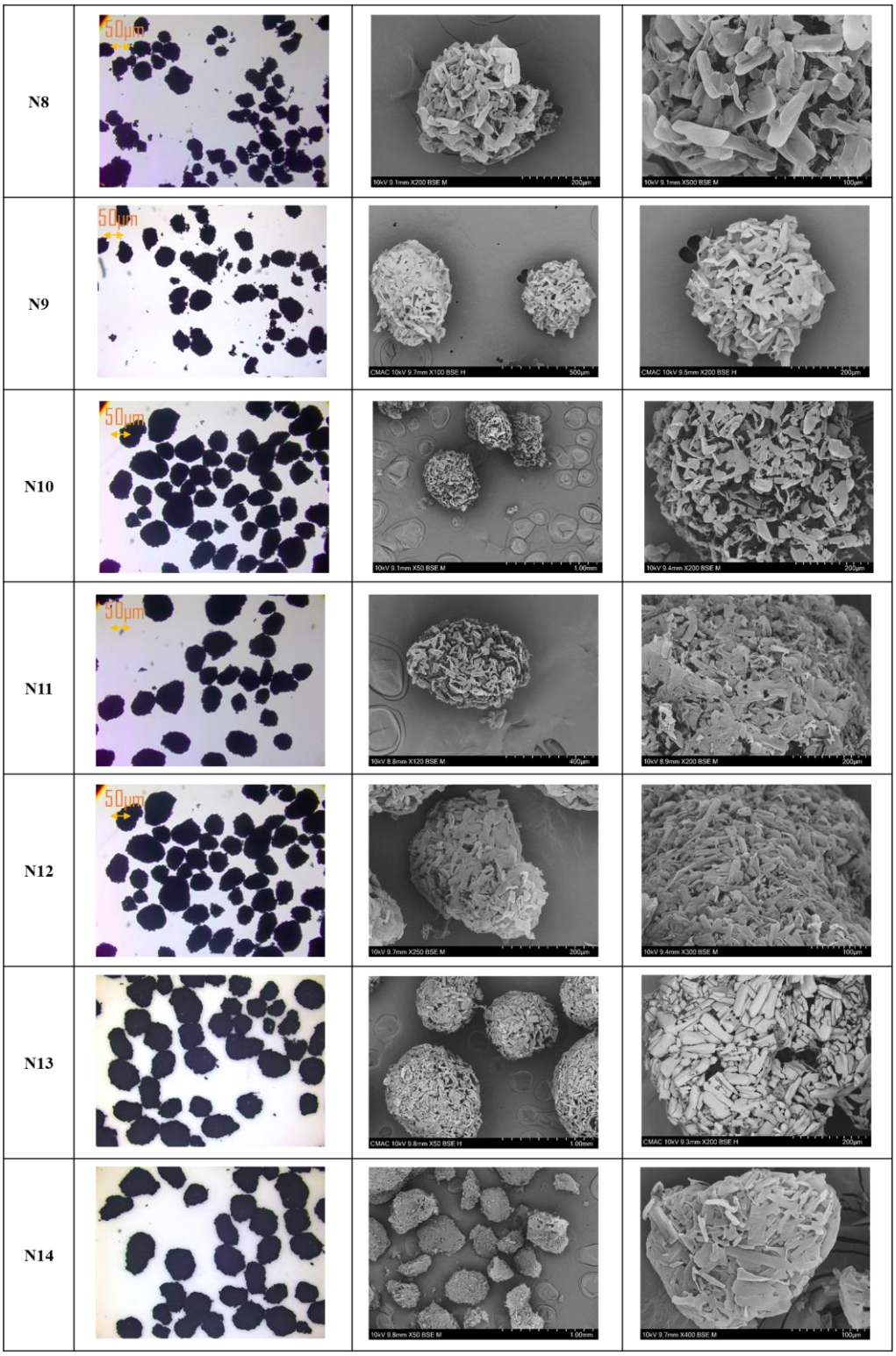

Figure 6-23 continue microscope (left column) and SEM images (centre and right column) of spherical agglomerates produced with HSWM mixing. Due to the agglomerate size variation, magnification has not been kept constant.

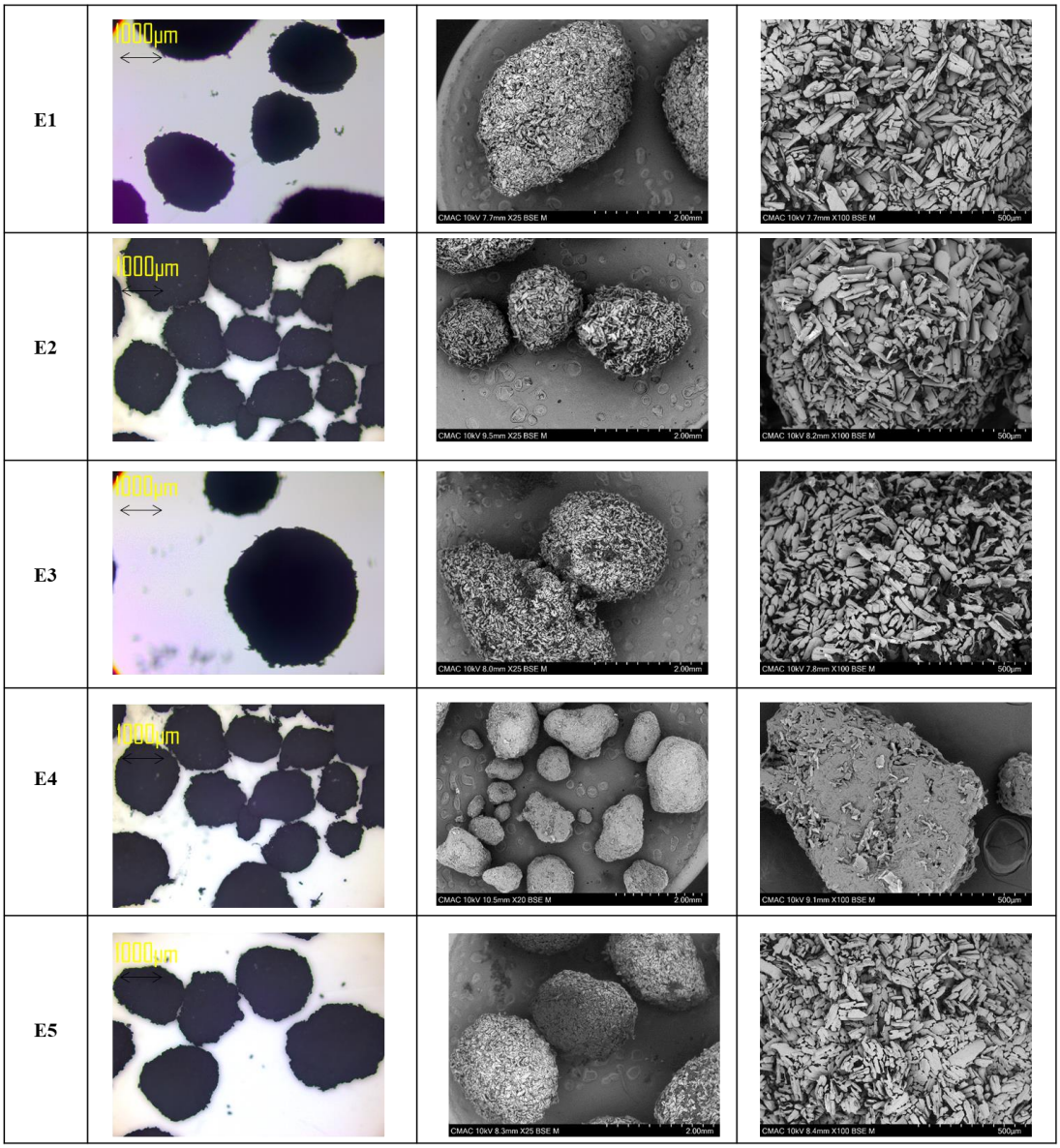

Figure 6-24 microscopes (left column) and SEM images (centre and right column) of spherical agglomerates produced with OHS-only mixing. Due to the agglomerate size variation, magnification has not been kept constant. The operating condition of each experiments are detailed in Table 6-8.

The flowability of a powder is also an important consideration in any pharmaceutical operation involving particle movement. It can significantly affect the processability of the material and, ultimately, the content uniformity of the final product [269]. However, common methods attempt to measure and quantify powder flow as a single property, such as the angle of repose, flow

through an orifice or as a function of the bulk and tapped density (Hausner ratio and Carr's index). The problem in doing so is that powders are highly functional materials, and flowability cannot be quantified as a discrete property. Therefore, powder flow properties of agglomerates generated from both types of mixing (HSWM and OHS) experiments were measured using FT4 powder rheometer summarised in **Table 6-7** and **Table 6-8**, respectively and presented graphically in the below section.

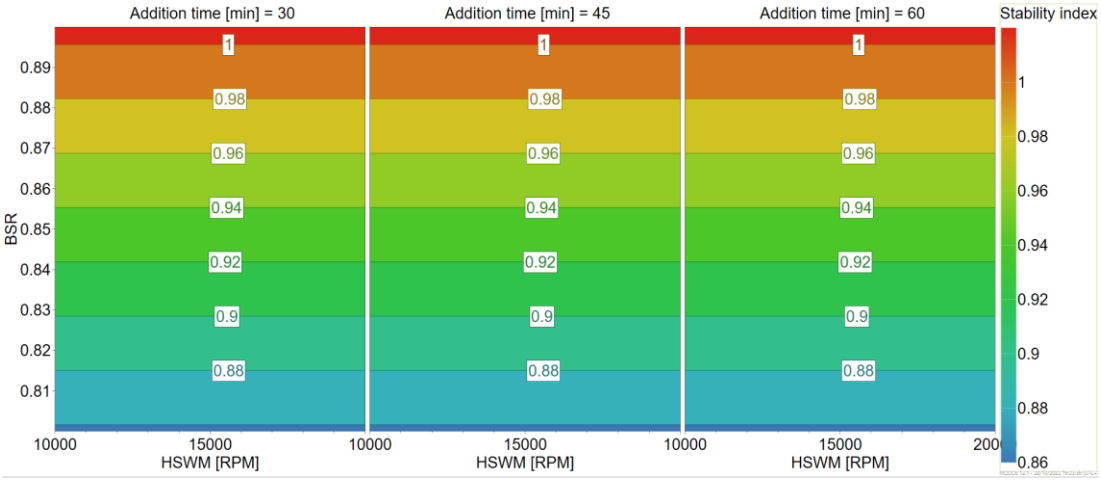

Figure 6-25 shows the effect of process parameters (BSR, mixing and addition time) on produced spherical agglomerates SI. The SI value of 0.90−1.10 require for good agglomerate stability

A stability index (SI), the ratio of the energy required to traverse the particle bed during the seventh test to the energy required during the first test, is a measure of the stability of the particles. In this test, the FT4 blade traverses downward through the particle bed at a set rotation speed for seven tests (at 100 mm/s). An SI value within 0.90−1.1 is normally defined as good stability [138]. **Figure 6-25** shows that most experiments have acceptable stability. Addition time and HSWM mixing do not show any effect on SI, while BSR shows a positive impact on the SI value.

The flow rate index (FRI) measures how sensitive the agglomerates are when subjected to flow and is measured by the FT4 blade traversing downward through the particle bed at four different tests, each with a decreasing rotational

speed (100, 70, 40, 10 mm/s). The ratio of the energy required to traverse the particle bed during the fourth test to the energy required during the first test is called the flow rate index (FRI). An FRI value between 1.5 and 3.0 displays average sensitivity to flow, while an FRI value of 1 indicates insensitivity to flow. As Table 6-7 illustrates, all experiments with good stability also display average to low sensitivity to flow. This observation is typical of large particles and confirms the benefit of performing spherical crystallisation.

Surface energy (SE) is measured during the blade's upward motion as the impeller's flat surface generates mass displacement, but the powder is not confined by the vessel. It is, therefore, not prevented from dilating and moving upwards. An SE value less than 5 is considered Low cohesive powder, SE value $5 < SE < 10$ is considered moderate cohesion, and an SE value greater than 10 is considered high cohesive powder. As a result, the agglomerated products displayed low to moderate cohesive properties, as illustrated in Table 6-7. However, there was no profound co-relation derived between process variables (BSR, Addition time and mixing) versus the FRI and SE from the DOE. The Basic flowability energy (BFE) is measured during the blade's downward motion as the impeller's flat surface generates mass displacement. However, the powder is confined by the test vessel's closed bottom, which resembles forced flow conditions. Therefore, a lower BFE value means better flow properties. Overall all the product has shown good flow property. The average BFE value of the agglomerated product was around 120 mJ compared to 200 mJ for a single crystal.

The agglomerates' compressibility is measured in FT4 by applying increasing compressive force via a vented piston to a conditioned powder and measuring the change in volume as a function of the applied load. The vented piston ensures air within the powder and vessel can readily escape. Compressibility is defined as a percentage change in volume for a given applied normal stress. Compressibility of the BA agglomerates are in the region of 5 to 15 % compared to 22% in single-particle, which again empathise with the benefit of SA as the lower compressibility percentage means the powder is less

cohesive, which in turn improves the overall flow property of the powder. **Figure 6-26** shows the positive effect of BSR in conjunction with lower mixing speed on spherical agglomerates compressibility, while addition time did not show any correlation with compressibility.

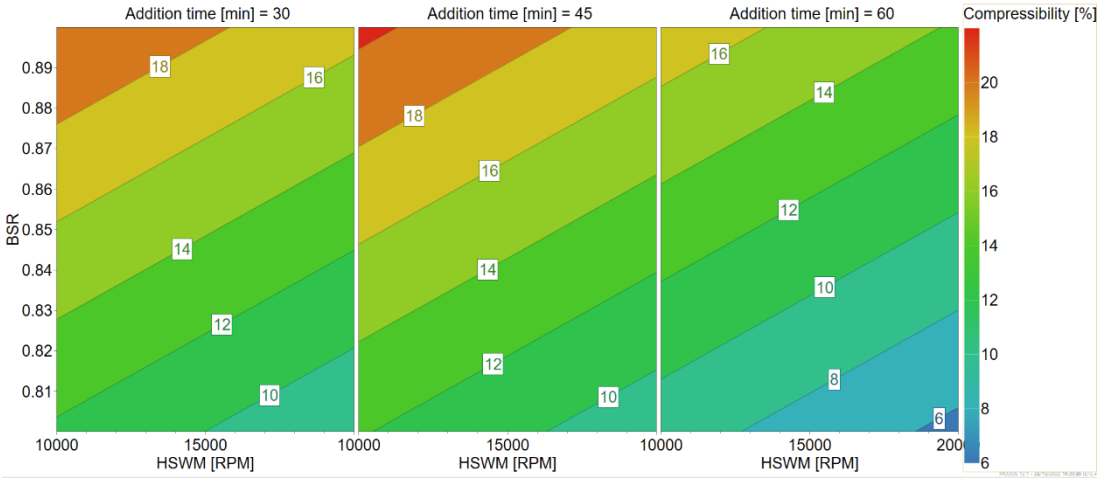

Figure 6-26 showing the effect of process parameters (BSR, mixing and addition time) on produced spherical agglomerates compressibility

Conditioned bulk density (CBD) was measured by creating uniform powder packing by performing the conditioning cycle and then using the split vessel to determine an exact volume. As a result, the CBD of the agglomerated product has increased to 1.5 g/ml compared to a single BA particle. In addition, the bulk porosity (ε), the ratio of agglomerated product to single-particle, was also observed to decrease with agglomerated product compared to single crystals, as summarised in **Table 6-7.**

In summary, The effect of individual operating parameters on the final agglomerates properties in the performed experiments shows that overall, BSR positively affects the agglomerate size for both HSWM and OHS-only mixing. Increasing the BSR leads to a higher agglomerate formation probability. This results in more energy dissipation during collisions and leads to an increase in agglomeration efficiency, ultimately yielding larger agglomerates, which is similar to the previously reported observation in literature [129, 178]. The mixing during the SA process can also directly

influence the final agglomerate's product property through the level of hydrodynamic forces produced. At a higher shear rate, the probability of collisions between crystal particles and the number of BL droplets increases [129]. Furthermore, the mixing also influences the BL droplet dispersion and size, increasing the high intensity of mixing and giving smaller droplet sizes. The BL droplet size generated with HSWM was around 30 µm, similar to the primary crystal size (31 µm). In comparison, the BL droplet size generated with OHS only was around 90 µm which is three times larger than the primary crystals. This suggests the different mechanism of agglomerate formation (distributive compared to immersive mechanism), resulting in a larger final agglomerates size.

The effect of high shear on collisions and producing smaller droplets within the SA leads to smaller agglomerates being produced under the higher shear regime in HSMW (mean size of < 700 µm) Compared to OHS only mixing, resulting in agglomerates with a mean size of > 1800 µm.

6.3.3.2 Batch 5 L scale

A batch scale-up experiment was performed in a 5L jacketed vessel with a similar setup used in the 1L vessel with HSWM as described in **section 6.2.3**. For the HSWM, the number of batch turnovers is a broadly accepted criterion for scaling up the milling time in wet milling processes [270]. Due to this, the HSWM circulation flow rate has increased to maintain a consistent half a volume of vessel turnover on both the scale and all other operating parameters were kept constant. Therefore, the operating conditions from experiment N5 at the 1 L batch scale were selected for a scale-up run based on achieving the targeted agglomerate mean size of 350 µm. The conditions shown in Table 6-7 and **Figure 6-29** show the FBRM trend of the agglomeration process for the scale-up experiment, which follows a similar trend to the 1 L scale shown in **Figure 6-16.** The agglomerates produced from the process were filtered using a 10L lab-scale filtration setup and dried at 40 °C under a vacuum oven before being analysed for size and flow properties. **Figure 6-28** shows the SEM images of the BA agglomerated product, showing that SA was successfully

achieved by producing the correct form and size of particles. The scale-up from conditions identified at 1L was also successful using HSWM. The product displays a compact, spherical shape with a targeted mean agglomerate size of 380 µm.

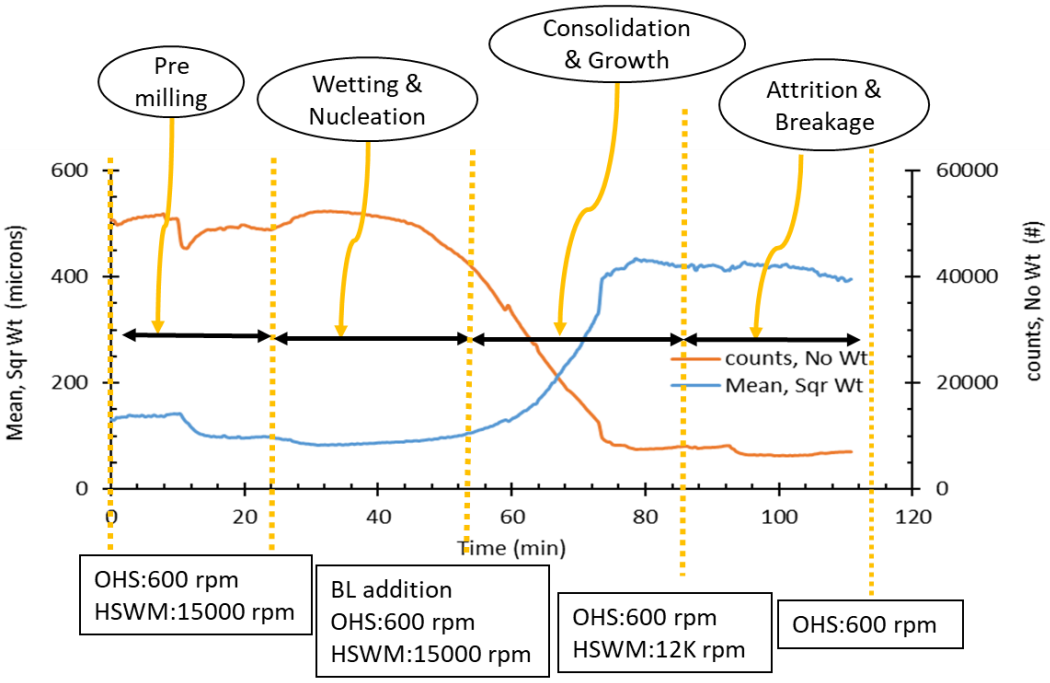

Figure 6-27 FBRM trend measured during the 5L process operation. Key stages in the SA process are highlighted.

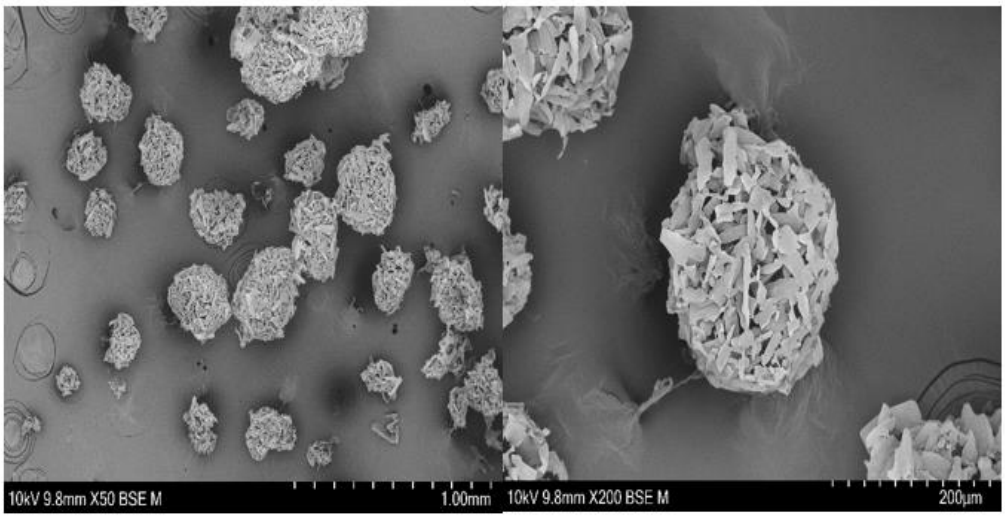

Figure 6-28 SEM images of spherical agglomerates produce from a 5-L scale-up batch.

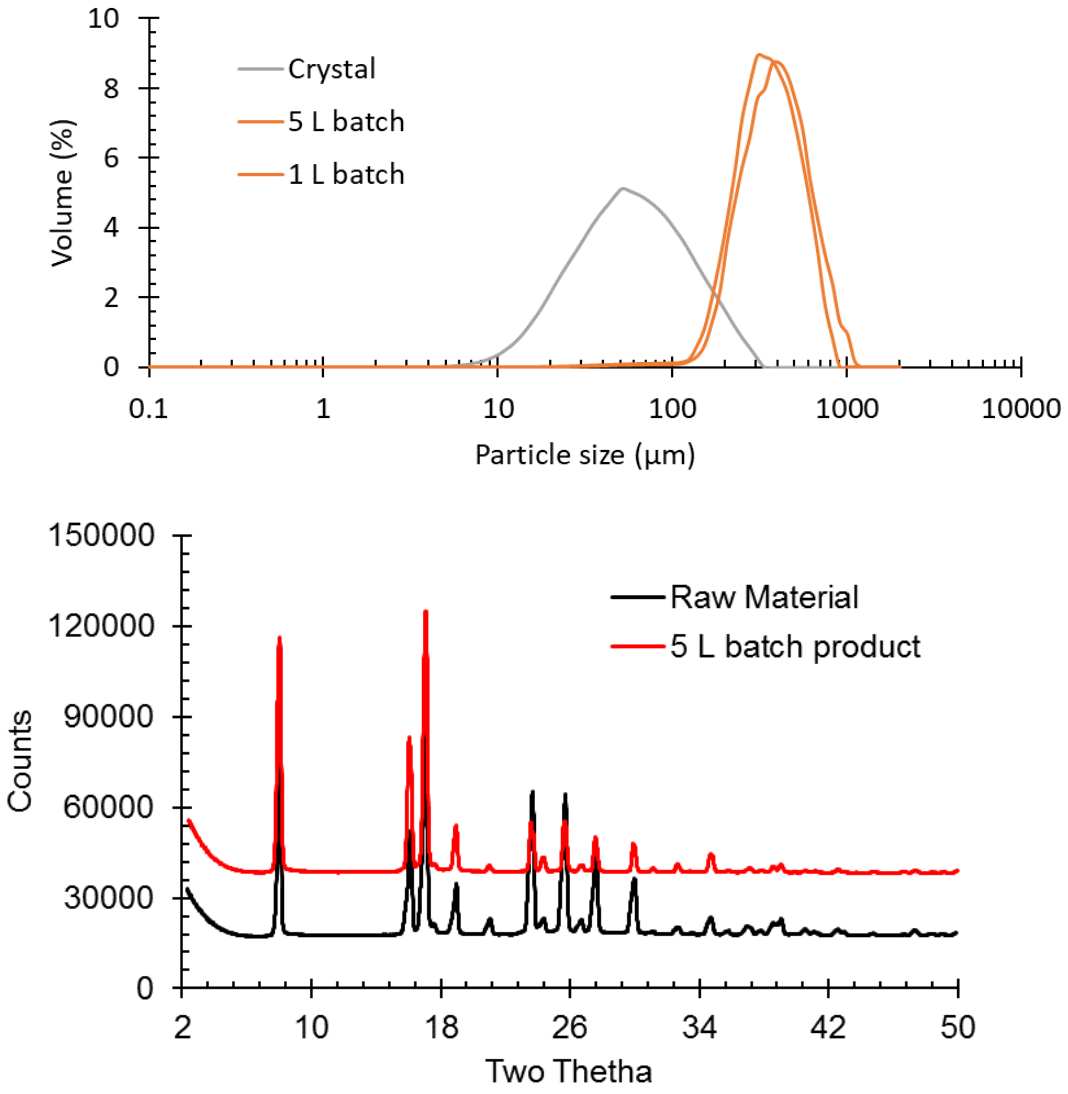

Figure 6-29 (Top) PSD comparison of primary BA crystals and produce agglomerates measured by Malvern Morphology G3 at 1 L and 5 L scale (Bottom) XRPD of product and raw material showing right polymorphic form.

This experiment demonstrates the scalability of the novel approach of using HSWM to produce smaller, compacted, and uniform spherical agglomerates later tested for direct compression and dissolution studies.

6.3.3.3 Continuous Six-stage MSMPR experiments

As demonstrated throughout the previous sections, SA provides potential advantages in suspended particles' micrometric properties, enabling improved

recovery of engineered, high-value solid particles. These advantages improve process design and efficiency, making SA a process intensification technique. Combining the inherent advantages of SA with the advantages of continuous operations demonstrated in this section further enhances efficiency, adaptability and productivity.

The control parameters for the continuous SA include the BSR, temperature, residence time, BL droplet size and high shear mixing. The detailed list of operating parameters for the continuous SA process is described in experimental **section 6.2.5**. The same rate processes and operating conditions dictate the final agglomerate properties as in the batch process. Stages-1, 2 and 3 were designed to serve as the crystal nucleation and growth-dominated stage by adding solution and anti-solvent. This stage's control parameters included the solvent to the anti-solvent ratio, residence time, and agitation rate as described in the P&ID diagram in **Figure 6-11**. Stage-4, 5 and 6 served as the agglomeration-dominated stage by adding slurry from stage-3 and bridging liquid addition. This stage's control parameters include BSR, residence time, and mixing by HSWM to generate controlled BL droplets on a par with the size of the primary particles. The advantage of the multi-stage system is tailoring both stages (crystallisation and agglomeration) individually to create conditions that control the required rate process in sequence at a steady state to achieve controlled formation of particles tailored to both primary and agglomerate particle specifications.

An FBRM probe was inserted in stage-6 for real-time monitoring of the steady-state operation of the process. **Figure 6-30** shows the trend of chord length means square weight. After one and a half residence times, the trend starts to level off at around 450 µm mean size, slightly higher than the offline volume-based measurement. The intense mixing imparted by HSWM tends to get adjacent particles to agitate too closely in the vessel, hence detected as the single-particle. However, approaching the steady-state operation is also visible by offline analysis of PSD and solid recovery measured in terms of the yield value as summarised in **Table 6-11.** The agglomerated product was collected

in a 10 L Duran bottle, filtered in a 10 L Nutsche filter with a 10-micron filter cloth, and dried overnight in a 40 °C vacuum oven. As shown in **Figure 6-30** well compacted spherical agglomerates were produced with the SEM images showing the targeted mean particle size of 355 µm with improved flow properties summarised in Table 6-8 improved bulk density 0.42 $g.ml^{-1}$ and flow property.

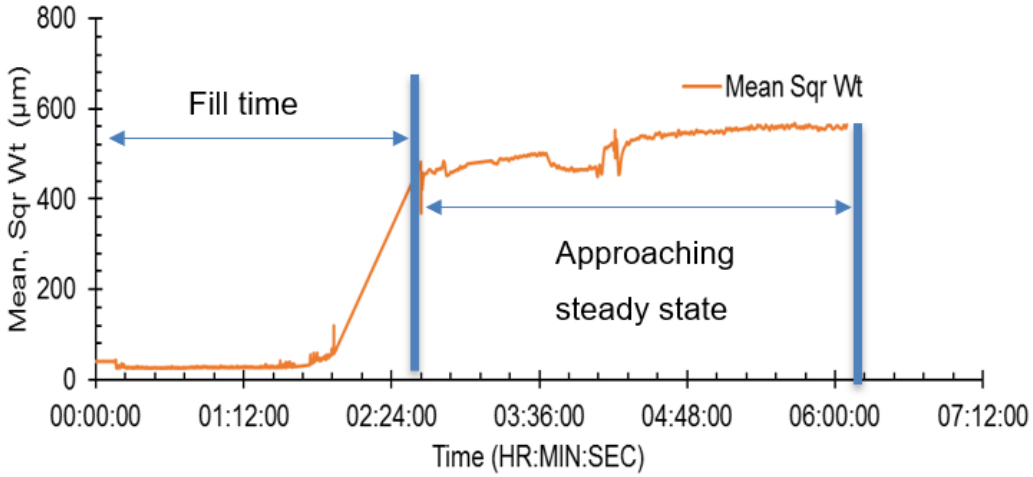

Figure 6-30 FBRM trend of mean square weight size inserted in stage-6 of continuous SA for real-time process monitoring.

Table 6-11 summary of size analysis and yield of spherical agglomerates after each residence time.

Sample Name	D[10] (µm)	D[50] (µm)	D[90] (µm)	Circularity Mean	Span	Yield (%)
RT-1	257.8	363.2	554.9	0.85	0.82	87
RT-2	235.7	341.1	449.3	0.77	0.63	91
RT-3	278.4	383.7	551.4	0.78	0.71	92
RT-4	261.3	378.7	641.8	0.85	1.00	93
RT-5	245.5	355.6	543.9	0.84	0.84	92

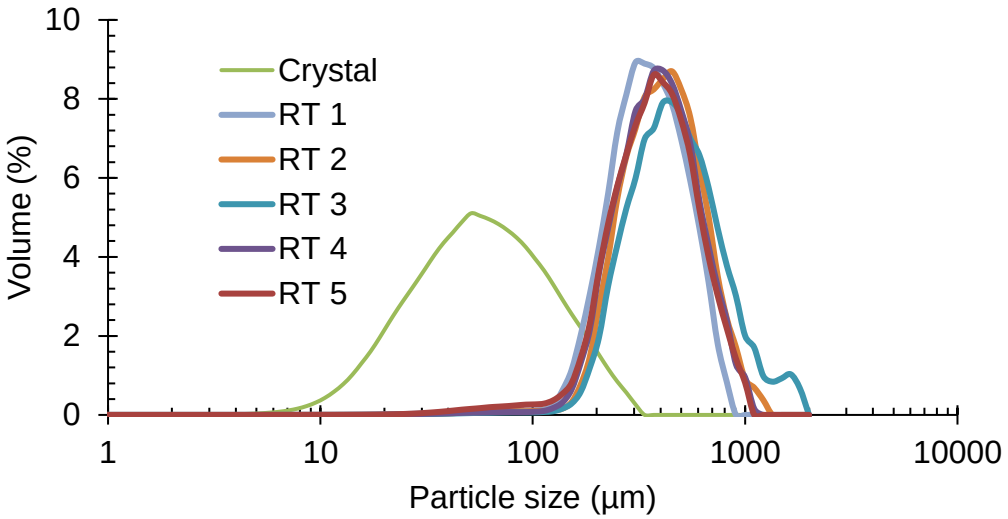

Figure 6-31 Evaluation of PSD of the spherical agglomerates after each residence time.

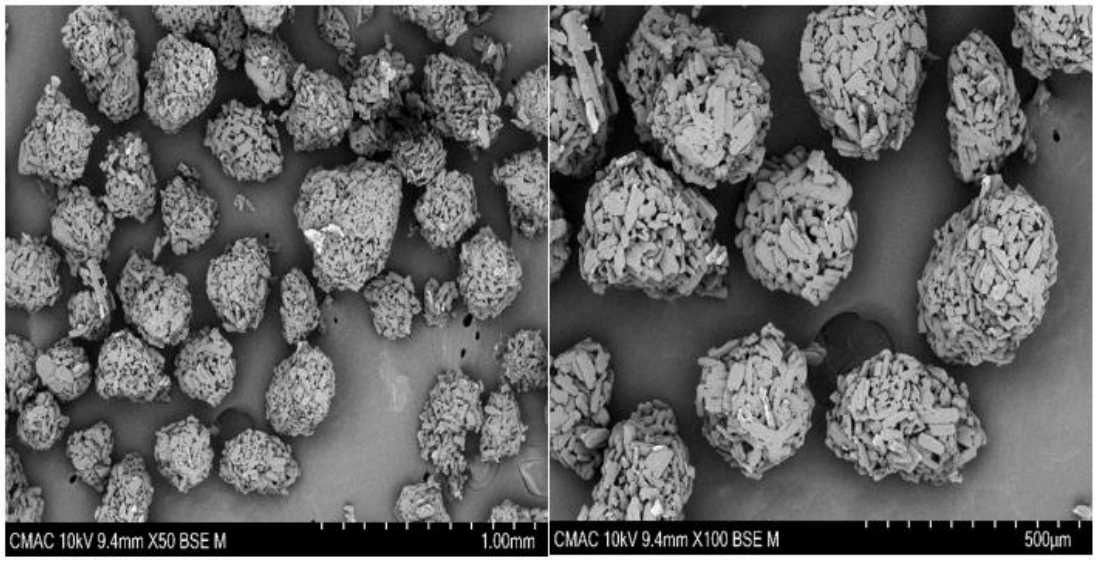

Figure 6-32 SEM images of the Spherical agglomerates produced by continuous operation.

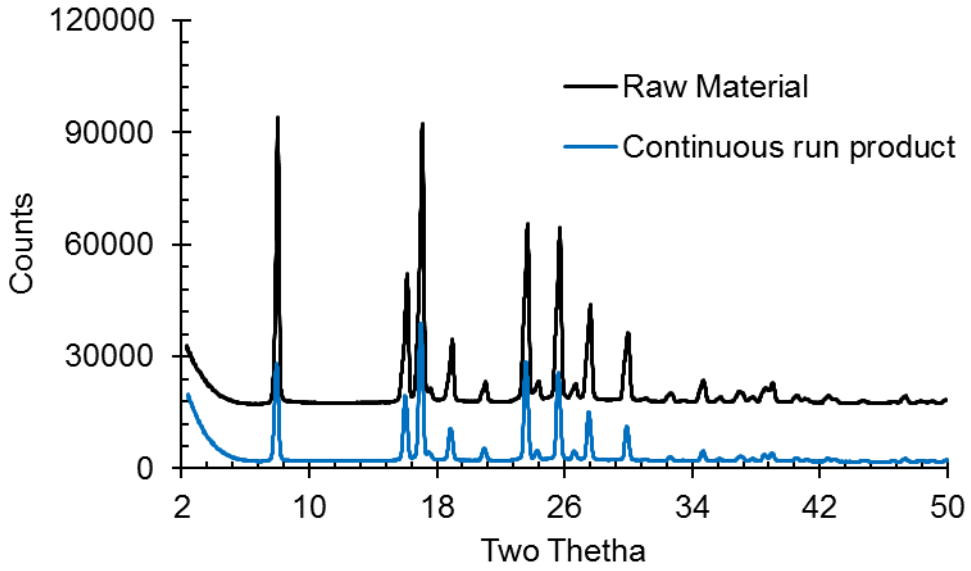

Figure 6-33 XRPD of the BA raw material and product from the continuous run.

A Powder X-ray diffraction study was carried out to exclude any polymorphic transition or solvate formation during the BA crystallisation. Only the known non-solvated form of benzoic acid was detected in the samples. XRPD data is obtained for the agglomerates prepared using chloroform, as BL is shown in **Figure 6-33**.

6.3.3.4 Tabletability and Dissolution performance

Tabletability, the ability of a powder to form a tablet upon compression, is another important property of a powder in pharmaceutical research [271]. It is represented by a plot of the tablet tensile strength as a function of compaction pressure. Tablet tensile strength of >2 MPa is required to withstand the stresses during shipping and handling to remain intact [127]. The total interparticle area and strength of bonding over a unit area determine the strength of a tablet. Bonding area and bonding strength can be assessed using compressibility and compactibility plots.

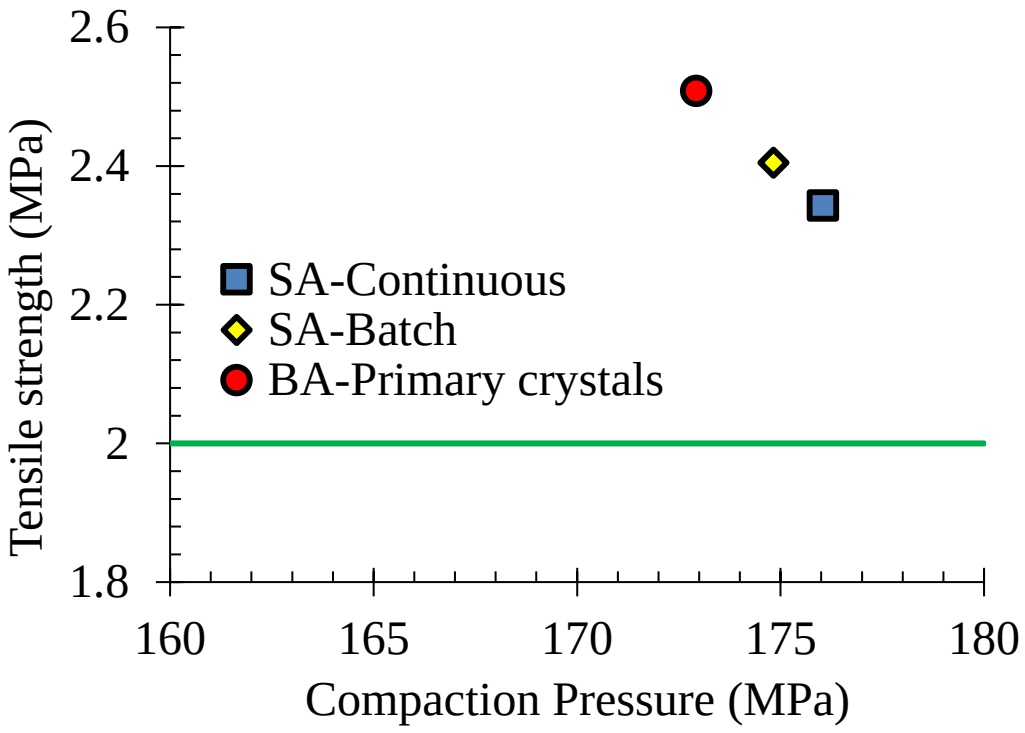

Figure 6-34 Comparison of tabletability of BA primary crystals, Spherical agglomerates produced via batch and continuous method. Tensile strength above 2 MPa considered to be industry relevant strength.

A compaction simulator (HB50 Huxley Bertram) was used to test the tabletability of the BA agglomerates. All tablets formulated using 35% w/w BA (drug load), 64% w/w microcrystalline cellulose (filler), 1% w/w magnesium stearate (lubricant). Tablet weight (200mg), thickness (9mm) and porosity (15%) were kept constant for all tablets. Preliminary results of the tablet produced with 170 MPa compaction pressure showed a tensile strength of greater than 2 MPa (**Figure 6-34**), which is the minimum tensile strength required for better handling of the tablet [127].

The enhanced tabletability is attributed to the smaller primary crystals favouring stronger tablets by affording a larger inter particulate bonding area.

Besides the manufacturability as discussed above, dissolution of BA from the dosage form is another property that is crucial for a successful formulation since it determines the bioavailability of a drug (e.g., flowability and

tabletability). The dissolution performance of the tablets was studied with 500 mL of (0.2 M potassium phosphate monobasic, 0.1 N NaOH) at pH 8 and 37 °C for 2 hr. A UV dip probe monitored the dissolved BA concentration in real-time.

Figure 6-35 demonstrates the dissolution performance of the BA primary crystals, spherical agglomerates produced via batch and continuous method. The tablet formulated with agglomerated BA showed much-improved drug release than a tablet containing primary crystals, mainly due to increased porosity in the SA and increased wettability of agglomerate driving faster dissolution [127]. More than 80% of drug release was achieved in a 2 hr dissolution time compared to 65% of drug release in primary crystal formulated tablets.

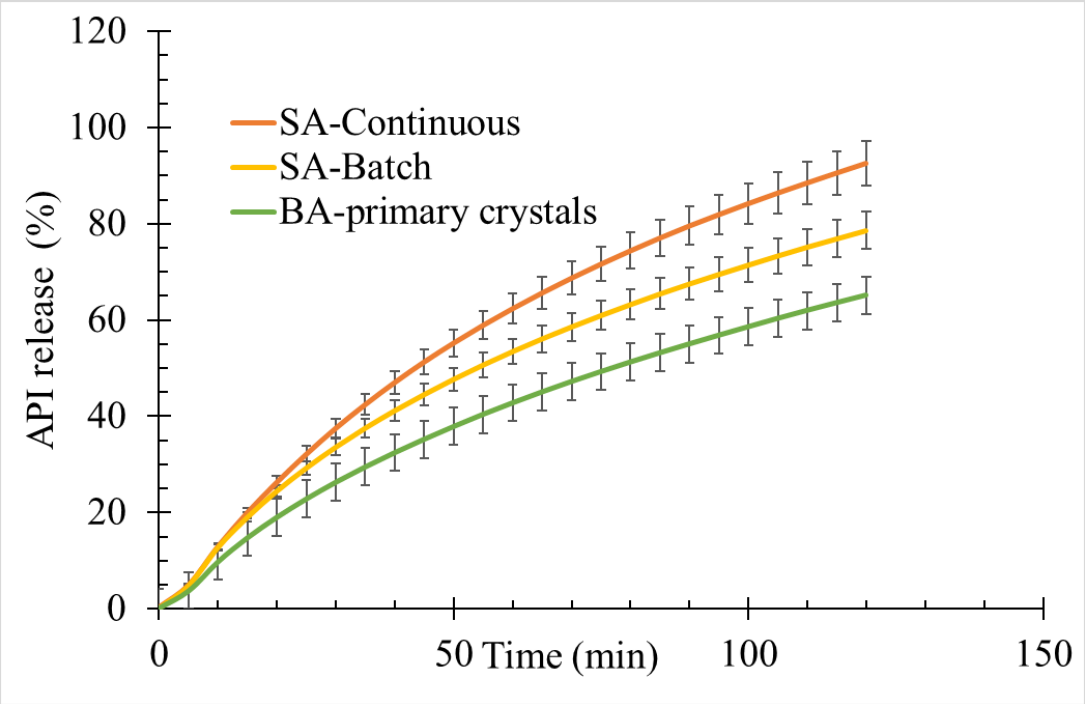

Figure 6-35 Comparison of dissolution performance of BA primary crystals, spherical agglomerates produced via batch and continuous method.

Thus, the dissolution data confirms that the SA approach can indeed be used to develop high-dose SA tablets of BA. A more detailed and in-depth analysis

of manufacturability and bioavailability will be carried out within CMAC by Jack Creswick (Daniel Markl group); later, inline Terahertz time-domain spectroscopy (THz-TDS) analysis will be incorporated to explore the effect of SA on porosity and content uniformity.

6.4 Operational consideration of spherical agglomeration process.

Several operational challenges were identified to efficient running of spherical agglomeration process. The main challenge is to operate within the tight BSR boundary range as small variability in the BL amount will have big impact on final agglomerate size. As this research progressed further, a more efficient way of adding BL were identified which is shown in **Figure 6-36**. Throughout this study, BL were added directly in to the vessel while the new approach was identified where the BL were added directly in to the HSWM via T-piece at the inlet, while circulating the dispersed slurry between the vessel and HSWM. By adding the BL directly in to the HSWM its make the generation of BL droplet much more efficient compared to the BL addition via vessel as BL directly pass through the HSWM as soon as it added to the process.

Figure 6-36 Modified BL addition point via T-Piece at the inlet of the HSWM

Strat up of continuous MSMPR operation from empty vessel has widely implemented for crystallisation operation. However, in spherical agglomeration mixing is one of the most influential parameter in controlling the target agglomerates size which is difficult to achieve when starting up with empty vessel. As lack of mixing has created big lumps of agglomerates, which were just stuck at the vessel's bottom. Following the few unsuccessful runs where MSMPR started with empty vessel the modified start up procedure in which stage-4 was allowed to filled with at least half the vessel volume with crystallising slurry from stage-3 before the BL addition begins. BL addition was not started until the vessel volume reached 500 g. After that, wet-mill circulation started, and the equivalent BL was added in the aliquot and let it run for a few minutes. following that the normal continuous operation resumed. This way, uninterrupted continuous operation is implemented without any blockage or fouling issues.

6.5 Summary

In summary, SA is a promising technique to control the micrometric properties of crystals to create products with improved flow properties. It has been demonstrated to improve downstream APIs manufacturability with needle-like habits, low bulk density and poor flowability by agglomerating them into spherical particles. The agglomerates of BA produced in this work are also suitable for direct compression, whilst the raw, unprocessed materials may not be or are more challenging to process, enabling cheaper, more streamlined manufacture of solid oral dosages.

This chapter has developed an effective approach to understanding the key steps in SA for the formation of < 500 µm SA using HSWM to control the BL droplet formation. Moreover, we have investigated the impact of product performance on downstream processing. Furthermore, combining SA with crystallisation also helps reduce the number of unit operations during industrial processing, which in turn helps reduce processing time and costs. Therefore, SA is inherently a process intensification technique that can potentially drive

the shift towards improved process efficiency in traditional industries such as pharmaceuticals and bulk chemicals.

Process understating at the 1 L scale carry out by DOE analysis highlighted that as the BSR amount has positive effect on agglomerate size and stability of the formed agglomerates while HSWM speed has negative effect on final agglomerates size. HSWM speed also showed negative effect on the compressibility behaviour of agglomerates. There was no profound effect of addition time on agglomerates size and flowability performance was identify within the addition time operating region. Moreover, the comparison with OHS only mixing shown with the similar condition can produce the agglomerates in millimetres compared to micron size with the HSWM approach, mainly driven by the smaller size droplet generation with HSWM.

This work has emphasised that many operational parameters influence the properties of the final agglomerates produced by SA and their consequent functional attributes. Therefore, optimising the operating conditions has been an important avenue of the SA process. BSR, BL droplet size, and mixing are the most critical parameters. In-situ BL droplets via HSWM have demonstrated its benefit by generating smaller droplets, which helps generate smaller, compact and more rounded spherical agglomerates. Many studies show a highly nonlinear relationship between BSR and critical product attributes such as agglomerate size. Furthermore, the size, morphology and concentration of solids in the system can affect the process parameters necessary for a successful agglomeration experiment and influence the controlling rate mechanisms, e.g. changing from immersion to distributive nucleation.

The scale-up experiment from 1L to 5 L scale while keeping the same turnover volume for HSWM over the different scales demonstrates the scalability of the novel approach of using HSWM to produce smaller, compacted, and uniform spherical agglomerates, which were later tested for direct compression and dissolution studies.

Combining the inherent advantages of SA with the advantages of continuous operations demonstrated successfully in a 6-stage MSMPR system, Continuous operation has further enhanced efficiency, adaptability and productivity of the pharmaceutical manufacturing of drug products., A DC tablet formulation containing 35% of the API, BA, was developed using SA based on the spherical crystallisation method. The resulting tablet met all critical quality attributes for direct compressions studies. In summary, This work highlights the potential for SA to significantly increase drug loading in DC tablet formulations when needed. Further investigation is also required in the filtration, washing and drying of SA. A systematic workflow must be developed for the selection of wash solvents and drying conditions (agitated/non-agitated).

There is a need to develop a rapid and efficient way of specifying process parameters, which deliver consistent agglomerates attributes, defined by the critical quality attribute, to optimise product performance and processability. Systematic, science-based process design workflow (**Figure 6-34**) for the robust design of spherical agglomeration process development for APIs have been proposed here, which can be refined further in the future from the learning gained from this research and be implemented in the future on a range of APIs. This workflow will provide an initial framework for designing a SA process but by no means covers all eventualities. It is not designed to be followed rigorously but instead emphasises a way of thinking leading to holistic SA process design. Initial SA workflow is divided into the following stages and can be refined further as it makes it through several SA processes.

Stage 1: Prior knowledge

All available information on the model compound is collected. This information can come from a range of sources, including but not limited to molecular design, synthetic route development, solid form screen, work-up development, previously published literature, analytical reports, physicochemical molecular properties and structural features of the API

Stage 2: Solvent selection and Decision 1

This stage guides the selection of a suitable solvent for spherical agglomeration. The aim is to rapidly identify solvents that show desirable solubility and immiscibility for BL to carry forward into stage 3. The choice of solvents for this screen can be narrowed by considering the information collected in stage 1 and neglecting any solvents that have shown any previous indication of an undesired polymorphic form, solvate formation or reactivity with the solute, for example. Further restrictions may be placed on the solvent library to only include solvents listed in the International Conference on Harmonisation (ICH) classification for residual solvents as class 2 (solvents to be limited) or class 3 (solvents with low toxic potential). At decision point 1, If suitable solvents that meet all criteria are carried on to stage 3, Failure to meet the criteria, consideration can be given to an agglomeration from the suspension route where agglomeration is carried out after the crystallisation and isolation and resuspend in the dispersant liquid again to carry out SA.

Stage 3: Operating range and decision 2

This stage is about defining the BSR operating range within which boundary agglomeration is possible as below the lower limit produces loose agglomerates, which will not survive isolation, and too high BSR will produce a paste. In this stage, attention should also be given to the wettability of primary crystals in dispersing liquid. If primary crystals are not wetted in DL, then DL can be saturated with BL before the agglomeration. At decision point 2, if the BSR operating range is too wide or the wettability of primary crystals remains the issue, then go back to stage 1 and consider alternative solvents.

Stage 4: System understanding

Small-scale experiments were developed to extract system understanding for process design to enable faster development using fewer materials. Following the success of finding suitable BL with the correct ratio in the previous stage, the aim is to investigate the influence of residence time, mixing and temperature in forming spherical agglomerates.

The spherical agglomeration mechanism (section 6.1.1.4) indicated that the relative size of API crystal to the droplet (formed of bridging and dispersing liquids) plays a key role in the crystals wetting; we hypothesised that smaller droplets with a larger surface area should result in more efficient wetting. Moreover, BL droplets must be stable enough to be formed and introduced to the API slurry and not coalesce. This stage aims to generate robust, stable and small droplets of BL with narrower mean size distribution (span) that can serve in wetting the API to form nuclei of spherical agglomerates.

Stage 5: Process understanding and decision 3

Following the system understanding stage 4, where we were able to identify the magnitude of the process parameters affecting the formation of spherical agglomerates, the task here is trying to select the proper equipment that can deliver these conditions, i.e. residence time, mixing and temperature. As well as the method of producing BL droplets (i.e. high shear wet mill, microchannel, homogeniser, higher mixing)

In this stage, a selective design of experiment (DoE) approach can be followed to build a model linking process parameters to product attribute to develop a predictive digital design. The measured attributes, i.e. bulk and tapped density, mean size, agglomerates strength, flowability and compressibility index as these attributes are known to affect the downstream processing in addition to enhancing suitability for direct compression of APIs by varying the process parameters (i,e. mixing intensity, temperature, droplets mean size and residence time.)

Stage 6: Proof of concept and decision 4

Having developed in stage 6 a model that reliably represents the SA behaviour of the system, taking into account the process conditions within a specific platform, in stage 7, the aim is to deploy this model to design a suitable process to achieve the required product attributes and translate the design into practice. A range of methods for process design can be utilised depending on the type of model developed.

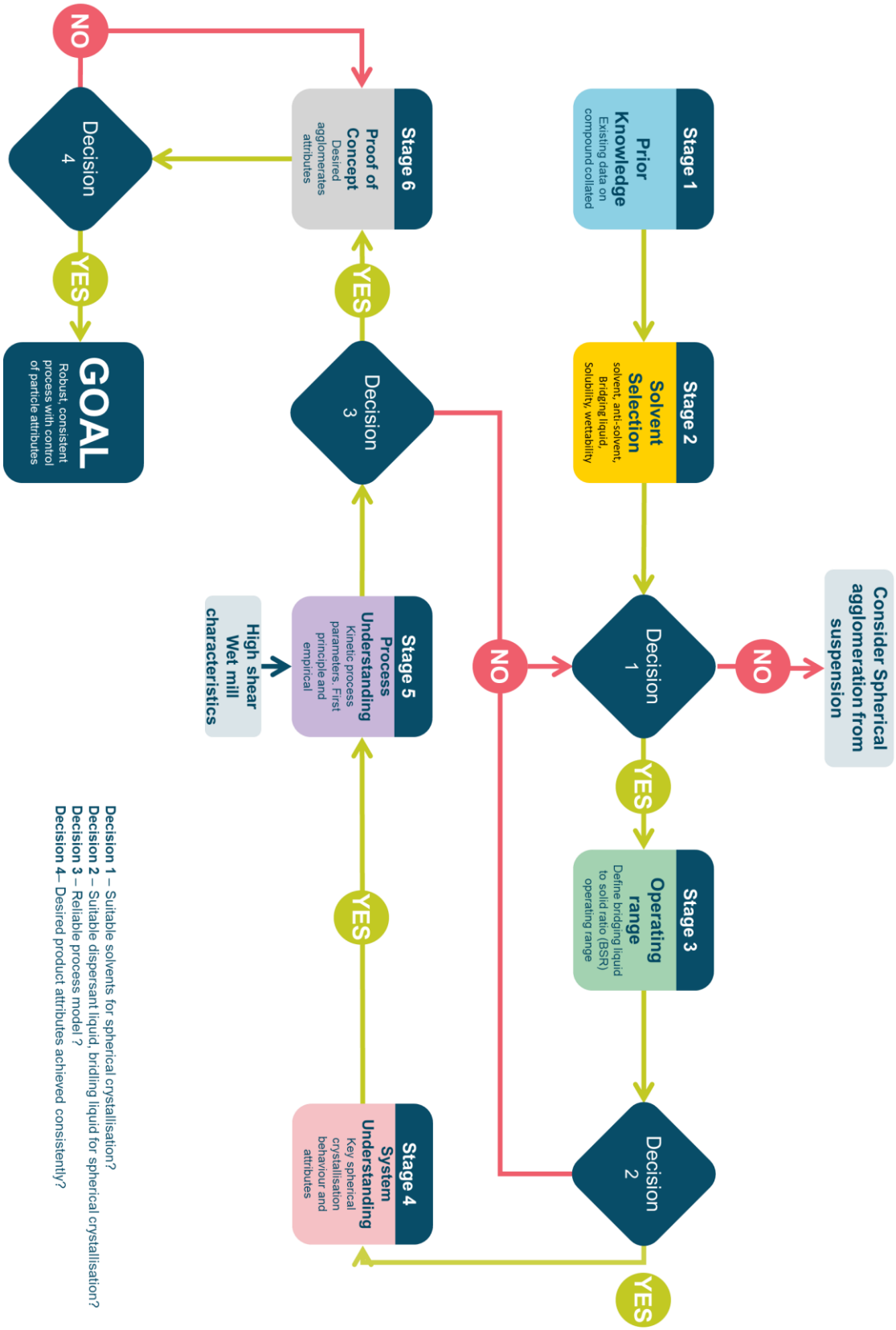

Figure 6-37 Proposed workflow for Spherical agglomeration

Chapter 7. Future work

In this thesis, the dynamics of the novel CMBOC were investigated. This thesis deals with designing and operating a novel platform to achieve required particle attributes with the help of platform hydrodynamics and process control strategies. The platform performance was evaluated for its mixing and heat transfer which proved its suitability to perform a range of crystallisation studies. The operability and platform performance were evaluated by performing ALM and PCM cooling crystallisation and the product met the target crystal size with a narrow span and yield.

Another significant aspect of this thesis was to design a continuous process with the help of a mechanistic model using the sequential parameter estimation approach to derive nucleation and growth rate by isolating different crystallisation phenomena which proved to be a effective approach. The mechanistic model developed for a crystallisation process then helped in designing a continuous crystallisation process (seeded and unseeded) to produce the crystals with targeted particle attributes. Predictions from the models were validated against the product collected from the continuous trial. The experimental measurements and model predictions within the defined model boundaries and uncertainties were obtained with good statistical agreements (±5 µm between simulated and experimental measured mean size). Moreover, the advantage of the moving baffle arrangement in the transfer of the kinetic model from batch to a continuous process was proved through experiments and simulation.

Finally, SA is another promising particle engineering technique to control particle attributes that was explored more in detail by implementing the PI's function domain by incorporating HSWM mixing. The focus of this work was to use this methodology to produce spherical agglomerates with enhanced particle attributes(improved filterability and flow property), which can resolve issues related to particles (needle-like morphology) difficult to handle during downstream processes. Process understating at the 1 L scale carried out by DOE analysis highlighted the positive effect of BSR and the negative effect of HSWM mixing on agglomerates size. Moreover, the comparison with OHS-

only mixing demonstrated that a similar condition could produce the agglomerates in millimetres size compared to micron size with the HSWM approach, mainly driven by the smaller size droplet generated with HSWM, which again validates the use of the HSWM approach to producing spherical agglomerates with workable size range for direct compression.

The scale-up experiment from 1L to 5 L scale while keeping the same turnover volume for HSWM over the different scales demonstrates the scalability of the novel approach of using HSWM to produce smaller, compacted, and uniform spherical agglomerates. Combining the inherent advantages of SA with the advantages of continuous operations demonstrated successfully in a 6-stage MSMPR system, Continuous operation has further enhanced the efficiency, adaptability and productivity of the pharmaceutical manufacturing of drug products. Based on the learnings from this research, below are a summary of some key research focuses for future work.

7.1 Development and characterisation of CMBOC

The study has shown that the developed platform is suitable for various continuous crystallisation processes. A linear mixing-based scaleup approach can be applied to move from lab scale to plant scale. This continuous crystallisation platform has been characterised and applied in continuous crystallisation; however, there is still room for improvement and further research. Another area that needs attention will be testing this platform for anti-solvent and pH-controlled crystallisation processes. The point of anti-solvent, acid, or base addition is crucial for running an uninterrupted crystallisation process. Mixing is a dominant factor in running anti-solvent and pH-controlled crystallisation, which can be explored more in-depth in future studies. From a process point of view, there is an abrupt temperature change when the slurry is transferred from one stage to another during the cooling crystallisation process. There is a need to investigate the effect of these variations on supersaturation and process kinetics.

7.2 Control System engineering- Lactose PBE modelling

This chapter focused on developing a population balance model for ALM. A sequential parameter estimation approach, combined with a customised solubility model including mutarotation kinetics, was used to estimate cooling crystallisation kinetics for ALM. Future work will focus on extending the current model to include agglomeration kinetics to improve PSD predictions. The model will be extended to generate seeds of the required particle size by applying kinetic parameters estimated and model optimisation. Future work will also focus on refining the continuous crystallisation model with additional data collected using continuous crystallisation. The current work used batch experiments to estimate kinetic parameters and then validated them for continuous crystallisation. There are other means to collect data for parameter estimation, such as running continuous crystallisation, collecting data by varying process parameters, and building a population balance model. Future work will focus on building the model from continuous crystallisation experiments to investigate the effect of net flow on the system's kinetics. Future work will focus on using a mechanistic model developed for ALM and model predictive control (using PharmaMV) to develop a digital twin and running these models to dial a particle size of ALM. Feedback control will be applied based on the response from PAT tools IR and FBRM to reach desired particle size.

7.3 Particle Engineering- Size controlled spherical agglomeration of benzoic acid.

SA is a promising technology to improve API crystals' mechanical properties and flowability. As demonstrated in chapter 6, by using the HSWM approach of producing <500 µm spherical agglomerates with improved flowability, compressibility and tabletability. Enables A better understanding of the process and scale-up is needed to bring the technology to the next level, from the “explorative/demonstration” stage in the laboratory to “commercial” application.

Areas investigated as the key to achieving the agglomerates of similar properties across the scales are accurate dosing of bridging liquid; A relatively small volume of bridging liquid is typically required for an SA process. It has been observed that small changes in BL can induce relatively large changes in agglomerate physical properties. Another area requiring investigation is quantifying residual BL after the SA process is finished. SA mechanism is well understood. However, further investigation is required to understand the transport mechanism of BL. Quantifying BL in the mother liquor and the agglomerate can help understand this mechanism. The spherical agglomeration process can also be explored further on the CMBOC platform to utilize its advantages (uniform mixing and narrow shear distribution) to perform spherical agglomeration, which was not possible with the current CMBOC 120 ml volume setup using HSWM.

Furthermore, different sizes and shapes of input material in conjunction with the BL quantity, droplet formation and available surface area are crucial parameters that can impact the achievable agglomerate size. Variable input in terms of the size and shape of raw material can lead to different agglomerate sizes. Required product size can be achieved with varying inputs using two different approaches. One approach is pre-processing raw materials to achieve desired input parameters (milling, etc.). However, this approach has limitations where there is a risk for polymorphic changes due to the mechanical disordering process and a thermally activated recrystallisation. The second approach is to use a well-designed experiment plan to develop a correlation between input size, BL and mixing. Recently, spherical co-agglomeration (agglomeration in the presence of polymer) has raised a lot of interest in the pharmaceutical industry, which can be explored further with the proposed HSWM technique. Within that, different polymer addition routes (i.e. depending on polymer solubility, dissolving a polymer in BL, suspending polymer in DL, dissolving a polymer in DL), different polymer types (i.e. HPMC, PEG, PVP), polymer concentrations can be explored along with the process demonstrated in chapter 6 to produce spherical agglomeration to further enhance attributes of an agglomerated product.

References

1. Statman, M., *The effect of patent expiration on the market position of drugs.* Managerial and Decision Economics, 1981. **2**(2): p. 61-66.
2. Domokos, A., et al., *Integrated Continuous Pharmaceutical Technologies—A Review.* Organic Process Research & Development, 2021. **25**(4): p. 721-739.
3. CMAC. *Personalised Product supply*. 2021; Available from: https://www.cmac.ac.uk/Hub_Research.htm.
4. Baxendale, I.R., et al., *Achieving Continuous Manufacturing: Technologies and Approaches for Synthesis, Workup, and Isolation of Drug Substance May 20–21, 2014 Continuous Manufacturing Symposium.* Journal of Pharmaceutical Sciences, 2015. **104**(3): p. 781-791.
5. Zhang, D., et al., *Progress of Pharmaceutical Continuous Crystallization.* Engineering, 2017. **3**(3): p. 354-364.
6. Byrn, S., et al., *Achieving Continuous Manufacturing for Final Dosage Formation: Challenges and How to Meet Them. May 20–21, 2014 Continuous Manufacturing Symposium.* Journal of Pharmaceutical Sciences, 2015. **104**(3): p. 792-802.
7. Badman, C. and B.L. Trout, *Achieving Continuous Manufacturing. May 20–21, 2014 Continuous Manufacturing Symposium.* Journal of Pharmaceutical Sciences, 2015. **104**(3): p. 779-780.
8. Badman, C., et al., *Why We Need Continuous Pharmaceutical Manufacturing and How to Make It Happen.* Journal of Pharmaceutical Sciences, 2019. **108**(11): p. 3521-3523.
9. Orehek, J., D. Teslić, and B. Likozar, *Continuous Crystallization Processes in Pharmaceutical Manufacturing: A Review.* Organic Process Research & Development, 2021. **25**(1): p. 16-42.
10. Mastrojohn, D. *Pfizer Announces Collaboration with GSK on Next-Generation Design of Portable, Continuous, Miniature and Modular (PCMM) Oral Solid Dose Development and Manufacturing Units*. 2015; Available from: https://www.businesswire.com/news/home/20151029005733/en/Pfizer-Announces-Collaboration-GSK-Next-Generation-Design-Portable.
11. Palmer, E. *Business wire*. 2019; Available from: https://www.businesswire.com/news/home/20151029005733/en/Pfizer-Announces-Collaboration-GSK-Next-Generation-Design-Portable.
12. Jiang, M. and R.D. Braatz, *Designs of continuous-flow pharmaceutical crystallizers: developments and practice.* CrystEngComm, 2019. **21**(23): p. 3534-3551.
13. Chen, J., et al., *Pharmaceutical Crystallization.* Crystal Growth & Design, 2011. **11**(4): p. 887-895.
14. Mascia, S., et al., *End-to-End Continuous Manufacturing of Pharmaceuticals: Integrated Synthesis, Purification, and Final Dosage Formation.* Angewandte Chemie-International Edition, 2013. **52**(47): p. 12359-12363.
15. Hu, C., et al., *An automated modular assembly line for drugs in a miniaturized plant.* Chemical Communications, 2020. **56**(7): p. 1026-1029.

16. Van Gerven, T. and A. Stankiewicz, *Structure, Energy, Synergy, Time—The Fundamentals of Process Intensification.* Industrial & Engineering Chemistry Research, 2009. **48**(5): p. 2465-2474.
17. Lee, S.L., et al., *Modernizing Pharmaceutical Manufacturing: from Batch to Continuous Production.* Journal of Pharmaceutical Innovation, 2015. **10**(3): p. 191-199.
18. Shekunov, B.Y. and P. York, *Crystallization processes in pharmaceutical technology and drug delivery design.* Journal of Crystal Growth, 2000. **211**(1-4): p. 122-136.
19. Bauer, J., et al., *Ritonavir: An Extraordinary Example of Conformational Polymorphism.* Pharmaceutical Research, 2001. **18**(6): p. 859-866.
20. Schoen, H.M., C.S. Grove, and J.A. Palermo, *The early history of crystallization.* Journal of Chemical Education, 1956. **33**(8): p. 373.
21. Mullin, J.W., *Crystallisation*. 4th ed, ed. Butterworth-Heinemann. 2001, Oxford.
22. Kraume, M. and P. Zehner, *Concept for scale-up of solids suspension in stirred tanks.* Canadian Journal of Chemical Engineering, 2002. **80**(4): p. 674-681.
23. Ma, Y., et al., *Recent Progress in Continuous Crystallization of Pharmaceutical Products: Precise Preparation and Control.* Organic Process Research & Development, 2020. **24**(10): p. 1785-1801.
24. Alvarez, A.J., A. Singh, and A.S. Myerson, *Crystallization of Cyclosporine in a Multistage Continuous MSMPR Crystallizer.* Crystal Growth & Design, 2011. **11**(10): p. 4392-4400.
25. Knox, M., M. Trifkovic, and S. Rohani, *Combining anti-solvent and cooling crystallization: Effect of solvent composition on yield and meta stable zone width.* Chemical Engineering Science, 2009. **64**(16): p. 3555-3563.
26. Nagy, Z.K., M. Fujiwara, and R.D. Braatz, *Modelling and control of combined cooling and antisolvent crystallization processes.* Journal of Process Control, 2008. **18**(9): p. 856-864.
27. Lindenberg, C., et al., *Design and Optimization of a Combined Cooling/Antisolvent Crystallization Process.* Crystal Growth & Design, 2009. **9**(2): p. 1124-1136.
28. Yazdanpanah, N. and Z.K. Nagy, *The handbook of continuous crystallization*. 2020. 630.
29. ter Horst, J.H., C. Schmidt, and J. Ulrich, *Fundamentals of Industrial Crystallization*, in *Handbook of Crystal Growth (Second Edition)*, P. Rudolph, Editor. 2015, Elsevier: Boston. p. 1317-1349.
30. Chew, J.W., P.S. Chow, and R.B.H. Tan, *Automated in-line technique using FBRM to achieve consistent product quality in cooling crystallization.* Crystal Growth & Design, 2007. **7**(8): p. 1416-1422.
31. Kim, S.J., C.K. Wei, and S. Kiang, *Crystallization process development of an active pharmaceutical ingredient and particle engineering via the use of ultrasonics and temperature cycling.* Organic Process Research & Development, 2003. **7**(6): p. 997-1001.

32. Lawton, S., et al., *Continuous Crystallization of Pharmaceuticals Using a Continuous Oscillatory Baffled Crystallizer.* Organic Process Research & Development, 2009. **13**(6): p. 1357-1363.
33. Myerson, A.S., *Nucleation Concluding Remarks* Faraday Discussions, 2015. **179**(0): p. 543-547.
34. Erdemir, D., A.Y. Lee, and A.S. Myerson, *Nucleation of Crystals from Solution: Classical and Two-Step Models.* Accounts of Chemical Research, 2009. **42**(5): p. 621-629.
35. Karthika, S., T.K. Radhakrishnan, and P. Kalaichelvi, *A Review of Classical and Nonclassical Nucleation Theories.* Crystal Growth & Design, 2016. **16**(11): p. 6663-6681.
36. Gebauer, D. and H. Cölfen, *Prenucleation clusters and non-classical nucleation.* Nano Today, 2011. **6**(6): p. 564-584.
37. Garside, J. and R.J. Davey, *Secondary Contact Nucleation - Kinetics, Growth and Scale-Up.* Chemical Engineering Communications, 1980. **4**(4-5): p. 393-424.
38. Briuglia, M.L., J. Sefcik, and J.H. ter Horst, *Measuring Secondary Nucleation through Single Crystal Seeding.* Crystal Growth & Design, 2019. **19**(1): p. 421-429.
39. Fujiwara, M., et al., *First-principles and direct design approaches for the control of pharmaceutical crystallization.* Journal of Process Control, 2005. **15**(5): p. 493-504.
40. Variankaval, N., A.S. Cote, and M.F. Doherty, *From form to function: Crystallization of active pharmaceutical ingredients.* Aiche Journal, 2008. **54**(7): p. 1682-1688.
41. Davey, R. and J. Garside, *From Molecules to Crystallizers*. 2000: Oxford University Press.
42. Beckmann, W., *Crystallisation - Basic Concepts and Industrial Applications*. 2013: Wiley-VCH.
43. Briggs, N.E.B., et al., *Seeded Crystallization of β-l-Glutamic Acid in a Continuous Oscillatory Baffled Crystallizer.* Organic Process Research & Development, 2015.
44. Schacht, U., *Control of nucleation in continuous crystallisation processes*, in *Department of Chemical and Process Engineering*. 2014, University of Strathclyde: Glasgow. p. 193.
45. Stoica, C., et al., *Understanding the effect of a solvent on the crystal habit.* Crystal Growth & Design, 2004. **4**(4): p. 765-768.
46. Berkovitchyellin, Z., et al., *Crystal Morphology Engineering by Tailor-Made Inhibitors - a New Probe to Fine Intermolecular Interactions.* Journal of the American Chemical Society, 1985. **107**(11): p. 3111-3122.
47. Davies, M.J., et al., *The crystal engineering of salbutamol sulphate via simulated pulmonary surfactant monolayers.* International Journal of Pharmaceutics, 2013. **446**(1-2): p. 34-45.
48. Joseph K. H. Ma, B.H., *Basic Physical Pharmacy*. 2013: Jones and Bartlett Learning.

49. Vasconcelos, T., B. Sarmento, and P. Costa, *Solid dispersions as strategy to improve oral bioavailability of poor water soluble drugs.* Drug Discovery Today, 2007. **12**(23-24): p. 1068-1075.
50. Nagy, Z.K., E. Aamir, and C.D. Rielly, *Internal Fines Removal Using Population Balance Model Based Control of Crystal Size Distribution under Dissolution, Growth and Nucleation Mechanisms.* Crystal Growth & Design, 2011. **11**(6): p. 2205-2219.
51. Saleemi, A., C. Rielly, and Z.K. Nagy, *Automated direct nucleation control for in situ dynamic fines removal in batch cooling crystallization.* Crystengcomm, 2012. **14**(6): p. 2196-2203.
52. Doherty, M.F., *Crystal Engineering for Product and Process Design.* 17th European Symposium on Computer Aided Process Engineering, 2007. **24**: p. 9-10.
53. Kim, S., et al., *Control of the particle properties of a drug substance by crystallization engineering and the effect on drug product formulation.* Organic Process Research & Development, 2005. **9**(6): p. 894-901.
54. Kovacic, B., F. Vrecer, and O. Planinsek, *Spherical crystallization of drugs.* Acta Pharmaceutica, 2012. **62**(1): p. 1-14.
55. Wang, J., F. Li, and R. Lakerveld, *Process intensification for pharmaceutical crystallization.* Chemical Engineering and Processing - Process Intensification, 2018. **127**: p. 111-126.
56. Whitesides, G.M., *The origins and the future of microfluidics.* Nature, 2006. **442**(7101): p. 368-373.
57. Siddique, H., et al., *Establishment of a Continuous Sonocrystallization Process for Lactose in an Oscillatory Baffled Crystallizer.* Organic Process Research & Development, 2015.
58. Peña, R., et al., *Process Intensification through Continuous Spherical Crystallization Using an Oscillatory Flow Baffled Crystallizer.* Crystal Growth & Design, 2017. **17**(9): p. 4776-4784.
59. Peña, R. and Z.K. Nagy, *Process Intensification through Continuous Spherical Crystallization Using a Two-Stage Mixed Suspension Mixed Product Removal (MSMPR) System.* Crystal Growth & Design, 2015. **15**(9): p. 4225-4236.
60. Wang, T., et al., *Recent progress of continuous crystallization.* Journal of Industrial and Engineering Chemistry, 2017. **54**: p. 14-29.
61. Brown, C., T. McGlone, and A. Florence, *Continuous Crystallisation*, in *Continuous Manufacturing of Pharmaceuticals*. 2017. p. 169-226.
62. McWilliams, J.C., et al., *The Evolving State of Continuous Processing in Pharmaceutical API Manufacturing: A Survey of Pharmaceutical Companies and Contract Manufacturing Organizations.* Organic Process Research & Development, 2018. **22**(9): p. 1143-1166.
63. Ferguson, S., et al., *Characterization of the anti-solvent batch, plug flow and MSMPR crystallization of benzoic acid.* Chemical Engineering Science, 2013. **104**: p. 44-54.
64. Zhao, L., et al., *From discovery to scale-up: α-lipoic acid : nicotinamide co-crystals in a continuous oscillatory baffled crystalliser.* CrystEngComm, 2014. **16**(26): p. 5769-5780.

65. Robertson, K., et al., *Design and Evaluation of a Mesoscale Segmented Flow Reactor (KRAIC).* Crystal Growth & Design, 2016. **16**(8): p. 4759-4764.
66. Khuu, Q., et al., *Pharmaceutical crystallization in Couette-Taylor crystallizer: A case study of polymorphism of amino acid L-glutamic acid.* Science and Technology Development Journal, 2016. **19**: p. 11-23.
67. Lee, S., C.-H. Lee, and W.-S. Kim, *Anti-solvent crystallization of l-threonine in Taylor crystallizers and MSMPR crystallizer: Effect of fluid dynamic motions on crystal size, shape, and recovery.* Journal of Crystal Growth, 2017. **469**: p. 119-127.
68. Nguyen, A.-T. and W.-S. Kim, *Effect of sinusoidal Taylor vortex flow on cooling crystallization of L-lysine.* Korean Journal of Chemical Engineering, 2017. **34**(7): p. 1896-1904.
69. Jiang, M. and X.-W. Ni, *Reactive Crystallization of Paracetamol in a Continuous Oscillatory Baffled Reactor.* Organic Process Research & Development, 2019. **23**(5): p. 882-890.
70. Ricardo, C. and N. Xiongwei, *Evaluation and Establishment of a Cleaning Protocol for the Production of Vanisal Sodium and Aspirin Using a Continuous Oscillatory Baffled Reactor.* Organic Process Research & Development, 2009. **13**(6): p. 1080-1087.
71. Plumb, K., *Continuous processing in the pharmaceutical industry - Changing the mind set.* Chemical Engineering Research & Design, 2005. **83**(A6): p. 730-738.
72. Chew, C.M. and R.I. Ristic, *Crystallization by oscillatory and conventional mixing at constant power density.* Aiche Journal, 2005. **51**(5): p. 1576-1579.
73. Chew, C.M., et al., *Characterisation of impeller driven and oscillatory mixing by spatial and temporal shear rate distributions.* Chemical Engineering Science, 2004. **59**(7): p. 1557-1568.
74. Brunold, C.R., et al., *Experimental-Observations on Flow Patterns and Energy-Losses for Oscillatory Flow in Ducts Containing Sharp Edges.* Chemical Engineering Science, 1989. **44**(5): p. 1227-1244.
75. Baird, M.H.I. and N.V.R. Rao, *Characteristics of a Countercurrent Reciprocating Plate Bubble Column .II. Axial Mixing and Mass-Transfer.* Canadian Journal of Chemical Engineering, 1988. **66**(2): p. 222-231.
76. Callahan, C.J. and X.W. Ni, *Probing into Nucleation Mechanisms of Cooling Crystallization of Sodium Chlorate in a Stirred Tank Crystallizer and an Oscillatory Baffled Crystallizer.* Crystal Growth & Design, 2012. **12**(5): p. 2525-2532.
77. Fritz K. Preikschat, E.P., *Apparatus and method for particle analysis*. **1989**.
78. Skala, D. and V. Veljkovic, *Mass-Transfer Characteristics in a Gas-Liquid Reciprocating Plate Column .1. Liquid-Phase Volumetric Mass-Transfer Coefficient.* Canadian Journal of Chemical Engineering, 1988. **66**(2): p. 192-199.

79. Hounslow, M.J. and X. Ni, *Population balance modelling of droplet coalescence and break-up in an oscillatory baffled reactor.* Chemical Engineering Science, 2004. **59**(4): p. 819-828.
80. Ristic, R.I., *Oscillatory mixing for crystallization of high crystal perfection pharmaceuticals.* Chemical Engineering Research & Design, 2007. **85**(A7): p. 937-944.
81. McGlone, T., et al., *Oscillatory Flow Reactors (OFRs) for Continuous Manufacturing and Crystallization.* Organic Process Research & Development, 2015. **19**(9): p. 1186-1202.
82. Stonestreet, P. and P.M.J. Van der Veeken, *The effects of oscillatory flow and bulk flow components on residence time distribution in baffled tube reactors.* Chemical Engineering Research & Design, 1999. **77**(A8): p. 671-684.
83. Dickens, A.W., M.R. Mackley, and H.R. Williams, *Experimental Residence Time Distribution Measurements for Unsteady-Flow in Baffled Tubes.* Chemical Engineering Science, 1989. **44**(7): p. 1471-1479.
84. Howes, T. and M.R. Mackley, *Experimental Axial-Dispersion for Oscillatory Flow through a Baffled Tube.* Chemical Engineering Science, 1990. **45**(5): p. 1349-1358.
85. Ni, X., *A Study of Fluid Dispersion in Oscillatory Flow-through a Baffled Tube.* Journal of Chemical Technology and Biotechnology, 1995. **64**(2): p. 165-174.
86. Smith, K.B. and M.R. Mackley, *An experimental investigation into the scale-up of oscillatory flow mixing in baffled tubes.* Chemical Engineering Research & Design, 2006. **84**(A11): p. 1001-1011.
87. Callahan, C.J., *The Influence of Hydrodynamic Environment on the Nucleation Mechanism of a Chiral Crystallization*, in *School of Engineering and Physical Sciences*. 2014, Heriot-Watt University: Edinburgh. p. 182.
88. Briggs, N.E.B., *Polymorph Control of Pharmaceuticals within a Continuous Oscillatory Baffled Crystalliser*, in *Strathclyde Institute of Pharmacy and Biomedical Sciences*. 2015, University of Strathclyde: Glasgow. p. 270.
89. Howes, T., *On the dispersion of unsteady flow in baffled tubes*, in *Dept. Chem. Eng.,*. 1988, Cambridge University,.
90. Reis, N.M.F., *Novel Oscillatory Flow Reactors for Biotechnological Applications*, in *School of Engineering*. 2006, University of Minho: Portugal.
91. Smith, K.B., *The Scale-Up of Oscillatory Flow Mixing*, in *Christ's College*. 1999, Cambridge. p. 187.
92. Yerdelen, S., *Continuous Crystallisation and Form Control in a Meso Oscillatory Baffled Reactor*, in *Faculty of Science*. 2018, University of Strathclyde: Glasgow. p. 228.
93. Doyle, B.J., et al., *Handling of Solids and Flow Characterization in a Baffleless Oscillatory Flow Coil Reactor.* Industrial & Engineering Chemistry Research, 2019.

94. Baird, M.H.I.R.R., N. V.; Prochazka, J.; Sovova, H., *Reciprocating plate columns in solvent extraction equipment design*, ed. M.J.G. Slater, J. Eds. 1994, Chichester UK: Wiley.
95. Levenspiel, O., *Chemical Reaction Engineering*. Third Edition ed. 1962, New York Chichester Weinheim Brisbane Singapore Toronto: John Wiley & Sons.
96. Levenspiel, O., *Chemical Reaction Engineering* 3rd ed. 1999, New York, USA: Wiley.
97. Liu, Y.Q.C., et al., *A comparative study of continuous operation between a dynamic baffle crystallizer and a stirred tank crystallizer.* Chemical Engineering Journal, 2019. **367**: p. 278-294.
98. Ni, X. and A. Liao, *Effects of Cooling Rate and Solution Concentration on Solution Crystallization of l-Glutamic Acid in an Oscillatory Baffled Crystallizer.* Crystal Growth & Design, 2008. **8**(8): p. 2875-2881.
99. Mackley, M.R., G.M. Tweddle, and I.D. Wyatt, *Experimental Heat-Transfer Measurements for Pulsatile Flow in Baffled Tubes.* Chemical Engineering Science, 1990. **45**(5): p. 1237-1242.
100. Mackley, M.R. and P. Stonestreet, *Heat-Transfer and Associated Energy-Dissipation for Oscillatory Flow in Baffled Tubes.* Chemical Engineering Science, 1995. **50**(14): p. 2211-2224.
101. Chen, Z.D. and J.J.J. Chen, *Local heat transfer for oscillatory flow in the presence of a single baffle within a channel.* Chemical Engineering Science, 1998. **53**(17): p. 3177-3180.
102. Stephens, G.G. and M.R. Mackley, *Heat transfer performance for batch oscillatory flow mixing.* Experimental Thermal and Fluid Science, 2002. **25**(8): p. 583-594.
103. Zhang, X.R., S. Maruyama, and S. Sakai, *Numerical investigation of laminar natural convection on a heated vertical plate subjected to a periodic oscillation.* International Journal of Heat and Mass Transfer, 2004. **47**(19-20): p. 4439-4448.
104. Benavides, E.M., *Heat transfer enhancement by using pulsating flows.* Journal of Applied Physics, 2009. **105**(9).
105. Jiang, M., et al., *Continuous-Flow Tubular Crystallization in Slugs Spontaneously Induced by Hydrodynamics.* Crystal Growth & Design, 2014. **14**(2): p. 851-860.
106. Vacassy, R., et al., *Calcium Carbonate Precipitation Using New Segmented Flow Tubular Reactor.* AIChE J., 2000. **46**(6): p. 1241.
107. Kubo, M. and T. Yonemoto, *Continuous Synthesis of TiO2 Fine Particles and Increase of Particle Size Using a Two-Stage Slug Flow Tubular Reactor.* Chem. Eng. Res. Des., 1999. **77**(4): p. 335.
108. Alvarez, A.J. and A.S. Myerson, *Continuous Plug Flow Crystallization of Pharmaceutical Compounds.* Crystal Growth & Design, 2010. **10**(5): p. 2219-2228.
109. Kunn Hadino, Y.Y., *Continuous and sustainable granulation of nanopharmaceuticals by spray coagulation encapsulation in alginate.* International Journal of Pharmaceutics, 2014. **473**(1-2): p. 644-652.

110. Raval, V., et al., *Development and characterisation of a cascade of moving baffle oscillatory crystallisers (CMBOC).* CrystEngComm, 2020. **22**(13): p. 2288-2296.
111. Kacker, R., S.I. Regensburg, and H.J.M. Kramer, *Residence time distribution of dispersed liquid and solid phase in a continuous oscillatory flow baffled crystallizer.* Chemical Engineering Journal, 2017. **317**: p. 413-423.
112. Derksen, J.J., *Numerical simulation of solids suspension in a stirred tank.* AIChE Journal, 2003. **49**(11): p. 2700-2714.
113. Hartmann, H., J.J. Derksen, and H.E.A. van den Akker, *Macroinstability uncovered in a Rushton turbine stirred tank by means of LES.* AIChE Journal, 2004. **50**(10): p. 2383-2393.
114. Hongyuan Wei, W.Z., and John Garside, *Computational Fluid Dynamics Modeling of the Precipitation Process in a Semibatch Crystallizer.* Industrial & Engineering Chemistry Research, 2001. **40**: p. 5255.
115. Jian, H. and X. Ni, *A numerical study on the scale-up behaviour in oscillatory baffled columns.* Chemical Engineering Research & Design, 2005. **83**(A10): p. 1163-1170.
116. Manninen, M., et al., *Evaluation of axial dispersion and mixing performance in oscillatory baffled reactors using CFD.* Journal of Chemical Technology and Biotechnology, 2013. **88**(4): p. 553-562.
117. Ni, X., H. Jian, and A.W. Fitch, *Computational fluid dynamic modelling of flow patterns in an oscillatory baffled column.* Chemical Engineering Science, 2002. **57**(14): p. 2849-2862.
118. Fitch, A.W., H.B. Jian, and X.W. Ni, *An investigation of the effect of viscosity on mixing in an oscillatory baffled column using digital particle image velocimetry and computational fluid dynamics simulation.* Chemical Engineering Journal, 2005. **112**(1-3): p. 197-210.
119. Ni, X., et al., *Mixing through oscillations and pulsations - A guide to achieving process enhancements in the chemical and process industries.* Chemical Engineering Research & Design, 2003. **81**(A3): p. 373-383.
120. Hamzah, A.A., et al., *Effect of oscillation amplitude on velocity distributions in an oscillatory baffled column (OBC).* Chemical Engineering Research & Design, 2012. **90**(8): p. 1038-1044.
121. Baird, M.H.I. and N.V.R. Rao, *Power Dissipation and Flow Patterns in Reciprocating Baffle-Plate Columns.* Canadian Journal of Chemical Engineering, 1995. **73**(4): p. 417-425.
122. Howes, T., M.R. Mackley, and E.P.L. Roberts, *The Simulation of Chaotic Mixing and Dispersion for Periodic Flows in Baffled Channels.* Chemical Engineering Science, 1991. **46**(7): p. 1669-1677.
123. Yang, H., et al., *The effect of oscillatory flow on nucleation kinetics of butyl paraben.* Crystal Growth & Design, 2015.
124. Martyn David Ticehurst , I.M., *Integration of active pharmaceutical ingredient solid form selection and particle engineering into drug product design.* J Pharm Pharmacol, 2015. **67**(6): p. Pages 782–802.

125. Videc, D., O. Planinšek, and D. Lamešić, *Design of Experiments for Optimization of the Lactose Spherical Crystallization Process.* Journal of Pharmaceutical Sciences, 2020. **109**(9): p. 2774-2786.
126. Li, L., S. Zhao, and Z. Xin, *Three-solvent spherical crystallization method with a model drug: Clopidogrel hydrogen sulfate.* Chemical Engineering Science, 2020. **212**: p. 115001.
127. Chen, H., *Improve the manufacturability and dissolution performance of drugs through spherical crystallisation*. 2020, University of Minnesota. p. 263.
128. Tahara, K., et al., *Development of Continuous Spherical Crystallization to Prepare Fenofibrate Agglomerates with Impurity Complexation Using Mixed-Suspension, Mixed-Product Removal Crystallizer.* Crystal Growth & Design, 2018. **18**(11): p. 6448-6454.
129. Pitt, K., et al., *Particle design via spherical agglomeration: A critical review of controlling parameters, rate processes and modelling.* Powder Technology, 2018. **326**: p. 327-343.
130. Javadzadeh, Y., S.M.D.a. Mastai, and M. Mokhtarpour, *Spherical Crystallization of Drugs*, in *Advanced Topics in Crystallization*, Z. Vazifehasl, Editor. 2015, IntechOpen: Rijeka.
131. Kawashima, Y., et al., *Direct preparation of spherically agglomerated salicylic acid crystals during crystallization.* J. Pharm. Sci., 1984. **73**: p. 1535.
132. Subero-Couroyer, C., et al., *Agglomeration in suspension of salicylic acid fine particles: Analysis of the wetting period and effect of the binder injection mode on the final agglomerate size.* Powder Technology, 2006. **161**(2): p. 98-109.
133. Pal, K., D. Ramkrishna, and Z.K. Nagy, *Mathematical Modeling of Emulsion Solvent Diffusion for Spherical Crystallization: How To Deconvolute Primary Crystal Size Distribution from Agglomerate Size Distribution?* Industrial & Engineering Chemistry Research, 2020. **59**(13): p. 6288-6300.
134. Kawashima, Y., M. Okumura, and H. Takenaka, *Spherical Crystallization: Direct Spherical Agglomeration of Salicylic Acid Crystals During Crystallization.* Science, 1982. **216**(4550): p. 1127-1128.
135. Jbilou, M., et al., *Ibuprofen Agglomerates Preparation by Phase Separation.* Drug Development and Industrial Pharmacy, 1999. **25**(3): p. 297-305.
136. Maghsoodi, M., *How spherical crystallization improves direct tableting properties: a review.* Advanced pharmaceutical bulletin, 2012. **2**(2): p. 253-257.
137. Orlewski, P.M., B. Ahn, and M. Mazzotti, *Tuning the Particle Sizes in Spherical Agglomeration.* Crystal Growth & Design, 2018. **18**(10): p. 6257-6265.
138. Peña, R., et al., *Further Understanding of Agglomeration Mechanisms in Spherical Crystallization Systems: Benzoic Acid Case Study.* Crystal Growth & Design, 2019. **19**(3): p. 1668-1679.

139. Peña, R., et al., *Modeling and optimization of spherical agglomeration in suspension through a coupled population balance model.* Chemical Engineering Science, 2017. **167**: p. 66-77.
140. Ahmed, B., et al., *Engineering of acetaminophen particle attributes using a wet milling crystallisation platform.* International Journal of Pharmaceutics, 2019. **554**: p. 201-211.
141. Pudasaini, N., et al., *Downstream Processability of Crystal Habit-Modified Active Pharmaceutical Ingredient.* Organic Process Research & Development, 2017. **21**.
142. Giulietti, M., et al., *Industrial crystallization and precipitation from solutions: State of the technique.* Brazilian Journal of Chemical Engineering, 2001. **18**(4): p. 423-440.
143. *Guidance for industry: PAT— A framework for innovative pharmaceutical development, manufacturing, and quality assurance*, F.a.D. Administration, Editor. 2004, Food and Drug Administration: Rockville, Maryland.
144. Kougoulos, E., et al., *Use of focused beam reflectance measurement (FBRM) and process video imaging (PVI) in a modified mixed suspension mixed product removal (MSMPR) cooling crystallizer.* Journal of Crystal Growth, 2005. **273**(3–4): p. 529-534.
145. Ferguson, S., et al., *Characterization of the anti-solvent batch, plug flow and MSMPR crystallization of benzoic acid.* Chemical Engineering Science, 2013. **104**(0): p. 44-54.
146. Hou, G.Y., et al., *Development and Characterization of a Single Stage Mixed-Suspension, Mixed-Product-Removal Crystallization Process with a Novel Transfer Unit.* Crystal Growth & Design, 2014. **14**(4): p. 1782-1793.
147. Keddon, P., et al., *Monitoring continuous crystallization of paracetamol in the presence of an additive using an integrated PAT array and multivariate methods.* 2016.
148. Ferguson, S., et al., *In-Situ Monitoring and Characterization of Plug Flow Crystallizers.* Chem. Eng. Sci., 2012. **77**: p. 105.
149. Tahir, F., et al., *Advanced control of a continuous oscillatory flow crystalliser.* Control Engineering Practice, 2017. **67**: p. 64-75.
150. Brown, C.J., et al., *Enabling precision manufacturing of active pharmaceutical ingredients: workflow for seeded cooling continuous crystallisations.* Molecular Systems Design & Engineering, 2018. **3**(3): p. 518-549.
151. Saleemi, A.N., C.D. Rielly, and Z.K. Nagy, *Monitoring of the combined cooling and antisolvent crystallisation of mixtures of aminobenzoic acid isomers using ATR-UV/vis spectroscopy and FBRM.* Chemical Engineering Science, 2012. **77**: p. 122-129.
152. Simon, L.L., Z.K. Nagy, and K. Hungerbuhler, *Comparison of external bulk video imaging with focused beam reflectance measurement and ultra-violet visible spectroscopy for metastable zone identification in food and pharmaceutical crystallization processes.* Chemical Engineering Science, 2009. **64**(14): p. 3344-3351.

153. Billot, P., M. Couty, and P. Hosek, *Application of ATR-UV Spectroscopy for Monitoring the Crystallisation of UV Absorbing and Nonabsorbing Molecules.* Organic Process Research & Development, 2010. **14**(3): p. 511-523.
154. Barrett, P. and B. Glennon, *Characterizing the metastable zone width and solubility curve using lasentec FBRM and PVM.* Chemical Engineering Research & Design, 2002. **80**(A7): p. 799-805.
155. Dr Jorg Worlitschek, D.J.d.b. *Crystallization studies with Focused Beam Reflectance Measurement and Multimax*. 2005; Available from: https://www.mt.com/dam/mt_ext_files/Editorial/Generic/4/Crystallization_MultiMax_FBRM_Editorial-Generic_1117648389578_files/application_notecrystallizationstudiesonmultimaxwithfbrm.pdf.
156. Toledo, M. *PVM V819 Technology*. 2018; Available from: https://www.mt.com/gb/en/home/products/L1_AutochemProducts/FBRM-PVM-Particle-System-Characterization/PVM/Lasentec_PVM_V819.html.
157. Liu, X., et al., *Monitoring of antisolvent crystallization of sodium scutellarein by combined FBRM–PVM–NIR.* Journal of Pharmaceutical Sciences, 2011. **100**(6): p. 2452-2459.
158. Barrett, P. and B. Glennon, *Characterizing the Metastable Zone Width and Solubility Curve Using Lasentec FBRM and PVM.* Chemical Engineering Research and Design, 2002. **80**(7): p. 799-805.
159. Malvernpanalytical. *Morphologi G3*. 2020; Available from: https://www.malvernpanalytical.com/en/support/product-support/morphologi-range/morphologi-g3.
160. Technologies, K., *Using a Compact Low Voltage FE-SEM in Evaluating Materials Nano-Porosity: Preliminary Study*. 2015: USA.
161. Bastos, I., et al., *Design, Synthesis, Experimental and Theoretical Characterization of a New Multitarget 2-Thienyl-N-Acylhydrazone Derivative.* Pharmaceuticals, 2018. **11**: p. 119.
162. Rheology, F.t.-p. *Freeman technology- poweder Rheology*. 2021; Available from: https://www.freemantech.co.uk/learn/powder-rheology.
163. Myerson, A.S., et al., *Control Systems Engineering in Continuous Pharmaceutical Manufacturing. May 20–21, 2014 Continuous Manufacturing Symposium.* Journal of Pharmaceutical Sciences, 2015. **104**(3): p. 832-839.
164. Nagy, Z.K., et al., *Recent advances in the monitoring, modelling and control of crystallization systems.* Chemical Engineering Research and Design, 2013. **91**(10): p. 1903-1922.
165. Randolph, A.D. and M.A. Larson, *Chapter 3 - The Population balance*, in *Theory of Particulate Processes (Second Edition)*, A.D. Randolph and M.A. Larson, Editors. 1988, Academic Press. p. 50-79.
166. Doki, N., et al., *Process Control of Seeded Batch Cooling Crystallization of the Metastable α-Form Glycine Using an In-Situ ATR-FTIR Spectrometer and an In-Situ FBRM Particle Counter.* Crystal Growth & Design, 2004. **4**(5): p. 949-953.

167. Kee, N.C.S., R.B.H. Tan, and R.D. Braatz, *Selective Crystallization of the Metastable α-Form of l-Glutamic Acid using Concentration Feedback Control.* Crystal Growth & Design, 2009. **9**(7): p. 3044-3051.
168. Simone, E., et al., *Active Polymorphic Feedback Control of Crystallization Processes Using a Combined Raman and ATR-UV/Vis Spectroscopy Approach.* Crystal Growth & Design, 2014. **14**(4): p. 1839-1850.
169. Pérez-Calvo, J.-F., S.S. Kadam, and H.J.M. Kramer, *Determination of kinetics in batch cooling crystallization processes—A sequential parameter estimation approach.* AIChE Journal, 2016. **62**(11): p. 3992-4012.
170. Aamir, E., *Population Balance Model-Based Optimal Control of Batch Crystallisation Processes for Systematic Crystal Size Distribution Design*, in *Department of Chemical Engineering*. 2010, Loughborough University.
171. Nagy, Z.K. and R.D. Braatz, *Robust nonlinear model predictive control of batch processes.* AIChE Journal, 2003. **49**(7): p. 1776-1786.
172. Aamir, E., et al., *Combined Quadrature Method of Moments and Method of Characteristics Approach for Efficient Solution of Population Balance Models for Dynamic Modeling and Crystal Size Distribution Control of Crystallization Processes.* Industrial & Engineering Chemistry Research, 2009. **48**(18): p. 8575-8584.
173. Hermanto, M.W., et al., *Robust optimal control of polymorphic transformation in batch crystallization.* AIChE Journal, 2007. **53**(10): p. 2643-2650.
174. Ono, T., et al., *Process Modeling of the Polymorphic Transformation of l-Glutamic Acid.* Crystal Growth & Design, 2004. **4**(6): p. 1161-1167.
175. McGraw, R., *Description of Aerosol Dynamics by the Quadrature Method of Moments.* Aerosol Science and Technology, 1997. **27**(2): p. 255-265.
176. Marchisio, D.L., et al., *Quadrature method of moments for population-balance equations.* AIChE Journal, 2003. **49**(5): p. 1266-1276.
177. Gunawan, R., I. Fusman, and R.D. Braatz, *Parallel high-resolution finite volume simulation of particulate processes.* AIChE Journal, 2008. **54**(6): p. 1449-1458.
178. Oliva, J.A., et al., *Continuous Spherical Crystallization of Lysozyme in an Oscillatory Baffled Crystallizer Using Emulsion Solvent Diffusion in Droplets.* Crystal Growth & Design, 2020. **20**(2): p. 934-947.
179. Raghavan, S.L., et al., *The bulk crystallization of α-lactose monohydrate from aqueous solution.* Journal of Pharmaceutical Sciences, 2001. **90**(7): p. 823-832.
180. McSweeney, P.L.H., Fox, P. F., *Advanced Dairy Chemistry, Lactose, Water, Salts and Minor Constituents*. Vol. 3. 2009, New York: Springer-Verlag
181. Mcleod, J., *Nucleation and growth of alpha Lactose monohydrate*, in *process engineering*. 2007, Massey University. p. 258.
182. Fujiwara, M., et al., *Paracetamol Crystallization Using Laser Backscattering and ATR-FTIR Spectroscopy: Metastability,*

Agglomeration, and Control. Crystal Growth & Design, 2002. **2**(5): p. 363-370.
183. Powell, K.A., et al., *Periodic steady-state flow crystallization of a pharmaceutical drug using MSMPR operation.* Chemical Engineering and Processing: Process Intensification, 2015. **97**(0): p. 195-212.
184. Brown, C.J. and X.W. Ni, *Evaluation of Growth Kinetics of Antisolvent Crystallization of Paracetamol in an Oscillatory Baffled Crystallizer Utilizing Video Imaging.* Crystal Growth & Design, 2011. **11**(9): p. 3994-4000.
185. Chew, C.M., et al., *Crystallization of paracetamol under oscillatory flow mixing conditions.* Crystal Growth & Design, 2004. **4**(5): p. 1045-1052.
186. Brown, C.J. and X.W. Ni, *Online Evaluation of Paracetamol Antisolvent Crystallization Growth Rate with Video Imaging in an Oscillatory Baffled Crystallizer.* Crystal Growth & Design, 2011. **11**(3): p. 719-725.
187. Jolliffe, H.G. and D.I. Gerogiorgis, *Process modelling, design and technoeconomic evaluation for continuous paracetamol crystallisation.* Computers & Chemical Engineering, 2018. **118**: p. 224-235.
188. Katta, J. and Å.C. Rasmuson, *Spherical crystallization of benzoic acid.* International Journal of Pharmaceutics, 2008. **348**(1): p. 61-69.
189. Harvey, A.P., M.R. Mackley, and T. Seliger, *Process intensification of biodiesel production using a continuous oscillatory flow reactor.* Journal of Chemical Technology and Biotechnology, 2003. **78**(2-3): p. 338-341.
190. Harrison, S.T.L. and M.R. Mackley, *A Pulsatile Flow Bioreactor.* Chemical Engineering Science, 1992. **47**(2): p. 490-493.
191. Gough, P., X.W. Ni, and K.C. Symes, *Experimental flow visualisation in a modified pulsed baffled reactor.* Journal of Chemical Technology and Biotechnology, 1997. **69**(3): p. 321-328.
192. Ni, X., Y. Zhang, and I. Mustafa, *An investigation of droplet size and size distribution in methylmethacrylate suspensions in a batch oscillatory-baffled reactor.* Chemical Engineering Science, 1998. **53**(16): p. 2903-2919.
193. Ni, X.W., S.W. Gao, and D.W. Pritchard, *Study of Mass-Transfer in Yeast in a Pulsed Baffled Bioreactor.* Biotechnology and Bioengineering, 1995. **45**(2): p. 165-175.
194. Ni, X.W., G. Nelson, and I. Mustafa, *Flow patterns and oil-water dispersion in a 0.38 m diameter oscillatory baffled column.* Canadian Journal of Chemical Engineering, 2000. **78**(1): p. 211-220.
195. Zhang, Y.M., X.W. Ni, and I. Mustafa, *A study of oil-water dispersion in a pulsed baffled reactor.* Journal of Chemical Technology and Biotechnology, 1996. **66**(3): p. 305-311.
196. Ni, X. and P. Gough, *On the discussion of the dimensionless groups governing oscillatory flow in a baffled tube.* Chemical Engineering Science, 1997. **52**(18): p. 3209-3212.
197. Ni, X., Y. Zhang, and I. Mustafa, *Correlation of polymer particle size with droplet size in suspension polymerisation of methylmethacrylate in a batch oscillatory-baffled reactor.* Chemical Engineering Science, 1999. **54**(6): p. 841-850.

198. Ni, X.W., et al., *On the effect of tracer density on axial dispersion in a batch oscillatory baffled column.* Chemical Engineering Journal, 2002. **85**(1): p. 17-25.
199. Stonestreet, P. and A.P. Harvey, *A mixing-based design methodology for continuous oscillatory flow reactors.* Chemical Engineering Research & Design, 2002. **80**(A1): p. 31-44.
200. Abbott, M.S., et al., *Biological processing in oscillatory baffled reactors: operation, advantages and potential.* Interface Focus, 2013. **3**(1): p. 20120036.
201. Kordikowski, A., T. Shekunov, and P. York, *Polymorph control of sulfathiazole in supercritical CO2.* Pharmaceutical Research, 2001. **18**(5): p. 682-688.
202. Houson, I., *Process Understanding - For Scale-up and Manufacture of Active Ingredients*. 2011: Wiley.
203. Ni, X., et al., *A Systematic Study of the Effect of Geometrical Parameters on Mixing Time in Oscillatory Baffled Columns.* Chemical Engineering Research and Design, 1998. **76**(5): p. 635-642.
204. Ni, X., et al., *A systematic study of the effect of geometrical parameters on mixing time in oscillatory baffled columns.* Chemical Engineering Research & Design, 1998. **76**(A5): p. 635-642.
205. Phan, A.N., A. Harvey, and J. Lavender, *Characterisation of fluid mixing in novel designs of mesoscale oscillatory baffled reactors operating at low flow rates (0.3-0.6 ml/min).* Chemical Engineering and Processing, 2011. **50**(3): p. 254-263.
206. Su, Q., et al., *Mathematical modelling and experimental validation of a novel periodic flow crystallization using MSMPR crystallizers.* AIChE Journal, 2017. **63**(4): p. 1313-1327.
207. Cui, Y., et al., *Custom-Built Miniature Continuous Crystallization System with Pressure-Driven Suspension Transfer.* Organic Process Research & Development, 2016. **20**(7): p. 1276-1282.
208. Harvey, A.P., M.R. Mackley, and P. Stonestreet, *Operation and optimization of an oscillatory flow continuous reactor.* Industrial & Engineering Chemistry Research, 2001. **40**(23): p. 5371-5377.
209. Engineering, P. *Perceptive Engineering* 2018; Available from: http://www.perceptiveapc.com/.
210. Tahir, F., et al., *Advanced control of a continuous oscillatory flow crystalliser.* Control Engineering Practice, 2017. **67**(Supplement C): p. 64-75.
211. Cruz, P., et al., *The axial dispersion of liquid solutions and solid suspensions in planar oscillatory flow crystallizers.* AIChE Journal, 2019. **65**(9): p. e16683.
212. Zheng, M.Z. and M. Mackley, *The axial dispersion performance of an oscillatory flow meso-reactor with relevance to continuous flow operation.* Chemical Engineering Science, 2008. **63**(7): p. 1788-1799.
213. Su, Q., Z.K. Nagy, and C.D. Rielly, *Pharmaceutical crystallisation processes from batch to continuous operation using MSMPR stages: Modelling, design, and control.* Chemical Engineering and Processing: Process Intensification, 2015. **89**: p. 41-53.

214. Onyemelukwe, I.I., Z.K. Nagy, and C.D. Rielly, *Solid-liquid axial dispersion performance of a mesoscale continuous oscillatory flow crystalliser with smooth periodic constrictions using a non-invasive dual backlit imaging technique.* Chemical Engineering Journal, 2019: p. 122862.
215. Danish, M., et al., *Effect of Operating Conditions on CSTR performance: an Experimental Study.* International Journal of Engineering Research and Applications, 2015. **5**: p. 2248-962274.
216. A.Javinsky, m., *optimal control of a continuous flow stirred tank chemicl reactor.* Aiche Journal, 1970.
217. Wong, S.Y., et al., *Modeling the Crystallization Kinetic Rates of Lactose via Artificial Neural Network.* Crystal Growth & Design, 2010. **10**(6): p. 2620-2628.
218. Wong, S.Y., et al., *Determination of the dynamic metastable limit for alpha-lactose monohydrate crystallization.* International Dairy Journal, 2011. **21**(11): p. 839-847.
219. Wong, S.Y. and R.W. Hartel, *Crystallization in Lactose Refining—A Review.* Journal of Food Science, 2014. **79**(3): p. R257-R272.
220. Wong, S.Y., et al., *Development of Continuous Crystallization Processes Using a Single-Stage Mixed-Suspension, Mixed-Product Removal Crystallizer with Recycle.* Crystal Growth & Design, 2012. **12**(11): p. 5701-5707.
221. Shi, Y., B. Liang, and R.W. Hartel, *Crystallization Kinetics of Alpha-Lactose Monohydrate in a continuous cooling crystallizer.* Journal of Food Science, 1990. **55**(3): p. 817-820.
222. Liang, B., Y. Shi, and R.W. Hartel, *Growth-Rate Dispersion Effects on Lactose crystal size distributions from a continuous cooling crystallizer.* Journal of Food Science, 1991. **56**(3): p. 848-854.
223. Hou, G., et al., *Development and Characterization of a Single Stage Mixed-Suspension, Mixed-Product-Removal Crystallization Process with a Novel Transfer Unit.* Crystal Growth & Design, 2014. **14**(4): p. 1782-1793.
224. Onyemelukwe, I.I., et al., *The Role of Residence Time Distribution in the Continuous Steady-State Mixed Suspension Mixed Product Removal Crystallization of Glycine.* Crystal Growth & Design, 2019. **19**(1): p. 66-80.
225. Mubeen ur Rehman, S. and S. Qamar, *Application of the Method of Characteristics to Population Balance Models Considering Growth and Nucleation Phenomena*. Vol. 05. 2014. 1853-1862.
226. Qamar, S. and G. Warnecke, *Numerical solution of population balance equations for nucleation, growth and aggregation processes*. Vol. 31. 2007. 1576-1589.
227. Marchisio, D.L., L. Rivautella, and A.A. Barresi, *Design and scale-up of chemical reactors for nanoparticle precipitation.* 2006. **52**(5): p. 1877-1887.
228. MacFhionnghaile, P., et al., *Crystallization Diagram for Antisolvent Crystallization of Lactose: Using Design of Experiments To Investigate*

Continuous Mixing-Induced Supersaturation. Crystal Growth & Design, 2017. **17**.
229. Nagy, Z., et al., *Comparative performance of concentration and temperature controlled batch crystallizations.* Journal of Process Control - J PROCESS CONTROL, 2008. **18**.
230. Schram, C.J., et al., *Understanding Crystal Growth Kinetics in the Absence and Presence of a Polymer Using a Rotating Disk Apparatus.* Crystal Growth & Design, 2016. **16**(5): p. 2640-2645.
231. Garside, J., A. Mersmann, and J. Nývlt, *Measurement of crystal growth and nucleation rates*. 2002: IChemE.
232. Vetter, T., C.L. Burcham, and M.F. Doherty, *Regions of attainable particle sizes in continuous and batch crystallization processes.* Chemical Engineering Science, 2014. **106**: p. 167-180.
233. Sano, A., et al., *Particle Design of Tolbutamide by the Spherical Crystallization Technique. V. Improvement of Dissolution and Bioavailability of Direct Compressed Tablets Prepared Using Tolbutamide Agglomerated Crystals.* chemical & Pharmaceutical Bulletin, 1992. **40**(11): p. 3030-3035.
234. Krishna, E., R.M.G. Vankadari, and S. Jyothi, *Spherical crystallisation - A modern technique for direct compression of pharmaceutical substances.* Asian Journal of Pharmaceutical and Clinical Research, 2012. **5**: p. 114-117.
235. Ueda, et al. *Particle Design of Enoxacin by Spherical Crystallization Technique. I. : Principle of Ammonia Diffusion System (ADS)*. 1990.
236. Puechagut, H.G., J. Bianchotti, and C.A. Chiale, *Preparation of norfloxacin spherical agglomerates using the ammonia diffusion system.* Journal of pharmaceutical sciences, 1998. **87 4**: p. 519-23.
237. Kawashima, Y., et al., *An experimental study of the kinetics of the spherical crystallization of aylline sodium theophylline monohydrate.* Powder Technology, 1983. **34**(2): p. 255-260.
238. Nocent, M., et al., *Definition of a Solvent System for Spherical Crystallization of Salbutamol Sulfate by Quasi-Emulsion Solvent Diffusion (QESD) Method.* Journal of Pharmaceutical Sciences, 2001. **90**(10): p. 1620-1627.
239. Sano, A., et al., *Particle design of tolbutamide by the spherical crystallization technique. III. Micromeritic properties and dissolution rate of tolbutamide spherical agglomerates prepared by the quasi-emulsion solvent diffusion method and the solvent change method.* Chem Pharm Bull (Tokyo), 1990. **38**(3): p. 733-9.
240. Martino, P.D., et al., *Improved Dissolution Behavior of Fenbufen by Spherical Crystallization.* Drug Development and Industrial Pharmacy, 1999. **25**(10): p. 1073-1081.
241. Zajac, M., W. Musial, and L. Pawlowski, *Stability of cefotaxime sodium in solid state.* Pharmazie, 2000. **55**: p. 917.
242. Viswanathan, C.L., S.K. Kulkarni, and D.R. Kolwankar, *Spherical agglomeration of mefenamic acid and nabumetone to improve micromeritics and solubility: A technical note.* AAPS PharmSciTech, 2006. **7**(2): p. E122-E125.

243. Thati, J. and Å.C. Rasmuson, *Particle engineering of benzoic acid by spherical agglomeration.* European Journal of Pharmaceutical Sciences, 2012. **45**(5): p. 657-667.
244. Gohel, M., et al., *Improvement in flowability and compressibility of ampicillin trihydrate by spherical crystallization.* Indian Journal of Pharmaceutical Sciences, 2003. **65**: p. 634-637.
245. Bhadra, S., et al. *Spherical crystallization of mefenamic acid*. in *Pharmaceutical Technology*. 2004.
246. Mahanty, S., Sruti, J., Niranjan Patra, C., & Bhanoji Rao, M. E., *Particle design of drugs by spherical crystallization techniques.* Int.J.Pharm.Sci.Nanotechnol., 2010. **3**(2): p. 912-918.
247. Thati, J. and Å.C. Rasmuson, *On the mechanisms of formation of spherical agglomerates.* European Journal of Pharmaceutical Sciences, 2011. **42**(4): p. 365-379.
248. Blandin, A.F., et al., *Agglomeration in suspension of salicylic acid fine particles: Influence of some process parameters on kinetics and agglomerate final size.* Powder Technol., 2003. **130**: p. 316-323.
249. Thati, J., F.L. Nordström, and Å.C. Rasmuson, *Solubility of Benzoic Acid in Pure Solvents and Binary Mixtures.* Journal of Chemical & Engineering Data, 2010. **55**(11): p. 5124-5127.
250. Arjmandi-Tash, O., et al., *A new mathematical model for nucleation of spherical agglomerates by the immersion mechanism.* Chemical Engineering Science: X, 2019. **4**: p. 100048.
251. Atanassova, T., et al., *Synthesis of cefotaxime sodium salt.* Pharmazie, 1998. **53**: p. 418.
252. Chen, M., et al., *Spherical Crystallization and the Mechanism of Clopidogrel Hydrogen Sulfate.* Chemical Engineering & Technology, 2018. **41**(6): p. 1259-1265.
253. Thati, J., *Particle Engineering by Spherical Crystallization: Mechanisms and Influence of Process Conditions*, in *Department of Chemical Engineering and Technology*. 2011, KTH Chemical Engineering and Technology. p. 86.
254. Kawashima, Y., Y. Kurachi, and H. Takenaka, *Preparation of spherical wax matrices of sulfamethoxazole by wet spherical agglomeration technique using a CMSMPR agglomerator.* Powder Technology, 1982. **32**(2): p. 155-161.
255. Zhang, H., et al., *Investigation on the Spherical Crystallization Process of Cefotaxime Sodium.* Industrial & Engineering Chemistry Research, 2010. **49**(3): p. 1402-1411.
256. Chow, A.H.L. and M.W.M. Leung, *A study of the Mechanisms of Wet Spherical Agglomeration of Pharmaceutical Powders.* Drug Development and Industrial Pharmacy, 1996. **22**(4): p. 357-371.
257. Capes, C.E. and J.P. Sutherland, *Formation of spheres from finely divided solids in liquid suspension.* Ind. Eng. Chem. Proc. Des. Dev., 1967. **6**: p. 146.
258. Chen, M., et al., *Strategy of selecting solvent systems for spherical agglomeration by the Lifshitz-van der Waals acid-base approach.* Chemical Engineering Science, 2020: p. 115613.

259. Butt, H.-J. and M. Kappl, *Normal capillary forces.* Advances in Colloid and Interface Science, 2009. **146**(1): p. 48-60.
260. Amaro-González, D. and B. Biscans, *Spherical agglomeration during crystallization of an active pharmaceutical ingredient.* Powder Technology, 2002. **128**(2): p. 188-194.
261. Kerkhofs, S., et al., *Mayonnaise production in batch and continuous process exploiting magnetohydrodynamic force.* Journal of Food Engineering, 2011. **106**(1): p. 35-39.
262. Paradkar, A.R., et al., *Spherical Crystallization of Celecoxib.* Drug Development and Industrial Pharmacy, 2002. **28**(10): p. 1213-1220.
263. Wu, S., et al., *Size Control of Atorvastatin Calcium Particles Based on Spherical Agglomeration.* Chemical Engineering & Technology, 2015. **38**(6): p. 1081-1087.
264. Maghsoodi, M., *Effect of process variables on physicomechanical properties of the agglomerates obtained by spherical crystallization technique.* Pharmaceutical Development and Technology, 2011. **16**(5): p. 474-482.
265. Usha, A.N., et al., *Preparation and, in vitro, preclinical and clinical studies of aceclofenac spherical agglomerates.* European Journal of Pharmaceutics and Biopharmaceutics, 2008. **70**(2): p. 674-683.
266. Morishima, K., et al., *Micromeritic characteristics and agglomeration mechanisms in the spherical crystallization of bucillamine by the spherical agglomeration and the emulsion solvent diffusion methods.* Powder Technology, 1993. **76**(1): p. 57-64.
267. Bos, A.S. and F.J. Zuiderweg, *Size of agglomerates in batchwise suspension agglomeration.* Chem. Eng. Res. Des., 1987. **65**: p. 187.
268. Müller, M. and F. Löffler, *Development of Agglomerate Size and Structure during spherical agglomeration in suspension.* Particle & Particle Systems Characterization, 1996. **13**(5): p. 322-326.
269. Yu, C., et al., *Design of the spherical agglomerate size in crystallization by developing a two-step bridging mechanism and the model.* AIChE Journal, 2021. **68**(2).
270. Luciani, C.V., E.W. Conder, and K.D. Seibert, *Modeling-Aided Scale-Up of High-Shear Rotor–Stator Wet Milling for Pharmaceutical Applications.* Organic Process Research & Development, 2015. **19**(5): p. 582-589.
271. Lamešić, D., et al., *Spherical Agglomerates of Lactose Reduce Segregation in Powder Blends and Improve Uniformity of Tablet Content at High Drug Loads.* AAPS PharmSciTech, 2021. **23**(1): p. 17.

Publications

1) Development and characterisation of a cascade of moving baffle oscillatory crystallisers (CMBOC) DOI: 10.1039/d0ce00069h

Vishal Raval, Humera Siddique, Cameron J. Brown, Alastair J.Florence

Abstract: *A novel four-stage Cascade of Moving Baffle Oscillatory Crystallisers (CMBOC) is developed, characterised, and implemented for the continuous crystallisation of pharmaceuticals. The platform was fully automated with pressure controlled slurry transfer and process analytical tools (PAT) to support process monitoring and control. Model predictive control was used to achieve precise temperature control during the operation of crystallisations. Mixing and flow characterisation for liquids and slurries was performed, confirming near-ideal mixing performance for mean residence times in the range of 20–90 min. Heat transfer characteristics were determined and shown to be well suited to the demands of cooling crystallisation processes. Heat transfer efficiency increased with increasing oscillatory Reynolds number (Reo). This cascade is shown to provide the advantages of more uniform mixing and efficient heat transfer performance compared to a traditional cascade of stirred tank crystallisers. Continuous crystallisations of alpha lactose monohydrate (ALM) and Paracetamol (PCM) were carried out in which the target size, form, agglomeration and encrustation were controlled. For ALM, the products showed a narrow particle size distribution (PSD) with d[50] = 65 ± 5 μm and a span of 1.4 ± 0.2 and achieved a yield of 70%. The continuous crystallisation of Paracetamol in the CMBOC produced a non-agglomerated product with d[50] = 398 ± 20 μm with a span of 1.5 ± 0.2 and achieved an 85% yield. No fouling or encrustation in the vessels or transfer lines was observed during the processes. The flexible configuration and operation of the platform coupled with well-characterised shear rate distribution, residence time distributions and heat transfer show that this platform is well suited to a range of crystallisation modes, including seeded, antisolvent, cooling or reactive processes, where careful control of crystal attributes is required.*

2) *Control system engineering- Lactose PBE modelling of Lactose (drafting)*

3) *Particle Engineering- Size controlled spherical agglomeration of benzoic acid (drafting***)**

Appendices

All the raw data are structured in to chapter wise folder and uploaded on the Pure (https://pure.strath.ac.uk)